

# **TOWARDS A MECHANISTIC UNDERSTANDING OF R-LOOP REGULATION AND FUNCTION AT TELOMERES**

**Dissertation**

PhD Thesis Co-Supervision

University of Porto and Johannes Gutenberg University Mainz

Submitted to attain the academic degree

„Doctor of Natural Sciences“

at the Department of Biology

of the Johannes Gutenberg University Mainz

**Vanessa Borges Pires**

Born in 19.09.1991 in Aigle, Switzerland

Mainz, 2023



Dean of the Faculty of Biology at JGU: -

Dean of ICBAS at UP: -

1. Reviewer: -

2. Reviewer: -

3. Reviewer: -

Day of the oral exam: 19.06.2023



# TABLE OF CONTENTS

---

List of Publications .....	V
Summary .....	VII
Zusammenfassung .....	IX
Resumo .....	XI
List of Figures .....	XIII
List of Tables .....	XV
Abbreviations .....	XVII
Acknowledgements .....	XIX
1 Introduction .....	1
1.1 Telomeres .....	1
1.1.1 TELOMERE STRUCTURE AND TELOMERIC PROTEINS .....	1
1.1.2 TELOMERE CAPPING (END PROTECTION PROBLEM) .....	4
1.1.3 TELOMERES VERSUS DOUBLE-STRANDED BREAKS (DSBs) .....	4
1.1.4 TELOMERE REPLICATION .....	12
1.1.5 TELOMERE MAINTENANCE MECHANISMS .....	16
1.1.6 TELOMERIC REPEAT CONTAINING RNA (TERRA) .....	23
1.2 RNA-DNA Hybrids .....	26
1.2.1 R-LOOP FORMATION .....	27
1.2.2 R-LOOP FUNCTION .....	28
1.2.3 R-LOOP REGULATION .....	30
1.2.4 TELOMERIC R-LOOPS .....	34
1.3 Rationale .....	37
2 Results .....	39
2.1 RNA-DNA hybrids prevent resection at dysfunctional telomeres .....	39
2.1.1 RNA-DNA Hybrids Prevent Telomere Dysfunction-Induced Cell Death .....	39
2.1.2 Telomeric RNA-DNA Hybrids Prevent Exo1- And Pif1-Mediated Resection Independent of G-Quadruplex (G4) Structures .....	50
2.1.3 RNA-DNA Hybrids Prevent ssDNA Formation at Dysfunctional Telomeres .....	54

2.2	RNase H1 and H2 Are Differentially Regulated to Process RNA-DNA Hybrids ..	59
2.2.1	The Chromatin Association of RNase H2 Is Cell Cycle Regulated .....	59
2.2.2	RNase H1 Associates to Chromatin upon R-Loop Stabilization Independently of the Cell Cycle .....	61
2.3	RNA-DNA Hybrids are Tightly Regulated at Critically Short Telomeres .....	63
2.3.1	RNase H1 and Sen1 are Epistatic in Replicative Senescence .....	63
2.3.2	Hyper-Stabilization of RNA-DNA Hybrids Leads to a Fast Senescence Phenotype .....	67
2.3.3	Exo1 Deletion is Epistatic with RNases H .....	68
2.3.4	RNA-DNA Hybrids do not Affect Rates of Telomere Shortening .....	70
3	Discussion .....	73
3.1	RNA-DNA Hybrids Prevent Resection at Dysfunctional Telomeres.....	73
3.2	RNase H1 and H2 Are Differentially Regulated to Process RNA-DNA Hybrids..	80
3.3	RNA-DNA Hybrids are Tightly Regulated at Critically Short Telomeres .....	82
3.4	Future Perspectives .....	88
4	Materials and methods.....	89
4.1	Materials .....	89
4.1.1	Yeast Strains .....	89
4.1.2	Plasmids.....	96
4.1.3	Oligonucleotides .....	96
4.1.4	Media .....	97
4.1.5	Buffers and Solutions.....	99
4.1.6	Antibodies, Kits and Reagents .....	101
4.1.7	Additional Materials .....	105
4.1.8	Electronic Devices and Software .....	105
4.2	Methods.....	107
4.2.1	Yeast Strains and Culture .....	107
4.2.2	Bacterial Transformation.....	109
4.2.3	Spotting Assay.....	109
4.2.4	Growth Curve Assay.....	109

4.2.5	Senescence Curve .....	110
4.2.6	Senescence Spotting Assay .....	110
4.2.7	Cell Cycle Synchronization and Release .....	111
4.2.8	Protein Extraction and Western Blot .....	111
4.2.9	DNA Content Analysis by Flow Cytometry .....	112
4.2.10	Telomere PCR (TELO-PCR).....	112
4.2.11	Chromatin Binding Assay (CBA).....	113
4.2.12	Chromatin Immunoprecipitation (ChIP), DNA-RNA Immunoprecipitation (DRIP) and qPCR .....	114
4.2.13	ssDNA Dot Blot.....	115
4.2.14	Mass Spectrometry.....	115
5	References .....	117
	Curriculum Vitae .....	137





## LIST OF PUBLICATIONS

---

Lockhart A, **Pires VB**, Bento F, Kellner V, Luke-Glaser S, Yakoub G, Ulrich HD, Luke B. RNase H1 and H2 Are Differentially Regulated to Process RNA-DNA Hybrids. *Cell Rep.* 2019 Nov 26; **29(9)**:2890-2900.e5. DOI: 10.1016/j.celrep.2019.10.108. PMID: 31775053.

**Pires VB**, Lohner N, Wagner T, Wagner CB, Wilkens M, Hajikazemi M, Paeschke K, Butter F, Luke B. RNA-DNA hybrids prevent resection at dysfunctional telomeres. *Cell Rep.* 2023 Feb 1; **42(2)**:112077. DOI: 10.1016/j.celrep.2023.112077. PMID: 36729832.

## FUNDING

---

This thesis was funded by Fundação para a Ciência e a Tecnologia (FCT), Portugal through a doctoral grant with the reference PD/BD/127999/2016.



## SUMMARY

---

RNA-DNA hybrids are generated during transcription, DNA replication and DNA repair, due to base pairing of RNA with DNA. They are crucial intermediates in these processes and, therefore, require a tight regulation concerning their formation, localization, and removal. RNA-DNA hybrids are present throughout the genome, and display important regulatory functions for transcription regulation, chromatin structure, DNA repair, and telomere maintenance. However, RNA-DNA hybrid misregulation poses a threat to genome stability, with accumulation of pathological hybrids contributing to several diseases.

Telomeres are nucleoprotein structures at the ends of linear eukaryotic chromosomes, which are essential for genome stability and integrity. Importantly, they protect chromosome ends from degradation and prevent their recognition as DNA double-strand breaks (DSBs), thereby avoiding chromosomal rearrangements and the loss of genomic information. At telomeres, RNA polymerase II transcribed the long non-coding RNA TERRA (Telomeric repeat-containing RNA), which forms physiologically relevant RNA-DNA hybrids. Indeed, at critically short telomeres, TERRA RNA-DNA hybrids become stabilized and drive homology-directed repair (HDR) to delay the onset of replicative senescence. Importantly, even at long- and intermediate-length telomeres, which are not subject to HDR, transient TERRA RNA-DNA hybrids form. This suggests that an additional role may be required of RNA-DNA hybrids at telomeres, not only being required to promote HDR at critically short telomeres.

Here, we demonstrate that, in *Saccharomyces cerevisiae*, telomeric RNA-DNA hybrids prevent Exo1-mediated resection when telomeres become non-functional. We employed the well-characterized *cdc13-1* allele, where telomere resection can be induced in a temperature-dependent manner, to demonstrate that telomeric RNA-DNA hybrid accumulation can rescue the viability defects and the ssDNA accumulation in *cdc13-1* mutants. Additionally, the removal and destabilization of hybrids, through RNase H1 overexpression, exacerbates Exo1-mediated resection as well as affecting cell viability. Moreover, telomeric RNA-DNA hybrids do not overtly affect the shortening rate of bulk telomeres. Overall, these results support a model whereby TERRA hybrids require dynamic regulation to drive HDR at short telomeres, where RNA-DNA hybrid presence may initiate HDR through replication stress, and their removal allow strand resection for efficient completion of repair.



## ZUSAMMENFASSUNG

---

RNA-DNA-Hybride können bei der Transkription der DNA-Replikation und der Reparatur der DNA durch Basenpaarung von RNA und DNA entstehen. Diese Hybridstrukturen sind wichtige Zwischenprodukte in diesen Prozessen und erfordern eine strenge Regulierung betreffend ihrer Bildung, Lokalisation und ihres Abbaus. RNA-DNA-Hybride sind im gesamten Genom präsent und haben dort regulatorische Funktionen. Beispielsweise regulieren sie die Transkription, die Chromatinstruktur, die DNA-Reparatur und die Erhaltung der Telomere. Eine Fehlregulierung von RNA-DNA-Hybriden kann jedoch die Stabilität des Genoms beeinträchtigen, wobei die Akkumulation pathologischer Hybride zu verschiedenen Krankheiten beiträgt.

Telomere sind Nukleoproteinstrukturen an den Enden linearer eukaryotischer Chromosomen, die für die Stabilität und Integrität des Genoms von wesentlicher Bedeutung sind. Eine wichtige Funktion der Telomere ist der Schutz der Chromosomenenden vor deren Degradation. Des Weiteren verhindern sie, dass die Chromosomenenden als DNA-Doppelstrangbrüche (DSB) erkannt werden, wodurch Chromosomenmutationen und der Verlust genomischer Informationen verhindert werden. An Telomeren transkribiert RNA-Polymerase II die lange nicht-kodierende RNA TERRA (Telomeric repeat-containing RNA), die physiologisch relevante RNA-DNA-Hybride bildet. Sobald die Telomere eine kritische Länge erreichen werden TERRA-RNA-DNA-Hybride stabilisiert, was die Reparatur durch homology directed repair (HDR) auslöst, um den Beginn der replikativen Seneszenz zu verzögern. Wichtig ist, dass sich auch an Telomeren mit langer und mittlerer Länge, an welchen keine HDR stattfindet, vorübergehende TERRA-RNA-DNA-Hybride bilden. Dies deutet darauf hin, dass RNA-DNA-Hybride an Telomeren eine weitere Rolle spielen und nicht ausschließlich zur Förderung der HDR an kritisch kurzen Telomeren erforderlich sind.

In dieser Arbeit zeigen wir, dass RNA-DNA-Hybride an nicht mehr funktionsfähigen Telomeren in *Saccharomyces cerevisiae* die Exo1-vermittelte Resektion verhindern. Dabei wurde das ausführlich charakterisierte *cdc13-1* Allel verwendet, bei dem die Telomerresektion temperaturabhängig induziert werden kann. Mit Hilfe dieses Allels konnten wir zeigen, dass die Akkumulation von RNA-DNA-Hybriden an Telomeren die Letalität und die ssDNA-Akkumulation in *cdc13-1*-Mutanten verhindern kann. Zusätzlich verschlimmert der Abbau und Destabilisierung von Hybriden durch Überexpression von RNase H1 die Exo1-vermittelte Resektion und beeinträchtigt die Vitalität der Zellen. Darüber hinaus haben RNA-DNA-Hybride an Telomeren keinen offensichtlichen Einfluss auf deren Verkürzungsraten. Insgesamt unterstützen diese Ergebnisse ein Modell, bei dem TERRA-Hybride dynamisch reguliert werden müssen, um die HDR an kurzen Telomeren voranzutreiben. Dabei kann

Vorhandensein von RNA-DNA-Hybriden durch Replikationsstress HDR auslösen und ihr Abbau Strangresektion ermöglichen, wodurch die Reparatur erfolgreich abgeschlossen werden kann.

## RESUMO

---

Os híbridos de RNA-DNA são gerados durante a transcrição, replicação de DNA e reparação de DNA, devido ao emparelhamento de bases de RNA com DNA. Estes são intermediários cruciais nestes processos e, por conseguinte, requerem uma regulação rigorosa relativamente à sua formação, localização e remoção. Os híbridos de RNA-DNA estão presentes em todo o genoma e apresentam importantes funções regulatórias na transcrição, estrutura de cromatina, reparação de DNA e manutenção de telómeros. No entanto, a sua desregulação representa uma ameaça à estabilidade do genoma, contribuindo para o desenvolvimento de várias doenças com a sua acumulação.

Os telómeros são estruturas nucleoproteicas nas extremidades dos cromossomas eucarióticos lineares, que são essenciais para a estabilidade e a manutenção da integridade do genoma. Essencialmente, protegem as extremidades dos cromossomas da degradação e impedem o seu reconhecimento como quebras duplas de DNA (DSBs), evitando assim rearranjos cromossómicos e a perda de informação genómica. Em telómeros, a RNA polimerase II transcreve o lncRNA TERRA, que forma híbridos de RNA-DNA fisiologicamente relevantes. De facto, em telómeros criticamente curtos, os híbridos de TERRA RNA-DNA tornam-se estáveis e persistentes, ativando a reparação dirigida por recombinação homóloga para atrasar o início da senescência replicativa. É de salientar que, mesmo em telómeros de comprimento intermédio e longo que não estão sujeitos a recombinação homóloga, formam-se híbridos de TERRA RNA-DNA transitórios. Isto sugere que pode ser necessário um papel adicional dos híbridos de RNA-DNA em telómeros, não sendo apenas necessário promover recombinação homóloga em telómeros criticamente curtos.

Aqui, demonstramos que, em *Saccharomyces cerevisiae*, os híbridos teloméricos de RNA-DNA impedem a ressecção mediada por Exo1 quando os telómeros se tornam disfuncionais. Utilizámos o alelo bem caracterizado *cdc13-1*, onde a ressecção telomérica pode ser induzida de uma forma dependente da temperatura, para demonstrar que a acumulação de híbridos de RNA-DNA nos telómeros pode reverter os defeitos de viabilidade e a acumulação de ssDNA em mutantes *cdc13-1*. Além disso, a remoção e desestabilização dos híbridos, através da sobre-expressão de RNase H1, exacerba a ressecção mediada por Exo1, assim como afecta a viabilidade celular. Ademais, os híbridos teloméricos de RNA-DNA não afectam diretamente a taxa de encurtamento dos telómeros. Em geral, estes resultados apoiam um modelo em que os híbridos TERRA requerem uma regulação dinâmica para conduzir a recombinação homóloga em telómeros curtos, onde a sua presença pode iniciar a recombinação homóloga através de conflitos

com a maquinaria de replicação, e a sua remoção permite a ressecção da cadeia para uma conclusão eficiente da reparação.



## LIST OF FIGURES

---

Figure 1. DNA structure and major protein components of <i>S. cerevisiae</i> telomeres.....	3
Figure 2. Overview of DNA damage response (DDR) at DNA double-stranded breaks (DSBs) in <i>S. cerevisiae</i> .....	7
Figure 3. The DNA damage response (DDR) at double-stranded breaks (DSBs) and uncapped telomeres.....	11
Figure 4. The end replication problem in <i>S. cerevisiae</i> .....	13
Figure 5. Telomere replication problem.....	14
Figure 6. Telomere elongation by telomerase in <i>S. cerevisiae</i> .....	17
Figure 7. Replicative senescence model.....	20
Figure 8. The telomeric transcript TERRA and its functions.....	25
Figure 9. Functional RNA-DNA hybrids and its impact on the genome.....	26
Figure 10. Factors that suppress and resolve R-loops.....	29
Figure 11. HR-mediated re-elongation of short telomeres is mediated by RNA-DNA hybrids.....	36
Figure 12. RNA-DNA hybrids prevent telomere dysfunction-induced cell death.....	39
Figure 13. RNA-DNA hybrids accumulate at telomeres in <i>cdc13-1</i> when RNases H are depleted.....	41
Figure 14. RNA-DNA hybrids removal by RNase H1 overexpression exacerbates telomere dysfunction-induced cell death.....	42
Figure 15. Liquid growth assays do not reiterate spotting assays in <i>cdc13-1</i> when RNA-DNA hybrids are misregulated.....	44
Figure 16. RNA-DNA hybrids rescue is specific to <i>cdc13-1</i> telomere dysfunction.....	45
Figure 17. RNase H1 overexpression leads to very few proteome changes.....	46
Figure 18. Telomeric RNA-DNA hybrids prevent Exo1- and Pif1-mediated resection.....	49

Figure 19. Telomeric RNA-DNA hybrids do not affect Mre11- nor Sae2-mediated resection.....	50
Figure 20. Telomeric RNA-DNA hybrids prevent resection independently of G4 DNA.....	52
Figure 21. RNA-DNA hybrids prevent resection-mediated ssDNA formation at telomeres..	54
Figure 22. RNA-DNA hybrid removal slightly enhances resection-mediated ssDNA formation at telomeres.....	55
Figure 23. RNA-DNA hybrid removal barely impacts the DNA damage checkpoint.....	56
Figure 24. Resection into the subtelomere is affected by RNA-DNA hybrids.....	57
Figure 25. . RNase H2 associates with chromatin at the onset of S phase.....	59
Figure 26. RNase H1 associates with chromatin when stress arises.....	60
Figure 27. RNase H1 and RNase H2 affect senescence rates differently.....	63
Figure 28. RNase H1 and Sen1 are epistatic in the absence of telomerase ( <i>est2</i> ).....	65
Figure 29. Removal or hyper-stabilization of RNA-DNA hybrids leads to fast senescence..	67
Figure 30. Exo1 deletion is epistatic with RNases H senescence phenotype.....	68
Figure 31. RNA-DNA hybrids do not affect telomere shortening rate in pre-senescent cells.....	70
Figure 32. Length-dependent Regulation of TERRA RNA-DNA Hybrids.....	72
Figure 33. RNA-DNA hybrids can prevent resection of uncapped telomeres.....	73
Figure 34. Cdc13 at the crossroad of telomerase action.....	76
Figure 35. Temporal Consequences of RNase H expression.....	80
Figure 36. RNase H1 and Sen1 are candidates for RNA-DNA hybrid resolution at critically short telomeres.....	83
Figure 37. Model of action of RNA-DNA hybrids at critically short telomeres.....	86

## LIST OF TABLES

---

Table 1. Major proteins involved in the DNA damage response and telomere capping in <i>S. cerevisiae</i> and <i>H. sapiens</i> .....	5
Table 2. Up and down-regulated proteins enriched in analysis of WT + EV vs WT + <i>RNH1</i> OE by Mass Spectrometry (MS).....	48



## ABBREVIATIONS

---

<b>5-FOA</b>	5-Fluoroorotic Acid	<b>G4</b>	G-Quadruplex
<b>A</b>	Adenine	<b>Gal</b>	Galactose
<b>Aa</b>	Amino Acid	<b>gDNA</b>	Genomic DNA
<b>AGS</b>	Aicardi-Goutières Syndrome	<b>h</b>	Hours
<b>AID</b>	Auxin-Inducible Degron	<b>HA</b>	Hemmagglutinin
<b>ALT</b>	Alternative Lengthening Of Telomeres	<b>HBD</b>	Hybrid Binding Domain
<b>AOA2</b>	Ataxia-Ocular Apraxia 2	<b>HDR</b>	Homology-Directed Repair
<b>ARS</b>	Autonomously Replicating Sequence	<b>HIS</b>	Histidine
<b>BIR</b>	Break-Induced Replication	<b>hnRNP</b>	Heterogeneous Nuclear Ribonucleoproteins
<b>Bp</b>	Base Pairs	<b>HR</b>	Homologous Recombination
<b>C</b>	Cytosine	<b>HU</b>	Hydroxyurea
<b>CBA</b>	Chromatin Binding Assay	<b>HYG</b>	Hygromycin
<b>CEN</b>	Centromeric	<b>IAA</b>	Indole-3-Acetic Acid
<b>ChIP</b>	Chromatin Immunoprecipitation	<b>IgG</b>	Immunoglobulin G
<b>CSR</b>	Class Switch Recombination	<b>IPF</b>	Idiopathic Pulmonary Fibrosis
<b>CST</b>	Cdc13-Stn1-Ten1	<b>K</b>	Lysine
<b>DDR</b>	DNA Damage Response	<b>KAN</b>	Kanamycin
<b>DKC</b>	Dyskeratosis Congenita	<b>kb</b>	Kilobases
<b>D-loop</b>	Displacement-Loop	<b>kDA</b>	Kilodaltons
<b>DNA</b>	Deoxyribonucleic Acid	<b>KO</b>	Knockout
<b>DNA pol</b>	DNA Polymerase	<b>LEU</b>	Leucine
<b>DRIP</b>	DNA-RNA Immunoprecipitation	<b>lncRNA</b>	Long Non-Coding RNA
<b>Ds</b>	Double Strand	<b>mDNA</b>	Mitochondrial DNA
<b>DSB</b>	Double Stranded Break	<b>me</b>	Methylation
<b>dsDNA</b>	Double Stranded DNA	<b>min</b>	Minutes
<b><i>E. coli</i></b>	<i>Escherichia Coli</i>	<b>MMS</b>	Methyl Methanesulfonate
<b>EV</b>	Empty Vector	<b>mRNP</b>	Messenger Ribonucleoprotein Particle
<b>Exp</b>	Exponential	<b>MRX</b>	Mre11-Rad50-Xrs2
<b>FLC</b>	Flowering Locus C	<b>MS</b>	Mass Spectrometry
<b>G</b>	Guanine	<b>NAT</b>	Nourseothricin
<b>ncRNA</b>	Non-Coding RNA	<b>RT</b>	Room Temperature
<b>NER</b>	Nucleotide Excision Repair	<b>sec</b>	Seconds

<b>NHEJ</b>	Non-Homologous End Joining	<b>S.</b>	<i>Saccharomyces Cerevisae</i>
<b>NMD</b>	Nonsense Mediated Decay	<b><i>cerevisae</i></b>	
<b>nt</b>	Nucleotides	<b><i>S. pombe</i></b>	<i>Schizosaccharomyces Pombe</i>
<b>OE</b>	Overexpression	<b>SC</b>	Synthetic Complete
<b>ORF</b>	Open Reading Frame	<b>SD</b>	Standard Deviation
<b>P</b>	Phosphorylation	<b>SEM</b>	Standard Error Of The Mean
<b>PAP</b>	Peroxidase Anti-Peroxidase	<b>SIR</b>	Silent Information Regulator
<b>PCNA</b>	Proliferating Cell Nuclear Antigen	<b>ss</b>	Single Strand
<b>PCR</b>	Polymerase Chain Reaction	<b>ssDNA</b>	Single Stranded DNA
<b>PD</b>	Population Doubling	<b>STR</b>	Subtelomeric Repeated Elements
<b>PIP</b>	PCNA-Interacting Protein Motif	<b>T</b>	Thymine
<b>Pol</b>	Polymerase	<b>TAP</b>	Tandem Affinity Purification
<b>PTM</b>	Post-Translational Modification	<b>TAS</b>	Telomere Associated Sequences
<b>qPCR</b>	Quantitative PCR	<b>TBD</b>	Telomere Biology Disorders
<b>RAFF</b>	Raffinose	<b>TERRA</b>	Telomeric Repeat Containing RNA
<b>RBP</b>	RNA Binding Protein	<b>THO</b>	Hrp1, Tho2, Thp1, And Mft1 Complex
<b>rcf</b>	Relative Centrifugal Force	<b>TPE</b>	Telomere Position Effect
<b>rDNA</b>	Ribosomal DNA	<b>tRNA</b>	Transfer RNA
<b>RER</b>	Ribonucleotide Excision Repair	<b>TRP</b>	Tryptophan
<b>RNA</b>	Ribonucleic Acid	<b>ts</b>	Temperature Sensitive
<b>RNA Pol</b>	RNA Polymerase	<b>TSS</b>	Transcription Start Site
<b>RNase H</b>	Ribonuclease H	<b>TTS</b>	Transcription Termination Site
<b>rNMP</b>	Ribonucleoside Monophosphate	<b>UAS</b>	Upstream Activating Sequence
<b>RNP</b>	Ribonucleoprotein	<b>URA</b>	Uracil
<b>rNTP</b>	Ribonucleoside Triphosphate	<b>WB</b>	Western Blot
<b>rRNA</b>	Ribosomal RNA	<b>WT</b>	Wild Type
<b>ROS</b>	Reactive Oxygen Species	<b>YPD</b>	Yeast Peptone Dextrose
<b>RPA</b>	Replication Protein A		

## ACKNOWLEDGEMENTS

---

Thank you to all the people involved in this work!





# 1 INTRODUCTION

---

## 1.1 TELOMERES

Telomeres are nucleoprotein structures at the ends of linear eukaryotic chromosomes that are essential for the maintenance of the genome's stability and integrity. Importantly, they protect chromosome ends from degradation and prevent their recognition as DNA double-strand breaks (DSBs), thereby avoiding chromosomal rearrangements and the loss of genomic information. Understanding how telomere capping prevents the recognition of natural ends as DSBs, how telomeres are replicated and solve the end-replication problem, and how telomere length is regulated have been major focus points of research throughout the last decades. Undeniably, comprehending telomere biology has relevant implications in the ageing and cancer fields, and potential medical implications. In this thesis, the budding yeast *Saccharomyces cerevisiae* was used as a model organism, and is consequently the focus of this introduction.

### 1.1.1 TELOMERE STRUCTURE AND TELOMERIC PROTEINS

Telomeres are the ends of linear eukaryotic chromosomes, that are composed of simple non-coding repetitive DNA sequences and specialized telomere-associated proteins, varying in length and protein composition depending on the organism, nonetheless their general structure and functions are evolutionary conserved<sup>1-3</sup>. In *S. cerevisiae*, telomeres consist of double stranded DNA (dsDNA) repeats of an heterogeneous C<sub>1-3</sub>A/TG<sub>1-3</sub> sequence comprising around 300 ± 75 base pairs (bp) at the end of the chromosomes<sup>4-6</sup> (Figure 1). These chromosome ends are not blunt, and rather form a 3' extension of the G-rich strand dubbed 'G-tail' or 'G-overhang'<sup>7</sup> (Figure 1). This 3' G-overhang remains short through most of the cell cycle, only 12-15 nucleotides (nt) in length<sup>4</sup>. However, in late S phase, the G-overhang can expand to ≥ 30-100 nt in size<sup>5,8-10</sup>, due to elongation of the G-strand by Telomerase but also degradation of the C-strand in a mechanism that is coordinated with genomic DNA replication<sup>9,11</sup>.

In addition to the repetitive telomeric sequences, chromosome ends possess subtelomeric, middle, repetitive elements, often called TAS elements (telomere associated sequences)<sup>6</sup>. In budding yeast, two classes of TAS elements occur at subtelomeric regions, X and Y<sup>6,12,13</sup>. X elements are present in all yeast telomeres, while Y' elements can be found in zero to four tandem copies immediately internal to the telomeric repeats, distally to

the X element<sup>12–14</sup>. The X elements present a more heterogeneous sequence than the Y' elements, and are composed of a “core X” sequence and subtelomeric repeats (STR), which include binding sites for the essential transcription factor Tbf1<sup>15,16</sup> (Figure 1). In addition, the core X contains an ARS (autonomously replicating sequence) consensus sequence and a binding site for the multifunctional regulator ARS-binding factor 1 (Afb1)<sup>16</sup>. Y' elements have been identified to present two sizes, Y' long (6.7 kb) and Y' short (5.2 kb)<sup>14,17</sup>, which differ by multiple small insertions/deletions<sup>18</sup>. TG repeats can be found between the X and Y' elements, as well as between Y' repeat elements<sup>19</sup>. Overall, subtelomeric regions are dynamic, since they undergo frequent recombination<sup>13,20</sup>.

Highly specialized proteins, bind the subtelomeric and telomeric DNA in *S. cerevisiae* telomeres (Figure 1), and orchestrate telomere-related processes<sup>6,21</sup>. These telomere-related processes include roles in end protection, DNA replication, and chromatin establishment and maintenance<sup>7</sup>. In budding yeast, telomeres are bound by Rap1, Rif1 and Rif2 (Rap1-Interacting Factor 1 and 2), the SIR (Silent Information Regulator) complex (Sir2/3/4) and the CST (Cdc13-Stn1-Ten1) complex<sup>6,21</sup> (Figure 1).

The essential protein Rap1 binds the telomeric double-stranded repeats in a sequence-specific manner, where 15-20 Rap1 molecules bind a normal length telomere via its tandem Myb-like domains<sup>22–24</sup>. Rap1 is responsible for the recruitment of other telomere-associated proteins. However, its function is not restricted to telomeres, being also involved in transcription activation and repression at multiple genomic loci<sup>25</sup>. At telomeres, Rap1 is responsible for Rif1 and Rif2 recruitment, key factors for regulation of telomere length and end protection<sup>26–29</sup>. The Rif1 proteins distribution throughout the telomere is not random, with Rif1 associating to centromere-proximal telomeric sequences while Rif2 localizes more distally towards the end of the chromosome<sup>30</sup>. In addition, Rap1 also recruits the SIR histone deacetylase complex (HDAC)<sup>31,32</sup>. The subtelomeric region of telomeres is organised in nucleosomes (Wright et al 1992), and is characterised by heterochromatin formation, causing silencing of genes proximal to the chromosome ends, in a process referred to as telomere position effect (TPE)<sup>33</sup>. The Sir2/3/4 complex is responsible for the establishment of transcriptional silencing at subtelomeres<sup>34,35</sup>, not only through its interaction with Rap1<sup>36</sup>, but also through the interaction of Sir4 with the Ku complex<sup>37</sup>.

The single-stranded G-overhang is bound by Cdc13, through a single OB-fold<sup>3</sup>, and recruits Stn1 and Ten1 forming the CST complex<sup>38–40</sup>, an ‘RPA-like’ complex<sup>23</sup>. Cdc13 has been proposed to outcompete RPA for binding to the ssDNA G-overhang, due to its sequence specificity and high affinity for telomeric repeats, even though RPA is detected, in particular in S phase, at telomeres when the G-overhang is the longest<sup>41,42</sup>. The minimum

binding site for Cdc13 is 11 nt of telomeric repeats<sup>43</sup>, indicating that during most of the cell cycle only one CST complex molecule is bound per telomere. Stn1 and Ten1 also act independently of Cdc13<sup>44,45</sup>, since their combined overexpression acts as a chromosome cap in the absence of Cdc13<sup>46–48</sup>. The N-terminal domain of Stn1 is necessary for its interaction with Ten1<sup>48,49</sup>, while the Stn1's C-terminal domain interacts with both Cdc13 and Pol12 (DNA Pol $\alpha$  complex subunit)<sup>50</sup>. The CST complex is essential for telomere protection by preventing nucleolytic degradation of the telomeric sequence and its recombination<sup>51,52</sup>. Moreover, the CST complex promotes the elongation of the telomeric repeats by telomerase, through the interaction of Cdc13 with telomerase<sup>53</sup>. The CST complex also interacts with the DNA polymerase alpha-primase (pol $\alpha$ -primase) complex, supporting the synthesis of the telomeric C-rich strand<sup>39,54–57</sup>.

The Ku complex, composed by the Yku70 and Yku80 subunits, also binds telomeres although in a sequence-unspecific manner<sup>58</sup>. The Ku complex binds at the border between the subtelomeric and telomeric repeats, as well as at internal telomeric repeats<sup>59</sup>. Moreover, it is able to directly bind to the telomeric DNA, but also to additionally localise to telomeres via a Sir4 protein-protein interaction<sup>60,61</sup>.

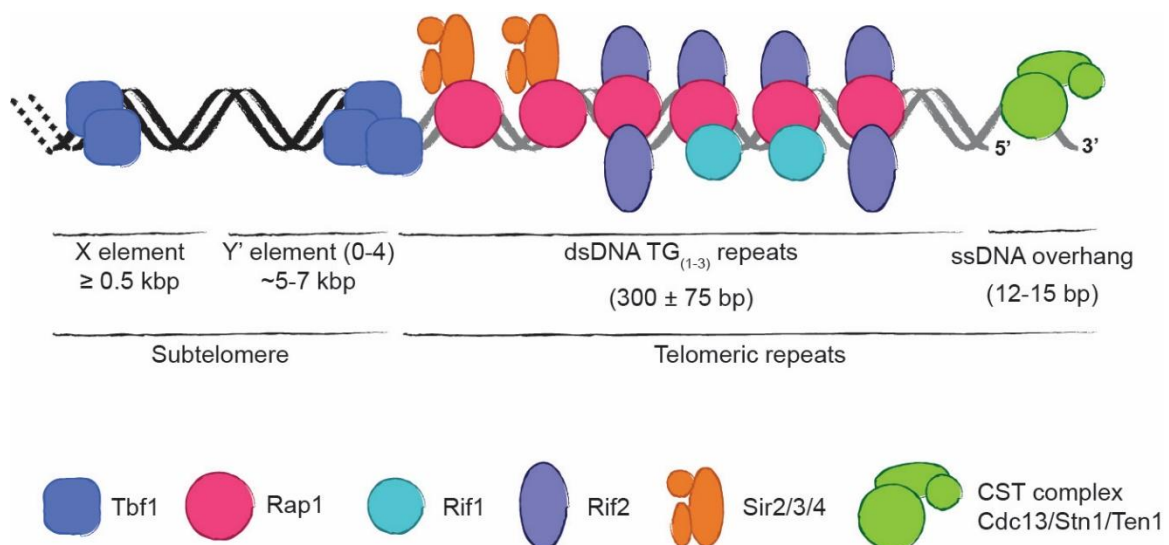


**Figure 1. DNA structure and major protein components of *S. cerevisiae* telomeres.**

The DNA structure at telomeres comprises the subtelomeric X and Y' elements, and terminal repeat sequences composed of TG<sub>(1-3)</sub> repeats and a 3' ssDNA overhang. In budding yeast, telomeres either only contain the X element (X-only telomeres) or can additionally harbour one to four Y' elements (Y' telomeres). Within the X and Y' elements, Tbf1-binding sites are present to regulate gene expression and telomere length. The Rap1 protein binds double-stranded telomeric repeats, and recruits the Sir2/3/4 complex, Rif1 and Rif2. The 3' ssDNA overhang is bound by the CST complex (Cdc13-Stn1-Ten1). Telomeric binding proteins are schematically positioned on the telomere drawing and the identity of the symbols explained at the bottom. Figure 12 Dapted from Wellinger and Zakian 2012.

### 1.1.2 TELOMERE CAPPING (END PROTECTION PROBLEM)

The ends of linear eukaryotic chromosomes structurally resemble one half of a DNA double-stranded break (DSB), and have the potential to be recognized and processed as such<sup>7,62,63</sup>. Telomeres have therefore the essential function of providing “capping” of the ends of linear chromosomes, thereby preventing unwanted repair activities and solving the “end protection problem”<sup>7</sup>. In *S.cerevisiae*, the telomere “capping” proteins comprise the CST (Cdc13-Stn1-Ten1) complex, Ku (yKu70/80) complex, and Rap1-Rif1-Rif2 proteins. Inactivation of any of these complexes causes telomere “uncapping”, stimulating a DNA damage response (DDR), which ultimately leads to cell cycle arrest. This telomere binding proteins not only distinguish telomeres from DNA breaks, preventing DNA repair activities, but also regulate telomere maintenance by telomerase, telomere replication and telomeric chromatin state<sup>6,7,21,64,65</sup>. Additionally, the telomeric architectural structure itself may mediate chromosome end protection, since telomeres are capable to fold into telomeric lariat structures<sup>66–71</sup>. In particular, telomeres have been proposed to fold-back into the subtelomeric region in *S. cerevisiae*<sup>35,72–74</sup>. Moreover, the formation of G-quadruplexes (G4s) at telomeres prevents resection<sup>75</sup>. Likewise, the presence of RNA-DNA hybrids at telomeres might promote a capping effect and inhibit resection, as is the case for DSBs<sup>76</sup>.

### 1.1.3 TELOMERES VERSUS DOUBLE-STRANDED BREAKS (DSBs)

The specialized proteins and structural properties of telomeres provide telomere protection by “capping” the chromosome ends, and consequently allowing them to be distinguished from intrachromosomal DNA double-strand breaks (DSBs)<sup>64,77,78</sup> (Table 1). Inactivation of these end protection proteins results in telomere “uncapping”, stimulating a DNA damage response (DDR), which leads to cell cycle arrest and unscheduled repair activities<sup>7,62,63</sup>. “Uncapping” is not the only source of telomere dysfunctionality and consequent genome instability. The inability of DNA replication to completely replicate the chromosome ends<sup>79,80</sup> coupled with the downregulation of telomerase activity in most somatic human tissues<sup>81</sup>, leads to telomere shortening with each cell cycle division and consequently, the loss of telomere protection capacity. This telomere attrition also causes DDR activation, irreversible cell-cycle arrest, and as a result replicative senescence<sup>82,83</sup>. Overall, defective telomere protection leads to telomeres being recognized as one half of a DSB that can be processed by nucleases, to generate single-stranded DNA (ssDNA) for repair by homologous recombination (HR) or the presence of blunt ends can lead to repair by non-homologous end joining (NHEJ)<sup>65</sup>. The recognition of telomeres as DNA damage is

believed to play a role in different pathologies, as for instance cellular ageing and tumorigenesis<sup>84–87</sup>.

**Table 1. Major proteins involved in the DNA damage response and telomere capping in *S. cerevisiae* and *H. sapiens*.** Table taken from Casari et al 2022.

<i>S. cerevisiae</i>	<i>H. sapiens</i>	Description
Mre11-Rad50-Xrs2	MRE11-RAD50-NBS1	DSB sensor; telomere length regulator
Ku70-Ku80	KU70-KU80	DSB sensor; telomere length regulator
Tel1	ATM	Apical protein kinase; telomere length regulator
Sae2	CtIP	Activator of MRX/MRN endonuclease
Exo1	EXO1	Exonuclease
Sgs1	BLM	DNA helicase
Dna2	DNA2	DNA helicase and nuclease
Mec1-Ddc2	ATR-ATRIP	Apical protein kinase and interacting factor
Rad9	53BP1	Checkpoint adaptor/mediator
Mrc1	Claspin	Replisome component; checkpoint activator
Rad53	CHK2	Downstream protein kinase
Chk1	CHK1	Downstream protein kinase
Cdc13-Stn1-Ten1	CTC1-STN1-TEN1	Telomere binding complex; telomere capping regulator
Rap1-Rif1-Rif2	TRF1-TRF2-RAP1-TIN2-TPP1-POT1	Telomere binding complex; telomere capping and length regulator

### 1.1.3.1 DNA Damage Response

In eukaryotic cells, the DDR comprises pathways to repair DNA breaks and the DNA damage checkpoint, which inhibits cell cycle progression and signals for the need of a DNA lesion to be repaired<sup>88</sup> (Figure 2). Upon the induction of a DSB, DNA ends are repaired by either HR or NHEJ<sup>89,90</sup>. The cell type and phase of the cell cycle affects the type of repair to ensue upon a DSB. The NHEJ pathway is the preferred mechanism during G1 phase, even though error-prone<sup>91</sup>. The HR pathway, is employed preferentially for DSB repair in the S and G2 phases of the cell cycle, when the sister chromatid is available as a template to promote error-free repair<sup>92</sup>. The choice between repair pathways is also influenced by the generation or not of ssDNA: the presence of ssDNA stimulates HR, while its absence, i.e. blunt ends, stimulates NHEJ<sup>89</sup>. The presence of ssDNA in the cell, not only drives HR, but

also leads to the activation of DNA damage checkpoint, causing cell cycle arrest while repair takes place<sup>89,93</sup>.

### 1.1.3.1.1 DSB Repair

The main mechanisms for DSB repair are non-homologous end-joining (NHEJ) and homologous recombination (HR) (Figure 2). The MRX complex (Mre11-Rad50-Xrs2) in association with the nuclease Sae2 and the Ku protein (yKu70-yKu80) complex are recruited to the DSB site upon damage (Figure 2 and Table 1). The key step to determine which pathway is used to repair the DSB is the initial nucleolytic degradation of the DSB ends. While NHEJ requires minimal to no DSB end-processing, HR initiation depends upon the generation of 3'-ended single stranded DNA (ssDNA), in a process called resection<sup>94</sup>. In NHEJ, the Ku complex acts as a hub for the recruitment of downstream NHEJ factors, such as Lif1, Nej1 and DNA ligase IV (Dnl4) that catalyses the direct ligation of the DSB ends<sup>95</sup> (Figure 2). Ku's presence at DSBs protects the DNA ends from degradation by the Exo1 nuclease, since it inhibits its recruitment<sup>96,97</sup> (Figure 2).

The MRX complex, stimulated by Sae2 (MRX/Sae2), provides the initial nuclease activity at DSBs, by creating small, step-wise cuts on the 5' strand in order to generate 50-100 nucleotide overhangs of 3' ssDNA<sup>98-100</sup> (Figure 2). Rapid end resection of the 5' strand leads to the eviction of the Ku complex from DNA<sup>101-103</sup>. For commitment to DSB repair by HR, these short ssDNA overhangs generated by Sae2/MRX, require further processing by a second nuclease activity dependent upon Exo1 to generate long 3' ssDNA overhangs<sup>100,104,105</sup> (Figure 2 and Table 1). Extensive resection of the DSB ends commits the repair pathway choice to HR, and also makes the DNA ends refractory to ligation by the NHEJ machinery<sup>106</sup>. An additional nuclease activity is involved in both the generation of the initial overhang as well as extensive resection, this activity is dependent upon the RecQ helicase Sgs1 and the multifunctional helicase-nuclease Dna2<sup>100,105,107,108</sup> (Figure 2 and Table 1). Sgs1/Dna2 cooperates with the MRX/Sae2 complex in the initial overhang generation and with Exo1 in extensive resection<sup>100,105</sup>.

The 3' ssDNA generated by resection becomes coated with the ssDNA binding heterotrimeric Replication Protein A (RPA) complex (Rfa1-Rfa2-Rfa3 subunits)<sup>109,110</sup>. Subsequently, RPA is replaced by the recombinase Rad51, with the assistance of the recombination protein Rad52 in the exchange<sup>111-113</sup>. This leads to the formation of a right-handed helical nucleoprotein filament, which is crucial for homology search and strand invasion into the homologous template for repair<sup>114</sup> (Figure 2).

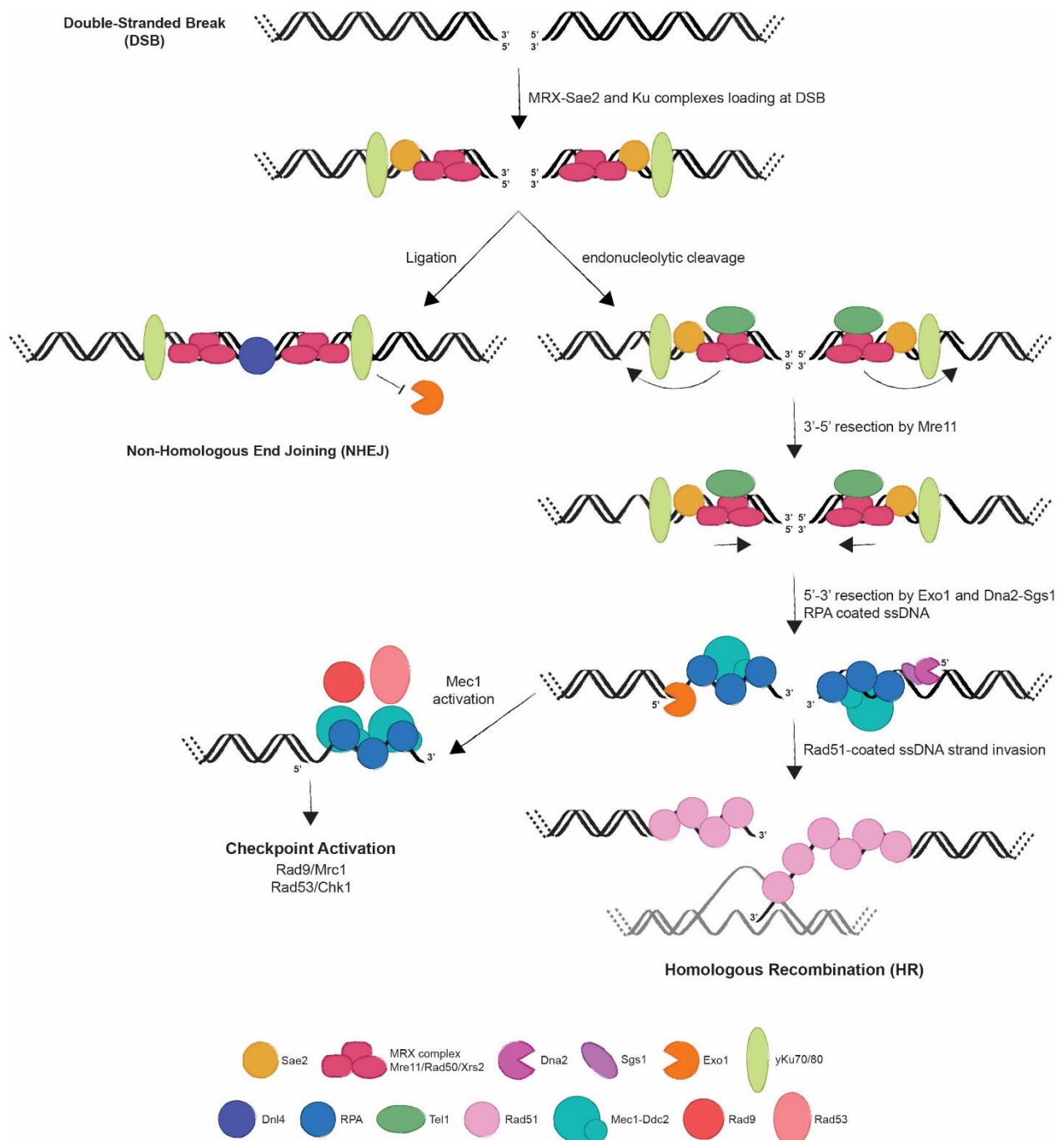


**Figure 2. Overview of DNA damage response (DDR) at DNA double-stranded breaks (DSBs) in *S. cerevisiae*.**

DSB repair can occur via non-homologous end-joining (NHEJ) or homologous recombination (HR). The MRX-Sae2 and Ku protein complexes are recruited to the DSB. The MRX complex is required to load Tel1. In NHEJ, Ku acts as a hub to recruit NHEJ factors, including DNA ligase IV that catalyses the direct ligation of the DSB ends, and Ku also inhibits Exo1 activity. If repair by NHEJ does not occur, upon ATP hydrolysis by Rad50, Mre11 together with Sae2 catalyse an endonucleolytic cleavage of the 5'-terminated strands. Bidirectional resection ensues and is catalysed by Mre11 in the 3'-5' direction and by Exo1 or Dna2-Sgs1 in the 5'-3' direction. RPA binds to the 3'-ended ssDNA overhangs and is subsequently replaced by Rad51. The Rad51-ssDNA intermediate initiates the homology search, invades the dsDNA, and pairs with the homologous DNA strand. RPA-coated ssDNA recruits the Mec1-Ddc2 complex, which eventually leads to checkpoint activation by activating Rad53 and/or Chk1 through the adaptor Rad9 or Mrc1. Proteins are schematically positioned on the drawing and the identity of the symbols is depicted at the bottom. Figure and Legend adapted from Casari et al. 2022.

### 1.1.3.1.2 DNA Damage Checkpoint

In parallel to repair, DSB occurrence can elicit the activation of the DNA damage checkpoint, coupling DSB repair with cell cycle progression<sup>88</sup>. The protein kinases Tel1 and Mec1 are key DNA damage checkpoint players (Table 1). Tel1 is the kinase involved in sensing and signaling unprocessed or minimally processed DNA DSBs, and the MRX complex is required to load Tel1 at the break site<sup>115–119</sup>. Once loaded, Tel1 supports MRX function in a positive feedback loop by promoting/stabilizing its association to the DSB<sup>120</sup>. Upon resection, the RPA-coated 3' ssDNA is recognized and bound by a heterodimer of Mec1 and Ddc2, required for checkpoint activation<sup>121,122</sup> (Figure 2). For signal initiation by Mec1-Ddc2, the cell requires extensive ssDNA (>100 nt)<sup>108</sup>. Upon Mec1 activation, the mediator protein Rad9 is recruited to break sites and permits Mec1 to activate the effector kinases Rad53 and Chk1, thus activating the checkpoint<sup>122–125</sup> (Figure 2 and Table 1). In addition, the checkpoint components are able to limit the generation of ssDNA, with Mec1, Rad53, and Rad9 all having roles in resection inhibition<sup>126–128</sup>. Moreover, Rad9 allows Rad53 phosphorylation and checkpoint activation in response to DNA damage in the G1 and G2 phases<sup>129,130</sup>, whereas Mrc1, which is a component of the replisome, promotes Rad53 activation during S phase<sup>131–134</sup>.

### 1.1.3.2 Telomere De-protection

Upon a DSB, the cell requires a rapid DNA damage response that leads to checkpoint activation and repair of the damage. Although telomeres structurally resemble DSBs, they exert an “anti-checkpoint” activity<sup>135,136</sup>. Telomere capping, i.e. the suppression of DNA repair and DNA damage checkpoint at telomeres, relies on specialized proteins that are present at single-stranded and double-stranded telomeric DNA (Table 1).

#### 1.1.3.2.1 CST complex

The evolutionarily conserved Cdc13-Stn1-Ten1 (CST) complex binds to the 3' ssDNA overhang of telomeres in *S. cerevisiae*<sup>51,137–139</sup>. The CST complex has structural similarities with the single-stranded DNA binding complex RPA<sup>23</sup>. However, it presents preferential binding to telomeric G-rich ssDNA overhangs<sup>23</sup>. In addition, it is believed to prevent telomere processing as DSBs by outcompeting RPA binding at ssDNA, thus



preventing Mec1 loading and activation<sup>23,140</sup>. The CST complex exerts its capping function during late S and G2/M phases of the cell cycle, but not in G1 or early S<sup>141,142</sup>.

Cdc13 is an essential protein, nonetheless through the usage of the temperature sensitive allele *cdc13-1*, the CST complex can be inactivated leading to telomere uncapping<sup>51,143</sup>. The *cdc13-1* allele leads to mislocalization of Cdc13 to the cytoplasm, preventing its nuclear capping function upon temperature increase<sup>144</sup>. Cdc13 inactivation induces resection of telomeric DNA, generating extensive ssDNA tracts that cause viability loss and activation of the Rad9/Mec1-dependent checkpoint, culminating in a robust G2 phase cell cycle arrest<sup>51,128,145</sup>. Inactivation of Stn1 or Ten1, through temperature sensitive alleles, also results in telomere degradation and checkpoint-mediated cell cycle arrest<sup>38,39,146</sup>. Loss of Cdc13 is related with an increase in genome instability, which is associated to defects in telomere replication<sup>147</sup>. Cdc13, as well as Stn1, physically interacts with the pol $\alpha$ -primase complex and promote its recruitment to the telomeric DNA to fill-in the C-strand<sup>50,56,57</sup>. While telomeric proteins can represent intrinsic obstacles for replication for progression<sup>148,149</sup>, it appears the CST complex could facilitate repriming on the lagging strand, compensating for fork stalling that inherently occurs during telomere replication<sup>65</sup>.

Although telomeres and DSBs are structurally similar, the nuclease activities that function at both are somewhat distinct. At DSBs, MRX/Sae2 initiates resection while at telomeres, in *cdc13-1* mutants, MRX inhibits resection<sup>150</sup> (Figure 3A). Exo1 is involved in resection at both DSBs and telomeres. However, while elimination of Exo1 alone at DSBs has relatively little effect on the efficiency and extent of resection<sup>104,151</sup>, at telomeres, Exo1 appears to be the major nuclease activity present at uncapped telomeres<sup>152,153</sup> (Figure 3B). The Sgs1/Dna2 complex is also involved in DSB resection, and the combined deletion of Sgs1 and Exo1 abolishes extensive resection<sup>100,154</sup>. At uncapped telomeres, Sgs1 also plays a role in resection<sup>155</sup>. However, extensive telomeric resection still occurs following inactivation of Cdc13 in the absence of both Exo1 and Sgs1<sup>155</sup>, indicating that the combined activities of Exo1 and Sgs1 are not responsible for all telomeric resection<sup>105</sup>. Indeed, the Pif1 helicase appears to have a critical role in the resection of uncapped telomeres<sup>156</sup> (Figure 3B). Pif1 is also implicated in replisome stability, processing of G-quadruplexes, telomerase regulation, and Okazaki fragment processing<sup>157-161</sup>. Elimination of both Exo1 and Pif1 abolishes resection following Cdc13 inactivation, also eliminating the requirement for telomere capping by Cdc13<sup>156</sup>, suggesting a pivotal role for Cdc13 in inhibiting Exo1- and Pif1-mediated resection. Overall, the CST complex presents a dual role to inhibit a DSB-like DDR initiated by Exo1 and a replication-associated DDR initiated by Pif1<sup>64</sup>.

### 1.1.3.2.2 Ku complex

The Ku complex is an evolutionarily conserved heterodimer, composed of Ku70 and Ku80 subunits, which contributes to telomere capping in the G1 phase of the cell cycle<sup>52,58,152,162</sup>. Ku inactivation results in drastically short telomeres, longer G-overhangs and deregulated subtelomeric chromatin<sup>58,163</sup>. The Ku complex inhibits Exo1 resection at DSBs and telomeres, hence restricting telomeric DNA degradation and checkpoint activation<sup>96,152,162,164</sup>. Cells lacking Ku display a temperature-sensitive growth defect related to telomere uncapping, since it can be partially suppressed by deletion of Exo1<sup>152</sup> or by overexpression of telomerase<sup>165,166</sup> (Figure 3C). In the absence of Ku, checkpoint activation occurs similarly at DSBs and telomeres, with both Rad 53 and Chk1 activation. However, at telomeres, Chk1 is primarily responsible for the arrest while Rad53 is only weakly activated<sup>152,166</sup>. In *yku70* mutants, resection at uncapped telomeres occurs less extensively than when compared to *cdc13-1* mutants, requiring multiple cell cycles for high ssDNA levels to accumulate upon telomere uncapping<sup>152,153</sup>, and resection is entirely dependent upon Exo1 activity<sup>152</sup> (Figure 3C).

### 1.1.3.2.3 Rap1-Rif1-Rif2

In budding yeast, the other protein complex with capping function is composed of Rap1, Rif1 and Rif2 proteins, with Rap1 binding directly double-stranded telomeric DNA. These proteins also negatively regulate telomere length by controlling different pathways<sup>26,167</sup>. Rap1 and Rif2, and to a lesser extent Rif1, can also repress NHEJ at telomeres, inhibit telomere degradation, and avoid checkpoint activation<sup>28,136,141,168,169</sup>. Rif2 also inhibits Tel1 activation, which promotes telomerase-mediated elongation<sup>170,171</sup>. Interestingly, Rif1 and Rif2 can have opposing roles in telomere stability, since telomere capping defects caused by CST or Ku inactivation are exacerbated by Rif1 loss but alleviated by loss of Rif2<sup>29,172</sup>. Thus, the Rap1-Rif1-Rif2 complex has capping activities with Rif1 and Rif2 having specific and separable roles in telomere capping. Rap1 inactivation leads to telomere uncapping and resection that is primarily dependent upon Exo1, although without Mec1-dependent checkpoint activation and leading to a G1 cell cycle arrest<sup>141</sup>. Even though Rap1 is an essential gene, a C-terminal deletion of Rap1 allows for cell viability impairing Rif1-Rif2 recruitment, consequently leading to telomere lengthening<sup>26</sup> and ssDNA accumulation<sup>162</sup>. Rap1 has been shown to directly inhibit resection by Exo1, moreover, by Rif1-Rif2 recruitment, it indirectly inhibits the MRX complex resection activity<sup>64,173</sup> (Figure 3D).

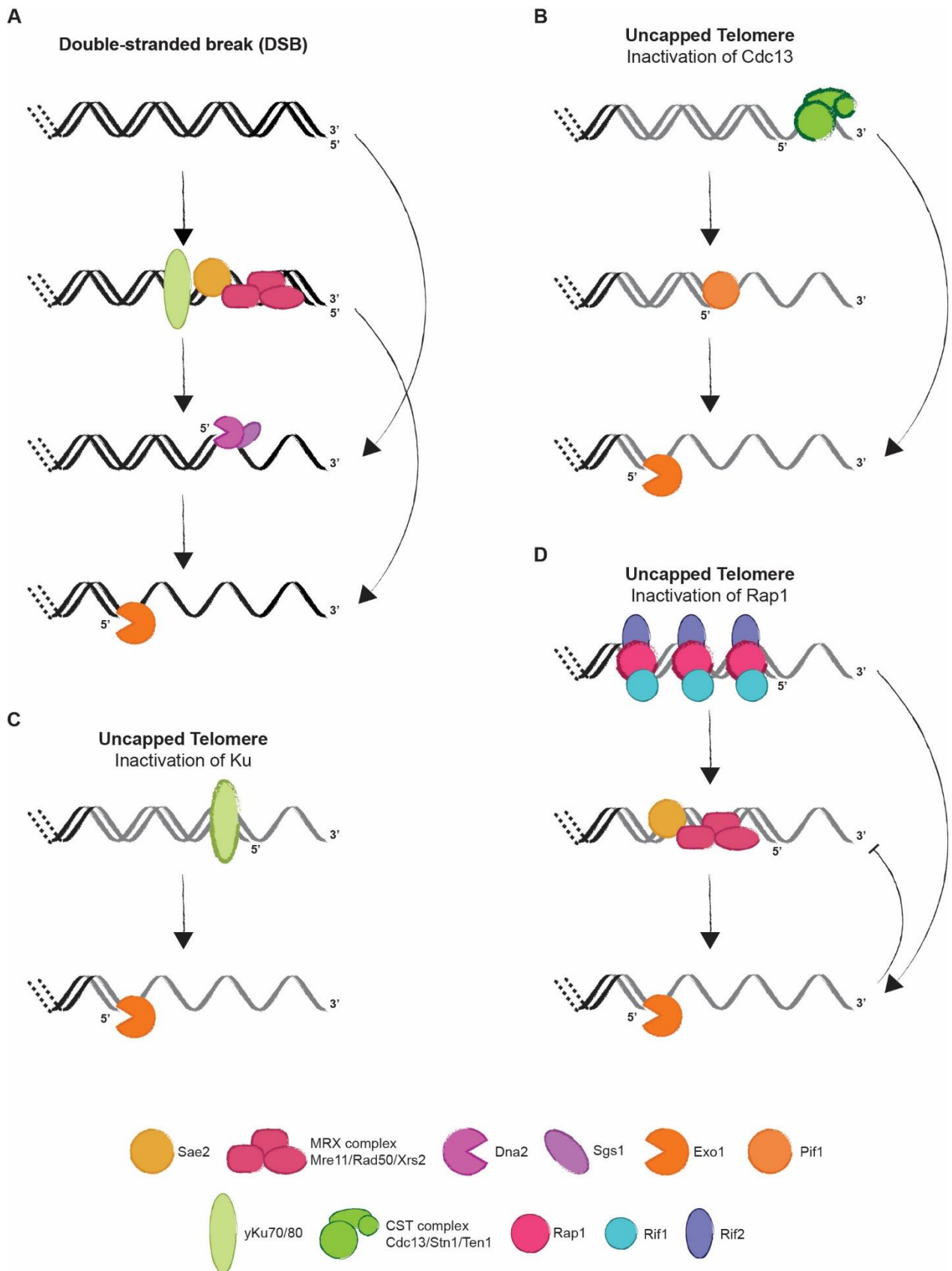


**Figure 3. The DNA damage response (DDR) at double-stranded breaks (DSBs) and uncapped telomeres.**

A) At DSBs, blunt end resection is initiated by the MRX/Sae2 complex to generate the initial overhang, and extensive resection is carried out by Exo1. The Sgs1/Dna2 complex has partially

overlapping function with both MRX/Sae2 and Exo1, and has roles in both generation of the initial overhang and extensive resection.

B) At telomeres, Cdc13 inactivation leads to resection by Exo1 and Pif1. Exo1 is capable of either initiating resection or extending Pif1-dependent 3' ssDNA.

C) At telomeres, Ku inactivation leads to resection that is entirely dependent upon Exo1.

D) At telomeres, Rap1 inactivation leads to resection primarily by Exo1. In the absence of Exo1, resection is carried out by MRX, which is inhibited when Exo1 is present.

Proteins are schematically positioned on the drawing, grey lines denote telomeric sequences, and the identity of the symbols is depicted at the bottom. Figure and Legend adapted from Dewar and Lydall 2012.

## 1.1.4 TELOMERE REPLICATION

Due to the nature of DNA synthesis, which requires a RNA primer and where DNA polymerases can only polymerise in the 5'-3' direction, the eukaryotic replication machinery is unable to completely duplicate chromosome ends, in a phenomenon denoted the end replication problem<sup>79,80,174,175</sup>. Consequently, information is lost at telomeres after every replication cycle, leading to progressive shortening in the absence of maintenance mechanisms<sup>175,176</sup> (Figure 4). This process can be counteracted by telomerase, a specialized ribonucleoprotein complex that is mechanistically related to reverse transcriptases, and is capable of adding telomeric repeats to 3' single-stranded telomeric ends<sup>177-179</sup>. Additionally to telomerase action, the canonical replication machinery accomplishes the bulk of telomeres replication. Replication origins proximal to telomeres or the autonomously replicating sequences (ARS) present in X and Y' elements can initiate telomere replication, which is unidirectional at telomeres<sup>180,181</sup>.

### 1.1.4.1 End Replication Problem

Leading strand synthesis occurs continuously, where the replication machinery starts from the replication origin, and DNA is synthesised until the chromosome end, generating a blunt end. After replication, the generated blunt end requires further processing via resection to create a 3' ssDNA overhang. This nucleolytic processing occurs after telomere replication, and is mediated by Tel1<sup>182</sup>. Resection generates a long G-overhang (~40 nt), and requires C-strand fill-in synthesis, which after removal of the RNA primer required leads to a shorter replication product from the lagging strand template<sup>176,182</sup> (Figure 4). Lagging strand synthesis is discontinuous, as it required Okazaki fragment synthesis, where each fragment is primed with its own RNA primer. After removal of the most distal primer, the 5' telomeric end is left with a gap, thus originating a 3' ssDNA overhang (Figure 4). Hence, the end replication problem derives from the leading strand replication, where the main loss of telomeric repeats through resection occurs with every replication cycle<sup>176,182</sup> (Figure 4). And, leads to a telomere shortening rate of 2.5-5 nt per replication<sup>182-185</sup>. In conclusion, telomere-

shortening rate is defined by a complex interplay between the end replication problem, the 3' overhang processing, and C-strand fill-in<sup>6,186</sup>.

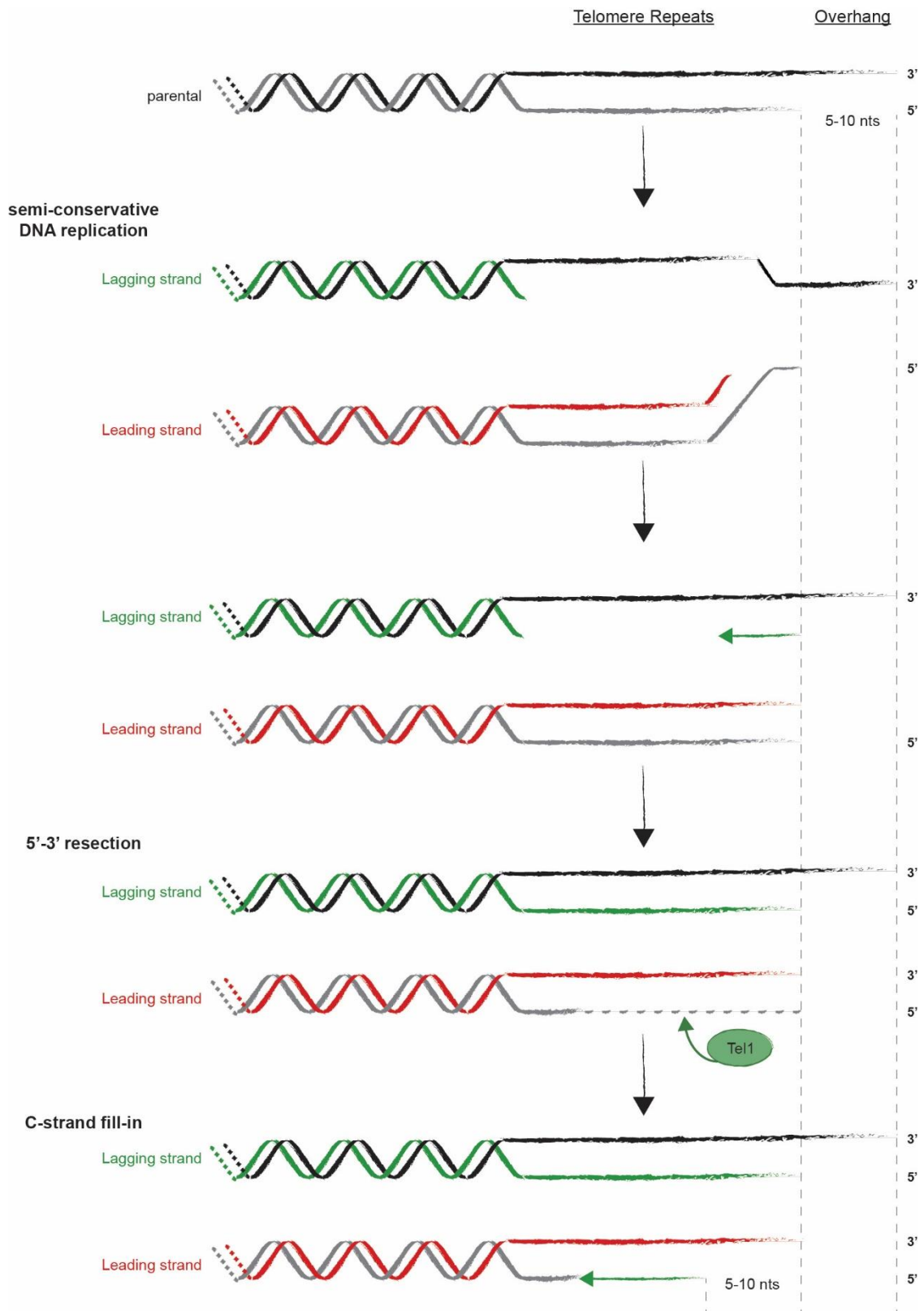


**Figure 4. The end replication problem in *S. cerevisiae*.**

For replication of the lagging strand (black), the last Okazaki fragment is initiated near the 3' end, resulting in a gap of 5-10 nt and creating a 3' overhang. Leading telomere replication (grey) may

proceed up the 5' end of the template, generating a blunt intermediate. This intermediate is rapidly processed through a Tel1-dependent pathway, generating a 3' overhang of about 40 nt. C-strand fill-in occurs, placing again a last Okazaki fragment at 5-10 nt from the end. In this scheme, telomeres shorten at a rate of 2.5-5 bp/population doubling (PD), which is due to leading strand replication. Figure and Legend adapted from Soudet et al 2014.

### 1.1.4.1 Telomere Replication Problem

Telomeres are one of the most difficult regions of the genome to replicate, and can trigger replication stress<sup>149,187-189</sup>. Chromosome end replication is subject to many obstacles derived from telomeric sequences and structures<sup>181</sup>. Hence, the effects of replication fork stalling on telomere maintenance are referred to as the telomere replication problem<sup>187</sup>. Fork stalling at telomeres can occur due to the heterochromatin structure, the strong association of telomeric binding proteins, the formation of complex secondary nucleic acid structures, as G-quadruplexes (G4s) or RNA-DNA hybrids<sup>181</sup> (Figure 5).

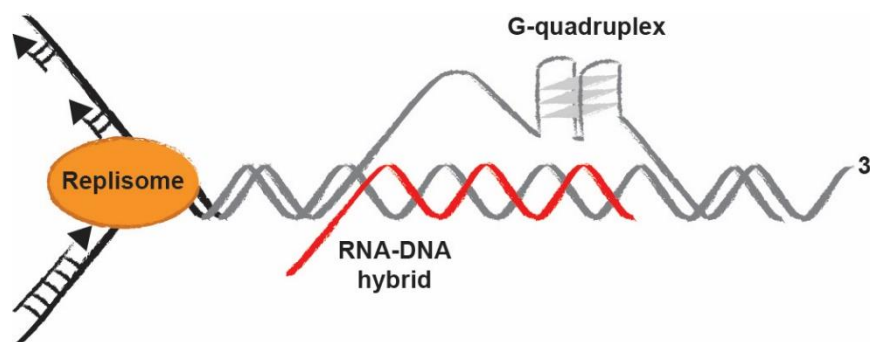


**Figure 5. Telomere replication problem.**

The C-rich strand (bottom strand) provides the template for RNA molecules to anneal, in *cis* or *trans*, to its genomic template generating RNA-DNA hybrids. G-quadruplex (G4) structures might form at the displaced G-rich strand (top strand) and stabilize the hybrid. To avoid collision during replication, this structures must be resolved, where dissolution requires nuclease and/or helicase activities. Figure and Legend adapted from Maestroni et al 2017.

Telomere associated proteins<sup>187,189-191</sup> as well as components of the fork protection complex (FPC)<sup>192</sup> are required to prevent fork stalling. Unsuccessful telomere replication is detrimental, potentially leading to fork collapse, if persistent fork stalling occurs at the telomeric repeats. Fork collapse leads to dissociation from the fork of the replication factors and the generation of a DSB<sup>193,194</sup>. If fork restart is unsuccessful at telomeres, this might lead to telomere breakage or extensive resection, and consequently resulting in abrupt telomere loss and telomere aberrations<sup>181</sup>. Therefore, different mechanisms have evolved to ensure efficient replication of telomeres. The telomere binding proteins themselves, by collaborating with the replisome, have been implicated in safeguarding efficient telomere replication and avoid fork stalling<sup>187,189-191</sup>. Additionally, several nucleases and helicases have evolved to resolve RNA-DNA hybrids and G4 structures at telomeres, and prevent

collisions with the replisome. The RNase H family composed of RNase H1 and RNase H2, as well as the helicase Sen1, are the main contributors in budding yeast to keep RNA-DNA hybrid levels in check<sup>195–198</sup>. The Pif1 helicase is the main contributor for G4 structure resolution in budding yeast, and plays critical roles in preventing replication pausing and DSBs at G4 structures<sup>199–207</sup>. In addition, several other helicases have been discovered to unfold G4 structures, including Sgs1, Srs2, Dna2 and Rrm3<sup>203</sup>. In addition to helicases, single-stranded DNA binding proteins might contribute in preventing or resolving G4 structures<sup>208–210</sup>.

### 1.1.4.2 Telomere Replication Timing

The firing of replication origins is tightly controlled, resulting in a subset of origins firing in early S phase while others fire in late S phase, without correlation to their chromatin environment or their nuclear positioning<sup>211–219</sup>. Moreover, early-replicating domains are more likely to be euchromatic, while late replicating domains usually lie within heterochromatin<sup>220,221</sup>. In budding yeast, telomere replication is coordinated in a timely manner, where telomeres replicate late in S phase<sup>218,222</sup>, independently of the replication origin sequence<sup>213</sup>. Different factors are responsible to restrict telomere replication timing in *S. cerevisiae*, with particular emphasis on the SIR complex, the Ku complex, and the telomeric binding protein Rif1 as important timing regulators. The SIR complex appears to delay replication initiation by introduction of a heterochromatin environment through its histone deacetylase function<sup>223</sup>, however how this affects the replication timing program is not fully understood. The Ku complex ensures late S replication, as impairment of the complex leads to early telomere replication<sup>224</sup>. Deletion of *RIF1* leads to anticipation of telomere replication, despite increased telomere length, indicating a role for Rif1 in regulating replication timing<sup>225,226</sup>, which is conserved from yeast to mammals<sup>227</sup>. Additionally, through its interaction with the PP1 phosphatase, Rif1 regulates the DDK-mediated phosphorylation of the pre-replication complex<sup>228–231</sup>. Moreover, telomere length dictates the timing of telomere replication: while wild type (WT) length telomeres replicate in late S phase<sup>218,222</sup>, short telomere replication occurs in early S phase<sup>232</sup>. Short telomere replication requires a Tel1-mediated pathway, where Tel1 binding is enhanced at short telomeres acting upstream of Rif1 in regulating telomeric origin firing<sup>233,234</sup>. Tel1 can also phosphorylate Rif1 at short telomeres, although this event is not sufficient to explain early replication of short telomeres, even though Tel1 dysfunction leads to short telomeres that replicate late<sup>234</sup>. Interestingly, replication timing and telomere transcription might be closely linked, since there is a connection between early replication and accumulation of telomeric transcripts at short telomeres<sup>223,232,235,236</sup>. The recruitment of telomerase at short

telomeres also appears to be facilitated by telomeric transcripts<sup>237</sup>, indicating a connection between telomere length, telomeric transcription, telomerase recruitment and replication timing. Additionally, telomere replication and telomerase action are tightly regulated, with early replication at short telomeres promoting telomerase recruitment and activity<sup>232</sup>.

## 1.1.5 TELOMERE MAINTENANCE MECHANISMS

To promote telomere integrity and protect chromosome ends, eukaryotes have evolved different strategies for telomere length regulation, counteracting the end replication problem and regulating telomere length maintenance. These strategies consist of telomerase-mediated telomere maintenance, alternative lengthening of telomeres (ALT) and non-canonical lengthening of telomeres.

### 1.1.5.1 TELOMERASE

One mechanism to counteract telomere shortening due to the end replication problem is telomerase, a specialized ribonucleoprotein complex that is capable of adding telomeric repeats to chromosome ends. Telomerase is a reverse transcriptase, which is composed of a catalytic protein component and an RNA moiety serving as a template for DNA synthesis<sup>177,179</sup>. Telomerase requires a 3' G-rich overhang for elongation, being incapable of adding telomeric repeats to blunt ends<sup>177-179</sup>. After telomere addition, the conventional DNA polymerases fill-in the C-strand using an RNA primer<sup>175</sup> (Figure 6).

In *S. cerevisiae*, telomerase is a ribonucleoprotein complex comprising of the proteins Est1, Est2, and Est3 and the RNA template TLC1. In budding yeast, telomerase is constitutively expressed, and the catalytic subunit Est2 allows polymerization of the telomeric DNA in 5'-3' orientation to the 3' G-overhang by reverse transcribing TLC1<sup>184,185,238,239</sup>. A 17 nt stretch in TLC1 serves as a template for telomere synthesis<sup>6</sup>, the Est2 subunit present the catalytic activity<sup>240</sup>, and the associated factors Est1 and Est3 are required for effective telomerase function and recruitment<sup>239,241</sup>. Completion of telomere elongation is provided by Cdc13-mediated recruitment of Pol $\alpha$ -primase to promote C-strand fill-in synthesis via conventional replication<sup>50,57</sup>. Inactivation of any telomerase component leads to progressive telomere shortening and onset of replicative senescence, leading to an irreversible cell cycle arrest and consequently cell death<sup>185</sup>.



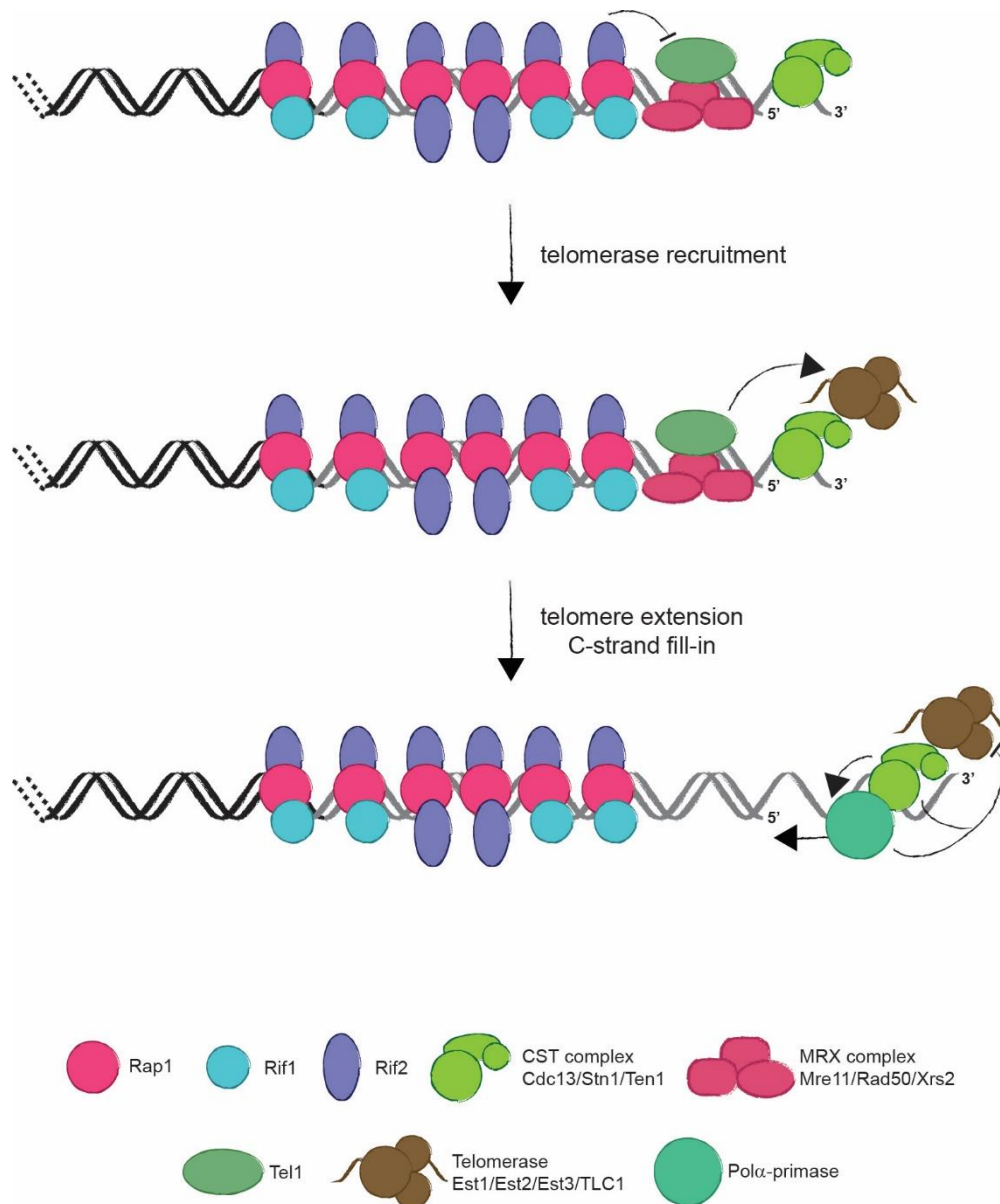


**Figure 6. Telomere elongation by telomerase in *S. cerevisiae*.**

Telomeres are bound by the MRX complex, whose binding allows for Tel1 recruitment. Tel1 promotes the association of telomerase, which is recruited to telomeres in an 'extensible' configuration. This step occurs preferentially at short telomeres. Rif2 inhibits Tel1 association by preventing its interaction with the MRX complex, and therefore its loading to DNA. Telomerase is recruited through an interaction between its Est1 component and the CST subunit Cdc13. The CST complex recruits the pol $\alpha$ -primase complex, which reconstitutes the double-stranded telomeric DNA by synthesizing the complementary C-strand. In turn, CST-mediated filling-in of the C-strand by the pol $\alpha$ -primase complex inhibits telomerase activity. Telomeric binding proteins are schematically positioned on the telomere drawing and the identity of the symbols is depicted at the bottom. Figure and Legend adapted from Bonetti et al 2014.

Telomerase recruitment and action at telomeres is a tightly coordinated process, considering the low abundance of telomerase, i.e. in late S phase there is approximately 30 telomerase copies per haploid cell for 64 telomeres<sup>242</sup>. Indeed, yeast telomerase is not active throughout the cell cycle it specifically adds telomeric repeats to chromosome ends

in late S and G2 phase<sup>56,243,244</sup>. Even though Est2 can bind telomeres throughout the cell cycle, through the interaction between TLC1 and Yku80, this localization alone is not sufficient to promote chromosome end elongation<sup>245</sup>. For formation of a functional telomerase complex, Est1 and Est3 are required for effective telomerase function and recruitment to telomeres<sup>239,241</sup>. Cdc13 phosphorylation by Cdk1, in late S and G2 phase, promotes the interaction of Cdc13 with Est1<sup>57,246–248</sup>, which in turn promotes the recruitment of Est3 and the establishment of a functional complex. Telomerase cannot promote elongation of blunt ends, which are generated after leading strand replication (Figure 4), therefore requiring the action of the MRX complex to degrade the C-strand of leading strand telomeres<sup>249</sup> (Figure 6). Cdk1 activity is also necessary for generation of the single-stranded overhang in late phase<sup>11</sup>. Additionally, the transit of the replication fork in S phase promotes recruitment of the MRX complex to telomeres<sup>9,249</sup>, indicating that the window of action for telomerase in late S/G2 phase is concomitant with the end of bulk replication and occurs after MRX-dependent telomere overhang formation. Which is consistent with the shortest telomere being preferentially elongated by telomerase<sup>183,232,250–253</sup>, i.e at leading strand telomeres where MRX processes blunt ends<sup>182,254</sup>. The Tel1 checkpoint kinase is the main regulator of telomere elongation, being recruited to telomeres by the MRX complex, where its kinase activity is necessary to promote telomere elongation<sup>30,255–258</sup> (Figure 6). Tel1-dependent phosphorylation of Cdc13 has been proposed to regulate the Cdc13-Est1 interaction<sup>259</sup>, and Tel1 has been shown to preferentially localize at short telomeres<sup>233,260</sup>. Importantly, Tel1 binding to telomeres is inhibited by Rif1 and Rif2, which act as negative regulators of telomerase action<sup>261</sup>. Rif2 inhibits Tel1 and MRX localization to telomeres by competing with Tel1 for association to Xrn2<sup>28,171</sup> (Figure 6), while the function of Rif1 in this regulation is still not completely understood<sup>171,258</sup>. Tel1 also promotes telomerase recruitment to critically short telomeres, where telomerase processivity is increased<sup>233,262,263</sup>. Indeed, with telomere shortening there is a reduction in the number of telomere-associated proteins, in particular of Rap1, Rif1, and Rif2 binding<sup>264</sup>. The loss of these proteins from the telomeric repeats allows for a ‘counting mechanism’, thereby connecting telomere length to the need for telomere extension<sup>264</sup>. In more detail, telomeres shortening would lead to the loss of Rap1 binding sites causing decreased Rif1-Rif2 recruitment to telomeres, allowing for Tel1 action, telomerase recruitment, and consequently, telomere elongation. Once the telomere is “long”, Rap1-Rif1-Rif2 binding sites are re-established, and therefore, Tel1 and telomerase action inhibited. Indeed, loss of telomeric repeats is associated to Rif2, and to a lesser extent Rif1, loss from short telomeres<sup>30,233</sup>, indicating that there is a differential distribution of the Rif proteins along the telomere, with Rif1 binding the centromere-proximal telomeric tract while Rif2 binds more towards the distal telomeric repeats. Additionally, the Pif1 helicase also promotes telomerase activity in a telomere-length-dependent manner,

therefore also being a telomerase regulator<sup>265</sup>. Pif1 preferentially binds to long telomeres<sup>266</sup>, where it can presumably displace telomerase from chromosome ends<sup>267</sup>, acting as a potent telomerase inhibitor.

### 1.1.5.2 TELOMERE SHORTENING AND SENESCENCE

In the absence of telomerase, telomeres gradually shorten with each cell cycle division, and progressively lose their protective capabilities. Consequently, these eroded telomeres cause DDR activation, resulting in an irreversible cell-cycle arrest, in a process referred to as replicative senescence<sup>82,83,268</sup> (Figure 7). Replicative senescence acts as a barrier against tumorigenesis, being considered a potent tumour suppressor mechanism, since telomere shortening limits a cell proliferative potential<sup>269,270</sup>. However, this barrier can be surpassed and create further genomic instability, that if coupled with re-stabilization of telomeres (telomerase reactivation or alternative lengthening of telomeres –‘ALT’), can drive tumorigenesis. Indeed, while telomerase is transcriptionally silenced in most human somatic cells, with the exception of the germline and certain stem cell compartments<sup>271,272</sup>, indefinite cell cycle proliferation is a hallmark of cancer<sup>273</sup>. Therefore, 73% of human cancers reactivate telomerase to counteract telomere shortening<sup>269,274</sup>, whereas 10-15% rely on homologous recombination (HR), via ALT, to maintain their proliferative potential<sup>274,275</sup>. Telomere shortening may also play a role in ageing, considering that with increasing age, there is a decrease in the mean telomere length and an increase in the proportion of senescent cells<sup>276–279</sup>. Overall, it is important to balance senescence onset in order to prevent premature ageing and at the same time prevent cancer development.

Telomerase is constitutively expressed in budding yeast, however, in the absence of catalytically active telomerase, i.e. by *EST2* or *TLC1* deletion, the growth potential of yeast cells progressively decreases<sup>185</sup>. After 60-80 population doublings (PDs), telomerase negative cells exhibit a G2/M cell cycle arrest, with increased cell volume over time<sup>184,185,239</sup>. Despite the permanent cell cycle arrest, these cells remain metabolically viable<sup>280,281</sup>. In *S. cerevisiae*, one critically short telomere is sufficient to anticipate the onset of senescence and elicit a DNA damage checkpoint response<sup>282,283</sup>. Critically short telomeres are recognized by Mec1, which activates the DNA damage checkpoint causing growth arrest<sup>283</sup>. Mec1 phosphorylates the effector kinase Rad53, requiring the adaptor proteins Rad9 and Rad24<sup>280,284</sup>. Rad53 phosphorylation additionally requires Mrc1, an S phase checkpoint protein needed for replication<sup>131</sup>. This indicates a mechanism, where eroded telomeres are recognized both as DSBs and replication stress<sup>284</sup>. While HR between telomeres can cause genome instability, it can also be a means to maintain telomere length in the absence of

telomerase, since recombination of the critically short telomere would lead to re-elongation of the chromosome ends, benefiting cell viability and preventing checkpoint activation<sup>285</sup>.

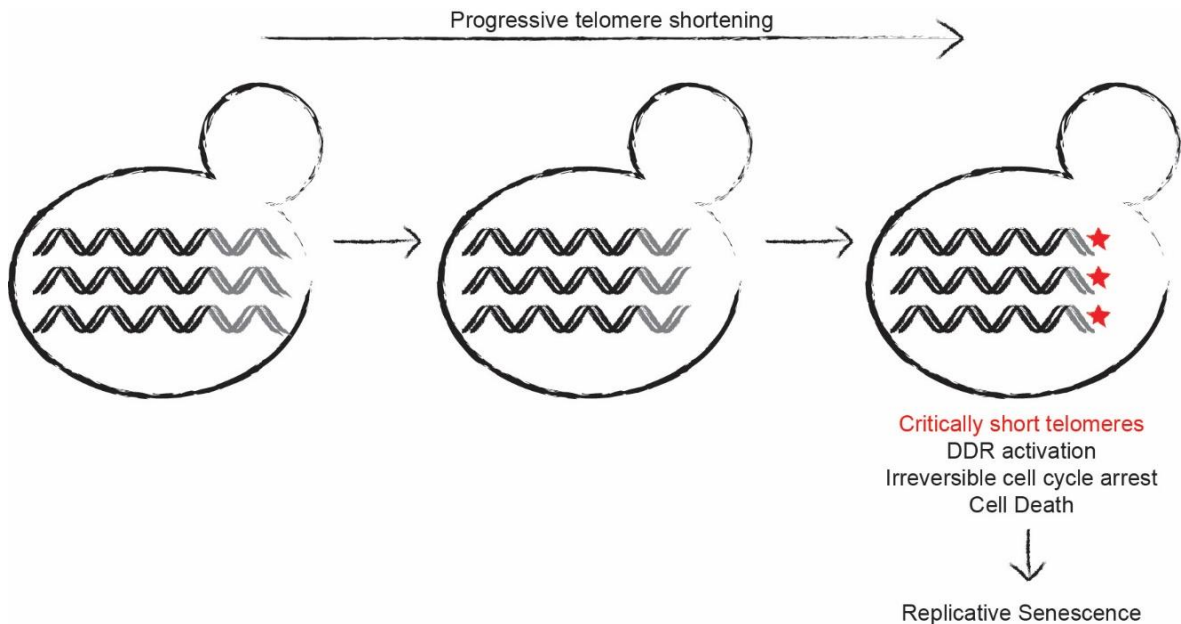


**Figure 7. Replicative senescence model.**

Telomere shortening occurs naturally with each round of cell division, ultimately leading to chromosome ends being recognised as DSBs and activating a DNA damage response, which results in an irreversible cell cycle arrest and consequently cell death. This process is called Replicative Senescence. Figure and Legend adapted from Victorelli and Passos 2017.

### 1.1.5.2.1 Telomere Recombination and Alternative Lengthening of Telomeres (ALT)

During senescence, telomerase negative cells lose viability due to checkpoint activation stemming from telomere de-protection of the short telomeres<sup>185</sup>. In *S. cerevisiae*, one critically short telomere is sufficient to trigger senescence, indicating that the length of the shortest telomere is the leading cause for growth arrest, and not bulk telomere shortening<sup>283</sup>. Indeed, most telomerase negative cells undergo subsequent terminal cell cycle arrests consequently causing cell death, which is consistent with telomeres reaching a critical (short) length<sup>286</sup>. Interestingly, approximately 40% of cells instead experience early cell cycle arrests followed by re-gain of cell proliferation capacity, in a process dependent on Pol32 and HR<sup>286</sup>. Therefore, telomere recombination can occur as a mean to elongate critically short telomeres, thereby delaying the onset of senescence, but not avoiding it completely<sup>287</sup>.

Strikingly, a rare number of telomerase negative cells can overcome senescence and re-gain almost wild type growth kinetics, these cells are called post-senescence 'survivors'. This survivor formation mechanism relies on homologous recombination<sup>288-290</sup>, and is dependent on Rad52-mediated recombination and on the Pol32-mediated break-induced replication (BIR) pathway for telomere elongation<sup>239,288-292</sup>. Survivors have been categorized into two types, Type I and II, based on the arrangement of their telomeric DNA and proteins required for their maintenance<sup>289,293</sup>. Type I survivors maintain telomeres by recombining the subtelomeric Y' elements, maintaining short telomeric repeats (50-150 bp)<sup>288,294</sup>, and rely on the HR proteins Rad51, Rad54, Rad57, and supposedly Rad55<sup>289,293</sup>. Y' element expansion can occur due to recombination between telomeres, but also possibly by amplification of extrachromosomal circular Y' repeats, which can be found in these cells<sup>294</sup>. Type I survivors arise with a high frequency, however, they present poor growth capability, due to constitutive activation of the DNA damage checkpoint<sup>290,295</sup>. Type II survivors maintain telomeres by recombining the telomeric repeats, which require the MRX complex, Rad59, and Sgs1 for telomere elongation<sup>261,289,290,293,296,297</sup>. Additionally, type II survivors contain extrachromosomal circles of telomeric repeats, which could be utilized to elongate telomeres by rolling circle amplification<sup>294</sup>. Type II survivor telomere length is extremely heterogeneous, varying from extremely long (up to 12 kb) to critically short<sup>290</sup>, presenting growth kinetics similar to wild type. Interestingly, as is the case for telomerase positive cells, type II survivor telomeres shorten with every replication round, with recombination happening at the critically short telomere<sup>261,268</sup>.

Indeed, the response to telomere shortening in *S. cerevisiae* is quite similar to what has been described for human fibroblasts and other mammalian cells, with post-senescence survivors presenting an ALT-like behaviour<sup>268</sup>. Telomere maintenance occurs via an HR-mediated mechanism and there is accumulation of extra chromosomal telomeric DNA<sup>294</sup>, making budding yeast a good model organism for studying ALT. Moreover, the regulation of the long noncoding RNA TERRA (Telomeric Repeat containing RNA), which is transcribed from telomeres, shares parallels in human ALT cells and yeast survivors, as both organisms exhibit increased TERRA levels<sup>298-301</sup>. Therefore, similar to human ALT cells, telomerase negative yeast cells likely require balanced replication stress levels, which promote HR-mediated telomere elongation yet still allow cell proliferation<sup>302</sup>.

### 1.1.5.2.2 Ageing and Telomere Biology Disorders

In human cells, telomeres progressively shorten due to the lack of telomerase activity in most somatic cells<sup>271,272</sup>, leading to DDR activation and an irreversible cell cycle arrest<sup>82,269,303</sup>. The permanent cell cycle arrest that limits cell proliferation is referred to as

cellular senescence<sup>304</sup>. Senescence limits a cells proliferative potential, and acts as a tumour suppressor mechanism<sup>269,270</sup>. Nevertheless, accumulation of senescent cells may negatively influence tissue regeneration and contribute to organismal ageing and age-related diseases<sup>87,277,279</sup>. Therefore, a balance must be achieve to prevent premature ageing and simultaneously prevent cancer development during senescence.

The onset of senescence can derive from a series of stimuli that include DNA damage, oxidative stress, proteotoxic stress, oncogene expression, chromatin alterations, continued cytokine signalling, and telomere dysfunction<sup>270,305</sup>. Senescence cells are characterized by a permanent growth arrest, even though metabolically active, apoptosis resistance and altered gene expression<sup>270,305</sup>. Moreover, both in human cells as in yeast, senescence onset results in increased cell size<sup>306,307</sup>, which causes dilution of the DNA content<sup>308</sup>. This phenomenon causes impaired gene expression and compromises cell cycle progression, which likely contributes to the limited proliferative capacity of senescent cells<sup>308</sup>. In cells with telomerase activity, i.e. cancer cells, germ cells and stem cells, telomerase can maintain telomere length and prevent entry into senescence<sup>309</sup>. However, most human cells do not harbour sufficient telomerase activity to prevent telomere shortening<sup>310</sup>, and consequently activates a DDR due to telomere dysfunction, which triggers replicative senescence entry<sup>82,83,311</sup>. In human cells, five dysfunctional telomeres are sufficient to drive senescence<sup>312</sup>, preventing proliferation of altered cells. Moreover, the amount of senescent cells increases as a function of age<sup>313,314</sup>, which can be due to the increased number of cells entering the senescent sate or also due to decreased ability to clear these cells, given the decline of the immune system function with age<sup>315</sup>. Genomic instability is a common driver for both ageing and cancer progression, with ageing actually being the most important cause of cancer, since cancer incidence drastically rises with advanced age<sup>87,316</sup>. Therefore, preserving genome stability is important to prevent cancer development and delay ageing-associated diseases.

Another subset of telomere associated diseases are telomeropathies or telomere biology disorders (TBDs), which are a group of rare premature ageing syndromes caused by telomere dysfunction<sup>317</sup>. These disorders are characterized by different severity of symptoms and ages of onset, with most patients showing pathogenic variants of genes involved in telomere maintenance<sup>317,318</sup>. Most mutations arise in genes that encode components of the telomerase complex, implicating reduction of telomerase activity, and consequently, telomere erosion. Overall several syndromes have been identified as TBDs, in particular dyskeratosis congenita (DKC) and idiopathic pulmonary fibrosis (IPF). In DKC, a rare cancer-prone bone marrow failure syndrome, mutations are found in the telomerase complex genes (TERC or TERT) or in the telomerase interactor dyskerin (DKC1)<sup>319–321</sup>. In

adulthood, IPF is the most common symptom of telomeropathy, which is characterized by progressive lung failure, linked to fibrosis and inflammation<sup>322,323</sup>, and in some cases also related to mutations in the telomerase complex itself<sup>324</sup>. These premature ageing syndromes are due to progressive organ failure and a predisposition to cancer, with patterns of onset that reflect ageing, and are not due to a progeria-like phenotype<sup>325,326</sup>. These disorders demonstrate clear links between impaired telomere maintenance, excessive telomere shortening and accelerated organismal ageing. Thereby implying that a tight regulation of telomere shortening must occur to prevent premature senescence onset and ageing.

### 1.1.6 **TELOMERIC REPPEAT CONTAINING RNA (TERRA)**

Telomeres are transcribed into a long noncoding RNA, named TERRA (Telomeric Reppeat containing RNA). TERRA transcription is evolutionary conserved and several biologically relevant functions have been described for TERRA at telomeres (Figure 8). Indeed, TERRA misregulation has been associated to dysfunctional telomere<sup>327–331</sup>, it is therefore important to regulate TERRA levels to promote telomere function and integrity. TERRA was suggested to act as a chromatin state regulator at telomeres and promote heterochromatin formation<sup>332,333</sup>. Moreover, TERRA can also act as a recruitment platform for auxiliary factors at telomeres, critical for telomere function<sup>334</sup> and as a role in telomere replication and the DNA damage response at telomeres<sup>235,335,336</sup>. In addition, TERRA was implicated in telomere length maintenance, potentially promoting telomerase recruitment or homology-directed repair (HDR) in order to support telomere elongation<sup>236,237,337</sup>.

#### 1.1.6.1 **TERRA TRANSCRIPTION**

Telomeres are characterized as heterochromatic structures, nonetheless they are transcribed into a long noncoding RNA, dubbed TERRA. TERRA transcription is evolutionary conserved and has been described in many eukaryotes, namely in yeast, plants and mammals<sup>335,338–340</sup>. RNA Polymerase II is primarily responsible for TERRA transcription from the C-rich strand of telomeres, from the subtelomeric sequence into the telomeric repeats<sup>338–342</sup>, however other polymerases also contribute to TERRA transcription<sup>340</sup>. TERRA length is heterogeneous, even within the same organism<sup>338–340</sup>. In budding yeast, TERRA varies between 100 and 1200 nt, with the bulk TERRA population averaging at 380 nt long<sup>339</sup>, a range that most likely stems from different transcription terminations sites (TTS) rather than multiple transcription start sites (TSS)<sup>342</sup>. In human and

budding yeast, TERRA carries a 5' 7-methyl-guanosine cap and a 3' poly-A-tail<sup>338–340,343</sup>, with these modifications likely promoting TERRA stabilization, localization and function<sup>336,339</sup>.

The subtelomeric chromatin environment regulates TERRA transcription. In budding yeast, TERRA transcription is limited by the Sir2/3/4 complex, which establishes heterochromatin at telomeres and represses TERRA transcription<sup>344</sup>. Additionally, TERRA levels are also regulated via RNA degradation, where the 5'-3' exonuclease Rat1 can degrade TERRA molecules, keeping TERRA levels low in the cell<sup>339</sup>. In *S. cerevisiae*, TERRA transcription is regulated by the telomere-binding proteins in a chromosome-end-specific manner that is dependent upon the subtelomeric X and Y' elements<sup>344</sup>. In more detail, at X-only telomeres, Rap1 dictates the regulation of TERRA transcription via Sir2/3/4 recruitment and TERRA degradation by promoting Rat1 nuclease activity<sup>344</sup>. While at Y' telomeres, Rap1 mediates repression of TERRA transcription through recruitment of Rif1-Rif2<sup>344</sup>. TERRA levels are regulated throughout the cell cycle and by telomere length in humans and budding yeast<sup>236,343</sup>. In human cells, TERRA accumulates at the G1/S phase transition and progressively decreases its levels during the S and G2 phases<sup>343</sup>. In budding yeast, the peak TERRA levels occur in early S phase, when TERRA is transcribed, decreasing as cells progress through S phase<sup>236</sup>. Indeed, the decrease in TERRA levels in late S phase is linked to Rat1 localization at telomeres<sup>236</sup>, where this regulation might facilitate telomere replication, since TERRA accumulation can cause replication fork stalling at telomeres<sup>181,236</sup>. Furthermore, when telomeres become critically short, in the absence of telomerase, there is accumulation of TERRA transcripts<sup>237,344</sup>. Importantly, there is loss of Rat1 binding to chromosome ends, which results in loss of the TERRA cell-cycle regulation, therefore leading to increased TERRA levels<sup>236</sup>. In budding yeast, transcription upregulation is not the cause of TERRA accumulation<sup>236</sup>, hence the increase of TERRA levels at short telomeres is due to loss of TERRA degradation. The accumulation of TERRA levels upon telomere shortening, likely promotes telomere elongation through telomerase recruitment or by promoting homology-directed repair (HDR)<sup>236,237,337</sup>. Furthermore, elevated TERRA levels can also be observed in post-senescent yeast survivors and ALT cancer cell lines<sup>298,300,301</sup>.



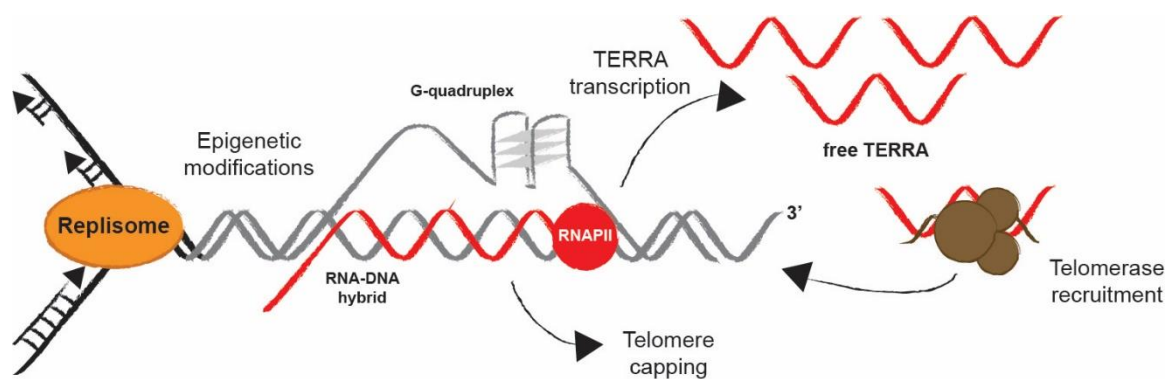


**Figure 8. The telomeric transcript TERRA and its functions.**

TERRA (red lines) can bind to the telomerase RNA component and block telomerase binding to telomeric ssDNA. In budding yeast, the telomerase RNA-TERRA clusters are localised at short telomeres to coordinate telomerase recruitment and activity. TERRA is implicated in chromosome-end protection by assembling secondary protective structures including R-loops and G-quadruplexes. Regulation of telomeres by TERRA can induce either telomere shortening by telomerase activity inhibition, or telomere elongation by promoting homologous recombination. TERRA remodels chromatin structure by recruit of different factors that contribute to epigenetic modifications at telomeres, and eventually affect telomere replication. Figure and Legend adapted from Kroupa et al 2022.

### 1.1.6.2 TERRA LOCALISATION

TERRA localises to the nucleoplasm and associates to chromosome ends<sup>338,339,343,345</sup>. In *S. cerevisiae*, TERRA derived from a single short telomere has been shown to move away from the telomere of origin and form a perinuclear focus, which acts as a scaffold for telomerase assembly in S phase, and returning preferentially to the telomere of origin<sup>237</sup>. In addition, TERRA can serve as a scaffold to recruit different nuclear factors responsible for telomere integrity<sup>327,343,346</sup>. Localisation of telomere transcripts may also be affected by damage, for e.g. TERRA relocates to the nuclear periphery and cytoplasm during diauxic shift due to an increase in oxidative stress<sup>347</sup>.

Moreover, by annealing to its template DNA, telomeric transcripts can form a three-stranded RNA-DNA hybrid structure, termed R-loop<sup>345,348,349</sup>. Telomere associated TERRA binds to the C-rich telomeric strand, therefore displacing the G-rich telomeric strand<sup>345,348</sup>. TERRA R-loop formation was proposed to primarily occur in a co-transcriptional manner<sup>350</sup>. However, recent evidence has also suggested a *trans* mechanism for TERRA R-loop formation after transcription<sup>351,352</sup>. R-loops can be a source of replication stress, since they impose barriers for the replication fork, ultimately causing genome instability and telomere loss<sup>334,353,354</sup>. Therefore, to preserve telomere integrity and prevent detrimental outcomes of R-loop deregulation, R-loops are tightly regulated by numerous mechanisms.

## 1.2 RNA-DNA HYBRIDS

RNA-DNA hybrids are generated during transcription, DNA replication and DNA repair, due to base pairing of RNA with DNA. They are crucial intermediates in these processes and, therefore, require a tight regulation concerning their formation, localization, and removal (Figure 9). RNA-DNA hybrids can arise from ribonucleotide (rNTP) incorporation into a DNA backbone during DNA replication<sup>355–357</sup>, generating a DNA backbone with intercalated rNMPs. Ribonucleotide mis-insertion is one of the most frequently occurring errors during DNA synthesis<sup>357–359</sup>, and if left unrepaired, DNA-embedded ribonucleotides ultimately lead to genome instability<sup>360,361</sup>. During replication there is also the formation of RNA-DNA hybrids, since RNA primers are required in particular for lagging strand replication<sup>362</sup>. Another form of RNA-DNA hybrids occurs when RNA molecules base pair with DNA strands. When stably formed in double-stranded DNA (dsDNA), there is displacement of one of the DNA strands, originating a three-stranded structure termed an R-loop<sup>353,363–365</sup>. R-loops are present throughout the genome and display important regulatory functions for gene expression, chromatin structure, and repair, however, when misregulated they pose a threat to genomic stability<sup>366–368</sup>. If R-loop regulation goes awry, there is accumulation of pathological R-loops, which contribute to several diseases, for instance neurodegeneration and cancer (Figure 9). Therefore, cells have evolved several mechanisms to regulate R-loop levels and consequently preserve genome integrity.

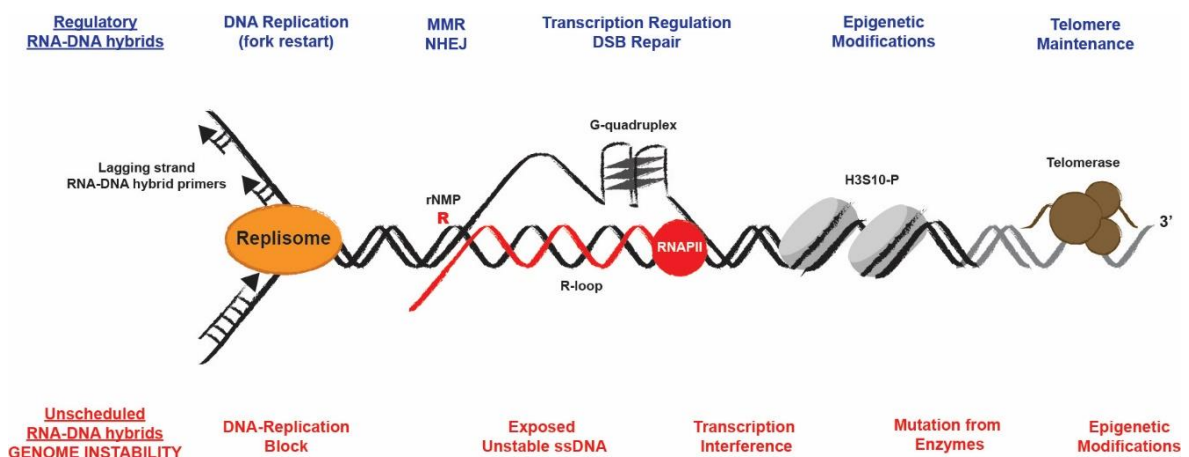


**Figure 9. Functional RNA-DNA hybrids and its impact on the genome.**

RNA has the capacity to localise to genomic regions in a sequence-specific manner and regulate downstream cellular processes. RNA-DNA hybrids, in particular R-loops are tightly regulated to prevent genome instability. R-loop formation is boosted by defects in RNA processing factors that coat, splice, export and degrade the nascent RNA, while R-loop resolution is promoted by nucleases and helicases, which degrade or unwind the RNA molecule, respectively. When unscheduled R-loops arise, they can interfere in transcription, cause replication stress and fork collapse, ultimately causing genome instability (red). Nonetheless, when scheduled, R-loops can positively contribute in transcription regulation, cause chromatin modifications and contribute to DSB repair efficiency (blue).

Grey lines denote telomeric sequences. Figure and Legend adapted from Costantino and Koshland 2015 and Niehrs and Luke 2020.

### 1.2.1 R-LOOP FORMATION

R-loops are three-stranded nucleic acid structures containing an RNA-DNA hybrid, that can be generated when an RNA transcript anneals co- or post-transcriptionally, i.e. in *cis* or *trans*, to its template DNA strand, causing displacement of the opposing DNA strand<sup>351,369–372</sup>. Moreover, R-loops do not form solely behind the RNA polymerase when the nascent RNA invades the duplex DNA but can also form anterior to the RNA polymerase during polymerase backtracking<sup>373</sup>. Co-transcriptional R-loops can form through an “extended hybrid model”, where the transcribed RNA remains annealed to its DNA template due to the high stability of the RNA-DNA interaction<sup>374</sup>, and the RNA polymerase extends the R-loop as it transcribes the DNA template. Alternatively, co-transcriptional R-loops can form through a “thread back model”, where the nascent transcripts denature shortly from the DNA template re-associating at a later stage before reannealing of the two DNA strands occurs<sup>375</sup>. Indeed, the transcribing RNA polymerases generate negative supercoils in the DNA behind them<sup>376</sup>, which facilitates dsDNA unwinding, and allows RNA invasion and the formation of an RNA-DNA hybrid. Post-transcriptional R-loops have been shown to form in a process mediated by the recombination protein Rad51<sup>351,372</sup>. RNA-DNA hybrids have thermodynamically more stability than dsDNA, in particular when presented with a high GC composition<sup>374</sup>. Indeed, R-loop formation is favoured by certain DNA characteristics, as for instance a high GC skew, meaning an asymmetric distribution of guanines (G) and cytosines (C)<sup>377</sup>. G-clustering promotes R-loop formation and the subsequent G-rich sequences on the template strand facilitate R-loop elongation<sup>377</sup>. The distance from G-rich sequences to promoter region may also determine R-loop formation efficiency, since G-rich sequences located further from promoters decrease R-loop formation<sup>378</sup>. Additionally, the presence of nicks in the non-template DNA strand<sup>378</sup> as well as the propensity of the displaced ssDNA strand to form G-quadruplex structures<sup>379</sup> are DNA characteristics favourable to R-loop formation. Finally, the negative DNA supercoiling behind the transcription machinery can also promote R-loop formation, as it may transiently facilitate RNA association to the open transcribed DNA<sup>378</sup>. R-loops can be found in different regions of the genome, nonetheless hotspots for R-loop accumulation have been identified at different loci, namely rDNA, telomeres, Ty transposons, tRNA genes and highly Pol II transcribed genes<sup>364,380,381</sup>.

## 1.2.2 R-LOOP FUNCTION

RNA-DNA hybrids and R-loops are generated during transcription, DNA replication and DNA repair, where they are crucial intermediates in these biological processes<sup>366–368</sup>. They can be found in different regions in the genome, including telomeres, centromeres, and non-coding RNAs (ncRNAs), exerting positive physiological roles<sup>366–368</sup>. However, formation of unscheduled R-loops, poses a threat to genome stability, since R-loops can cause transcription-replication conflicts and replication stress<sup>353,368</sup>.

DNA replication is aided by RNA-DNA hybrids, termed Okazaki fragments, which provide 3'OH substrate to DNA polymerases that are incapable of *de novo* DNA synthesis, thus facilitating lagging strand DNA replication<sup>80</sup>. R-loops also coordinate the replication initiation of bacterial, viral and mitochondrial DNA<sup>382–385</sup>, implicating R-loop regulation in circular DNA replication. Gene expression is also R-loop-coordinated through different mechanisms, including epigenetic regulation<sup>386–388</sup>. Active mammalian promoters present a strong GC skew, and R-loop formation capabilities, which prevent DNMT3B1-mediated promoter methylation maintaining these loci transcriptionally active<sup>389</sup>. R-loops can also recruit GADD45 and TET1 to specific loci, and promote DNA demethylation<sup>390</sup>. R-loops can also coordinate gene expression through histone modifications, triggering chromatin condensation, in particular, the H3S10-phosphorylation (H3S10-P) is an R-loop associated mark responsible for chromatin condensation<sup>387</sup>. At transcription termination sites, there is heterochromatin formation and R-loop accumulation, which may facilitate transcription termination by pausing RNA Pol II<sup>197,363,386,391</sup>. Indeed, in mammalian cells, Senataxin-mediated R-loop resolution promotes recruitment of the 5'-3' exoribonuclease Xrn2 and allows for termination of transcription<sup>386</sup>. Additionally, RNA Pol II pausing due to R-loops may allow for recruitment of the exonuclease Rat1, thus promoting efficient transcription termination<sup>197</sup>. Other examples of R-loop-mediated gene expression involve the floral repressor gene *FLC* in *A. thaliana*<sup>392</sup>, immunoglobulin class switch recombination (CSR) in activated B-cells<sup>375</sup>, and cellular differentiation by R-loop-mediated recruitment of chromatin remodelers and influencing pluripotency factors<sup>393</sup>.

R-loop formation has also been found to be required for efficient DSB repair, by facilitating the recruitment of repair factors and mediating DNA repair<sup>76,394–398</sup>. In fission yeast, R-loops can have a role in regulation of resection and RPA accumulation, indicating that R-loop formation as well as its timely resolution are critical to accomplish efficient DSB repair<sup>76</sup>. In human cells, RNA-DNA hybrid accumulation at DSB sites may derive from *de novo* transcription after DSB resection and Drosha-mediated processing<sup>395,399</sup>. Impairment of RNA-DNA hybrid formation at DSBs impairs the recruitment of repair factors, thus the

importance of the hybrids in this process is clear nonetheless the mechanism through which RNA-DNA hybrids promote DNA repair remains elusive, and it may depend on the type of DNA damage. Indeed, RNA-DNA hybrid accumulation at DSB sites has been linked to promotion of different types of repair, including NHEJ and HR in human cells<sup>399–404</sup>, and it was suggested that RNA-DNA hybrids might even play a role in pathway choice<sup>368,405</sup>. Nevertheless, RNA-DNA hybrids at DSBs must be tightly regulated to ensure efficient repair, since the accumulation of unscheduled hybrids interferes with repair and results in genomic instability<sup>76,398,400,406,407</sup>. In human cells, the regulation of RNA-DNA hybrids at DSBs has been linked to the recruitment and activity of RNase H2<sup>395</sup>, DDX1<sup>406</sup>, Senataxin<sup>400</sup> or XPG<sup>405</sup>.

Apart from their regulatory functions in gene regulation, telomere stability and DNA repair, when unscheduled R-loops are associated with DNA damage, transcription elongation defects, hyper-recombination and genome instability<sup>198,366–368</sup>. Genome instability due to aberrant R-loop accumulation can occur in multiple ways. Firstly, the exposed ssDNA strand, generated upon the formation of an R-loop, is chemically unstable, susceptible to damaging agents, mutagenic events, and may be targeted by specific enzymes that introduce DNA modifications or generate ssDNA breaks<sup>353,363,408,409</sup>. R-loops can also be targeted by the replication-coupled nucleotide excision repair (NER) machinery, resulting in DSB formation<sup>410</sup>. Additionally, R-loops may generate single-stranded breaks due to Top1 cleavage<sup>411</sup> or through RPA-mediated processing<sup>409</sup>. Moreover, in recent years, R-loop-induced genome instability has increasingly been linked to the replication process<sup>366</sup>, where R-loop accumulation may be the underlying cause of DSBs due to transcription-replication conflicts<sup>353,363,366,409,412</sup>. Replication through nicked DNA or a transcription-replication collision can lead to the generation of DSBs, and consequently compromise genome integrity<sup>353,363,366,409</sup>. R-loops may be a physical obstacle for replication fork progression<sup>354,413</sup>, where fork stalling can cause a DSB<sup>366,409,414</sup>. However, the orientation of the collision appears to influence the DNA repair response, with co-directional collision being less severe and may resolve R-loop structures at the collision site, while head-on collisions are more severe and lead to R-loop accumulation at the site of collision<sup>366,415</sup>. Co-directional collisions may resolve the R-loop through displacement of the transcription machinery by the replisome and its associated helicases, thus displacing the R-loop, however they can still activate the DNA damage response via ATM, which is indicative of DSBs<sup>415</sup>. At telomeres, transcription-replication conflicts occur in a co-directional orientation, furthermore there is the potential to over-stabilize telomeric R-loops through the association of certain RNA-binding proteins that could lead to a co-directional collision<sup>416</sup>. Consequently, telomeric R-loops may be a source of genome instability, their tight

regulation as well as the regulation of the telomeric R-loop regulatory proteins may determine the context of replication stress and genome instability, in a mechanism perhaps dependent on telomere-length and maintenance. Overall, accumulation of RNA-DNA hybrids and R-loops at different genomic loci may result in distinct DNA damage responses. Finally, the chromatin context associated to R-loops may also play a role in genome instability, since the chromatin mark H3S10-P is associated to R-loop-mediated genome instability, it is also possible that not the R-loop *per se* is the source of genome instability but rather the chromatin condensation environment can lead to increased conflicts<sup>371,387,417–420</sup>. Therefore, understanding R-loop regulation is of extreme importance, as misregulated R-loops can be a significant source of genome instability in cancer cells and other pathologies. In particular, telomeric R-loop misregulation may lead to replication stress and telomere dysfunction in an R-loop-dependent manner<sup>421–425</sup>.

### 1.2.3 R-LOOP REGULATION

R-loops are dynamic structures that can be controlled at many levels, namely their formation and resolution (Figure 10), where multiple factors and pathways are involved in this regulation<sup>412,426–429</sup> (Figure 10). Among R-loop formation inhibitors, topoisomerases can prevent RNA invasion of the duplex DNA by releasing the torsional stress generated after the transcription or replication machinery<sup>365,430–432</sup>. In budding yeast, Top1 and Top2 inactivation leads to R-loop accumulation at ribosomal DNA (rDNA) loci, causing RNA Pol I stalling and defective pre-rRNA synthesis<sup>430</sup>. In human cells, TOP1 defects lead to DNA breakage at highly transcribed genes<sup>414</sup>, and TOP3B can counteract R-loop formation consequently suppressing chromosomal translocations<sup>433</sup>. Similarly, proteins involved in RNA processing and export machinery allow for suppression of RNA-DNA hybrid formation by sequestering the nascent RNA from its template, promoting chromatin compaction, and/or RNA export from the nucleus<sup>353,420</sup>. In budding yeast, the inactivation of certain transcription factors and RNA binding proteins (RBPs), for instance heterogeneous nuclear ribonucleoproteins (hnRNPs) or splicing factors, have been associated to increase R-loop levels<sup>434–436</sup>. The sequestering of the nascent RNA is possible by targeting the RBPs to the nuclear pores, since increased physical distance from the nuclear pore increases R-loop levels, likely due to transcript accumulation in the nucleoplasm where it can reanneal to its template DNA<sup>437</sup>. Likewise, splicing factors can also prevent unscheduled R-loop formation, as for instance in vertebrates, where the splicing factor ASF/SRSF1 regulates R-loop levels<sup>438</sup>. Moreover, other RNA regulatory proteins have been implicated to contribute in R-loop regulation at different stages of transcription<sup>365,371</sup>. In particular, in both yeast and

humans, the THO/TREX complex has been well characterized in its role to prevent R-loop formation<sup>434,439–441</sup>. In addition, chromatin modifiers can also play a role in preventing R-loop formation, as an example loss of ARID1A, the core DNA-binding subunit of the BAF chromatin remodelling complex, leads to DNA replication stress associated with R-loops and transcription-replication conflict, associated with reduced TOP2A binding at R-loop sites<sup>442</sup>. Finally, modifications on the RNA strand of the hybrid by RNA methyltransferases, like METTL3 or TRDMT1, also helps regulate R-loop formation<sup>443–445</sup>.

Once formed, cells have several proteins and pathways to resolve or degrade R-loops. In the degradation front, the RNase H family of nucleases, comprising RNase H1 and RNase H2, selectively degrade the RNA moiety of an RNA-DNA hybrid<sup>446,447</sup>. RNase H1 is a highly conserved monomeric protein<sup>447–449</sup>, possessing in its N-terminus a hybrid binding domain (HBD), which binds to RNA-DNA hybrids with a higher preference over dsRNA<sup>450</sup>. The central region of RNase H1 is less conserved among eukaryotes, with this domain possibly providing a flexible linker between the N- and C-terminal regions, to facilitate activity on their substrates<sup>447,449</sup>. The C-terminal domain of RNase H1 contains the RNase H domain, which cleaves the RNA-DNA hybrid<sup>449</sup>. In fact, RNase H1 only recognizes and degrades RNA-DNA hybrids that contain at least a stretch of four consecutive ribonucleotides<sup>447,449,450</sup>. RNase H1 is, therefore, a specialized enzyme that hydrolyses “long” RNA-DNA hybrids to preserve genome integrity, preventing accumulation of toxic R-loops and mediating certain biological processes<sup>365,447</sup>. In particular, RNase H1 has roles in mitochondrial DNA replication, since RNase H1 inactivation impairs embryo development due to the incapacity to amplify mitochondrial DNA<sup>451</sup>, thus being an essential gene in higher eukaryotes. In *S. cerevisiae*, RNase H1 is not essential, and it is not required for mitochondrial DNA replication<sup>195</sup>. A possibility for RNase H1 recruitment to R-loop sites is due to its interaction with RPA, which binds the displaced strand of the R-loop, whereby RPA can potentially recruit RNase H1 to R-loops hence promoting its activity<sup>452</sup>. RNase H1 is also important for efficient DSB repair, since stabilization of R-loops at DNA breaks impairs DNA repair<sup>76,395,400</sup>.





attached to the newly synthesized DNA strand, to promote successful replication, nevertheless it still requires further processing by Rad27/Fen1<sup>457,459</sup>. Another reason why RNase H2 provides the majority of RNase H activity in yeast cells might be due to its cell cycle regulation, since RNase H2 has an essential function in G2/M for its activity while RNase H1 function is cell cycle independent, but occurs in response to damage<sup>464</sup>. Moreover, it might be the case that RNase H1 activity is restricted to specific loci, while RNase H2 may have a more general activity<sup>363,462</sup>. Finally, there is formation of different types of R-loops in the cell<sup>465</sup>, however it is still not understood how their regulation happens and which R-loop resolving pathways are involved in each pathway. In humans, RNase H2 mutations lead to the severe childhood inflammatory disorder Aicardi-Goutières syndrome (AGS), which results in neurological dysfunction and psychomotor retardation<sup>453</sup>. Moreover, RNase H2 activity impairment results in R-loop accumulation at a subset of genes, in a RNA Pol II transcription-dependent manner that leads to DNA damage and the activation of the immune response, demonstrating a mechanistic contribution of R-loops to AGS pathogenesis<sup>466,467</sup>. On another topic, RNase H activity is also important to regulate telomeric R-loops, in particular RNase H1 appears to be important in human ALT to sustain HR and promote telomere integrity<sup>348</sup>. In budding yeast, RNase H2 is recruited to long telomeres to keep R-loop levels in check, while its association decreases with telomere shortening, allowing for R-loop accumulation and promoting HR<sup>236</sup>. Thus revealing an important role for RNase H activity in telomere length regulation and cell viability.

In Archaea and bacteria, an additional RNase H can be found – RNase H3, which is closely related to H2 in sequence and structure, however has RNase H1-like biochemical properties<sup>449,468</sup>. Overall, in *S. cerevisiae*, loss of RNase H activity sensitizes cells to low doses of replication stress<sup>469</sup>. Indeed, RNase H2 loss is associated with increased genome instability, but not RNase H1 loss, due to R-loop accumulation<sup>462</sup>. However, combined loss of the RNase H enzymes leads to a synergistic increase of recombination rates, suggesting that there is some redundancy in RNase H1 and RNase H2 activities<sup>470</sup>. Interestingly, there are evidences that these two enzymes act at different loci in the genome, since *RNH1* overexpression cannot rescue the R-loop dependent sick phenotype observed in *rnh201 sgs1* mutants, where HR is impaired<sup>471</sup>. Suggesting that in this background, RNase H1 does not have access or cannot act on these fraction of R-loops that are normally regulated by RNase H2<sup>471</sup>.

To promote R-loop resolution, unwinding of the R-loop RNA component can be achieved with specialized helicases. One of the preferred helicases for R-loop resolution is the 5'-3' helicase Senataxin, encoded by the gene SETX in humans<sup>386</sup>. Senataxin resolves R-loop at transcription termination sites<sup>386,472</sup>, and DSBs<sup>400</sup> by unwinding R-loops. Senataxin

dysfunction leads to pathologies, in particular, Ataxia-ocular apraxia 2 (AOA2)<sup>473</sup>, demonstrating the relevance of regulating R-loop levels in human cells. In budding yeast, the Senataxin orthologue Sen1 regulates R-loops and prevents transcription-replication conflicts<sup>197</sup>. Moreover, Sen1 associates with the replisome, indicating a role in fork protection upon R-loop encounters<sup>474,475</sup>, with Sen1 being an S-phase-specific R-loop resolvase<sup>476</sup>. Furthermore, other replisome-associated helicases may facilitate replication progression through an R-loop region, particularly if the R-loop encounter is present on the leading strand<sup>409,415</sup>. The G4-unwinding helicases Pif1 and Rrm3 also play an important role in resolving R-loops, in particular at centromeres and telomeres<sup>477,478</sup>. Finally, Dead-box helicases can also mediate R-loop resolution. In mammalian cells, DDX1, DDX5, DDX19, DDX21, DDX23, DDX39 and DDX41 resolve R-loops and promote genome stability<sup>479–486</sup>. In particular, the dead-box helicase DDX39 plays a role in genome integrity and telomere protection<sup>487</sup>, indicating a possible role for this helicase in telomeric R-loop regulation.

Importantly, impairment of most of these R-loop restricting pathways leads to R-loop accumulation, indicating that most of these factors have access and specificity, in a spatial and temporal context, to a unique subset of R-loop substrates, thus not being completely redundant. The many factors implicated in R-loop formation and resolution (Figure 10), thus suggest that the cell needs to dynamically balance these processes.

## 1.2.4 TELOMERIC R-LOOPS

The chromosome ends by containing GC-rich sequences and a high ability for forming G4s<sup>377,379</sup>, are extremely prone to R-loop formation and accumulation<sup>345,349,350</sup>. Telomeric R-loops have been shown to play important regulatory roles in telomere maintenance and integrity<sup>348,488</sup>. To prevent detrimental outcomes of R-loop misregulation, there is a tight regulation of telomeric R-loops by several mechanisms. R-loops can be detected by the S9.6 antibody, which specifically recognizes RNA-DNA hybrids with a size of at least 6-8 bp<sup>489</sup>, and indeed, R-loops have been identified at telomeres in both yeast and human cells<sup>345,348,490–492</sup>. Telomeric R-loops can form in *cis* or *trans*<sup>328,331,350,351,493</sup>, and in yeast are correlated with telomere length and the cell cycle phase<sup>236,345</sup>. Telomeric R-loops become especially relevant in telomerase negative pre-senescent cells, where they are responsible for promoting homologous recombination to counteract telomere shortening, thus delaying replicative senescence onset<sup>285,345</sup>. At long telomeres, telomeric R-loop levels are low, potentially to prevent transcription-replication conflicts and telomere shortening<sup>236,416,436,490</sup>.

In the absence of telomerase, with telomere shortening there is accumulation of R-loops at short telomeres, which promote HDR-mediated repair and allow for telomere re-elongation<sup>236,345</sup>. In budding yeast, telomeric R-loops are regulated by the RNase H nucleases, RNase H1 and H2, and the THO-TREX complex<sup>195,345,490</sup>. At long telomeres, RNase H2 is recruited, through a Rif2-mediated mechanism, to degrade telomeric R-loops<sup>236</sup>. In the absence of telomerase, telomeric R-loops accumulate at the shortest telomere due to decrease RNase H2 recruitment<sup>236</sup>. This telomeric R-loop accumulation promotes HDR-mediated telomere maintenance, in telomerase negative cells<sup>236,345</sup>. Additionally, yeast hnRNP-like proteins cooperate to prevent unscheduled R-loop formation<sup>416,490,492,494</sup>, an example is the hnRNP-like protein Npl3 which associates to TERRA and telomeres, in an R-loop dependent manner, promoting HDR and preventing premature senescence onset<sup>495</sup>. Interestingly, telomeric R-loop accumulation influences the survivor pathway choice, preferentially generating type II survivors in an R-loop-dependent manner<sup>492</sup>. However, how mechanistically R-loops promote recombination at telomeres remains unknown, with the hypothesis that induction of R-loop-dependent replication stress at telomeres might be the cause for increase recombination<sup>236,302,345</sup>, since replication stress can trigger HDR<sup>302,409,496</sup>. It is possible that telomeric R-loops generate transcription-replication conflicts that trigger HR, and consequently R-loop-mediated telomere maintenance may thus regulate replicative senescence rate and yeast survivor formation<sup>236,298,299,492,497</sup>. The accumulation of R-loops at short telomeres may also require processing to prevent excessive replication stress and impaired recombination. Indeed, persistent telomeric R-loops are detrimental for HDR-mediated telomere maintenance, leading to accelerated senescence rates and impairing type II survivor formation<sup>416,495</sup>. Moreover, Sgs1 inactivation, in the absence of telomerase, leads to an accelerated senescence phenotype<sup>498</sup>, indicating that R-loop accumulation may interfere with recombination through formation of toxic intermediates. Therefore, several regulatory factors are in place to prevent R-loop associated replication stress and regulate senescence rate, as for instance the Mph1 helicase<sup>499,500</sup>. The Pif1 helicase has also been implicated in telomere length maintenance, however not through a mechanism associated with R-loops but by regulating telomerase activity<sup>266,478,501</sup>.

In human cells, TERRA has also been implicated in telomere maintenance in telomerase negative ALT cancer cells through the formation of recombinogenic R-loops at telomeres<sup>348,422,502–504</sup>. Telomeric R-loops have also been proposed to increase replication stress in mammalian cells, mainly through the generation of a DSB at telomeres and initiation of telomere recombination through the HR pathways of break-induced replication or MiDAS<sup>505–507</sup>. To regulate telomeric R-loops, there is accumulation of RNase H1 at



### 1.3 RATIONALE

RNA-DNA hybrids and R-loops are generated during transcription, DNA replication and DNA repair, where they are crucial intermediates in these biological processes, thus requiring a tight regulation concerning their formation, localization, and removal. However, when misregulated, the accumulation of pathological hybrids leads to genome instability, underlying several diseases, as for instance cancer and neurodegeneration. The growing evidence of the involvement of RNA-DNA hybrids in DSB repair efficiency, implicates these structures in recruitment of DSB repair factors to the break site, as well as RNA-DNA hybrid resolution factors<sup>76,395,400,405,406</sup>. Therefore proposing that, even though there is accumulation of hybrids at the DSB site, for completion of repair the RNA-DNA hybrids must be removed<sup>76</sup>. It appears that the type of repair and resolution factors recruited might be influenced by the location and type of damage. At chromosome ends, telomeric R-loops are an essential intermediate for telomere maintenance in ALT cancer cells and telomerase negative *S. cerevisiae* cells, by promoting homologous recombination leading to telomere elongation, and sustained cell viability<sup>345,348,492</sup>. Understanding how RNA-DNA hybrids are regulated at telomeres, which pathway of R-loop removal is involved, and how HR is promoted is of fundamental biological importance to dissect the molecular mechanisms of ALT telomere maintenance. The recapitulation of human ALT phenotypes in budding yeast<sup>298,299</sup>, has proved that *S. cerevisiae* is an excellent model for the study of replicative senescence and telomere maintenance in telomerase negative cells. The work in this thesis aims to gain a deeper understanding of RNA-DNA hybrid regulation at *S. cerevisiae* telomeres. In particular, to contribute to the understanding of how telomeric RNA-DNA hybrids affect end resection at dysfunctional telomeres, and during replicative senescence. The regulation of RNA-DNA hybrids by the RNase H enzymes and Sen1, was the focus of this thesis, due to their involvement in DNA damage repair processes<sup>76,400,511</sup>, and the synthetic lethality of the simultaneous impairment of this pathways, which indicates that they are the main RNA-DNA hybrid resolvases in budding yeast<sup>198,464</sup>.



## 2 RESULTS

---

### 2.1 RNA-DNA HYBRIDS PREVENT RESECTION AT DYSFUNCTIONAL TELOMERES

In the absence of telomerase, TERRA RNA-DNA hybrids become stabilized and drive homology-directed repair (HDR) at critically short telomeres, consequently delaying replicative senescence<sup>236,288,345,348,512,513</sup>. Nonetheless, during replicative senescence, transient TERRA RNA-DNA hybrids can form at long- and intermediate-length telomeres, which are not subject to HDR<sup>285</sup>. Interestingly, RNA-DNA hybrids can transiently form at double-stranded break (DSB) sites to promote HDR, but their subsequent removal is necessary to ensure efficient Rad51-mediated repair<sup>76,395,398</sup>. Hence, there is a well-established link between RNA-DNA hybrids and HDR at telomeres<sup>236,345,514</sup> and DSBs<sup>76,395,398</sup>. The aim of this section was to further understand how RNA-DNA hybrids might affect telomere maintenance. We employed a well-characterized telomere capping defective mutant, *cdc13-1* allele<sup>51</sup>, where telomere uncapping leads to unrestricted resection that can be induced in a temperature-dependent manner, to understand how ssDNA generation at telomeres may be impacted by RNA-DNA hybrids. The viability of *cdc13-1* cells was affected by the presence or absence of hybrids, i.e. we observed a rescue of *cdc13-1* phenotype when RNA-DNA hybrids became stable at telomeres (*rnh1 rnh201* mutants) or worsening of *cdc13-1* phenotype when RNA-DNA hybrids became destabilized (*RNH1* overexpression). We reported in Pires et al, 2023<sup>515</sup>, that hybrids prevent Exo1-mediated resection when telomeres become dysfunctional. Taken together, these results suggest that RNA-DNA hybrids mediate resection rates at dysfunctional telomeres, in addition to affecting replicative senescence rates through HDR activation.

#### 2.1.1 RNA-DNA Hybrids Prevent Telomere Dysfunction-Induced Cell Death

In budding yeast, genome-wide RNA-DNA hybrid removal occurs mainly through the RNase H nucleases, RNase H1 (Rnh1) and RNase H2 (Rnh201, Rnh202 and Rnh203 complex). Additionally, the Sen1 helicase, also contributes to RNA-DNA hybrid removal and genome stability maintenance<sup>197</sup>. The loss of these two RNA-DNA hybrid removal pathways leads to irreparable damage and cell death<sup>198</sup>. To assess how RNA-DNA hybrids affect telomere dysfunction, we either partially inactivated Sen1, with the *sen1-1* temperature

sensitive (*ts*) allele<sup>197</sup> (Figure 12A), or removed RNase H1 (*rnh1*) and RNase H2 (*rnh201*) function through deletion of the respective genes (Figure 12B), thus allowing for the accumulation of hybrids genome-wide. We observed that when RNA-DNA hybrids accumulate, irrespective of the genetic mutant employed (*sen1-1* or *rnh1 rnh201*), there was a partial rescue of the *cdc13-1* growth defect at semi-permissive temperatures (26°C) (Figures 12C and 12D). This observation indicates that hybrids protect telomeres from excessive resection. Moreover, only the complete ablation of RNase H activity (*rnh1 rnh201*) rescued the *cdc13-1* phenotype (Figure 12D), as deletion of the independent RNase H enzymes was not sufficient to improve growth. Indicating that both RNase H1 as RNase H2 alone have the potential to remove RNA-DNA hybrids at dysfunctional telomeres. Importantly, the partial removal of Sen1, through an auxin-inducible degron allele (*SEN1-AID\**), did not rescue the growth defects of *cdc13-1* cells (Figure 12E) despite the fact that Sen1-AID\* protein levels were strongly reduced at the concentration of auxin used (Figure 12F), potentially implying an indirect effect of the *sen1-1* allele for the *cdc13-1* rescue observed.

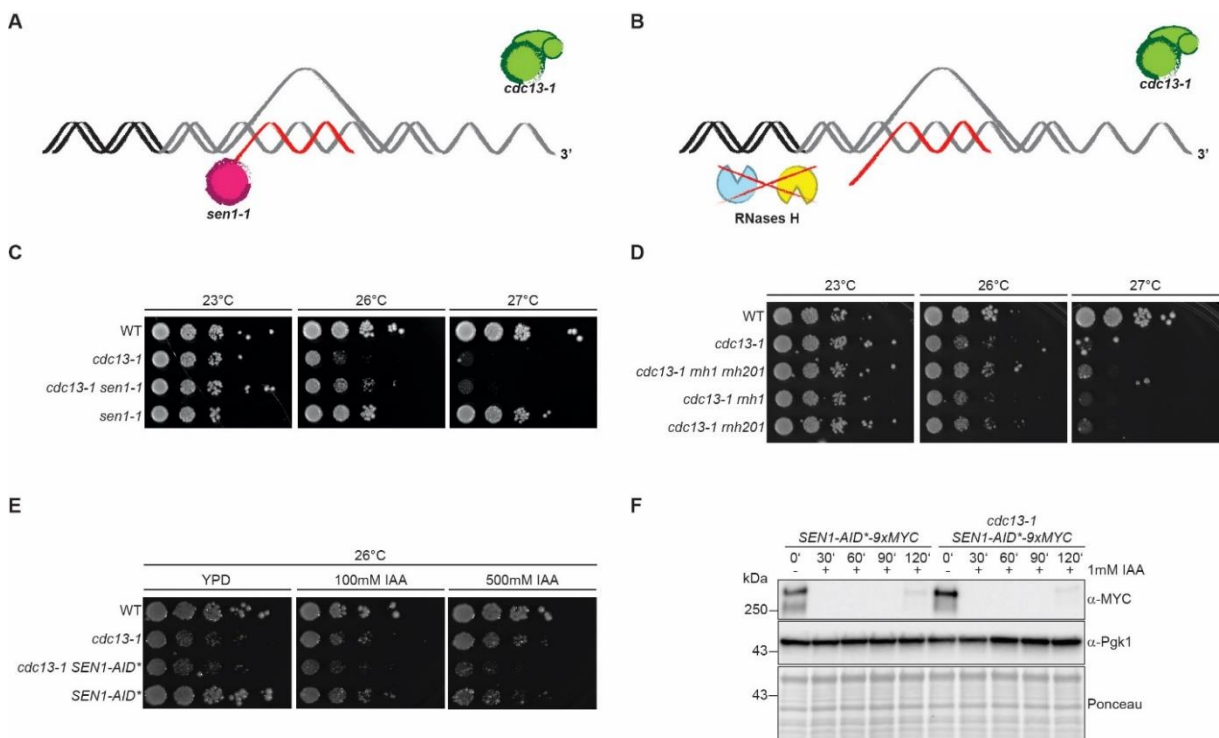


**Figure 12. RNA-DNA hybrids prevent telomere dysfunction-induced cell death.**

(A-B) Schematic representation of the genetic background for the experiments where RNA-DNA hybrids accumulate when Sen1 is inactivated (*sen1-1*; A) or the RNases H enzymes are deleted (*rnh1 rnh201*; B).

(C-D) 10-fold serial dilutions of the indicated strains were spotted onto YPD plates. Images were taken after 3 days growth at the indicated temperatures.

(E) 10-fold serial dilutions of the indicated strains were spotted onto YPD plates or with the indicated amount of auxin (IAA). Images were taken after 3 days growth at the indicated temperatures.

(F) Western blot analysis of the degron strains used in E. Exponentially growing cells were treated with 1mM IAA for 2h, 30min time-points were collected for protein extraction.



To confirm that RNA-DNA hybrids accumulate at telomeres in *cdc13-1* cells when RNase H or Sen1 activity was impaired, we quantified RNA-DNA hybrid levels using DNA-RNA immunoprecipitation (DRIP) with the S9.6 antibody<sup>197,516</sup>. We used the rDNA and the *SUF2* genes as control loci that are insensitive and highly sensitive to RNase H activity, respectively (Figure 13A). In a *cdc13-1* genetic background, RNA-DNA hybrids accumulated at telomeres in the absence of RNase H1/H2 at permissive temperature (23°C) (Figure 13A), consistent with our previous observations<sup>345</sup>. Interestingly, we do not detect an increase of RNA-DNA hybrid levels at telomeres in *rnh1 rnh201* mutants at 23°C, and again only a slight non-significant signal at 26°C (Figure 13A). However, when looking at a semi-permissive temperature (26°C), we only detect a slight, yet non-significant, increase in hybrid levels in *cdc13-1 rnh1 rnh201* when compared to *cdc13-1* cells (Figure 13A) at telomeres 1L and 15L. We speculate that the increased resection at 26°C may eliminate, to a certain extent, the DNA template where RNA-DNA hybrids can form. In addition, RNA-DNA hybrids are known to accumulate at telomeres in S-phase in WT cells at 30°C<sup>236</sup>, and we are detecting hybrid accumulation in exponential cells at lower temperatures.

No differences were detected in cell cycle distribution profiles at the permissive temperature of 23°C, or at the semi-permissive temperature of 26°C, in the presence or absence of RNase H1/H2 in the *cdc13-1* background (Figure 13B), setting aside the possibility that RNA-DNA hybrids are affecting cell cycle progression. Remarkably, in the *sen1-1* background, we did not detect increased RNA-DNA hybrids at telomeres via DRIP (Figure 13C). Nonetheless, since the inactivation of Sen1 occurs simultaneously with Cdc13 loss from telomeres, due to the presence of two temperature sensitive alleles, RNA-DNA hybrids may not be able to accumulate or even form at these loci before resection occurs. In terms of cell cycle distributions, we detect a G2-arrest for *cdc13-1* cells, independently of Sen1 status, after 2h at 30°C (Figure 13D). Considering the lack of rescue when using the degron system (Figure 12E) and the absence of RNA-DNA hybrids at telomeres detected by DRIP at 30°C (Figure 13C), these data suggest that the rescue of *cdc13-1* cells by the *sen1-1* mutant may be indirect.

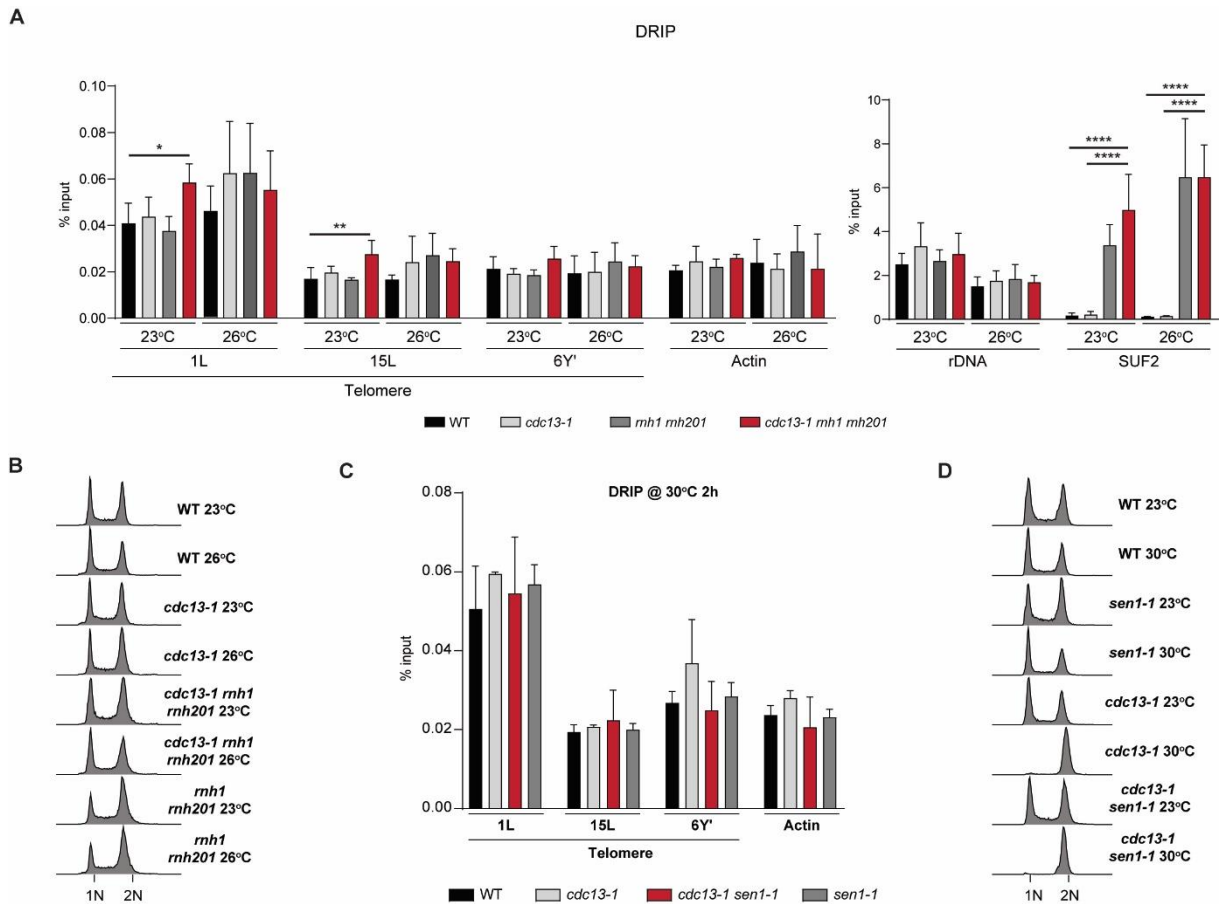


**Figure 13. RNA-DNA hybrids accumulate at telomeres in *cdc13-1* when RNases H are depleted.**

(A) DRIP. Chromatin immunoprecipitation with S9.6 antibody and qPCR analysis of the indicated strains at the indicated loci. Cells were grown at 23°C or shifted for 2h at 26°C until collection. Values are represented as %input of DNA recovered. Data are depicted as mean + SD,  $n = 3$ . p-values were obtained from One-Way ANOVA using the Tukey test to correct for multiple comparisons (\* $p < 0.05$ , \*\* $p < 0.01$ , \*\*\* $p < 0.001$ , \*\*\*\* $p < 0.0001$ ).

(B) DNA content analysis of depicted genotypes in exponentially growing cultures at 23°C or after a 2h shift to 26°C. 1N: DNA content, G1 phase; 2N: DNA content, G2/M phase. One representative histogram for each condition is shown.

(C) DRIP. Chromatin immunoprecipitation with S9.6 antibody and qPCR analysis of the indicated strains at the indicated loci. Cells were shifted to 30°C for 2h before collection. Values are represented as %input of DNA recovered. Data are depicted as mean + SEM,  $n = 3$ .

(D) DNA content analysis of depicted genotypes in exponentially growing cultures at 23°C or after a 2h shift to 30°C. 1N: DNA content, G1 phase; 2N: DNA content, G2/M phase. One representative histogram for each condition is shown.

Because RNA-DNA hybrid accumulation rescued the growth defects of the dysfunctional telomere mutant *cdc13-1*, we then wondered if the removal of hybrids might have the opposite effect and exacerbate the growth defects (Figure 14A). Indeed, we detected an increased growth defect when RNase H1 was overexpressed in *cdc13-1* cells at semi-permissive temperature (27°C) (Figure 14B). To understand if the phenotype observed in *cdc13-1 sen1-1* is RNA-DNA hybrid dependent, we overexpressed RNase H1 and observed the same growth defect present in *cdc13-1*, indicating that Sen1 has an

indirect effect at dysfunctional telomeres (Figure 14C). Nonetheless, we cannot completely discard a role for Sen1 regulating RNA-DNA hybrids at telomeres in other scenarios. No differences were detected in the cell cycle profiles of wild type nor *cdc13-1* cells when *RNH1* was overexpressed, at the permissive temperature of 23°C or semi-permissive temperature of 27°C (Figure 14D). The overexpression of *RNH1* reduced RNA-DNA hybrid levels detected by DRIP at telomeres, at the control 18s rDNA locus, in wild type and *cdc13-1* cells at permissive temperature (23°C), and at semi-permissive temperature (27°C) (Figure 14E). Together, these data suggest that RNA-DNA hybrid destabilize at telomeres when RNase H1 is overexpressed in the *cdc13-1* background.

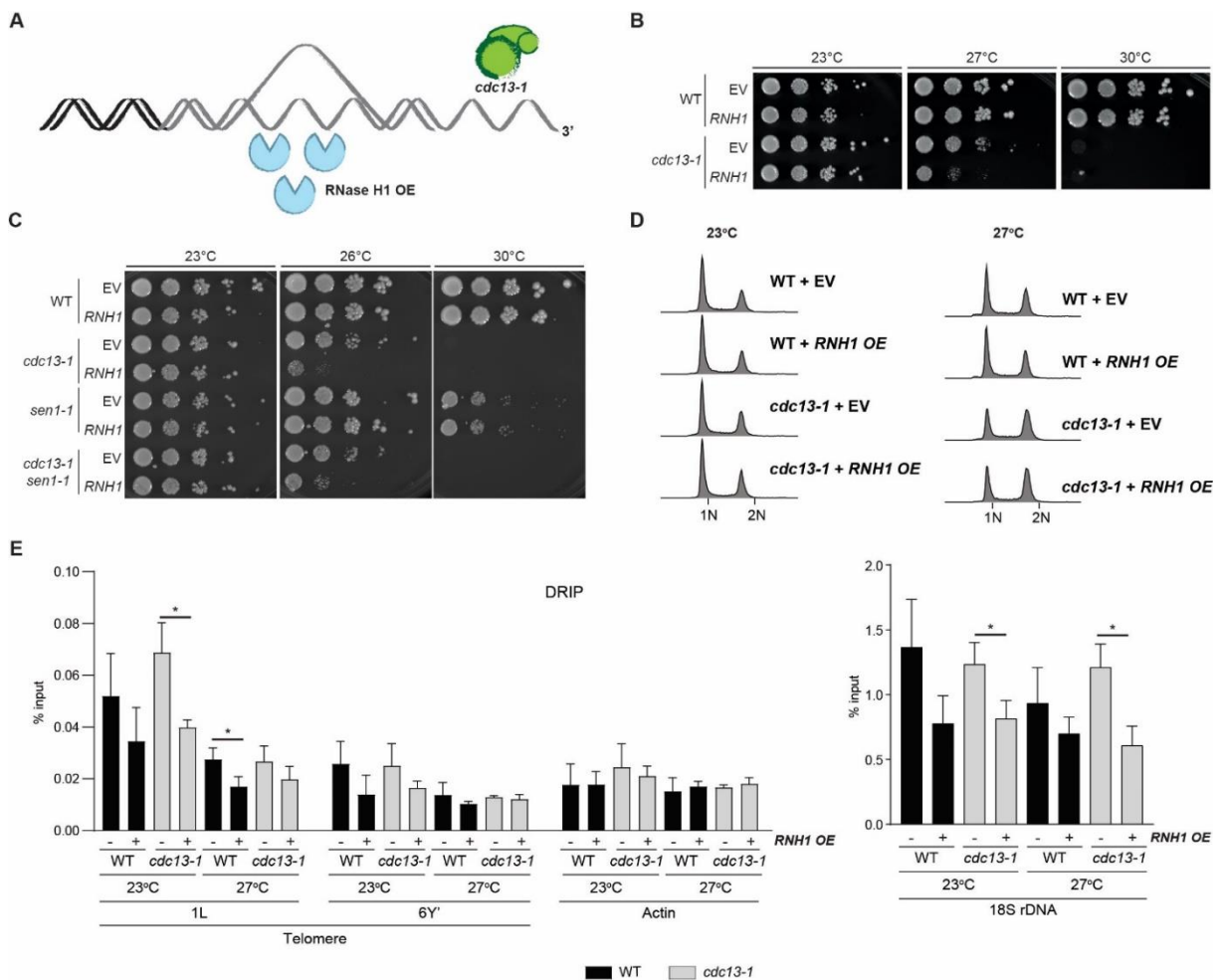


**Figure 14. RNA-DNA hybrids removal by RNase H1 overexpression exacerbates telomere dysfunction-induced cell death.**

(A) Schematic representation of the genetic background for the experiments where RNA-DNA hybrids are depleted by overexpression of RNase H1.

(B-C) 10-fold serial dilutions of the indicated strains transformed with the indicated plasmids were spotted onto SC-HIS (B) or SC-URA (C) plates. Images were taken after 3 days growth at the indicated temperatures.

(D) DNA content analysis of depicted genotypes in exponentially growing cultures at 23°C or after a 2h shift to 27°C. 1N: DNA content, G1 phase; 2N: DNA content, G2/M phase. One representative histogram for each condition is shown.

(E) DRIP. Chromatin immunoprecipitation with S9.6 antibody and qPCR analysis of the indicated strains at the indicated loci. Cells were grown at 23°C or shifted for 2h at 27°C until collection. Values

are represented as %input of DNA recovered. Data are depicted as mean + SD, n = 3. p-values were obtained from One-Way ANOVA using the Tukey test to correct for multiple comparisons (\*p < 0.05, \*\*p < 0.01, \*\*\*p < 0.001, \*\*\*\*p < 0.0001).

To get better insights regarding the link between RNA-DNA hybrids and resection at telomeres, we studied the dynamic of proliferation of cells by monitoring continuous cell growth, when RNA-DNA hybrid levels are altered at dysfunctional telomeres. We monitored the growth kinetics of strains that accumulated RNA-DNA hybrids (*rnh1 rnh201* and *sen1-1*) with hourly OD<sub>600</sub> measurements for 15 hours (Figures 15A and 15B, respectively), at semi-permissive temperatures (26°C-27°C) to allow the growth of the *cdc13-1* background. When looking at the doubling time of these mutants, we could not recapitulate the observed phenotypes in spotting assays either for the RNases H or Sen1 when impaired (Figures 15D and 15E). We do detect a decrease in doubling time when the RNases H enzymes are deleted, however this decrease is also observed in the single deletion mutants (Figure 15D). For *sen1-1*, we do not detect a decrease in doubling time in liquid culture at this temperature (Figure 15E). Upon *RNH1* overexpression, at the semi-permissive temperature of 27°C, we clearly detect an increase in doubling time as previously observed (FigureS 15C and 15F). However, we believe that due to the highly mutagenic nature of these mutants, the liquid culture assays would give fast growers/suppressing mutations a selective advantage. Hence, in this particular scenario, the spotting assays are more robust than the growth curves.

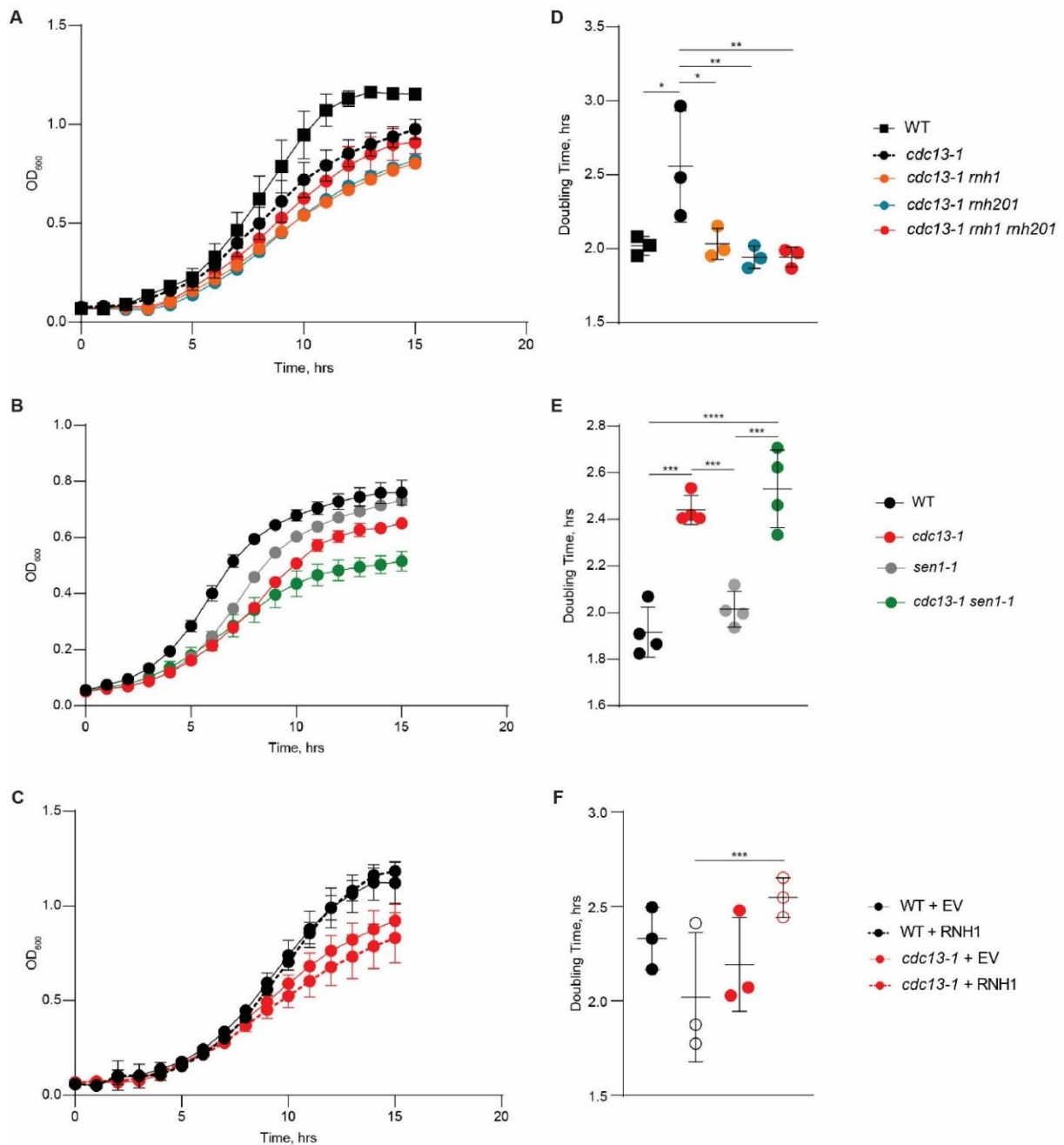


**Figure 15. Liquid growth assays do not reiterate spotting assays in *cdc13-1* when RNA-DNA hybrids are misregulated.**

(A-C) Kinetic growth analysis of the indicated strains. Cells were inoculated at 0.05 OD<sub>600</sub> in SC complete (A-B) or SC-HIS (C) and grown for 15 hours at 26°C (A), 26.5°C (B) and 27°C (C) in 96 well microtiter plates. OD<sub>600</sub> measurements were performed every hour. Mean values ± SD of 3 biological replicates are shown for each strain.

(D-F) Doubling time of the indicated genotypes, in hours (hrs). Data are depicted as mean + SD, n = 3. p-values were obtained from One-Way ANOVA using the Tukey test to correct for multiple comparisons (\*p < 0.05, \*\*p < 0.01, \*\*\*p < 0.001, \*\*\*\*p < 0.0001). WT, wild type; EV, empty vector.

We tested whether the rescue of *cdc13-1* cells through the deletion of the RNases H (*rnh1 rnh201*) was specific to telomere dysfunction, or if it was due to any temperature sensitive of the *rnh1 rnh201* deletion. We did not observe a growth improvement in either *cdc15-2* or *cdc7-4*, two temperature sensitive alleles not involved in telomere function, upon

loss of RNase H activity (*rnh1 rnh201*), suggesting that RNA-DNA hybrid accumulation is beneficial if it is only in the *cdc13-1* mutant (Figures 16A and 16B). The overexpression of *RNH1* does not reduce viability in *cdc15-2* mutants (Figure 16C), again indicating specificity for hybrids at dysfunctional telomeres.

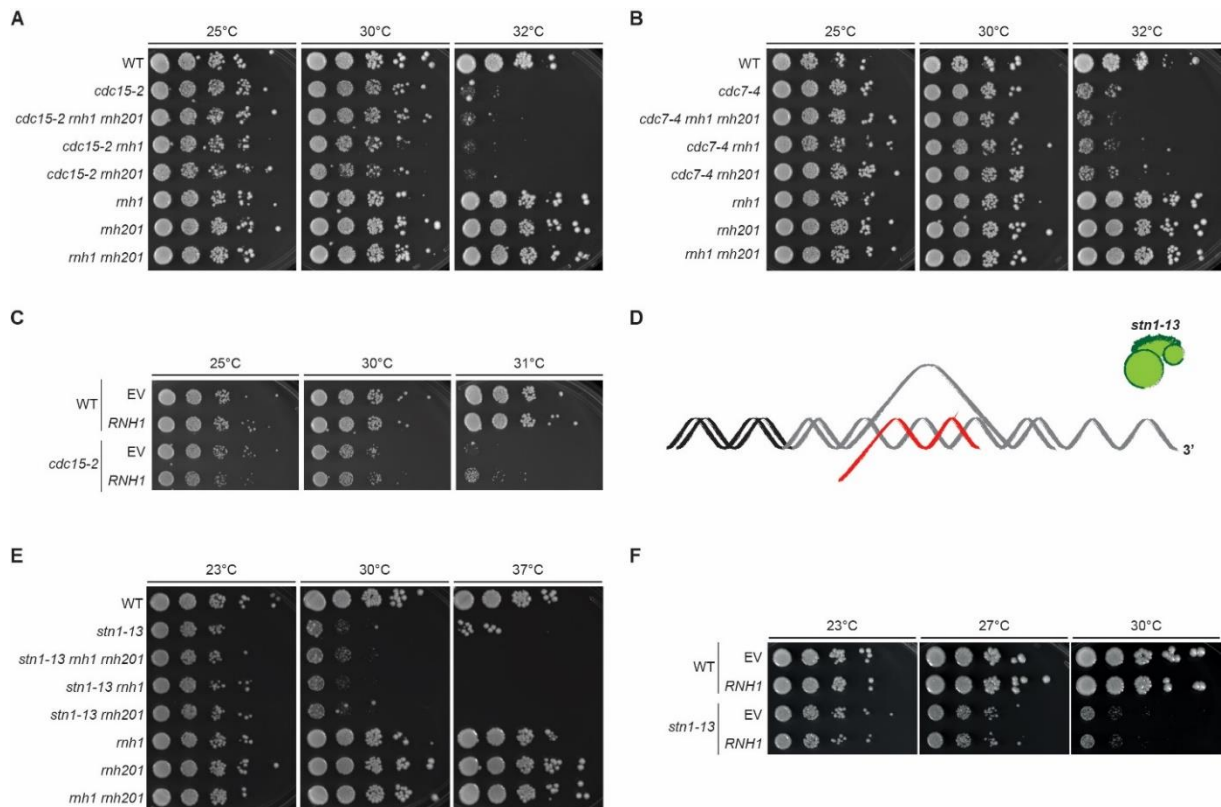


**Figure 16. RNA-DNA hybrids rescue is specific to *cdc13-1* telomere dysfunction.**

(A-B, E) 10-fold serial dilutions of the indicated strains transformed with the indicated plasmids were spotted onto YPD plates. Images were taken after 3 days growth at the indicated temperatures. (C, F) 10-fold serial dilutions of the indicated strains transformed with the indicated plasmids were spotted onto SC-HIS plates. Images were taken after 3 days growth at the indicated temperatures. (D) Schematic representation of the CST complex and the mutant *stn1-13*.

Interestingly, when looking at another member of the CST complex, Stn1, also using a temperature sensitive allele (*stn1-13*) (Figure 16D), we could not recapitulate the same phenotype present for *cdc13-1*, i.e. no growth rescues were observed upon depleting the RNases H nucleases (*rnh1 rnh201*, Figure 16E) nor any growth impairment was observed by RNase H1 overexpression (Figure 16F). Even though the deletion of any subunit of the CST complex leads to a lethal phenotype due to telomere deprotection<sup>38,39,51</sup>, it is known that Cdc13 has a predominant role over Stn1 and Ten1 in preventing chromosome end fusions<sup>517</sup>, and that Stn1 and Ten1 have Cdc13-independent functions<sup>23,44,45</sup>. This might explain why we cannot observe the same phenotype in the *stn1-13* background.

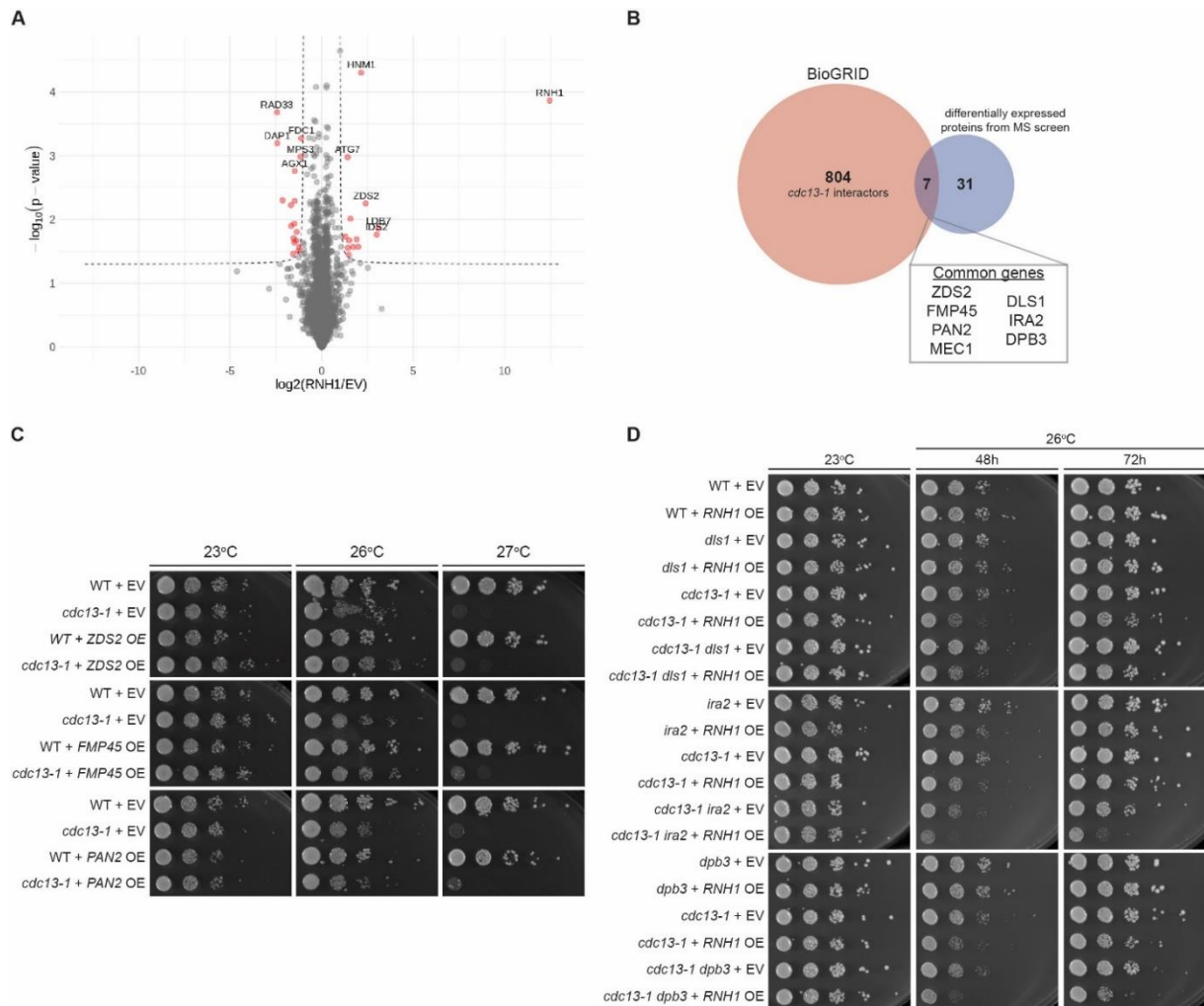


**Figure 17. RNase H1 overexpression leads to very few proteome changes.**

(A) Volcano plot of quantified proteins. Log<sub>2</sub> fold change was determined as the difference between the mean LFQ intensity of the four replicates of *RNH1* OE to EV, and p-values were calculated with a Welch's t-test. Proteins above the dashed line are enriched (p-value = 0.05, fold change = 2). Differentially expressed protein groups are highlighted in red and the 5 candidates showing the highest enrichment from each condition are labelled with their protein IDs. WT, wild type. EV, empty vector. Experiment performed by Carolin Wagner and Maya Wilkens (collaboration with Falk Butter's Laboratory).

(B) Venn diagram comparing the differentially expressed protein from (A) with the *cdc13-1* interactors from the BioGRID™ database, highlighting the common genes.

(C-D) 10-fold serial dilutions of the indicated strains were spotted onto YPD + Kanamycin (I) or SC-HIS (J) plates. Images were taken after 3 days growth at the indicated temperatures, unless indicated otherwise. WT, wild type. EV, empty vector.

Since the overexpression of *RNH1* affects RNA-DNA hybrids genome-wide, we wanted to exclude indirect effects that may be responsible for *cdc13-1* rescue. We compared the proteome of wild type cells harbouring an empty vector with those overexpressing *RNH1* (Figure 17A), and observed that *RNH1* overexpression generated hardly any significant changes in the proteome with only 31 proteins being either up- or down-regulated (Figure 17A) (Table 2). Of the 31 differentially regulated proteins identified, only seven have been documented to possess genetic or physical interactions with *cdc13-1* according to the BioGRID<sup>4,4</sup> database (Figure 17B). We tested six of the seven

candidates, we could not obtain an overexpression plasmid for MEC1, and were either unable to confirm the documented genetic interactions or determine that there was an additive interaction with RNase H1 overexpression (Figures 17C and 17D). This indicates that the differentially regulated proteins are not responsible for the growth effects observed upon *RNH1* overexpression. Taken together, these data suggest that the accumulation of telomeric RNA-DNA hybrids can rescue the viability of *cdc13-1* mutants, which undergo telomere dysfunction at temperatures above 25°C.



**Table 2. Up and down-regulated proteins enriched in analysis of WT + EV vs WT + *RNH1* OE by Mass Spectrometry (MS).**

Standard Name	Systematic Name	Fold change	log <sub>10</sub> (p-value)
RNH1	YMR234W	12.44731829	3.865610901
LDB7	YBL006C	3.089610808	1.86223146
IDS2	YJL146W	3.00088672	1.76251257
ZDS2	YML109W	2.40602119	2.25175823
HNM1	YGL077C	2.158061455	4.30034607
MEC1	YBR136W	1.990893732	1.572770903
ARO10	YDR380W	1.905957733	1.689899109
FMP45	YDL222C	1.7022662	1.570865707
PAN2	YGL094C	1.572418292	2.012417523
APM4	YOL062C	1.491282542	1.673288421
GPB1	YOR371C	1.476820468	1.449650722
	YPL247C	1.421042422	1.557003907
ATG7	YHR171W	1.414750934	2.978271029
KSH1	YNL024C-A	1.290665174	1.731588309
FDC1	YDR539W	-1.120053312	3.273522078
MPS3	YJL019W	-1.147310718	2.985363235
YJU2	YKL095W	-1.24079975	1.569324181
DLS1	YJL065C	-1.271795842	1.506829292
PST1	YDR055W	-1.362665645	1.806464377
CDD1	YLR245C	-1.391894094	1.670633918
AGX1	YFL030W	-1.466992447	2.761628134
CIN2	YPL241C	-1.470030701	2.289325687
DPB3	YBR278W	-1.491120278	1.63979064
IRA2	YOL081W	-1.497398376	1.933028144
MRPL27	YBR282W	-1.540021794	1.706395241
RSA1	YPL193W	-1.558423794	1.463798872
SND1	YDR186C	-1.66011106	1.899464253
SSU1	YPL092W	-1.669371525	2.22531649
ISA2	YPR067W	-2.136433342	2.301014137
DAP1	YPL170W	-2.425499897	3.19505422
RAD33	YML011C	-2.435441641	3.679694316

## 2.1.2 Telomeric RNA-DNA Hybrids Prevent Exo1- And Pif1-Mediated Resection Independent of G-Quadruplex (G4) Structures

The inactivation of the CST complex results in telomere uncapping, and ultimately leads to cell death<sup>51,64</sup>. At non-permissive temperature in the *cdc13-1* background, extensive ssDNA is generated by resection in an Exo1- and Pif1-dependent manner, resulting in the activation of the DNA damage checkpoint (Rad9, Rad53) and subsequently leading to cell cycle arrest<sup>51,145</sup> (Figure 18A). In wild type cells, Cdc13 prevents Exo1 and Pif1 access to telomeres<sup>55,64,156</sup> (Figure 18A). The *cdc13-1* growth phenotype can be rescued by deletion of *EXO1*, *PIF1* or impairment of the DNA damage checkpoint<sup>518</sup> (*rad9*, *rad53*). We wondered if telomeric RNA-DNA hybrids affect cell viability upon telomere dysfunction through either resection or checkpoint activation.

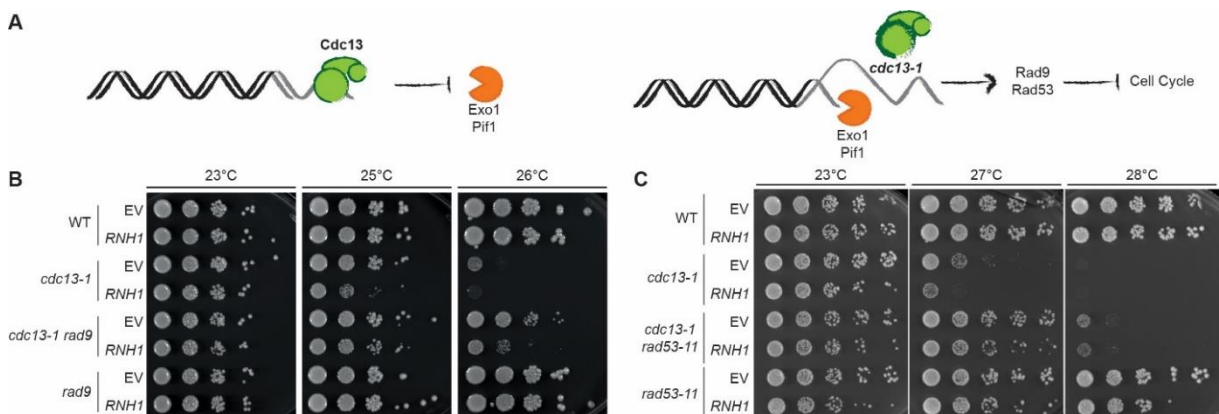


**Figure 18. Telomeric RNA-DNA hybrids prevent Exo1- and Pif1-mediated resection.**

(A) Schematic representation of Cdc13's role in resection and DNA damage checkpoint activation. (B-C) 10-fold serial dilutions of the indicated strains transformed with the indicated plasmids were spotted onto SC-HIS plates. Images were taken after 3 days growth at the indicated temperatures.

As expected, ablation of the checkpoint (through *RAD9* deletion) showed a rescue of the growth defect of *cdc13-1* cells (Figure 18B). Yet, when *RNH1* was overexpressed in the double mutants, it still resulted in toxicity (Figure 18B). Another important DNA damage checkpoint player is the DNA damage response kinase, Rad53. To test its involvement, we employed a checkpoint-defective allele of *RAD53*, *rad53-11*<sup>519</sup>, and recapitulated the rescue of *cdc13-1* growth when the checkpoint is impaired<sup>520</sup> (Figure 18C). Interestingly, in this background, when overexpressing *RNH1* we do not detect the same level of toxicity as for the *rad9* mutants (Figures 18B and 18C), even though we do detect a slight effect on growth at 28°C. These data suggest that the removal of RNA-DNA hybrids was lethal in *cdc13-1*

cells in a Rad9 independent manner and further indicates that RNA-DNA hybrid removal results in cell death in a Rad53-dependant manner.

Considering that there is extensive Exo1- and Pif1-mediated resection in *cdc13-1* mutants upon telomere uncapping, we wondered if other resection factors (Figure 19A) could possibly be involved in the rescue observed when telomeric RNA-DNA hybrids accumulate.

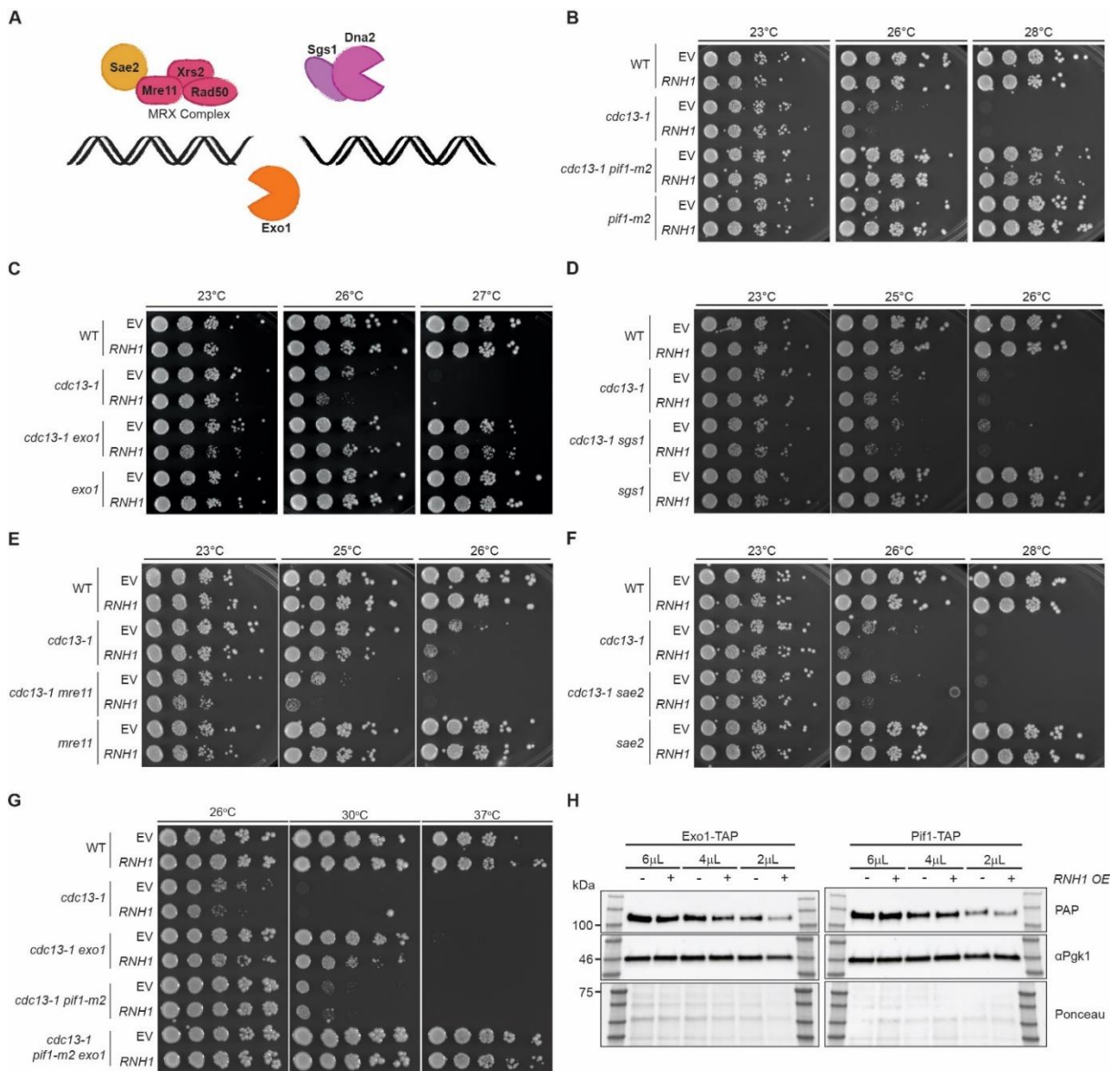


**Figure 19. Telomeric RNA-DNA hybrids do not affect Mre11- nor Sae2-mediated resection.**

(A) Schematic representation of the resection factors involved in DNA damage repair in budding yeast.

(B-G) 10-fold serial dilutions of the indicated strains transformed with the indicated plasmids were spotted onto SC-HIS plates, except (D-E) that were spotted onto SC-URA. Images were taken after 3 days growth at the indicated temperatures.

(H) Western blot analysis of the depicted TAP tagged resection factors, in decreasing amount of protein extracts, with or without overexpression of RNase H1 (*RNH1*). PAP (to detect TAP), peroxidase anti-peroxidase soluble complex antibody; TAP, tandem affinity purification tag.

The inactivation of the nuclear form of *PIF1* (*pif1-m2* allele which restricts Pif1 localization to mitochondria<sup>157</sup>) or the deletion of *EXO1* rendered *cdc13-1* cells insensitive to *RNH1* overexpression (Figures 19B and 19C). The inactivation of *MRE11*, *SAE2* or *SGS1* lead to the same toxicity observed in *cdc13-1* upon *RNH1* overexpression (Figures 19D-19F), excluding these factors as contributors to the observed resection phenotype. This genetic data indicates that the growth defects of *cdc13-1* cells that accumulate RNA-DNA hybrids is due to excessive end resection mediated by Exo1 and Pif1. Even though there is a slight effect of *RNH1* overexpression in *cdc13-1 pif1-m2* and *cdc13-1 exo1* strains, this was eliminated in the *cdc13-1 exo1 pif1-m2* triple mutant (Figure 19G). We looked at the protein expression of Exo1 and Pif1 upon *RNH1* overexpression, and detected no differences in exponential cells regarding protein levels (Figure 19H). Thus corroborating the lack of influence of the *RNH1* overexpression observed in the proteome on resection factors (Figure 17A).

The G-rich strand within telomeric ss and dsDNA has the ability to form G-quadruplex (G4) DNA structures<sup>521</sup>. A previous study reported that G4 stabilization can prevent resection of telomeres in a *cdc13-1* background<sup>75,522</sup>. Additionally, G4s may form on the displaced strand of an R-loop at telomeres<sup>334,367</sup>. Furthermore, the Pif1 helicase binds G4 structures and efficiently unwinds them *in vitro* and *in vivo*<sup>161,203</sup>. Hence, RNA-DNA hybrids at telomeres may prevent resection indirectly through the stabilization of G4 structures (Figure 20A). To understand the effect of RNA-DNA hybrids on telomeric G4 levels, we used the BG4 antibody<sup>523</sup> to monitor G4 formation at telomeres via ChIP followed by qPCR (as described in Hänsel-hertsch 2018<sup>524</sup>). We performed BG4 ChIP in *pif1-m2* cells to confirm the specificity of the antibody (Figure 20B) and, as expected, we detected a strong accumulation of G4 DNA at telomeres in this mutant in comparison to WT cells. An internal G4 site on chromosome XIII was used as a positive control for the experiment.

We detected slight, but non-significant, increases in G4 signal at telomeres in WT cells, upon *RNH1* overexpression or upon removal of RNase H activity (*rnh1 rnh201*) (Figure 20C). However, upon *RNH1* overexpression, we saw an increase in signal at a G4 positive locus on chromosome XIII and at the actin locus is also detected (Figure 20C), indicating that *RNH1* overexpression might have an overall effect in G4 structures and not specifically at telomeres. In *cdc13-1* mutants, we no longer detect the increased G4 levels upon *RNH1* overexpression at telomeres, at either permissive (23°C) or restrictive temperatures (30°C) (Figure 20D). When RNA-DNA hybrids accumulate upon removal of RNase H activity (*rnh1 rnh201*), there is an overall decrease in G4 levels in this background (Figure 20D). Remarkably, upon a two hour (2h) shift to 30°C, G4 structure levels were

considerably decreased in *cdc13-1*, independently of RNA-DNA hybrid load at telomeres (Figure 20D). These data indicate that RNA-DNA hybrids at telomeres may affect G4 levels, yet unlike with RNA-DNA hybrids, we cannot confirm that G4s are responsible for the phenotypes observed when hybrid levels are misregulated.

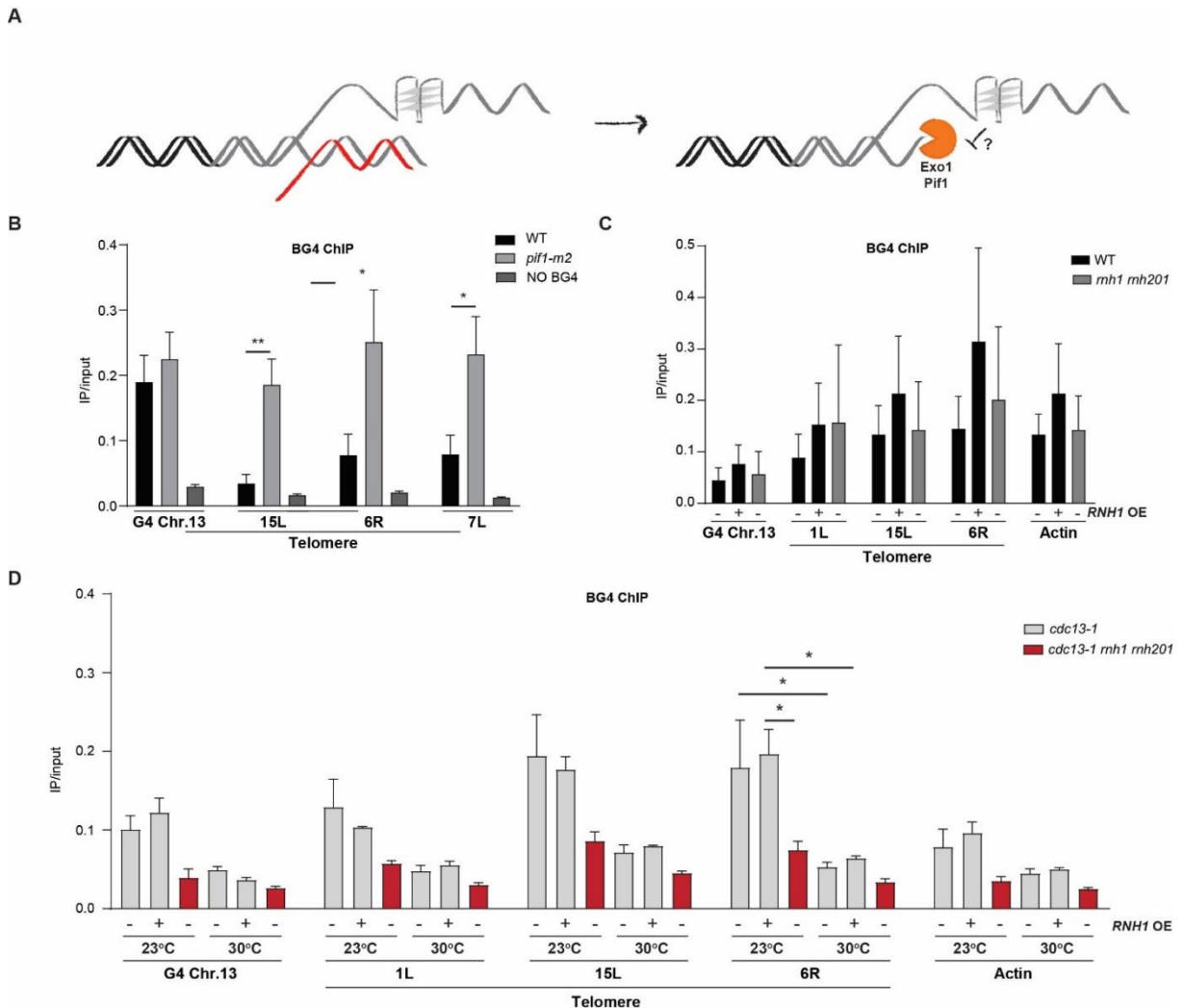


**Figure 20. Telomeric RNA-DNA hybrids prevent resection independently of G4 DNA.**

(A) Schematic representation of a G4 DNA structure at telomeres.

(B-D) BG4 ChIP. Chromatin immunoprecipitation with BG4 antibody and qPCR analysis of the indicated strains at the indicated loci. Cells were grown at 30°C until collection, except for (D) where the cells were grown at 23°C and shifted for 2h to 30°C. Data are depicted as mean + SD, n = 3. p-values were obtained from Student's t-test (\*p < 0.05) for (B) and obtained from One-Way ANOVA using the Tukey test to correct for multiple comparisons (\*p < 0.05, \*\*p < 0.01, \*\*\*p < 0.001, \*\*\*\*p < 0.0001) for (D). WT, wild type. EV, empty vector. Experiment performed by Mona Hajkazemi (collaboration with Katrin Paeschke's Laboratory).

In summary, RNA-DNA hybrids limit Exo1- and Pif1-mediated resection. Consequently, RNA-DNA hybrid removal, through *RNH1* overexpression, impairs cell viability when telomeres are dysfunctional. This is most likely due to a direct effect of R-loops on resection, rather than a direct consequence of G4 stabilization and prevention of

resection by the G4 structure, since less G4 levels are detected when RNA-DNA hybrids accumulate in a *cdc13-1* background.

### 2.1.3 RNA-DNA Hybrids Prevent ssDNA Formation at Dysfunctional Telomeres

To further understand the impact of RNA-DNA hybrids at dysfunctional telomeres, we quantified ssDNA at telomeres using two different approaches. We either made use of a strand specific dot blot hybridization technique on non-denatured telomeric DNA (as compared to denatured DNA) and probed it with a C-rich oligonucleotide probe<sup>73</sup>, or employed ChIP of the RPA ssDNA binding complex. The amount of ssDNA increased at telomeres when *cdc13-1* cells were shifted to 30°C for two hours (2h) (Figures 21A and 21B), as described in the literature<sup>519,525</sup>. We confirmed that the increased signal was ssDNA overhang-dependent and not replication intermediates, through its sensitivity to bacterial Exol (3'-5' nuclease) (Figure 21A). Consistent with the genetic data (Figure 12D), the increase in ssDNA was reduced in *cdc13-1* cells when the RNase H enzymes were deleted and RNA-DNA hybrids accumulated (Figures 1A and 1B). Analysis of the cell cycle profiles, through flow cytometry, revealed a G2-arrest for *cdc13-1* cells, independently of RNases H status, after 2h at 30°C (Figure 21C) and no difference in cell cycle profiles at 23°C (Figure 21C). We saw similar effects using RPA ChIP as a readout, following either a two hour (2h) shift to the semi-permissive temperature of 26°C or to the restrictive temperature of 30°C (Figure 21D). Although the intensity of the signal is reduced at 26°C, we see a clear decrease in RPA accumulation in the absence of the RNase H enzymes at telomeres (Figure 21D). As expected, the actin locus remained unaffected in terms of RPA accumulation following inactivation of the *cdc13-1* allele. Therefore, even though the production of ssDNA was attenuated in the absence of RNase H enzymes, it was not sufficient to prevent a checkpoint-mediated arrest (Figure 1C).

Although the overexpression of *RNH1* increased the temperature sensitivity of *cdc13-1* cells, we were unable to detect a significant increase of ssDNA using the dot blot approach (Figures 22A and 22B). Analysis of the cell cycle profiles, through flow cytometry, revealed a G2-arrest for *cdc13-1* cells, independently of RNase H1 overexpression, after 2h at 30°C (Figure 21C) and no difference in cell cycle profiles in the absence of *exo1* compared to wild type (Figure 22C). Using RPA ChIP, we observed only a slight increase in telomeric ssDNA, with strong variation between telomeres (Figure 22D), similar to the dot blot approach.

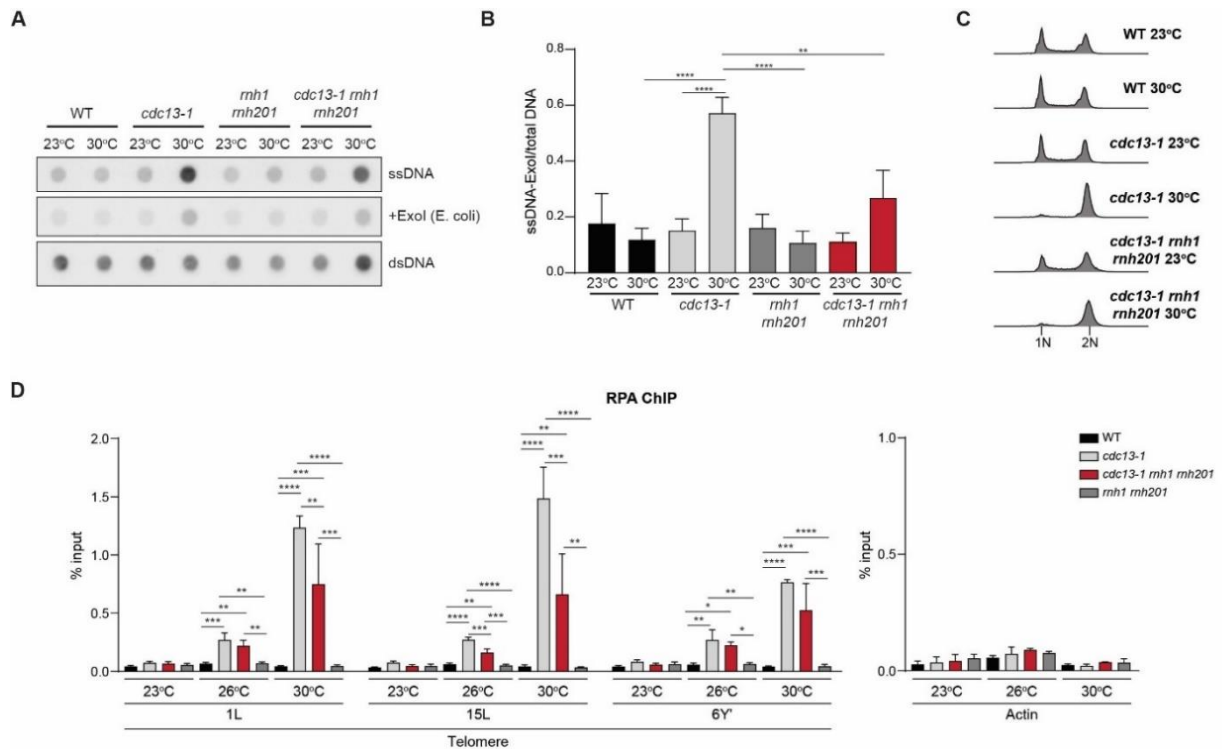


**Figure 21. RNA-DNA hybrids prevent resection-mediated ssDNA formation at telomeres.**

(A) ssDNA dot blot. Genomic DNA of the indicated strains was extracted under non-denaturing conditions after exponential growth at 23°C or a 2h shift to 30°C, spotted on a nylon membrane and probed with a DIG-labelled telomeric C-rich oligonucleotide (ssDNA). The same DNA samples were also digested with bacterial Exol, which digests 3'-5' DNA overhangs (+Exol), to check for ssDNA signal specificity. DNA samples were then denatured to control for equal blotting (dsDNA).

(B) Quantification of A. Data are depicted as mean + SD, n = 3 and calculations take into account the ssDNA signal, subtracting the background (+Exol signal), normalized to total amount of telomeric signal (dsDNA signal). p-values were obtained from One-Way ANOVA using the Tukey test to correct for multiple comparisons (\*p < 0.05, \*\*p < 0.01, \*\*\*p < 0.001, \*\*\*\*p < 0.0001).

(C) DNA content analysis of depicted genotypes in asynchronous exponentially growing cultures at 23°C or after a 2h shift to 30°C. 1N: DNA content, G1 phase; 2N: DNA content, G2/M phase. One representative histogram for each condition is shown.

(D) RPA ChIP. Chromatin immunoprecipitation with  $\alpha$ -RPA antibody and qPCR analysis of the indicated strains at the indicated loci. Cells were shifted to 26°C or 30°C for 2h before collection. Values are represented as % input of DNA recovered. Data are depicted as mean + SD, n = 3. p-values were obtained from One-Way ANOVA using the Tukey test to correct for multiple comparisons (\*p < 0.05, \*\*p < 0.01, \*\*\*p < 0.001, \*\*\*\*p < 0.0001).

When overexpressing *RNH1* in *cdc13-1* cells, the DNA damage checkpoint (using *RNR3* expression as a readout) was only weakly increased compared to an empty vector control (Figures 23A and 23B). Despite this observation, no detectable differences were observed in cell cycle distribution (Figure 23C). We speculate that ssDNA accumulation within the telomeric repeats in *cdc13-1* cells may already be saturating the signal and that a further increase cannot be detected upon *RNH1* overexpression. Subsequently, we decided to evaluate the resection distance into the subtelomeric region to see if differences here were detectable.

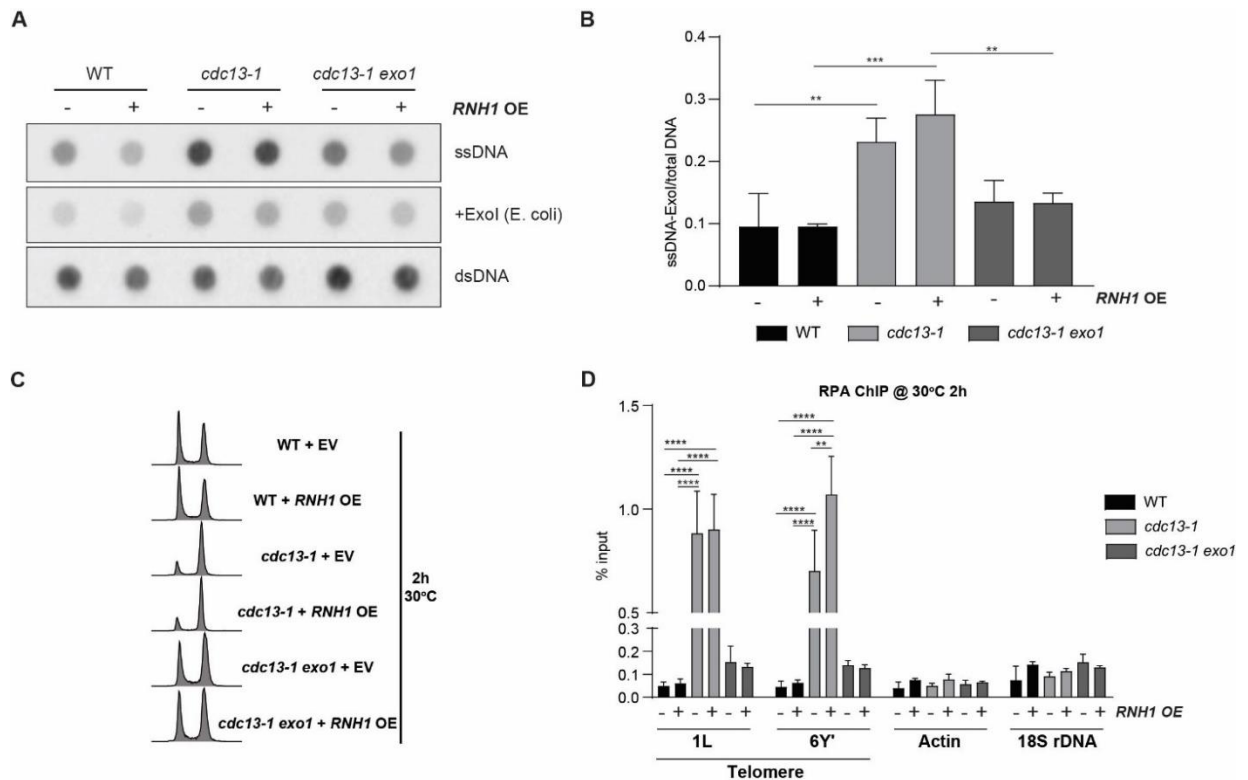


**Figure 22. RNA-DNA hybrid removal slightly enhances resection-mediated ssDNA formation at telomeres.**

(A) ssDNA dot blot. Genomic DNA of the indicated strains was extracted under non-denaturing conditions after a 2h shift to 30°C, spotted on a nylon membrane and probed with a DIG-labelled telomeric C-rich oligonucleotide (ssDNA). The same DNA samples were also digested with bacterial Exol, which digests 3'-5' DNA overhangs (+Exol), to check for ssDNA signal specificity. And DNA samples were also denatured to control for equal blotting (dsDNA).

(B) Quantification of A. Data are depicted as mean + SEM,  $n = 3$  and calculations take in account the ssDNA signal, subtracting the background (+Exol signal), normalized to total amount of telomeric signal (dsDNA signal). p-values were obtained from One-Way ANOVA using the Tukey test to correct for multiple comparisons (\* $p < 0.05$ , \*\* $p < 0.01$ , \*\*\* $p < 0.001$ , \*\*\*\* $p < 0.0001$ ).

(C) DNA content analysis of depicted genotypes in asynchronous exponentially growing cultures after a 2h shift to 30°C. 1N: DNA content, G1 phase; 2N: DNA content, G2/M phase. One representative histogram for each condition is shown.

(D) RPA ChIP. Chromatin immunoprecipitation with RPA antibody and qPCR analysis of the indicated strains at the indicated loci. Cells were shifted to 30°C for 2h before collection. Values are represented as % input of DNA recovered. Data are depicted as mean + SEM,  $n = 3$ . p-values were obtained from One-Way ANOVA using the Tukey test to correct for multiple comparisons (\* $p < 0.05$ , \*\* $p < 0.01$ , \*\*\* $p < 0.001$ , \*\*\*\* $p < 0.0001$ ).

The amount of ssDNA has been reported to decrease with increasing distance from the telomere when the *cdc13-1* allele is inactivated, through PCR-based methods<sup>525</sup>. We tested whether the distance of resection may differ when telomeric RNA-DNA hybrids are removed or accumulate. We used amplicons along the length of a single telomere (1L) to detect the spread of ssDNA by RPA ChIP (Figures 24A and 24B, upper diagram). We detected ssDNA up to ca. 10 kbp into the subtelomeric region in *cdc13-1* (Figure 24A, dashed red line). Consistent with our previous results, we could not detect significant changes in ssDNA levels directly proximal to the telomere when *RNH1* was overexpressed



(Figure 24A). However, we did observe increased ssDNA levels at loci located 2 and 4 kbp from the telomere in these conditions (Figure 24A). The *RNH1*-induced ssDNA increase at these loci, as well as the overall signal present in *cdc13-1*, was dependent on the presence of *EXO1* (Figure 24A, grey lines). When considering the accumulation of ssDNA in *rnh1 mh201* cells along the 1L telomere, we continue to detect a lower signal when RNA-DNA hybrids accumulate in *cdc13-1* (Figure 24B, red line), although with a lot of variability between replicates and consistent with our previous findings (Figure 21).

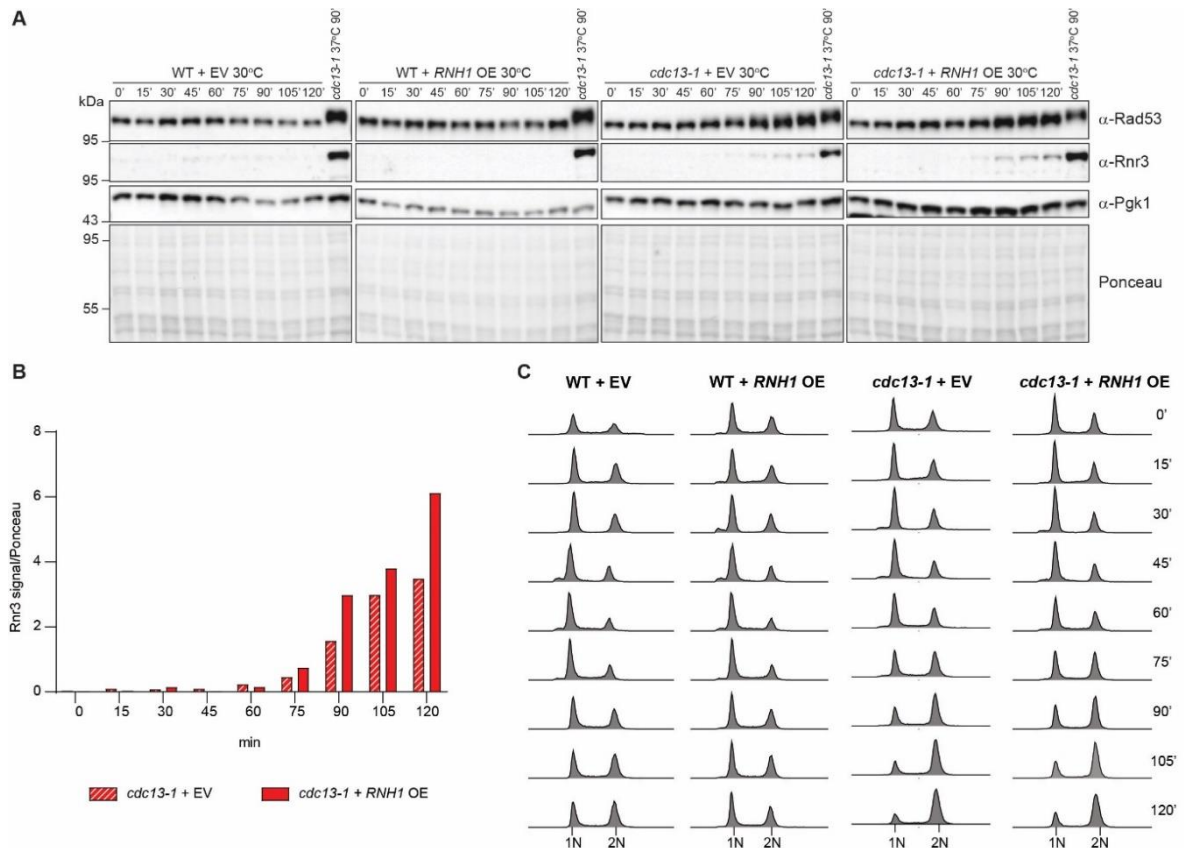


**Figure 23. RNA-DNA hybrid removal barely impacts the DNA damage checkpoint.**

(A) Western blot analysis showing DNA damage checkpoint activation upon shift to 30°C, by checking Rad53 phosphorylation and Rnr3 levels. Protein samples were collected at 15min intervals. (B) Quantification of Rnr3 protein levels, of the depicted genotypes in A upon a 2h shift to 30°C. (C) DNA content analysis of depicted genotypes upon shift to 30°C, samples were collected at 15min intervals. 1N: DNA content, G1 phase; 2N: DNA content, G2/M phase. One representative histogram for each condition is shown. WT, wild type. EV, empty vector.

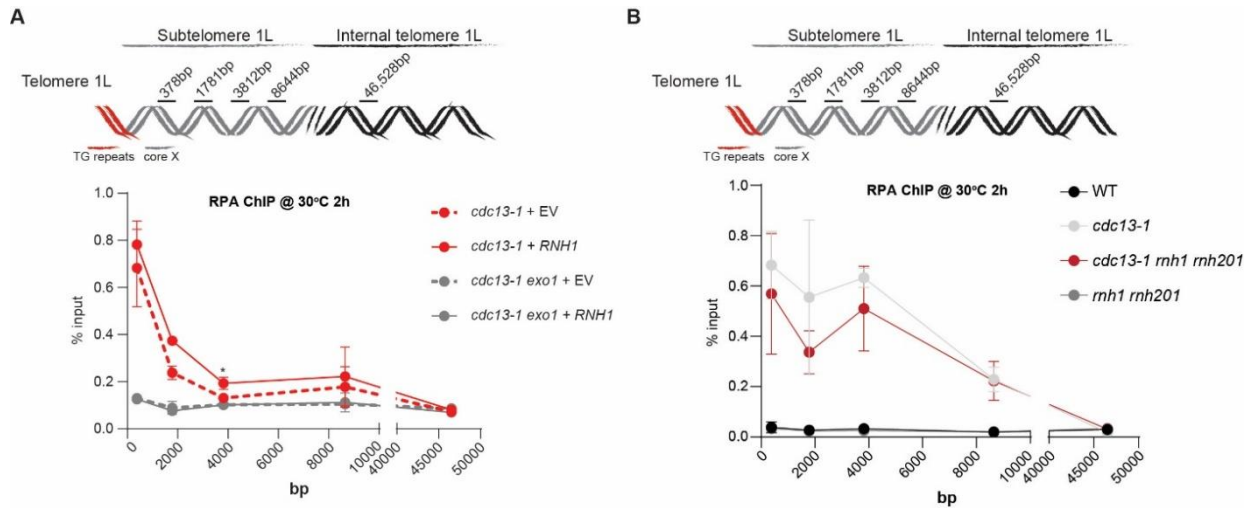


**Figure 24. Resection into the subtelomere is affected by RNA-DNA hybrids.**

(A-B) RPA ChIP. Chromatin immunoprecipitation with  $\alpha$ -RPA antibody and qPCR analysis of the indicated strains along the 1L telomere as depicted in upper diagram. Cells were shifted to 30°C for 2h before collection. Values are represented as % input of DNA recovered. Data are depicted as mean + SD, n = 3. p-values were obtained from Student's t-test (\*p < 0.05). WT, wild type. EV, empty vector.

In summary, these results confirm that RNA-DNA hybrids prevent Exo1-mediated resection at telomeres when capping is compromised.

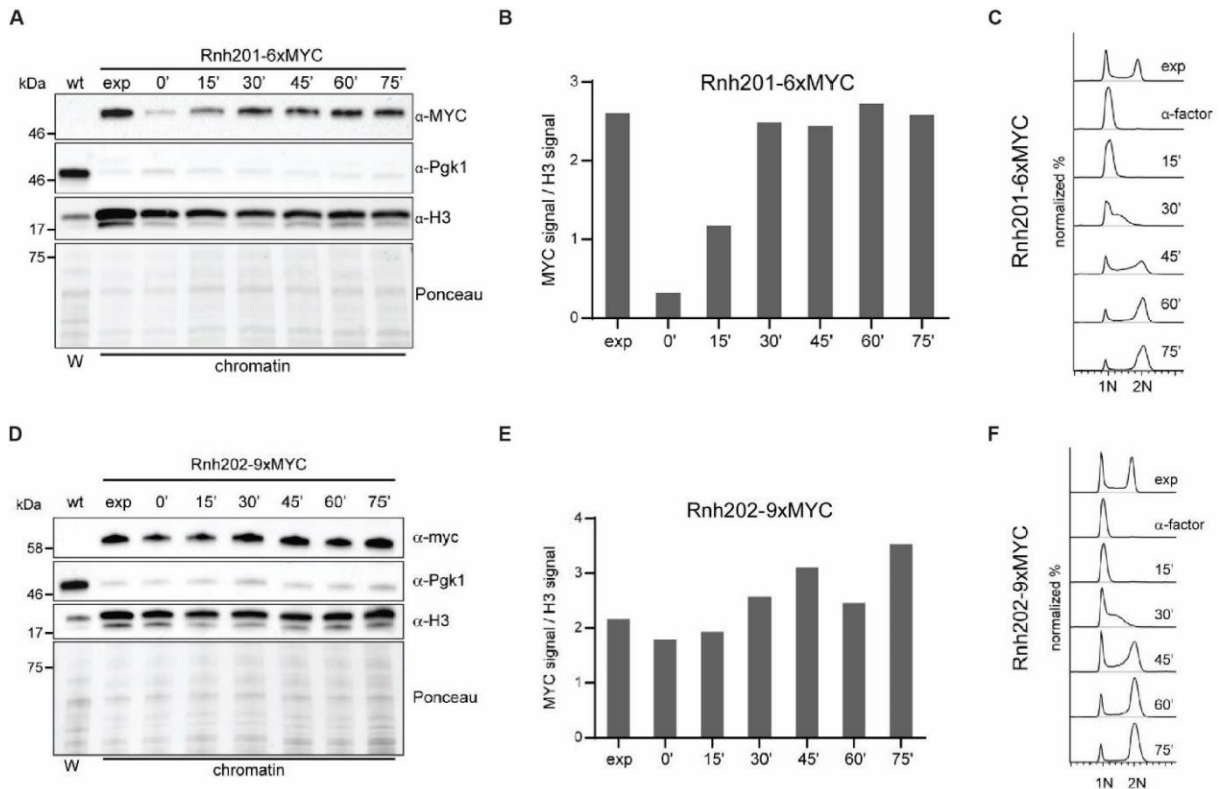
## 2.2 RNASE H1 AND H2 ARE DIFFERENTIALLY REGULATED TO PROCESS RNA-DNA HYBRIDS

RNA-DNA hybrids are tightly regulated to ensure genome stability, and the RNase H enzymes contribute to this stability by removing RNA-DNA hybrids and keeping their levels in check<sup>447</sup>. In order to understand RNA-DNA hybrid dynamics, we studied the dynamic regulation of the individual RNase H enzymes. We published in Lockhart et al., 2019 that the RNase H enzymes are controlled in different manners. Whereas RNase H2 has an essential function in G2/M for both R-loop processing and ribonucleotide excision repair, RNase H1, however, can function independently of the cell cycle to remove R-loops. Furthermore, RNase H1 is activated in response to high R-loop loads<sup>464</sup>. These results show that RNase H1 and RNase H2 may act in a context dependent manner.

### 2.2.1 The Chromatin Association of RNase H2 Is Cell Cycle Regulated

The endogenous subunits of RNase H2 are expressed throughout all phases of the cell cycle, however, the genetic and biochemical data from Lockhart et al., 2019 indicated an essential and sufficient function for RNase H2 activity in G2/M to execute both its RER and R-loop processing roles. To understand if some form of regulation on the level of localization or activity of RNase H2 could explain the genetic data, we looked at the chromatin recruitment of RNase H2 during the cell cycle (Figure 25). We fractionated chromatin-associated proteins in synchronized cells, after  $\alpha$ -factor arrest and release, to address the recruitment to chromatin of a tagged version of one subunit of RNase H2 (RNH201-6xMYC) (Figure 25A). In G1, the chromatin association detected was very weak. However, from early S phase (15 minutes post-release), the protein levels increased in the chromatin fraction (Figures 25A and 25B). Rnh201 continued to accumulate on the chromatin as cells progressed through the S phase and into G2/M (Figures 25A and 25B). Fractionation efficiency was controlled by re-probing the western blots for Pgk1 and histone H3, controls for the soluble and chromatin bound fractions, respectively (Figure 25A). The chromatin association timing was consistent with published data regarding telomere localization of Rnh201-TAP by ChIP<sup>236</sup>. Another RNase H2 subunit, Rnh202, presented a similar regulation (Figures 25D, 25E and 25F). Progression through the cell cycle was monitored by flow cytometry in 15-minute intervals (Figures 25C and 25F). Overall, the

regulation of the RNase H2 subunits appears to be through its chromatin association, which increases as cells progress through the S phase and into G2/M.



## 2.2.2 RNase H1 Associates to Chromatin upon R-Loop Stabilization Independently of the Cell Cycle

RNase H2 acts in ribonucleotide and R-loop processing functions and its activity accounts for the majority of RNase H activity in a cell<sup>195</sup>. Nevertheless, RNase H1 is efficient in the removal of R-loops<sup>447</sup>. The genetic data from Lockhart et al., 2019 indicated no cell cycle requirement for *RNH1* activity, and no regulation regarding chromatin association throughout the cell cycle (Figure 26A). Where RNase H1 was weakly but equally chromatin bound in all cell cycle phases (Figure 26A), and the progression through the cell cycle was monitored by flow cytometry (Figure 26B). This observation was consistent with a lack of an obvious cell cycle regulation. There is speculation in the literature that Rnh1 might become activated in response to stress<sup>462</sup>; to test this hypothesis, we evaluated the association of Rnh1 in backgrounds with R-loop accumulation. For this purpose, we employed the temperature sensitive allele *sen1-1*<sup>197</sup>, where R-loops are known to drastically accumulate<sup>198</sup>. Indeed, after a 90 minutes shift to the semi-permissive temperature of 30°C in the *sen1-1* background, increased levels of chromatin-bound Rnh1 were detected (Figure 26C). When using *rnh201* mutants, no visible increase in Rnh1 chromatin association was detected (Figure 26C). No effects were observed by flow cytometry regarding cell cycle profiles of these mutants (Figure 26D). Therefore, irrespective of cell cycle stage, Rnh1 appears to respond to increased R-loop levels.

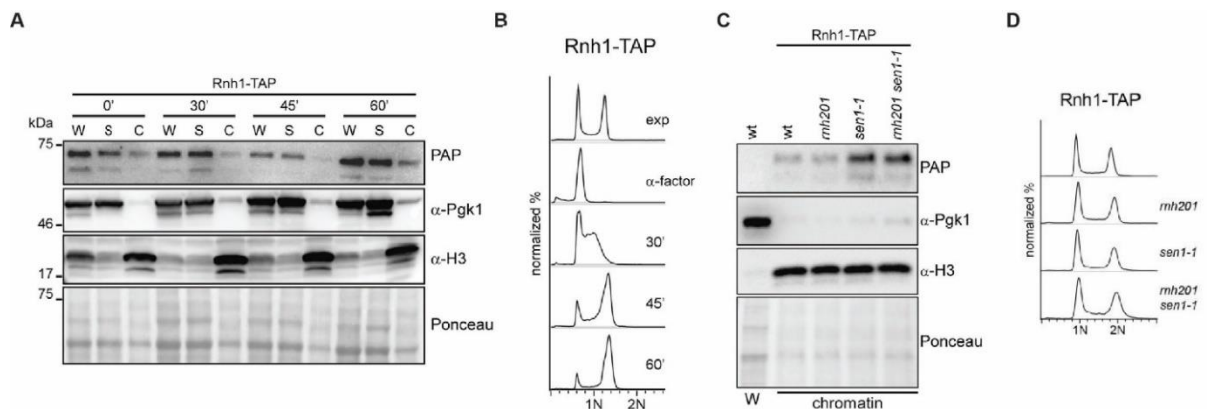


**Figure 26. RNase H1 associates with chromatin when stress arises.**

(A) Chromatin association of Rnh1 in the cell cycle. Exponentially growing cells were arrested in G1 with  $\alpha$ -factor and released in the cell cycle at 25°C. Protein samples were collected at the indicated time points and whole-cell extract (W), soluble (S) and chromatin (C) fractions were analyzed by western blotting. Chromatin fractions were loaded 4x relative to S and W. exp, exponential phase; PAP (to detect TAP), peroxidase anti-peroxidase soluble complex antibody; TAP, tandem affinity purification tag.

(B) DNA content analysis of samples shown in (A), samples were collected at the indicated time points. 1N: DNA content, G1 phase; 2N: DNA content, G2/M phase. One representative histogram for each condition is shown.

(C) Chromatin association of Rnh1 in RNA-DNA hybrid accumulation backgrounds. Cells of the indicated genotypes were grown exponentially at 25°C and then shifted to 30°C for 90 minutes. Protein samples were collected at the indicated time points and whole-cell extract (W) and chromatin fractions were analyzed by western blotting. Chromatin fractions were loaded 4x relative to S and W. exp, exponential phase; WT, wild type; PAP (to detect TAP), peroxidase anti-peroxidase soluble complex antibody; TAP, tandem affinity purification tag.

(D) DNA content analysis of samples shown in (C), samples were collected at the indicated time points. 1N: DNA content, G1 phase; 2N: DNA content, G2/M phase. One representative histogram for each condition is shown.

## 2.3 RNA-DNA HYBRIDS ARE TIGHTLY REGULATED AT CRITICALLY SHORT TELOMERES

In the absence of telomerase, cells undergo progressive telomere shortening with each cell cycle division<sup>176,182</sup>. Subsequently, telomere erosion leads to the activation of the DNA damage checkpoint resulting in a permanent cell cycle arrest, in a process referred to as replicative senescence<sup>176,182</sup>. TERRA RNA-DNA hybrids have been found to become stabilized and drive homology-directed repair (HDR) at critically short telomeres, consequently delaying replicative senescence onset<sup>288,345,348,512,513</sup>. However, how RNA-DNA hybrids promote HDR at critically short telomeres is still not understood. In this section, we aimed to further understand RNA-DNA hybrid regulation during replicative senescence, and elucidate the mechanism of when and how hybrids are required to promote HDR. We saw that RNase H1 and Sen1 are potential candidates to remove RNA-DNA hybrids at critically short telomeres, while it is already known that at long telomeres RNase H2 is responsible for hybrid removal<sup>236</sup>. Moreover, while at dysfunctional telomeres TERRA RNA-DNA hybrids can prevent nuclease-mediated resection (Section 1.1 of Results), in pre-senescent cells, with intermediate length telomeres, RNA-DNA hybrids do not affect telomere-shortening rates.

### 2.3.1 RNase H1 and Sen1 are Epistatic in Replicative Senescence

At critically short telomeres, the accumulation of TERRA RNA-DNA hybrids leads to increased rates of homology-directed repair (HDR)<sup>236,345</sup>. RNase H2 is responsible for the majority of RNase H activity in the cell, acting in both ribonucleotide as well as R-loop removal<sup>195</sup>, having its essential function in the G2/M phase of the cell cycle<sup>464</sup>. At long telomeres, RNase H2 is recruited, via the telomere binding protein Rif2, to keep RNA-DNA hybrid levels in check<sup>236</sup>. It is interesting that at telomeres, RNase H2 may be primarily responsible for TERRA RNA-DNA hybrid removal, while RNase H1 might play a compensatory role, considering it appears to respond to increased R-loop levels<sup>464</sup>. Remarkably, when tracking the senescence rates of the RNases H mutants (*rnh1*, *rnh201*, *rnh1 rnh201*) in telomerase negative cells (*est2*), we could observe a different regulation for RNase H1 and RNase H2 at telomeres (Figure 27A). While *RNH1* deletion led to a fast senescence phenotype (Figure 27A, green line) when compared to *est2* mutants (Figure 27A, black line), the deletion of *RNH201* produced an even bigger delay in senescence

onset (Figure 27A, blue line) than observed in *est2 rnh1 rnh201* cells (Figure 27A, red line). This result indicates that the loss of RNase H1 is detrimental for senescent cells, since it accelerated senescence onset (Figure 27A). However, how RNase H1 regulates senescence rates is still unclear.

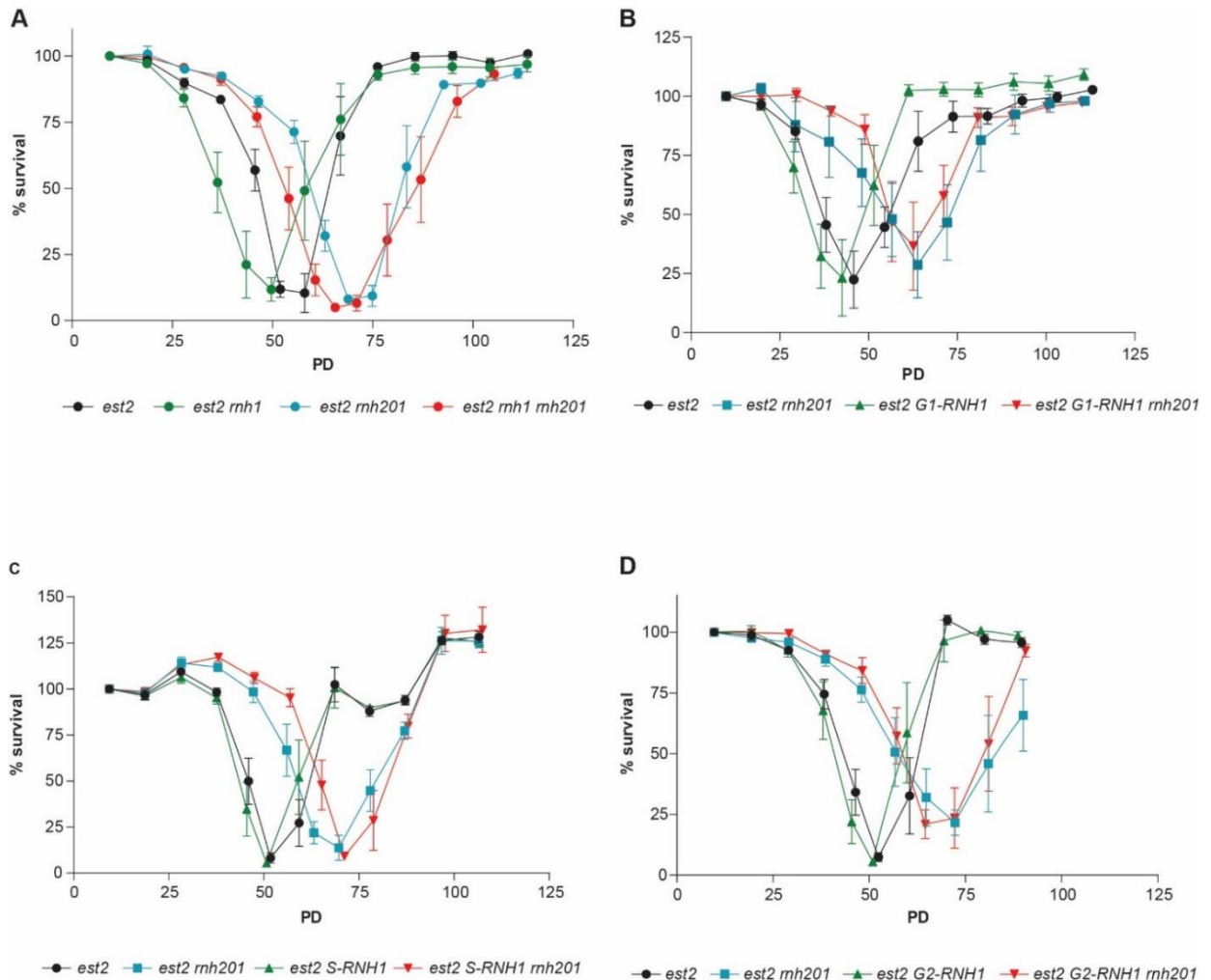


**Figure 27. RNase H1 and RNase H2 affect senescence rates differently.**

(A-D) Senescence curves were performed in telomerase defective cells (*est2*), and viability was estimated daily by measuring cell culture density, with the first measurement set to 100%. Data are shown as mean  $\pm$  SEM;  $n \geq 5$  biological replicates per genotype.

To further understand the requirements for RNase H1 at telomeres, we employed cell cycle regulated alleles of *RNH1*, where protein expression was restricted to either G1, S or G2/M phase of the cell cycle<sup>464,500,526</sup>. Briefly, the promoter and N-terminal portion of the CDK inhibitor Sic1 was used to obtain a late M/G1 phase-specific expression; while the promoter and N-terminal degenon elements of the cyclins Clb6 and Clb2 were used to achieve a S phase- and G2/M phase-specific expression<sup>464,500,526,527</sup>. When analysing senescent rates of the cell cycle regulated alleles of *RNH1*, we observed that restricting



*RNH1* to any phase of the cell cycle led to a *est2*-like senescence rate, except when *RNH1* was restricted to G1 (Figures 27B, 27C, 27D, green lines - *RNH1* alleles, black lines - *est2*). In the *G1-RNH1* mutants, we have a very slight acceleration of the senescent rate (Figure 27B, green line), but still not to the same extent as the deletion of *RNH1* (Figure 27A, green line). Considering the slight expression in late M phase of the G1-allele<sup>526</sup>, this might be sufficient to allow R-loop removal by RNase H1 during replicative senescence at telomeres. However, when looking at senescence rates in the absence of RNase H2 (*rnh201* mutants), we continue to observe a delay in senescence onset independently of the cell cycle phase where *RNH1* expression is restricted (Figures 27B, 27C, 27D, red lines – *RNH1* alleles, blue lines – *est2 rnh201*). This indicates that RNase H1 has the potential to remove RNA-DNA hybrids at telomeres independently of the cell cycle. However, when *RNH1* expression is restricted to S-phase it appears to further delay senescence onset (Figure 27C, red line). This suggests that RNase H1 activity is required for the maximum delay on senescence onset, and although RNase H1 can act on any phase of the cell cycle, to achieve the best conditions to postpone senescence, *RNH1* activity in S-phase might be required.

Besides the RNase H nucleases, the cell has other pathways for RNA-DNA hybrid processing, in particular, the helicase Sen1 makes significant contributions to RNA-DNA hybrid removal, and maintenance of genome stability<sup>197</sup>. Inactivation of Sen1 leads to a drastic accumulation of R-loops in the genome<sup>198</sup>, and Sen1 has been identified to associate with the replisome and play key functions at the replication fork during DNA replication, promoting fork progression and chromosome stability<sup>475</sup>. The progression through replicative senescence has been associated with increased replication stress, not only by phosphorylation of the replication stress sensor Mrc1 but also by linking this stress specifically to short telomeres<sup>284,528</sup>. Considering this, we wondered if Sen1 might have a role in RNA-DNA hybrid removal during senescence. For this purpose, we employed the temperature sensitive allele *sen1-1*<sup>197</sup>. Unfortunately, due to the high mutagenic potential of this mutant, liquid senescence curves at non-permissive temperatures lead to formation of suppressor mutations. And so, we could not proceed with experiments in this context. Therefore, we performed senescence spotting assays in order to qualitatively test the senescence rate of *sen1-1* in the absence of telomerase (*est2*). After 2 days, the first dilution of each genotype was re-spotted, from the permissive temperature of 25°C, to 25°C and semi-permissive temperatures (28-29°C) to inactivate *SEN1* and track cell viability (senescence) through consecutive passages (Figure 28A). At permissive temperature (25°C), we can detect senescence through the passages but no Sen1 effect (Figures 28B and 28C, *est2* mutants at 25°C), and no loss of viability is detected in telomerase positive cells (Figures 28B and 28C).

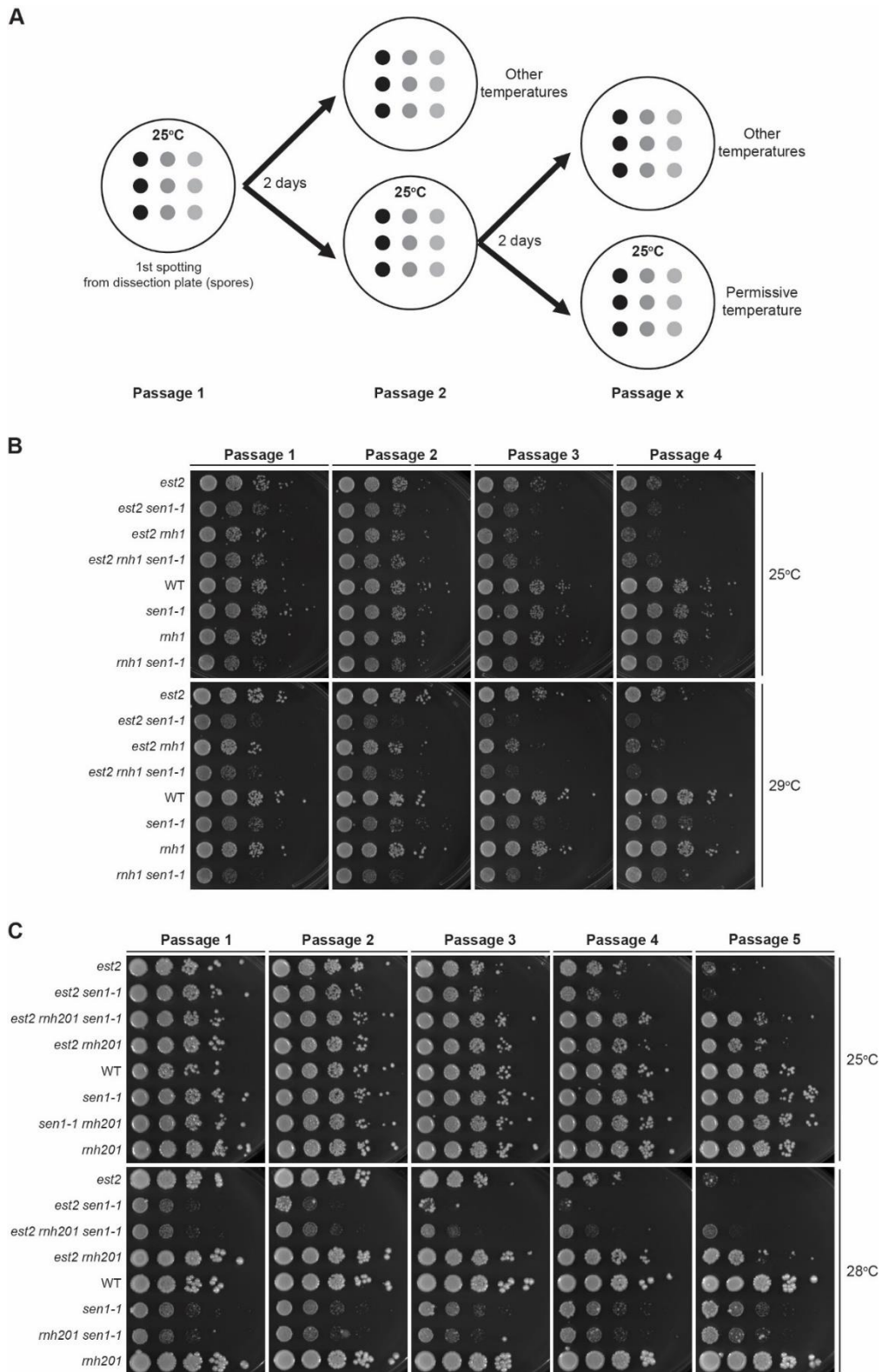


**Figure 28. RNase H1 and Sen1 are epistatic in the absence of telomerase (*est2*).**

(A) Schematic representation of the senescence spotting assay – due to the temperature allele *sen1-1*, cells were maintained at 25°C, and re-spotted every 2 days to acquire the different passages from the first spot. To inactivate *sen-1*, the cells were also spotted onto YPD plates placed at other semi-permissive temperatures (28-29°C) and senescence was tracked through consecutive passages.

(B-C) Senescence spotting - 10-fold serial dilutions of the indicated strains were spotted onto YPD plates and incubated at the indicated temperatures. After 2 days, the first dilution at 25°C was re-spotted onto new YPD plates for a new passage and placed at 25°C and other semi-permissive

temperatures (28-29°C). Images were taken after 3 days growth at the indicated temperatures. Images are representative of 5 biological replicates with 2 technical replicates for re-spotting.

At semi-permissive temperatures, with the inactivation of Sen1 (*sen1-1*), we detected growth defects of *sen1-1* mutants independently of telomerase status (Figures 28B and 28C). However, a fast senescence phenotype can also be detected in *est2 sen1-1* mutants when comparing the growth to *est2* cells (Figures 28B and 28C). The RNase H nucleases and the Sen1 helicase are the two major families of RNA-DNA hybrid resolution in budding yeast, especially considering that there is toxic accumulation of R-loops leading to cell death in *rnh1 rnh201 sen1-1* mutants<sup>198</sup>. Next, we tested if the RNA-DNA hybrid regulators work in the same pathway at telomeres. Therefore, we deleted *RNH1* and *RNH201* individually in *est2 sen1-1*, and compared senescence rates with the same senescence spotting setup (Figures 28B and 28C). We observed a fast senescence phenotype that is similar to the one observed when *RNH1* is deleted in *est2 rnh1* mutants (Figure 27A and PB). Sen1 inactivation promotes faster senescence when compared to *RNH1* deletion (Figure 28B). Nonetheless, when evaluating the senescence rate of the triple mutant *est2 rnh1 sen1-1* we do not detect any additive effect (Figure 28B), indicating that most likely RNase H1 and Sen1 are epistatic in replicative senescence. When evaluating the effect of RNase H2, we can repeat the observed phenotype of delayed senescence for the *est2 rnh201* mutants (Figures 27A and 28C). Analysing the growth of the triple mutant *est2 rnh201 sen1-1*, we can detect an additive effect, where similarly to the *est2 rnh1 rnh201* senescence rate (Figure 27A). We observe a delay in senescence onset in *est2 rnh201 sen1-1* when compared to *est2* but not to the same extent as *est2 rnh201* (Figure 28C). These observations suggest that RNase H1 and Sen1 might act in a similar fashion at telomeres, but differently than RNase H2 in order to remove RNA-DNA hybrids at the critically short telomere and promote HDR.

### 2.3.2 Hyper-Stabilization of RNA-DNA Hybrids Leads to a Fast Senescence Phenotype

The overexpression of *RNH1* greatly accelerates the senescence rates in the absence of telomerase, also impacting telomere recombination which decreases when RNA-DNA hybrids are removed from telomeres<sup>345</sup>. RNA-DNA hybrids have been shown to promote DNA repair at DSB sites, forming at the break site and consequently recruiting DNA repair factors<sup>76,394,395</sup>. However, for completion of repair and HDR to occur, the RNA-DNA hybrid needs to be removed, and several nucleases and helicases have been found

to be recruited to sites of DSB for this purpose<sup>76,395,400</sup>. It appears that for efficient HDR to occur, the RNA-DNA hybrid needs to be removed. To understand the impact of hyper-stabilized RNA-DNA hybrids at telomeres during senescence, we used a catalytic dead version of *RNH1* (*RNH1-D193N*), where RNA-DNA hybrid accumulation at telomeres is known to occur<sup>529</sup> and evaluated the senescence rate. In telomerase negative (*est2*) cells, both the removal of RNA-DNA hybrids by *RNH1* overexpression (Figure 29, red line) as well as the hyper-stabilization of RNA-DNA hybrids by overexpression of a catalytic dead version of *RNH1* (*RNH1-D193N*, Figure 29, blue line) lead to a fast senescence phenotype when compared to *est2* mutants transformed with an empty vector (Figure 29, black line). This data indicates that, also at telomeres, there is a requirement for RNA-DNA hybrids to promote HDR<sup>345</sup>. Nonetheless, timely removal of the RNA-DNA hybrids is also necessary<sup>416,530</sup> (Figure 29).

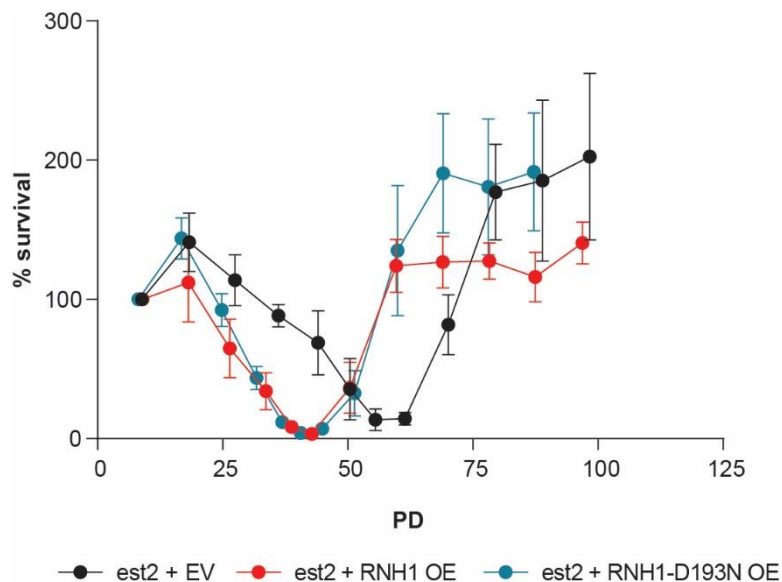


**Figure 29. Removal or hyper-stabilization of RNA-DNA hybrids leads to fast senescence.**

Senescence curve was performed in telomerase defective cells (*est2*) with the indicated plasmids, and viability was estimated daily by measuring cell culture density, with the first measurement set to 100%. Data are shown as mean  $\pm$  SEM;  $n \geq 5$  biological replicates per genotype.

### 2.3.3 Exo1 Deletion is Epistatic with RNases H

We observed that RNA-DNA hybrids prevent resection at dysfunctional telomeres in the *cdc13-1* background (Section 1.1 of Results). *EXO1* is known for contributing to telomere maintenance independently of telomerase<sup>531</sup>, playing a role in survivor formation<sup>532</sup>, and leading to a delay in senescence onset when impaired in telomere deficient cells (*est2 exo1*)<sup>285,532,533</sup>. Therefore, we questioned how *EXO1* deletion influences

rates of senescence when the RNase H nucleases are deleted, either in combination (*rnh1 rnh201*) or individually (*rnh1*; *rnh201*).

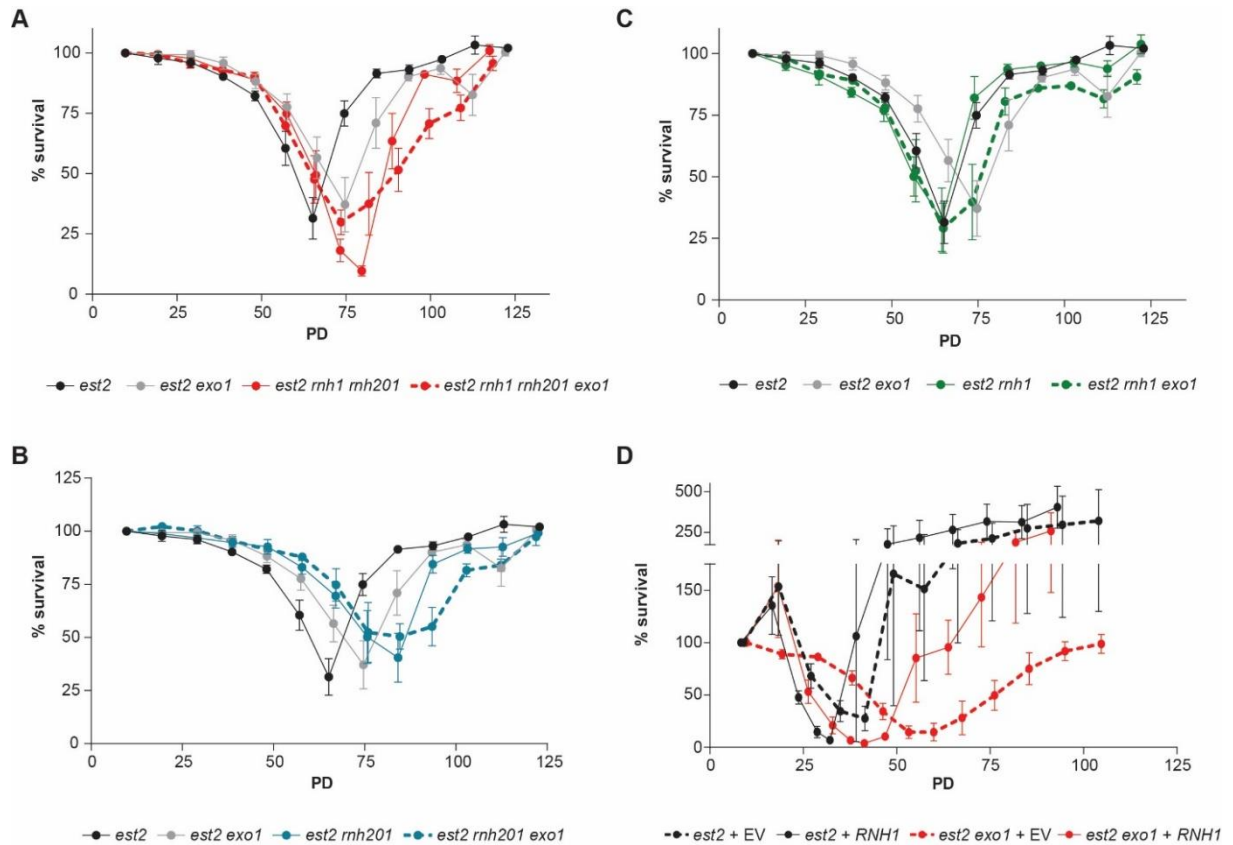


**Figure 30. Exo1 deletion is epistatic with RNases H senescence phenotype.**

(A-D) Senescence curves were performed in telomerase defective cells (*est2*), and viability was estimated daily by measuring cell culture density, with the first measurement set to 100%. In (D), the telomerase defective cells (*est2*) were transformed with the indicated plasmids. Data are shown as mean  $\pm$  SEM;  $n \geq 5$  biological replicates per genotype.

We could recapitulate the delay in senescence observed for *est2 exo1* when compared to *est2* cells (Figures 30A, 30B and 30C, grey versus black lines). When accounting for the RNase H presence or absence, we detect the same senescence onset behaviour, i.e. epistasis, when *EXO1* is deleted in combination with either or both RNase H1 and H2 (Figures 30A, 30B, 30C). Meaning that when comparing *est2 rnh1 rnh201* with *est2 rnh1 rnh201 exo1* we detect the same senescence rate (Figure 30A, full red line versus dashed red line). The same is true when comparing *est2 rnh1* with *est2 rnh1 exo1* (Figure 30B, full green line versus dashed green line) and *est2 rnh201* with *est2 rnh201 exo1* (Figure 30C, full blue line versus dashed blue line). The only observable difference is a delay in survivor formation in the absence of RNase H activity (Figures 30A, 30B and 30C). Upon *RNH1* overexpression, in both *est2* as well as *est2 exo1* mutants, we can observe a faster rate of senescence when compared to the empty vector transformed counterparts

(Figure 30D, full versus dashed lines). Taken together, these data suggest that the senescence rate delay observed when *EXO1* is impaired is RNA-DNA hybrid dependent (Figure 30D), however, when entering senescence, and until the crisis point is reached, the presence or absence of Exo1 is redundant to which RNase H nuclease is present (Figures 30A, 30B and 30C). Indicating a role for RNA-DNA hybrid regulation upstream from resection in replicative senescence.

### 2.3.4 RNA-DNA Hybrids do not Affect Rates of Telomere Shortening

Together with the prevention of resection at dysfunctional telomeres (Section 1.1 of Results), and the epistasis observed between *exo1* and the RNases H nucleases, we wondered if RNA-DNA hybrids might prevent resection, and hence rate of shortening, during replicative senescence when telomerase is deleted. We derived telomerase mutant cells (*est2*) in the absence and presence of RNase H activity. It is known that the loss of RNase H function delays replicative senescence onset<sup>345</sup> (Figure 31A). Even though telomeres were consistently longer in the absence of RNase H enzymes (*rnh1 rnh201*) (Figures SB and SC), the rate of telomere shortening was unaltered (Figure 31D). Consistent with the literature, the overexpression of *RNH1* greatly accelerated the onset of senescence in the absence of telomerase<sup>345</sup> (Figure 31E). Also here, although telomeres were in general shorter when RNase H was overexpressed (Figures SF and SG), the rate of telomere shortening was only slightly altered (Figure 31H). Taken together, even though RNA-DNA hybrids can prevent nuclease-mediated resection at dysfunctional telomeres, in a *cdc13-1* context, they appear to not contribute to telomere shortening in pre-senescent cells with intermediate length telomeres. Hence, with the data collected so far, TERRA appears to have two critical roles at telomeres: 1. Hindering nucleolytic processing and 2. Promoting HDR at critically short telomeres.

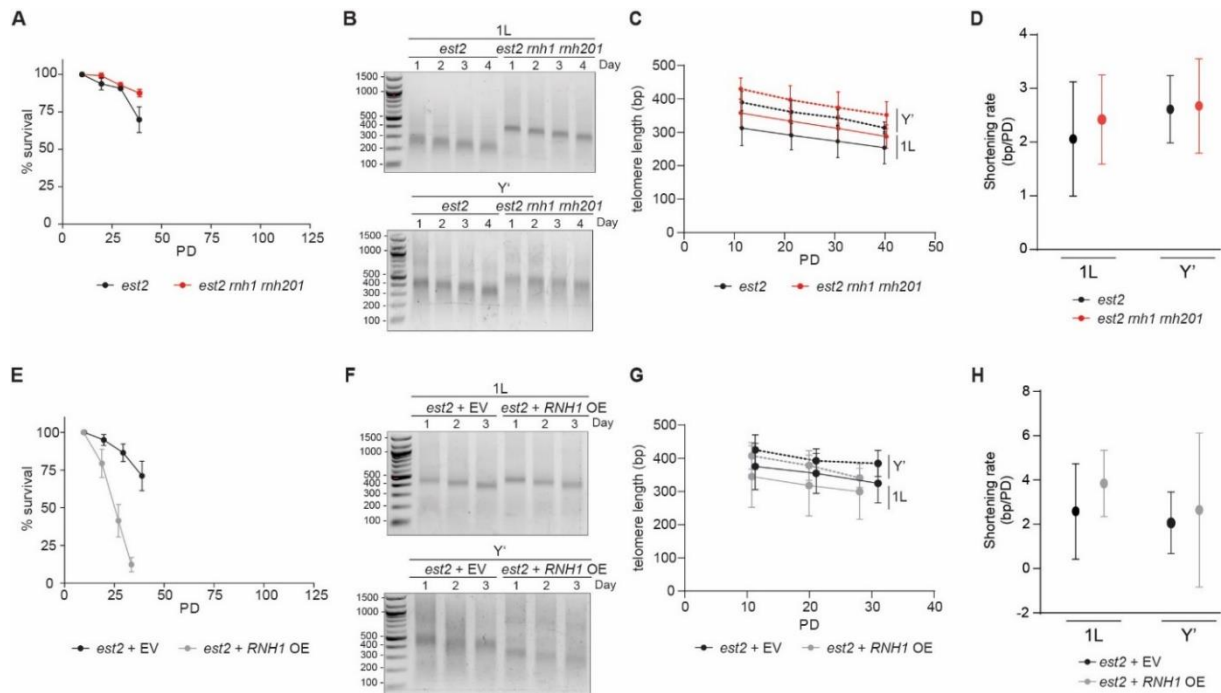


**Figure 31. RNA-DNA hybrids do not affect telomere shortening rate in pre-senescent cells.**

(A) Senescence curves were performed in telomerase defective cells (*est2*), and viability was estimated daily by measuring cell culture density, with the first measurement set to 100%. Data are shown as mean ± SEM; n ≥ 5 biological replicates per genotype.

(B-C) Telo-PCR analysis of telomere length in *est2* and *est2 mh1 mh201* cells during pre-senescence (Days 1-4). Representative gels (B) and telomere length (C) of Telomeres 1L and Y' are described. Experiment performed by Nina Lohner.

(D) Quantification of shortening rate (bp/PD) for the telomeres analysed (1L, Y') depicted in (C). Data are depicted as mean + SD, n = 4.

(E) Senescence curves were performed in telomerase defective cells (*est2*) transformed with the indicated plasmids, and viability was estimated daily by measuring cell culture density, with the first measurement set to 100%. Data are shown as mean ± SEM; n ≥ 5 biological replicates per genotype.

(F-G) Telo-PCR analysis of telomere length in *est2 + EV* and *est2 + RNH1 OE* cells during pre-senescence (Days 1-3). Representative gels (F) and telomere length (G) of Telomeres 1L and Y' are described. Experiment performed by Nina Lohner.

(H) Quantification of shortening rate (bp/PD) for the telomeres analysed (1L, Y') depicted in (G). Data are depicted as mean + SD, n = 4. EV, empty vector.





### 3 DISCUSSION

---

When critically short telomeres arise in budding yeast, TERRA RNA-DNA hybrids become stabilized and drive homology-directed repair (HDR) in order to delay replicative senescence onset<sup>236,285,345</sup>. However, even at long- and intermediate-length telomeres, which are not subjected to HDR<sup>285</sup>, there is the formation of transient RNA-DNA hybrids, suggestive of additional roles. Here, we showed that telomeric RNA-DNA hybrids can prevent Exo1-mediated resection when telomeres become dysfunctional. Using the well-characterized *cdc13-1* allele, where telomere resection can be induced in a temperature-dependent manner, we demonstrated that ssDNA generation at telomeres is either prevented when RNA-DNA hybrids are stabilized or increased when RNA-DNA hybrids are destabilized. The viability of *cdc13-1* cells is affected by the presence of such hybrids, which promote cell viability. On the contrary, the absence of RNA-DNA hybrids leads to cell death. Additionally, telomeric RNA-DNA hybrids do not affect the shortening rate of bulk telomeres. Taken together, these data suggest that TERRA RNA-DNA hybrids require a dynamic regulation in order to promote HDR at short telomeres. In particular, hybrids may initiate HDR through replication stress, although hybrid removal is required for strand resection, completion of repair, and subsequently telomere re-elongation.

#### 3.1 RNA-DNA HYBRIDS PREVENT RESECTION AT DYSFUNCTIONAL TELOMERES

RNA-DNA hybrids are required at a subset of DSBs to ensure efficient HDR, and promote DSB repair completion<sup>76,395,398</sup>. In agreement with this, at critically short telomeres in the absence of telomerase, RNA-DNA hybrids become stable and promote HDR at the short telomere<sup>236,285,345</sup> (Figure 32). Nevertheless, TERRA RNA-DNA hybrids can also form at long- and intermediate-length telomeres, where they are transient. Indeed, RNase H2 is recruited to these telomeres, through its interaction with the telomeric protein Rif2<sup>236</sup>, and is able to remove RNA-DNA hybrids before potential encounters with the replication machinery might occur (Figure 32). It is not yet understood if TERRA and telomeric RNA-DNA hybrids might have a role at longer telomeres. Nevertheless, if they do, since long telomeres are not subject to HDR<sup>285</sup>, their role is most likely different from that at short telomeres. In Pires et al., 2023<sup>515</sup>, we demonstrated that RNA-DNA hybrids can prevent Exo1-mediated resection at uncapped telomeres, using the *cdc13-1* background (Section 2.1 of Results). The resection inhibition observed here was limited to dysfunctional

telomeres, as we were unable to detect effects on telomere shortening rates when RNA-DNA hybrid were misregulated at telomeres during replicative senescence, i.e. in the absence of telomerase (Section 2.3.4 of Results).

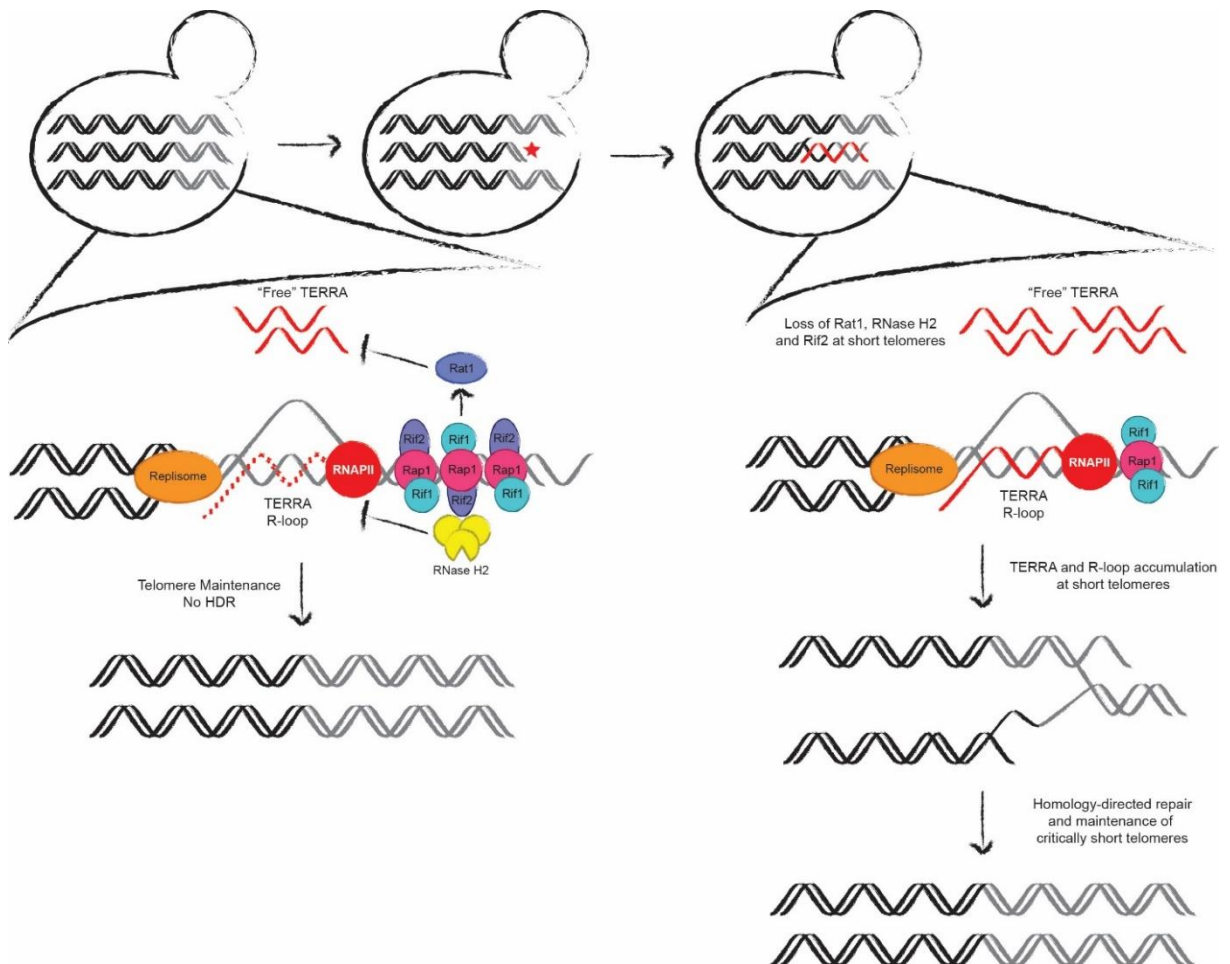


**Figure 32. Length-dependent Regulation of TERRA RNA-DNA Hybrids.**

At long- and intermediate-length telomeres, the presence of Rif2 molecules allows for the recruitment of RNase H2 to telomeres that mediates an RNase H2-dependent degradation of TERRA RNA-DNA hybrids. The exonuclease Rat1, which can genetically interact with Rap1 and Rif1, suppresses high “free” TERRA levels through degradation. Through Rat1 and RNase H2 activity, “free” TERRA and TERRA telomeric hybrids are regulated at long- and intermediate-length telomeres (left diagram). Upon telomere shortening, Rif2 binding to telomeres decreases, leading to loss of recruitment of RNase H2 to telomeres, thereby accounting for the increase in TERRA RNA-DNA hybrids at short telomeres. Additionally, Rat1 recruitment is also impaired, resulting in accumulation of “free” TERRA. The accumulation of TERRA RNA-DNA hybrids at short telomeres promotes activation of the DNA damage response (DDR) and Homology-directed repair (HDR)-mediated re-elongation to prevent premature senescence onset (right diagram). Figure and Legend adapted from Graf et al 2017.

The ssDNA telomeric binding Cdc13-Stn1-Ten1 (CST) complex is able to prevent resection at chromosome ends<sup>156</sup>. Through its association with the G-rich ssDNA 3' overhang, the CST complex can protect telomeres from the resection factors Exo1 and Pif1<sup>156</sup> (Figure 33). When the CST complex is impaired, for e.g. when the *cdc13-1* allele is

inactivated, at temperatures above 26°C, the Exo1 nuclease resects the 5' strand, thus creating an extended 3' G-rich overhang, which gets coated with the ssDNA binding factor RPA (Figure 33). The accumulation of RPA at telomeres leads to the activation of the DNA damage checkpoint through Mec1, Rad9, and Rad53, resulting in a G2 phase cell cycle arrest, which ultimately leads to halting of cell growth and proliferation. Even though TERRA RNA-DNA hybrids form in *cdc13-1* cells (Figure 33, Top), they are not stable and are therefore rapidly removed by endogenous RNase H activity. In this scenario, where RNase H activity is intact, the inactivation of the CST complex renders telomeres vulnerable to nuclease-mediated resection (Figure 33, left). However, when the RNase H enzymes are compromised (e.g. deleted), RNA-DNA hybrids become stabilized at telomeres, and prevent Exo1 from resecting the 5' strand (Figure 33, right). Indeed, by using two independent methods, we detected less ssDNA accumulating in *cdc13-1 rh1 rh201* cells at semi-permissive temperature (Section 2.1.3 Figure 21 of Results) and more ssDNA accumulating when RNA-DNA hybrids were removed through *RNH1* overexpression (Section 2.1.3 Figure 22 of Results). Moreover, *in vitro* studies have shown that RNA-DNA hybrid substrates strongly suppress Exo1 resection, when compared to dsDNA substrates<sup>534</sup>. In addition, the removal of hybrids at DSBs through RNase H overexpression has been shown to promote end resection *in vivo*<sup>535</sup>. Taken together, these data strongly suggest that the accumulation of RNA-DNA hybrids at telomeres prevents Exo1-mediated resection, conferring a capping-like protection of dysfunctional telomeres.

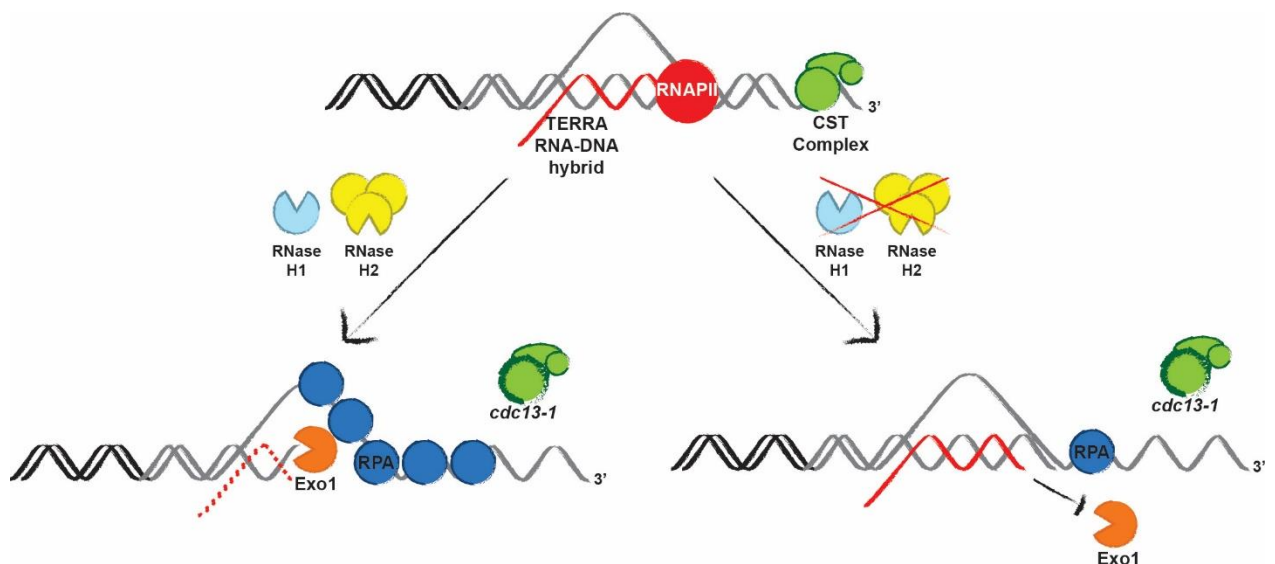


**Figure 33. RNA-DNA hybrids can prevent resection of uncapped telomeres.**

Schematic representation of the role of RNA-DNA hybrids in *cdc13-1* to impede Exo1-mediated resection and protect uncapped dysfunctional telomeres. With the increase in temperature, and the consequent induction of telomere uncapping in the *cdc13-1* mutant, if the RNase H enzymes are present, RNA-DNA hybrids are removed from telomeres (red dashed line, left diagram), extensive

Exo1-mediated resection occurs leading to cell cycle arrest and cell death (left diagram). When RNA-DNA hybrids accumulate at dysfunctional telomeres, in the absence of the RNase H enzymes, Exo1-mediated resection is impaired and this allows for telomere capping and subsequently cell survival. Figure and Legend adapted from Pires et al 2023.

Even though we observed a rescue in *cdc13-1* viability when accumulating RNA-DNA hybrids with the *sen1-1* allele, we could not recapitulate this rescue with an auxin-inducible degron allele of *SEN1* (*SEN1-AID\**) (Section 2.1.1 Figure 12 of Results). In addition, upon *RNH1* overexpression in *cdc13-1 sen1-1* cells, we observe the same growth defect present in *cdc13-1* cells, indicating that the rescue phenotype observed in *cdc13-1 sen1-1* might not be dependent on RNA-DNA hybrids (Section 2.1.1 Figure 14 of Results). Moreover, when trying to confirm that RNA-DNA hybrids accumulate at telomeres in *cdc13-1* cells when Sen1 activity was impaired, we could not detect increased RNA-DNA hybrids at telomeres via S9.6 DRIP<sup>197,516</sup> (Section 2.1.1 Figure 13 of Results). Taken together, this suggests that the rescue observed in *cdc13-1* cells by the *sen1-1* mutant may be indirect. However, these experiments have a potential caveat, regarding technical limitations for the DRIP assay with *sen1-1* cells. We cannot rule out a lack of RNA-DNA hybrid accumulation due to the simultaneous inactivation of Sen1 and Cdc13, since both *sen1-1* and *cdc13-1* alleles are temperature sensitive at slightly different temperatures. It is possible that RNA-DNA hybrids cannot accumulate or even form at these loci before resection happens, due to the loss of Cdc13 from telomeres occurring potentially before the accumulation of the RNA-DNA hybrids even occurs. To further understand if Sen1 indeed does not play a role at dysfunctional telomeres, it might be important in the future to perform DRIP experiments with the *SEN1-AID\** allele, where inactivation of Sen1, and consequently RNA-DNA hybrid accumulation can be induced before the shift to a higher temperature in the *cdc13-1* background, thus separating the RNA-DNA hybrid accumulation from telomere uncapping. This might shed some light if the *sen1-1* rescue observed is direct or indirect in the *cdc13-1* background, when looking at RPA and ssDNA accumulation in this scenario.

To rule out a potential indirect effect due to any temperature sensitivity of the *rnh1 rnh201* deletion, we tested whether the rescue of *cdc13-1 rnh1 rnh201* cells was specific to telomere dysfunction. Using temperature sensitive alleles not involved in telomere function, *cdc15-2* and *cdc7-4* mutants, we did not observe a growth improvement in either mutant upon loss of RNase H activity (*rnh1 rnh201*), suggesting that RNA-DNA hybrid accumulation is not benefiting temperature sensitive alleles in general but specifically *the cdc13-1* background (Section 2.1.1 Figure 16 of Results). Moreover, *RNH1* overexpression did also not reduce the viability of *cdc15-2* mutants (Section 2.1.1 Figure 16 of Results), further indicating a specificity for hybrids at dysfunctional telomeres.

Cdc13 is a part of the CST complex, and so we wondered if other members of the complex would have similar phenotypes and effects on resection. We therefore used a temperature sensitive allele of Stn1, *stn1-13*. Interestingly, in this background, we could not recapitulate the same phenotype present for *cdc13-1*, i.e. no rescue was observed upon RNA-DNA hybrid accumulation (*rnh1 rnh201* deletion) nor any growth impairment was observed upon *RNH1* overexpression (Section 2.1.1 Figure 16 of Results). Despite the fact that deletion of any subunit of the CST complex leads to a lethal phenotype, due to telomere deprotection<sup>38,39,51</sup>, it is known that Stn1 and Ten1 have Cdc13-independent functions<sup>23,44,45</sup>. Moreover, it has been shown that Cdc13 has a predominant role over Stn1 and Ten1 in preventing chromosome end fusions<sup>517</sup>. It would therefore be interesting to understand how Ten1 responds to the stabilization and destabilization of hybrids, through the usage of a temperature sensitive allele, for e.g. *ten1-31*<sup>39</sup>, to further understand how the CST complex as a whole is affected by RNA-DNA hybrids.

Cdc13 not only regulates the protection of the telomeric ends, but also has a role in telomerase recruitment and C<sub>1-3</sub>A strand re-synthesis by DNA polymerase  $\alpha$ <sup>54</sup>. Through its association with Ten1 and Stn1, Cdc13 forms the CST complex that is essential for telomere capping<sup>38,39,51</sup>. On the other hand, at the expense of the Cdc13-Stn1 interaction, Cdc13 can associate with the Est1 subunit of telomerase, and promote its recruitment to chromosome ends<sup>53,241,248,536,537</sup>. Moreover, Cdc13 plays a role in the synthesis of both strands at telomeres, and by promoting C-strand synthesis, it can limit continuous telomerase action<sup>40,57,538</sup>. Cdc13 and Stn1 physically interact with the DNA polymerase  $\alpha$ -primase complex, promoting its recruitment to telomeric DNA<sup>49,50,56,57</sup>. Therefore, Cdc13 is at the crossroads of telomerase action, where its activity is dependent on post-translational modifications, and the phase of the cell cycle<sup>142,539-542</sup> (Figure 34).

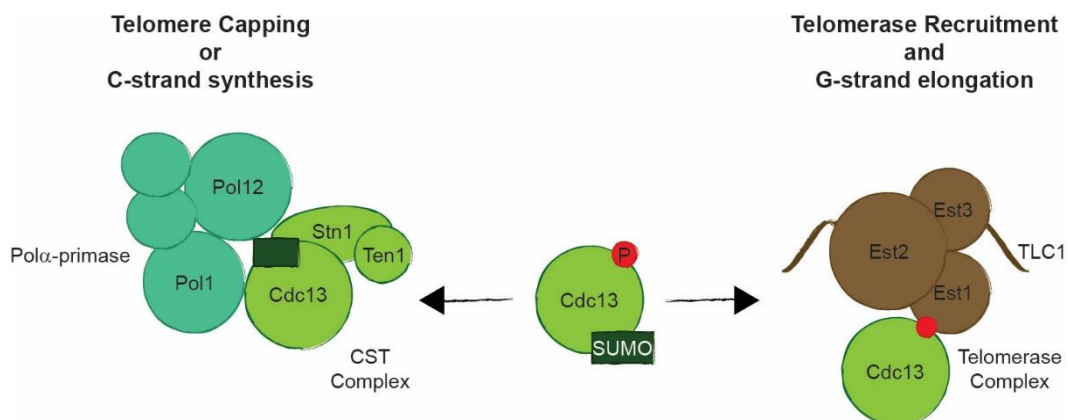


**Figure 34. Cdc13 at the crossroad of telomerase action.**

Cdc13 forms separate complexes with different functions at telomeres. Cell-cycle regulated post-translational modifications control the balance between these complexes. SUMOylation in the C-

terminus of Cdc13 promotes Stn1 interaction, and formation of the CST complex. Cyclin-dependent kinase phosphorylation of Cdc13 favours the interaction with Est1, at the expense of its interaction with Stn1, thus promoting telomere uncapping and telomerase recruitment. When telomerase action is accomplished, Cdc13 switches back to interaction with Stn1, and the CST complex recruits the pol $\alpha$ -primase complex for C-strand synthesis. Figure and Legend adapted from Churikov et al 2013.

It is also known that inactivation of Cdc13 leads to generation of Exo1-dependent ssDNA leading to unstable chromosomes, which are an additional source of genome instability in these cells<sup>147</sup>. This genome instability is due to defects in telomere replication, indicating that the CST capping function relies on its involvement in supporting telomeric DNA replication<sup>147</sup>. Indeed, telomere-binding proteins themselves can represent intrinsic obstacles for replication fork progression<sup>148,149</sup>, thereby the role of the CST complex in supporting pol $\alpha$ -primase activity could facilitate lagging strand repriming, to compensate for fork stalling during telomere replication<sup>65</sup>. Considering the involvement of the CST complex in C-strand fill-in synthesis, we did not investigate the possibility of the rescue present in *cdc13-1* mutants when RNA-DNA hybrids accumulate being somehow due to Pol $\alpha$ -primase activity. Considering that the impairment of Cdc13 or Ten1 in combination with Pol1, the catalytic subunit of Pol $\alpha$ -primase complex, or Stn1 and Pol12, the B subunit of Pol $\alpha$ -primase complex, leads to a synthetic growth defects<sup>50,146</sup>, suggesting that Pol $\alpha$ -primase activity is important for cell viability. Therefore, investigating how *pol1-* or *pol12-ts* alleles in combination with the *cdc13-1* background, might be affected by the stabilization or destabilization of RNA-DNA hybrids, i.e. *rnh1 rnh201* deletion or *RNH1* overexpression, respectively, might shed more light into how resection is being affected at these dysfunctional telomeres. It is important to note that no increase in ssDNA accumulation was observed in *ten1-ts pol1-ts (cdc17-1)* mutants, indicating that the growth defect present is not due to increased DNA end resection<sup>146</sup>. It could also be interesting to check how other Cdc13 mutants react to RNA-DNA hybrids, namely in the case of *cdc13-2* and *cdc13-5*, where telomerase regulation is impaired<sup>55,538</sup>, in order to further understand mechanistically how RNA-DNA hybrids are promoting capping at dysfunctional telomeres.

G-quadruplex (G4) structures have been reported to form on the G-rich displaced strand of an R-loop<sup>543</sup>. Furthermore, the stabilization of G4 DNA with small molecules or peptides leads to the rescue of viability defects of *cdc13-1* mutants, by preventing DNA end resection<sup>75</sup>. Therefore, we wondered if RNA-DNA hybrids at telomeres might be preventing resection through the stabilization of G4s, on the G-rich displaced strand. Through BG4 ChIP<sup>523</sup> in a *cdc13-1* background, we detected less G4 levels at telomeres in *rnh1 rnh201* mutants, and no difference in cells that were overexpressing *RNH1* (Section 2.1.2 Figure 20 of Results). In a *CDC13* WT background, i.e. with functional Cdc13, we can detect slight increases in G4 levels in *rnh1 rnh201* mutants, and upon the *RNH1* overexpression in WT

cells (Section 2.1.2 Figure 20 of Results). Considering these results, it seems unlikely that the influence of RNA-DNA hybrids on DNA end resection are an indirect effect of G4 stabilization in *cdc13-1* cells.

We also considered that *RNH1* overexpression may be suppressing the *cdc13-1* phenotype in an indirect manner, i.e. through the up- or down-regulation of factors that affect *cdc13-1* viability. However, analysis of the proteome upon *RNH1* overexpression revealed that only a handful of proteins are detected as differentially expressed (Section 2.1.1 Figure 17 and Table 2 of Results). Of those, only a few were previously identified to be *cdc13-1* interactors according to the BioGRID database (Section 2.1.1 Figure 17 of Results). In some cases, we were unable to recapitulate the genetic interactions reported from the BioGRID database, thereby ruling them out as potential indirect effectors. In the instances where we could detect the reported genetic interaction, we found that they were not epistatic with misregulation of RNA-DNA hybrids (Section 2.1.1 Figure 17 of Results).

These results raise the interesting question of how RNA-DNA hybrids promote HDR at critically short telomeres, when at the same time they prevent DNA end-resection, which is a critical step to generate 3' ssDNA for strand invasion in HDR. We can speculate that at critically short telomeres, the stabilization of RNA-DNA hybrids might cause replication stress, which has been observed at short telomeres<sup>528</sup>. The stalled polymerase in combination with the RNA-DNA hybrid may cause a conflict with the replication machinery at critically short telomeres<sup>366,544,545</sup>. This may lead to the recruitment of the recombination machinery, while at the same time prevent extensive resection. Eventually, the RNA-DNA hybrid would have to be removed to allow resection and generation of the 3' ssDNA. Indeed, at DSBs in human cells, although the factors involved may differ depending on the context of repair, it appears that following 5'-end resection at the DSB, an RNA-DNA hybrids forms at the exposed 3' end, which leads to the recruitment of repair factors, as for e.g. RAD52, XPG, BRCA1, and BRCA2<sup>395,397,405</sup>. Moreover, the RNA is subsequently removed by nucleases or helicases that are recruited to the DSB site, as for e.g. Senataxin, RNase H1, RNase H2, DDX1 or DDX5<sup>76,395,400,406,480,546</sup>, thereby allowing RAD51 loading and efficient completion of homologous recombination<sup>395,397,400,406</sup>.

Overall, these data demonstrate that TERRA and its associated RNA-DNA hybrids are able to prevent telomere end resection in the *cdc13-1* model. These observations add another layer to the regulation that occurs at short telomeres, in order to promote HDR, and prevent accelerated senescence. In the end, TERRA, like other non-coding RNAs (ncRNAs) that form RNA-DNA hybrids at sites of damage must be allowed to form an hybrid, which must subsequently be removed in a timely manner<sup>367</sup>, in this instance to allow end resection.

Therefore, RNA-DNA hybrids at DSBs and telomeres require a dynamic regulation to allow for efficient repair.

### 3.2 RNASE H1 AND H2 ARE DIFFERENTIALLY REGULATED TO PROCESS RNA-DNA HYBRIDS

RNase H2 provides the majority of the RNase H activity in the cell, however it is only weakly associated with chromatin by ChIP<sup>462</sup>. On the other hand, RNase H1 was found associated with multiple R-loop loci along the genome, but this association does not always translate into active processing of R-loops from chromatin<sup>462</sup>. For this reason, it has been speculated that the RNase H enzymes might be differentially regulated, with RNase H2 being regulated in terms of cell cycle, and RNase H1 regulation responding to R-loop-associated cellular stress<sup>462</sup>. Moreover, since *RNH1* overexpression promotes R-loop degradation throughout the genome, this suggests that a potential repressor may exist and need to be inhibited in order for RNase H1 activity to be unleashed<sup>462</sup>. Indeed, *E.coli* RNase H has been shown to bind different RNA-DNA hybrid substrates, yet its activity is determined by the type of overhang present at the RNA-DNA hybrid<sup>547</sup>. Moreover, when overexpressed, there is no longer any substrate discrimination, since RNase H1 can act without restriction<sup>547</sup>.

In Lockhart et al 2019, using cell-cycle-restricted alleles of RNase H1 and RNase H2, we were able to confirm the cell cycle requirement for RNase H2 recruitment and activity, in R-loop as well as ribonucleotide removal (Figure 35). In addition, we were able to demonstrate that RNase H1 is likely reacting to R-loop-mediated stress, in a cell cycle-independent manner (Figure 35). With endogenously tagged strains for RNase H1 and RNase H2, *RNH1-TAP* and *RNH201-MYC*, respectively, we could track chromatin association through the cell cycle (Section 2.2 of Results).

Indeed, the RNase H2 activity coincided with its association to chromatin in a post-replicative manner in the G2/M phase of the cell cycle, with RNase H2 being present in chromatin in early S-phase but its recruitment increasing with progression of the cell cycle (Section 2.2.1 Figure 25 of Results). Moreover, at telomeres, RNase H2 recruitment is also cell-cycle regulated, since through ChIP assays it was demonstrated that the recruitment of RNase H2 occurs only very late in the S phase<sup>236</sup>.

RNase H1 can interact with RPA, which may explain its constitutive localization to stable R-loops and chromatin, since RPA coats the displaced ssDNA<sup>452,548</sup>. When R-loops



accumulate and become stable, as for e.g. in *sen1-1* mutants, we detect an increase in Rnh1 association to chromatin that is cell cycle-independent (Section 2.2.2 Figure 26 of Results). Indicating, that irrespective of the cell-cycle phase, RNase H1 is able to function in scenarios where R-loops accumulate to otherwise toxic levels, and induce stress. One hypothesis remains, that in order for persistent R-loop removal to occur via RNase H1, activation of this protein has to somehow occur, either by potential post-translational modifications or by removal of an inhibitor protein.

Telomere length also influences recruitment of RNase H2, since it was shown that at short telomeres, due to the loss of Rif2 bound protein, RNase H2 is also lost from the chromosome ends thus allowing accumulation of RNA-DNA hybrids to occur<sup>236</sup>. Moreover, RNase H1 was not detected at long- and intermediate-length telomeres, in telomerase-positive cells, indicating the efficient removal of R-loops by RNase H2 in this context<sup>236</sup>. Taken together, these data suggest a differential role for the RNase H enzymes at telomeres. It is therefore of interest to understand the regulation of these enzymes and their contribution in genome maintenance with respect to RNA-DNA hybrid regulation and misregulation.

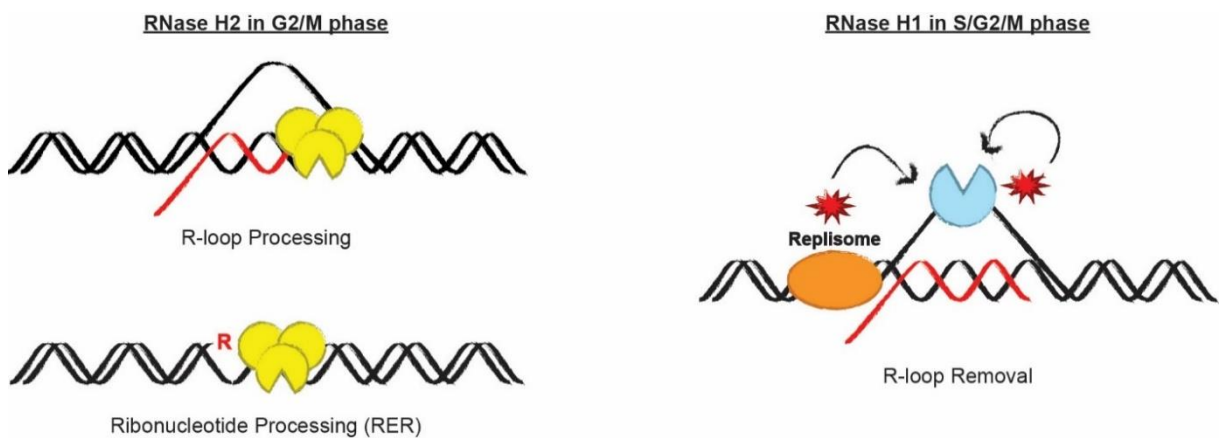


**Figure 35. Temporal Consequences of RNase H expression.**

The expression of RNase H2 in a post-replicative manner is sufficient to promote WT-like survival in the presence of excess rNMPs and stabilized R-loops. The nicks created in G2 can be repaired in a Rad52-independent manner. R-loops are processed in a non-toxic manner in G2/M (left diagram). Rnh1 is equally associated to chromatin throughout the cell cycle and accumulates in the face of R-loop-induced stress (e.g. in *sen1-1* mutants). There may be signalling from sites of R-loop stress to RNase H1 to trigger the association to chromatin/R-loops (right diagram). Figure and Legend adapted from Lockhart et al 2019.

### 3.3 RNA-DNA HYBRIDS ARE TIGHTLY REGULATED AT CRITICALLY SHORT TELOMERES

In the absence of telomerase, with each cell cycle division there is progressive telomere shortening<sup>176,182</sup>. This telomere erosion triggers the activation of the DNA damage checkpoint and, in budding yeast, one critically short telomere is sufficient to trigger an irreversible cell cycle arrest in a process called replicative senescence<sup>176,182</sup>. At telomeres, there is transcription of a long non-coding RNA TERRA<sup>335,338–340</sup>, which can form RNA-DNA hybrids<sup>236,237,33</sup>. TERRA RNA-DNA hybrids have been shown to become stabilized and aid in promoting homology-directed repair (HDR) at critically short telomeres, therefore delaying replicative senescence onset<sup>288,345,348,512,513</sup>. It is known, that in *S. cerevisiae*, repair of the shortest telomere has the effect of delaying the onset of replicative senescence<sup>285</sup>. However, how mechanistically RNA-DNA hybrids promote HDR at critically short telomeres is still not understood. Hence, we aimed to further understand how RNA-DNA hybrids are regulated during replicative senescence, and how they promote HDR.

Once formed, there are several proteins and pathways to resolve or degrade RNA-DNA hybrids in the cell. In budding yeast, the RNase H family of nucleases, comprising the RNase H1 and RNase H2 enzymes, selectively degrade the RNA moiety of an RNA-DNA hybrid<sup>446,447</sup>. Moreover, the specialized 5'-3' helicase Sen1, Senataxin in humans, can resolve RNA-DNA hybrids at transcription termination sites<sup>386,472</sup>, and DSBs<sup>400</sup> by unwinding the hybrid. The loss of these two RNA-DNA hybrid removal pathways, by the loss and impairment of these three enzymes (*rnh1 rnh201 sen1-1*), leads to irreparable damage and cell death<sup>198,464,475</sup>. While the deletion of only two of these factors still leads to viable spores, and colony growth<sup>464</sup>, which may indicate a somewhat redundant role for the RNase H enzymes genome-wide. Overall, it indicates the importance of RNA-DNA hybrid removal for cell survival, and the essential role of these RNA-DNA removal pathways for genome stability and proliferation of budding yeast cells.

At long- and intermediate-length telomeres, it was demonstrated that RNase H2 is recruited to these telomeres, through its interaction with Rif2<sup>236</sup>. Moreover, with telomere shortening, loss of Rif2 binding at telomeres occurs, and consequently loss of RNase H2, which leads to an accumulation of RNA-DNA hybrids at short telomeres<sup>236</sup>. It has been proposed that at telomeres RNase H2 plays a major role in RNA-DNA hybrid removal, while RNase H1 might play a compensatory role, since it appears to respond, genome-wide, to increased RNA-DNA hybrid levels<sup>464</sup>. Indeed, when looking at the senescence rates of RNase H mutants (*rnh1*, *rnh201*, *rnh1 rnh201*) in telomerase negative cells (*est2*), we observed a different regulation for RNase H1 and RNase H2 at telomeres (Section 2.3.1

Figure 27 of Results). The deletion of *RNH1* led to a fast senescence phenotype, while the deletion of *RNH201* produced a delay in senescence onset when compared to telomerase negative cells (*est2*). The triple mutants, *est2 rnh1 rnh201*, demonstrated a delay in senescence onset compared to *est2* mutants, however not to the same extent as *est2 rnh201* cells. Considering these results, it appears that, at telomeres, the role of the RNase H enzymes is not redundant when it comes to RNA-DNA hybrid removal. Moreover, it appears that for a maximum delay in senescence onset, removal of the RNA-DNA hybrid by RNase H1 is required. Therefore, we propose a model where RNase H2 is responsible to keep RNA-DNA hybrid levels in check at long- and intermediate-length telomeres, where it is recruited to telomeres via Rif2 (Figure 36). At short telomeres, RNase H1 might be responsible for the removal of the RNA-DNA hybrid to promote efficient HDR and re-elongation of the telomere (Figure 36). Indeed, RNase H1 is important for efficient DSB repair, since stabilization of RNA-DNA hybrids at DNA breaks impairs DNA repair<sup>76,395,400</sup>. In this direction, we also observed that stabilization of RNA-DNA hybrids using a catalytic dead version of RNase H1 (*RNH1-D193M*), which has been shown to accumulate RNA-DNA hybrids genome-wide and at telomeres<sup>529</sup>, leads to a fast senescence phenotype (Section 2.3.2 Figure 29 of Results), similar to the one observed for *RNH1* overexpression. These results indicate that the presence of RNA-DNA hybrids is important to delay senescence. In this regard *RNH1* overexpression has been linked to less HDR at telomeres<sup>345</sup>. Moreover, the stabilization of RNA-DNA hybrids at telomeres is also detrimental, demonstrating the importance of removing the hybrid to allow completion of repair, as previously observed for DSB repair<sup>76,407</sup>. We have detected that upon RNA-DNA hybrid accumulation, RNase H1 recruitment to chromatin increased<sup>464</sup>; however, how RNase H1 is recruited to telomeres is not fully understood. A potential mechanism for recruitment of RNase H1 to RNA-DNA hybrids may be stochastically through its HBD domain that can bind hybrids present in the genome. Another possibility is that RNase H1 is recruited to telomeres through its interaction with RPA<sup>452</sup>, which binds the displaced strand of R-loops, thus RPA accumulation can potentially be a signal for RNase H1 recruitment to R-loops, hence promoting its activity and R-loop removal. Nonetheless, to further understand the involvement of RNase H1 in replicative senescence, it remains to be determined if RNase H1 is recruited to critically short telomeres during senescence, by ChIP experiments.

Another candidate for removal of RNA-DNA hybrids at critically short telomeres is Sen1. Indeed, inactivation of Sen1 leads to RNA-DNA hybrids accumulation in the genome<sup>198</sup>, and Sen1 has been identified to associate with the replisome to promote genome stability<sup>475</sup>. Moreover, Sen1 has been shown to prevent transcription-replication

conflicts<sup>197,472</sup>. Therefore, we investigated the role of Sen1 during senescence (Section 2.3.1 Figure 28 of Results). Using the temperature sensitive allele, *sen1-1*, inactivation of Sen1 upon a temperature shift was possible, and we monitored replicative senescence via spotting assays. Upon Sen1 inactivation, at semi-permissive temperatures, we were able to detect a fast senescence phenotype for *est2 sen1-1* cells, when compared to *est2* cells. When combining the inactivation of Sen1 with the deletion of the RNase H enzymes, we observed a fast senescence phenotype for *est2 sen1-1 rnh1*, epistatic to the *est2 sen1-1* phenotype and a slow senescence phenotype for *est2 sen1-1 rnh201*, when compared to *est2* but not to the same extent has the delay observed in *est2 rnh201* cells. These observations indicate that RNase H1 and Sen1 might act similarly at telomeres, resolving hybrids that persist at critically short telomeres; hence, differently from RNase H2's role in RNA-DNA hybrid removal at long- and intermediate-length telomeres (Figure 36).

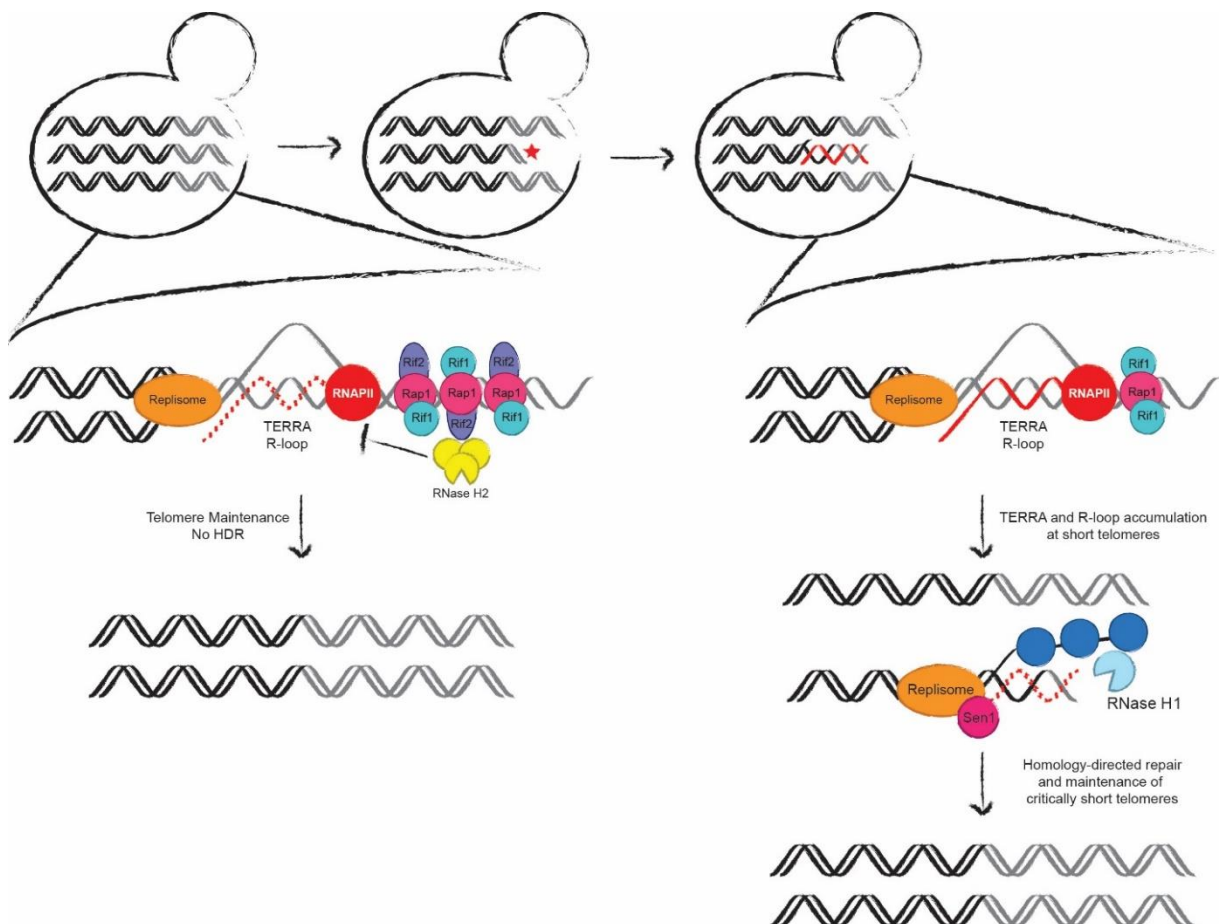


**Figure 36. RNase H1 and Sen1 are candidates for RNA-DNA hybrid resolution at critically short telomeres.**

At long- and intermediate-length telomeres, Rif2 recruits RNase H2 to telomeres, which mediates an RNase H2-dependent degradation of TERRA RNA-DNA hybrids. Upon telomere shortening, Rif2 and consequently RNase H2 are lost from telomeres, thereby increasing TERRA RNA-DNA hybrids at short telomeres. At critically short telomeres, RNase H1 or Sen1 might be recruited to promote

RNA-DNA hybrid removal, with the recruitment being potentially mediated by RPA or the replisome, respectively.

Indeed, while at dysfunctional telomeres TERRA RNA-DNA hybrids can prevent nuclease-mediated resection (Section 1.1 of Results), in pre-senescent cells, with intermediate length telomeres, RNA-DNA hybrids do not affect telomere-shortening rates. However, when analysing the telomere shortening rates, we cannot distinguish if added recombination could mask the rate of shortening. Considering that at telomeres that have persistent/stable RNA-DNA hybrids there is increased recombination<sup>345</sup>. Therefore, the mechanism by which RNA-DNA hybrids promote HDR at critically short telomeres, while at the same time preventing DNA end-resection, which is critical to generate a 3' ssDNA for strand invasion, is puzzling. At the moment we can only speculate, further studies are required to elucidate the mechanistic details of this process. However, we hypothesize that at critically short telomeres, stabilization of RNA-DNA hybrids, following TERRA transcription, may lead to replication stress. Actually, during replicative senescence, it was demonstrated that there is an increase in replication stress, which is associated to phosphorylation of the replication sensor Mrc1, and related to the critically short telomere<sup>284,528</sup>. Additionally, in human ALT cancer cells, it was reported that RNA-DNA hybrids lead to replication stress that facilitates recombination<sup>422</sup>. Hence, we have speculated that a collision between the replisome and the stable RNA-DNA hybrid may occur at critically short telomeres, which would occur in a co-directional manner, and might lead to either a break<sup>415</sup> or replication stress, and subsequently trigger HDR (Figure 37). The stalled polymerase together with the RNA-DNA hybrid would then recruit the recombination machinery, while at the same time preventing extensive DNA end-resection. Eventually, the RNA-DNA hybrid would have to be removed in order to finally allow resection, and generation of the 3' ssDNA required for strand invasion. Indeed, removal of the RNA-DNA hybrid in a timely manner appears to be critical for completion of repair, and the potential candidates to remove RNA-DNA hybrids at critically short telomeres are RNase H1 and Sen1 (Figure 37).

Moreover, in human cells, RNA-DNA hybrids have been shown to recruit HR repair factors to DSBs, where hybrid removal needs to occur to allow resection and completion of repair<sup>76,367,394–398</sup>. In particular, a repair factor that might be recruited to DSBs due to its direct interaction with RNA-DNA hybrids is Rad52 itself. It has been recently show that in human cells, Rad52 can directly bind RNA-DNA hybrids at telomeres, upon reactive oxygen species (ROS)-induced DNA damage<sup>404</sup>. In this context of ROS-induced DNA damage, there is accumulation of telomeric RNA-DNA hybrids that promote repair of telomeric DSBs through RAD52 recruitment to stimulate break-induced replication (BIR)<sup>404</sup>. Moreover, in

this study they have identified a separation of function mutant, RAD52-K144A, which can no longer bind RNA-DNA hybrids<sup>404</sup>. When comparing the RAD52 protein sequence alignment between budding yeast and human, there is conservation of this lysine in *S. cerevisiae*, at position 126. It would be interesting to investigate if budding yeast Rad52 can also bind directly to RNA-DNA hybrids *in vitro* and *in vivo*, and if this lysine is also responsible for this binding as is the case for human cells. In budding yeast, there is also another lysine at position 125, it might be of interest to see if mutation of both lysines are required for this potential binding.

At telomeres, the Ku complex is extremely important to prevent extensive DNA-end resection and protect the chromosome ends of nucleolytic activity<sup>28,96,549</sup>. At replication forks, Ku has also been implicated in regulating end-resection of unbroken forks and in fine-tuning the HR-mediated replication restart upon damage<sup>550</sup>. At DSBs, Ku's involvement in preventing long-range resection has been well established<sup>96,97,551</sup>. Moreover, it has been recently shown that the Ku complex can be recruited to DSBs in a RNA-DNA hybrid dependent manner, in the absence of Sen1<sup>401</sup>. Sen1 inactivation leads to increased recruitment of the Ku complex to DSB ends, activating an alternative resection pathway that promotes classical and microhomology-mediated NHEJ<sup>401</sup>, an error-prone mechanism for DNA DSB repair. Several DNA repair factors have been implicated in associating with the Ku complex<sup>552-554</sup>, and the complex itself has been shown to have affinity for RNA-DNA hybrid structures<sup>552</sup>. Considering this, it will be of interest to explore the role of the Ku complex in maintaining genomic stability through RNA-DNA hybrid interactions at telomeres. The Ku complex has been shown to promote both the formation and stabilization of RNA-DNA hybrids at DSB sites to promote NHEJ<sup>366</sup>. Dissecting its potential role in preventing extensive DNA-end resection at telomeres during replicative senescence, might shed some light in the timely regulation of RNA-DNA hybrids required for repair to occur, ultimately leading to telomere re-elongation.

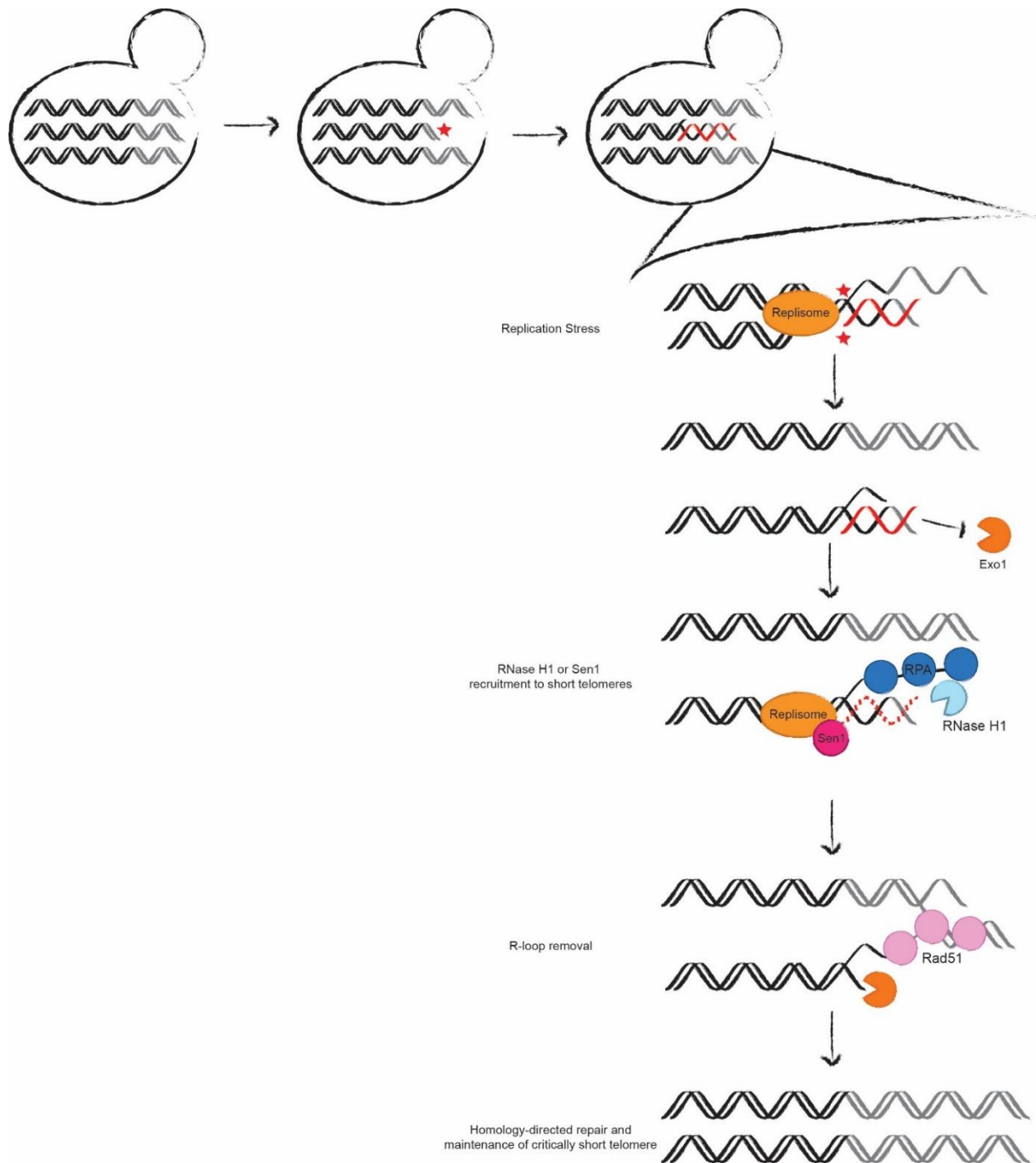


**Figure 37. Model of action of RNA-DNA hybrids at critically short telomeres.**

At critically short telomeres, accumulation of stable RNA-DNA hybrids might lead to replication stress, due to co-directional encounters between the transcription and replication machineries. This encounter might signal the need to repair this critically short telomere and promote the HDR process. The presence of the RNA-DNA hybrid might prevent DNA end resection and loss of genetic information. Through the replisome, Sen1 can be recruited to short telomeres; or through the presence of RPA in the displaced strand of the R-loop, RNase H1 recruitment can occur. These enzymes can remove the RNA-DNA hybrid allowing the resection machinery to create a long strand of ssDNA for strand invasion by Rad51 and HDR to be completed, thus re-elongating the short telomere.

### 3.4 FUTURE PERSPECTIVES

In budding yeast, TERRA RNA-DNA hybrids become stabilized at critically short telomeres and drive homology-directed repair (HDR) in order to delay replicative senescence onset<sup>236,285,345</sup>. Moreover, at long- and intermediate-length telomeres, there is formation of transient RNA-DNA hybrids; however, these telomeres are not subjected to HDR<sup>285</sup>. We uncovered a role for telomeric RNA-DNA hybrids in preventing Exo1-mediated resection at dysfunctional telomeres<sup>515</sup>. Furthermore, we demonstrated that telomeric RNA-DNA hybrids do not affect the shortening rate of bulk telomeres<sup>515</sup>. Taken together, it appears RNA-DNA hybrids require a dynamic regulation in order to promote HDR at short telomeres, where the stable hybrids may initiate HDR through replication stress. In addition, RNA-DNA hybrid removal is required for strand resection and completion of repair, for subsequent telomere re-elongation to occur. Several details of this process are still not understood, and therefore further investigation is still required to determine exactly how RNA-DNA hybrids are promoting HDR at the critically short telomere. Of importance, understanding if RNase H1 and/or Sen1 are recruited to critically short telomeres, might uncover who is responsible for the removal of the RNA-DNA hybrid to allow completion of repair. Moreover, dissecting the potential recruitment of Rad52 or the Ku complex to the critically short telomere, in an RNA-DNA hybrid dependent manner, might also shed some light on how mechanistically resection is impaired at dysfunctional telomeres and how HDR is promoted to ensure re-elongation of the critically short telomere.

Our work contributes to the understanding of RNA-DNA hybrid regulation at telomeres. Further elucidating how telomere capping and resection are impacted by RNA-DNA hybrids at dysfunctional telomeres. These observations add another layer to the regulation that occurs at critically short telomeres to promote HDR, and prevent accelerated senescence. Moreover, it demonstrates that TERRA, like other non-coding RNAs that can form RNA-DNA hybrids at damaged DNA, requires a dynamic regulation. Understanding TERRA and telomere regulation, has relevant implications in cancer and ageing research, and can have potential medical repercussions.



## 4 MATERIALS AND METHODS

### 4.1 MATERIALS

#### 4.1.1 Yeast Strains

The yeast strains used in this study are derivatives of the BY4741 background (MATa *his3Δ1 leu2Δ0 met15Δ0 ura3Δ0*)<sup>555</sup>.

Strain number	Genotype	Source
yAL352	MATa/ MATalpha <i>his3Δ1/his3Δ1 leu2Δ0/leu2Δ0 ura3Δ0/ura3Δ0 met15Δ0/met15Δ0 EST2/est2::KAN RNH201/rnh201::HYG RNH1/NAT-S-RNH1-TAP-HIS</i>	A. Lockhart
yAL842	MATa/ MATalpha <i>his3Δ1/his3Δ1 leu2Δ0/leu2Δ0 ura3Δ0/ura3Δ0 met15Δ0/met15Δ0 EST2/est2::KAN RNH1/NAT-G2-RNH1-TAP-HIS RNH201/rnh201::HYG</i>	A. Lockhart
yBB236	MATa/MATalpha <i>his3Δ1/his3Δ1 leu2Δ0/leu2Δ0 ura3Δ0/ura3Δ0 MET15/met15Δ0 EST2/est2::HYG RNH1/rnh1::KAN RNH201/rnh201::NAT</i>	Balk et al., 2013
yBL7	MATa <i>his3Δ1 leu2Δ0 ura3Δ0 met15Δ0</i>	Euroscarf
yFB357	MATa <i>his3Δ1 leu2Δ0 ura3Δ0 rnh1::KAN rnh2::HYG + pBL189 (2μ GPD-URA3)</i>	F. Bento
ySLG252	MATa <i>his3Δ1 leu2Δ0 ura3Δ0 RNH1-TAP-HIS3MX6</i>	Dharmacon
yTW602	MATa <i>his3Δ1 leu2Δ0 ura3Δ0 + pBL190 (2μ GPD-HIS EV)</i>	T. Wagner
yTW603	MATa <i>his3Δ1 leu2Δ0 ura3Δ0 + pBL192 (2μ GPD-RNH1-HA-HIS)</i>	T. Wagner
yTW614	MATa <i>his3Δ1 leu2Δ0 ura3Δ0 stn1-13::KAN + pBL190 (2μ GPD-HIS EV)</i>	T. Wagner
yTW615	MATa <i>his3Δ1 leu2Δ0 ura3Δ0 stn1-13::KAN + pBL192 (2μ GPD-RNH1-HA-HIS)</i>	T. Wagner
yTW695	MATa <i>his3Δ1 leu2Δ0 ura3Δ0 met15Δ0 + pBL189 (2μ GPD-URA3)</i>	T. Wagner
yTW696	MATa <i>his3Δ1 leu2Δ0 ura3Δ0 met15Δ0 + pBB39 (2μ GPD-RNH1-HA-URA3)</i>	T. Wagner
yTW701	MATa <i>his3Δ1 leu2Δ0 ura3Δ0 met15Δ0 cdc13-1::HIS + pBL189 (2μ GPD-URA3)</i>	T. Wagner
yTW702	MATa <i>his3Δ1 leu2Δ0 ura3Δ0 met15Δ0 cdc13-1::HIS + pBB39 (2μ GPD-RNH1-HA-URA3)</i>	T. Wagner
yTW707	MATa <i>his3Δ1 leu2Δ0 ura3Δ0 met15Δ0 cdc13-1::HIS rad9::NAT + pBL189 (2μ GPD-URA3)</i>	T. Wagner
yTW708	MATa <i>his3Δ1 leu2Δ0 ura3Δ0 met15Δ0 cdc13-1::HIS rad9::NAT + pBB39 (2μ GPD-RNH1-HA-URA3)</i>	T. Wagner
yTW713	MATa <i>his3Δ1 leu2Δ0 ura3Δ0 met15Δ0 rad9::NAT + pBL189 (2μ GPD-URA3)</i>	T. Wagner
yTW714	MATa <i>his3Δ1 leu2Δ0 ura3Δ0 met15Δ0 rad9::NAT + pBB39 (2μ GPD-RNH1-HA-URA3)</i>	T. Wagner
yVP226	MATa <i>his3Δ1 leu2Δ0 ura3Δ0</i>	Pires et al., 2023

yVP230	MATa his3Δ1 leu2Δ0 ura3Δ0 rnh1::KAN	Pires et al., 2023
yVP232	MATa his3Δ1 leu2Δ0 ura3Δ0 rnh201::HYG	Pires et al., 2023
yVP242	MATa his3Δ1 leu2Δ0 ura3Δ0 rnh1::KAN rnh201::HYG	Pires et al., 2023
yVP317	MATa his3Δ1 leu2Δ0 ura3Δ0 RNH1-TAP-HIS3MX6 rnh201::HYG	Lockhart et al., 2019
yVP319	MATa his3Δ1 leu2Δ0 ura3Δ0 RNH1-TAP-HIS3MX6 sen1-1::KAN	Lockhart et al., 2019
yVP321	MATa his3Δ1 leu2Δ0 ura3Δ0 RNH1-TAP-HIS3MX6 sen1-1::KAN rnh201::HYG	Lockhart et al., 2019
yVP475	MATa his3Δ1 leu2Δ0 ura3Δ0 RNH201-6xMYC-HIS	Lockhart et al., 2019
yVP483	MATa his3Δ1 leu2Δ0 ura3Δ0 RNH202-9xMYC-HIS	Lockhart et al., 2019
yVP537	MATa/MATalpha his3Δ1/his3Δ1 leu2Δ0/leu2Δ0 ura3Δ0/ura3Δ0 EST2/est2::NAT SEN1/sen1-1::KAN RNH201/rnh201::HYG	this study
yVP670	MATa/MATalpha his3Δ1/his3Δ1 leu2Δ0/leu2Δ0 ura3Δ0/ura3Δ0 EST2/est2::NAT SEN1/sen1-1::KAN RNH1/rnh1::KAN	this study
yVP726	MATalpha his3Δ1 leu2Δ0 ura3Δ0 stn1-13::KAN	this study
yVP730	MATa his3Δ1 leu2Δ0 ura3Δ0 stn1-13::KAN rnh1::HIS	this study
yVP734	MATa his3Δ1 leu2Δ0 ura3Δ0 stn1-13::KAN rnh201::HYG	this study
yVP738	MATa his3Δ1 leu2Δ0 ura3Δ0 stn1-13::KAN rnh201::HYG rnh1::HIS	this study
yVP773	MATa his3Δ1 leu2Δ0 ura3Δ0 pBL189 (2μ GPD-URA3)	Pires et al., 2023
yVP773	MATa his3Δ1 leu2Δ0 ura3Δ0 + pBL189 (2μ GPD-URA3)	this study
yVP776	MATa his3Δ1 leu2Δ0 ura3Δ0 pBB39 (2μ GPD-RNH1-HA-URA3)	Pires et al., 2023
yVP776	MATa his3Δ1 leu2Δ0 ura3Δ0 + pBB39 (2μ GPD-RNH1-URA3)	this study
yVP779	MATa his3Δ1 leu2Δ0 ura3Δ0 cdc13-1::HIS pBL189 (2μ GPD-URA3)	Pires et al., 2023
yVP779	MATa his3Δ1 leu2Δ0 ura3Δ0 cdc13-1::HIS + pBL189 (2μ GPD-URA3)	this study
yVP782	MATa his3Δ1 leu2Δ0 ura3Δ0 cdc13-1::HIS pBB39 (2μ GPD-RNH1-HA-URA3)	Pires et al., 2023
yVP782	MATa his3Δ1 leu2Δ0 ura3Δ0 cdc13-1::HIS + pBB39 (2μ GPD-RNH1-URA3)	this study
yVP785	MATa his3Δ1 leu2Δ0 ura3Δ0 sen1-1::KAN + pBL189 (2μ GPD-URA3)	this study
yVP788	MATa his3Δ1 leu2Δ0 ura3Δ0 sen1-1::KAN + pBB39 (2μ GPD-RNH1-URA3)	this study
yVP791	MATa his3Δ1 leu2Δ0 ura3Δ0 sen1-1::KAN cdc13-1::HIS + pBL189 (2μ GPD-URA3)	this study
yVP794	MATa his3Δ1 leu2Δ0 ura3Δ0 sen1-1::KAN cdc13-1::HIS + pBB39 (2μ GPD-RNH1-URA3)	this study
yVP830	MATa his3Δ1 leu2Δ0 ura3Δ0 cdc7-4::KAN	Pires et al., 2023

yVP833	MATa his3Δ1 leu2Δ0 ura3Δ0 cdc7-4::KAN rnh1::HIS	Pires et al., 2023
yVP836	MATa his3Δ1 leu2Δ0 ura3Δ0 cdc7-4::KAN rnh201::HYG	Pires et al., 2023
yVP839	MATa his3Δ1 leu2Δ0 ura3Δ0 cdc7-4::KAN rnh1::HIS rnh201::HYG	Pires et al., 2023
yVP842	MATa his3Δ1 leu2Δ0 ura3Δ0 cdc15-2::KAN	Pires et al., 2023
yVP845	MATa his3Δ1 leu2Δ0 ura3Δ0 cdc15-2::KAN rnh1::HIS	Pires et al., 2023
yVP848	MATa his3Δ1 leu2Δ0 ura3Δ0 cdc15-2::KAN rnh201::HYG	Pires et al., 2023
yVP851	MATa his3Δ1 leu2Δ0 ura3Δ0 cdc15-2::KAN rnh1::HIS rnh201::HYG	Pires et al., 2023
yVP869	MATa/MATalpha his3Δ1/his3Δ1 leu2Δ0/leu2Δ0 ura3Δ0/ura3Δ0 EST2/est2::HIS RNH1/rnh1::KAN RNH201/rnh201::HYG EXO1/exo1::NAT	this study
yVP882	MATa his3Δ1 leu2Δ0 ura3Δ0	Pires et al., 2023
yVP885	MATalpha his3Δ1 leu2Δ0 ura3Δ0 cdc13-1::KAN	Pires et al., 2023
yVP888	MATa his3Δ1 leu2Δ0 ura3Δ0 met15Δ0 cdc13-1::KAN SEN1-AID-HIS AFB2::LEU	Pires et al., 2023
yVP892	MATa his3Δ1 leu2Δ0 ura3Δ0 met15Δ0 SEN1-AID-HIS AFB2::LEU	Pires et al., 2023
yVP978-983	MATa his3Δ1 leu2Δ0 ura3Δ0 est2::KAN exo1::NAT + pBL354 ("ERTO" EST2 URA3 CEN) + pBL190 (2μ GPD-HIS EV)	this study
yVP984-989	MATa his3Δ1 leu2Δ0 ura3Δ0 est2::KAN exo1::NAT + pBL354 ("ERTO" EST2 URA3 CEN) + pBL192 (2μ GPD-RNH1-HA-HIS)	this study
yVP1001, 1002, 1003	MATa his3Δ1 leu2Δ0 ura3Δ0	Pires et al., 2023
yVP1005, 1006, 1007	MATa his3Δ1 leu2Δ0 ura3Δ0 cdc13-1::HIS	Pires et al., 2023
yVP1018	MATa his3Δ1 leu2Δ0 ura3Δ0 cdc13-1::HIS rnh1::KAN	Pires et al., 2023
yVP1022	MATalpha his3Δ1 leu2Δ0 ura3Δ0 cdc13-1::HIS rnh201::HYG	Pires et al., 2023
yVP1025, 1026	MATa his3Δ1 leu2Δ0 ura3Δ0 rnh1::KAN rnh201::HYG	Pires et al., 2023
yVP1027	MATalpha his3Δ1 leu2Δ0 ura3Δ0 rnh1::KAN rnh201::HYG	Pires et al., 2023
yVP1029, 1030, 1031	MATa his3Δ1 leu2Δ0 ura3Δ0 cdc13-1::HIS rnh1::KAN rnh201::HYG	Pires et al., 2023
yVP1036, 1037, 1038	MATa his3Δ1 leu2Δ0 ura3Δ0 pBL190 (2μ GPD-HIS EV)	Pires et al., 2023
yVP1040, 1041, 1042	MATa his3Δ1 leu2Δ0 ura3Δ0 pBL192 (2μ GPD-RNH1-HA-HIS)	Pires et al., 2023
yVP1044, 1045	MATa his3Δ1 leu2Δ0 ura3Δ0 cdc13-1::KAN pBL190 (2μ GPD-HIS EV)	Pires et al., 2023
yVP1046	MATalphaa his3Δ1 leu2Δ0 ura3Δ0 cdc13-1::KAN pBL190 (2μ GPD-HIS EV)	Pires et al., 2023

yVP1048, 1049	MATa his3Δ1 leu2Δ0 ura3Δ0 cdc13-1::KAN pBL192 (2μ GPD-RNH1-HA-HIS)	Pires et al., 2023
yVP1050	MATalpha his3Δ1 leu2Δ0 ura3Δ0 cdc13-1::KAN pBL192 (2μ GPD-RNH1-HA-HIS)	Pires et al., 2023
yVP1052	MATalpha his3Δ1 leu2Δ0 ura3Δ0 exo1::NAT pBL190 (2μ GPD-HIS EV)	Pires et al., 2023
yVP1056	MATalpha his3Δ1 leu2Δ0 ura3Δ0 exo1::NAT pBL192 (2μ GPD-RNH1-HA-HIS)	Pires et al., 2023
yVP1060, 1061	MATalpha his3Δ1 leu2Δ0 ura3Δ0 cdc13-1::KAN exo1::NAT pBL190 (2μ GPD-HIS EV)	Pires et al., 2023
yVP1062	MATa his3Δ1 leu2Δ0 ura3Δ0 cdc13-1::KAN exo1::NAT pBL190 (2μ GPD-HIS EV)	Pires et al., 2023
yVP1064, 1065	MATalpha his3Δ1 leu2Δ0 ura3Δ0 cdc13-1::KAN exo1::NAT pBL192 (2μ GPD-RNH1-HA-HIS)	Pires et al., 2023
yVP1066	MATa his3Δ1 leu2Δ0 ura3Δ0 cdc13-1::KAN exo1::NAT pBL192 (2μ GPD-RNH1-HA-HIS)	Pires et al., 2023
yVP1292	MATa his3Δ1 leu2Δ0 ura3Δ0	Pires et al., 2023
yVP1293, 1294	MATa his3Δ1 leu2Δ0 ura3Δ0	Pires et al., 2023
yVP1295, 1296	MATa his3Δ1 leu2Δ0 ura3Δ0 cdc13-1::HIS	Pires et al., 2023
yVP1297	MATalpha his3Δ1 leu2Δ0 ura3Δ0 cdc13-1::HIS	Pires et al., 2023
yVP1301	MATalpha his3Δ1 leu2Δ0 ura3Δ0 sen1-1::KAN	Pires et al., 2023
yVP1302, 1303	MATa his3Δ1 leu2Δ0 ura3Δ0 sen1-1::KAN	Pires et al., 2023
yVP1304, 1306	MATalpha his3Δ1 leu2Δ0 ura3Δ0 cdc13-1::HIS sen1-1::KAN	Pires et al., 2023
yVP1305	MATa his3Δ1 leu2Δ0 ura3Δ0 cdc13-1::HIS sen1-1::KAN	Pires et al., 2023
yVP1316-1318	MATalpha his3Δ1 leu2Δ0 ura3Δ0 est2::KAN + pBL190 (EV) + pBL352 (EST2-URA3)	Pires et al., 2023
yVP1319	MATa his3Δ1 leu2Δ0 ura3Δ0 est2::KAN + pBL190 (EV) + pBL352 (EST2-URA3)	Pires et al., 2023
yVP1340, 1342	MATalpha his3Δ1 leu2Δ0 ura3Δ0 est2::KAN + pBL192 (2μ GPD-RNH1-HA-HIS) + pBL352 (EST2-URA3)	Pires et al., 2023
yVP1344, 1345	MATa his3Δ1 leu2Δ0 ura3Δ0 est2::KAN + pBL192 (2μ GPD-RNH1-HA-HIS) + pBL352 (EST2-URA3)	Pires et al., 2023
yVP1364-1366	MATalpha his3Δ1 leu2Δ0 ura3Δ0 est2::KAN + pBL710 (2μ GPD-RNH1-D193N-HA-HIS) + pBL352 (EST2-URA3)	this study
yVP1367-1369	MATa his3Δ1 leu2Δ0 ura3Δ0 est2::KAN + pBL710 (2μ GPD-RNH1-D193N-HA-HIS) + pBL352 (EST2-URA3)	this study
yVP1390	MATa his3Δ1 leu2Δ0 ura3Δ0	Pires et al., 2023
yVP1393	MATa his3Δ1 leu2Δ0 ura3Δ0 cdc13-1::HIS	Pires et al., 2023
yVP1399	MATalpha his3Δ1 leu2Δ0 ura3Δ0 sen1-1::KAN	Pires et al., 2023
yVP1405	MATa his3Δ1 leu2Δ0 ura3Δ0 cdc13-1::HIS sen1-1::KAN	Pires et al., 2023

yVP1604	MATa his3Δ1 leu2Δ0 ura3Δ0 met15Δ0 cdc15-2::KAN pBL190 (2μ GPD-HIS EV)	Pires et al., 2023
yVP1607	MATa his3Δ1 leu2Δ0 ura3Δ0 met15Δ0 cdc15-2::KAN pBL192 (2μ GPD-RNH1-HA-HIS)	Pires et al., 2023
yVP1724	MATa his3Δ1 leu2Δ0 ura3Δ0 + pBL189 (2μ GPD-URA3)	this study
yVP1726	MATa his3Δ1 leu2Δ0 ura3Δ0 + pBB39 (2μ GPD-RNH1-URA3)	this study
yVP1728	MATa his3Δ1 leu2Δ0 ura3Δ0 cdc13-1::HIS + pBL189 (2μ GPD-URA3)	this study
yVP1730	MATa his3Δ1 leu2Δ0 ura3Δ0 cdc13-1::HIS + pBB39 (2μ GPD-RNH1-URA3)	this study
yVP1732	MATa his3Δ1 leu2Δ0 ura3Δ0 cdc13-1::HIS sgs1::NAT + pBL189 (2μ GPD-URA3)	this study
yVP1734	MATa his3Δ1 leu2Δ0 ura3Δ0 cdc13-1::HIS sgs1::NAT + pBB39 (2μ GPD-RNH1-URA3)	this study
yVP1736	MATa his3Δ1 leu2Δ0 ura3Δ0 sgs1::NAT + pBL189 (2μ GPD-URA3)	this study
yVP1738	MATa his3Δ1 leu2Δ0 ura3Δ0 sgs1::NAT + pBB39 (2μ GPD-RNH1-URA3)	this study
yVP1740	MATa his3Δ1 leu2Δ0 ura3Δ0 EXO1-TAP-HIS + pBL189 (2μ GPD-URA3)	this study
yVP1743	MATa his3Δ1 leu2Δ0 ura3Δ0 EXO1-TAP-HIS + pBB39 (2μ GPD-RNH1-URA3)	this study
yVP1770	MATa his3Δ1 leu2Δ0 ura3Δ0 PIF1-TAP-HIS + pBL189 (2μ GPD-URA3)	this study
yVP1773	MATa his3Δ1 leu2Δ0 ura3Δ0 PIF1-TAP-HIS + pBB39 (2μ GPD-RNH1-URA3)	this study
yVP1954	MATalpha his3Δ1 leu2Δ0 ura3Δ0 pBL190 (2μ GPD-HIS EV)	Pires et al., 2023
yVP1957	MATalpha his3Δ1 leu2Δ0 ura3Δ0 pBL192 (2μ GPD-RNH1-HA-HIS)	Pires et al., 2023
yVP1960	MATalpha his3Δ1 leu2Δ0 ura3Δ0 cdc13-1::KAN pBL190 (2μ GPD-HIS EV)	Pires et al., 2023
yVP1963	MATalpha his3Δ1 leu2Δ0 ura3Δ0 cdc13-1::KAN pBL192 (2μ GPD-RNH1-HA-HIS)	Pires et al., 2023
yVP1966	MATa his3Δ1 leu2Δ0 ura3Δ0 cdc13-1::KAN pif1-m2-URA3 pBL190 (2μ GPD-HIS EV)	Pires et al., 2023
yVP1969	MATa his3Δ1 leu2Δ0 ura3Δ0 cdc13-1::KAN pif1-m2-URA3 pBL192 (2μ GPD-RNH1-HA-HIS)	Pires et al., 2023
yVP1972	MATa his3Δ1 leu2Δ0 ura3Δ0 pif1-m2-URA3 pBL190 (2μ GPD-HIS EV)	Pires et al., 2023
yVP1975	MATa his3Δ1 leu2Δ0 ura3Δ0 pif1-m2-URA3 pBL192 (2μ GPD-RNH1-HA-HIS)	Pires et al., 2023
yVP1977	MATa his3Δ1 leu2Δ0 ura3Δ0 + pBL190 (2μ GPD-HIS EV)	this study
yVP1980	MATa his3Δ1 leu2Δ0 ura3Δ0 met15Δ0 + pBL192 (2μ GPD-RNH1-HA-HIS)	this study
yVP1983	MATa his3Δ1 leu2Δ0 ura3Δ0 cdc13-1::KAN + pBL190 (2μ GPD-HIS EV)	this study
yVP1986	MATa his3Δ1 leu2Δ0 ura3Δ0 cdc13-1::KAN + pBL192 (2μ GPD-RNH1-HA-HIS)	this study
yVP1989	MATalpha his3Δ1 leu2Δ0 ura3Δ0 cdc13-1::KAN sae2::NAT + pBL190 (2μ GPD-HIS EV)	this study

yVP1992	MATalpha his3Δ1 leu2Δ0 ura3Δ0 cdc13-1::KAN sae2::NAT + pBL192 (2μ GPD-RNH1-HA-HIS)	this study
yVP1995	MATalpha his3Δ1 leu2Δ0 ura3Δ0 sae2::NAT + pBL190 (2μ GPD-HIS EV)	this study
yVP1998	MATalpha his3Δ1 leu2Δ0 ura3Δ0 sae2::NAT + pBL192 (2μ GPD-RNH1-HA-HIS)	this study
yVP2001	MATa his3Δ1 leu2Δ0 ura3Δ0 + pBL189 (2μ GPD-URA3)	this study
yVP2004	MATa his3Δ1 leu2Δ0 ura3Δ0 met15Δ0 + pBB39 (2μ GPD-RNH1-URA3)	this study
yVP2007	MATa his3Δ1 leu2Δ0 ura3Δ0 cdc13-1::KAN + pBL189 (2μ GPD-URA3)	this study
yVP2010	MATa his3Δ1 leu2Δ0 ura3Δ0 cdc13-1::KAN + pBB39 (2μ GPD-RNH1-URA3)	this study
yVP2013	MATalpha his3Δ1 leu2Δ0 ura3Δ0 cdc13-1::KAN mre11::KAN + pBL189 (2μ GPD-URA3)	this study
yVP2016	MATalpha his3Δ1 leu2Δ0 ura3Δ0 cdc13-1::KAN mre11::KAN + pBB39 (2μ GPD-RNH1-URA3)	this study
yVP2019	MATalpha his3Δ1 leu2Δ0 ura3Δ0 mre11::KAN + pBL189 (2μ GPD-URA3)	this study
yVP2022	MATalpha his3Δ1 leu2Δ0 ura3Δ0 mre11::KAN + pBB39 (2μ GPD-RNH1-URA3)	this study
yVP2104	MATa his3Δ1 leu2Δ0 ura3Δ0 pBL190 (2μ GPD-HIS EV)	Pires et al., 2023
yVP2107	MATa his3Δ1 leu2Δ0 ura3Δ0 pBL192 (2μ GPD-RNH1-HA-HIS)	Pires et al., 2023
yVP2110	MATalpha his3Δ1 leu2Δ0 ura3Δ0 cdc13-1::KAN pBL190 (2μ GPD-HIS EV)	Pires et al., 2023
yVP2113	MATalpha his3Δ1 leu2Δ0 ura3Δ0 cdc13-1::KAN pBL192 (2μ GPD-RNH1-HA-HIS)	Pires et al., 2023
yVP2116	MATa his3Δ1 leu2Δ0 ura3Δ0 cdc13-1::KAN exo1::NAT PIF1::URA3-pif1-m2 pBL190 (2μ GPD-HIS EV)	Pires et al., 2023
yVP2119	MATa his3Δ1 leu2Δ0 ura3Δ0 cdc13-1::KAN exo1::NAT PIF1::URA3-pif1-m2 pBL192 (2μ GPD-RNH1-HA-HIS)	Pires et al., 2023
yVP2122	MATa his3Δ1 leu2Δ0 ura3Δ0 exo1::NAT PIF1::URA3-pif1-m2 pBL190 (2μ GPD-HIS EV)	Pires et al., 2023
yVP2125	MATa his3Δ1 leu2Δ0 ura3Δ0 exo1::NAT PIF1::URA3-pif1-m2 pBL192 (2μ GPD-RNH1-HA-HIS)	Pires et al., 2023
yVP2216, 2217, 2218, 2219, 2220	MATa his3Δ1 leu2Δ0 ura3Δ0 met15Δ0 + pBL190 (2μ GPD-HIS EV)	Pires et al., 2023
yVP2221, 2222, 2223, 2224, 2225	MATa his3Δ1 leu2Δ0 ura3Δ0 met15Δ0 + pBL192 (2μ GPD-RNH1-HA-HIS)	Pires et al., 2023
yVP2466	MATa his3Δ1 leu2Δ0 met15Δ0 + pBL190 (2μ GPD-HIS EV)	this study
yVP2469	MATa his3Δ1 leu2Δ0 met15Δ0 + pBL192 (2μ GPD-RNH1-HA-HIS)	this study
yVP2472	MATa his3Δ1 leu2Δ0 met15Δ0 cdc13-1::KAN + pBL190 (2μ GPD-HIS EV)	this study
yVP2475	MATa his3Δ1 leu2Δ0 met15Δ0 cdc13-1::KAN + pBL192 (2μ GPD-RNH1-HA-HIS)	this study
yVP2478	MATa his3Δ1 leu2Δ0 met15Δ0 rad53-11::URA + pBL190 (2μ GPD-HIS EV)	this study

yVP2481	MATa his3Δ1 leu2Δ0 met15Δ0 rad53-11::URA + pBL192 (2μ GPD-RNH1-HA-HIS)	this study
yVP2484	MATa his3Δ1 leu2Δ0 met15Δ0 cdc13-1::KAN rad53-11::URA + pBL190 (2μ GPD-HIS EV)	this study
yVP2487	MATa his3Δ1 leu2Δ0 met15Δ0 cdc13-1::KAN rad53-11::URA + pBL192 (2μ GPD-RNH1-HA-HIS)	this study
yVP2532	MATa his3Δ1 leu2Δ0 ura3Δ0 met15Δ0 + pBL1000 (2μ YGR045C, KanMX, LEU2)	Pires et al., 2023
yVP2535	MATa his3Δ1 leu2Δ0 ura3Δ0 met15Δ0 cdc13-1::HIS + pBL1000 (2μ YGR045C, KanMX, LEU2)	Pires et al., 2023
yVP2538	MATa his3Δ1 leu2Δ0 ura3Δ0 met15Δ0 + pBL975 (2μ FMP45, KanMX, LEU2)	Pires et al., 2023
yVP2541	MATa his3Δ1 leu2Δ0 ura3Δ0 met15Δ0 cdc13-1::HIS + pBL975 (2μ FMP45, KanMX, LEU2)	Pires et al., 2023
yVP2580	MATa his3Δ1 leu2Δ0 ura3Δ0 met15Δ0 + pBL982 (2μ ZDS2, KanMX, LEU2)	Pires et al., 2023
yVP2583	MATa his3Δ1 leu2Δ0 ura3Δ0 met15Δ0 cdc13-1::HIS + pBL982 (2μ ZDS2, KanMX, LEU2)	Pires et al., 2023
yVP2586	MATa his3Δ1 leu2Δ0 ura3Δ0 met15Δ0 + pBL983 (2μ PAN2, KanMX, LEU2)	Pires et al., 2023
yVP2589	MATa his3Δ1 leu2Δ0 ura3Δ0 met15Δ0 cdc13-1::HIS + pBL983 (2μ PAN2, KanMX, LEU2)	Pires et al., 2023
yVP2601	MATa his3Δ1 leu2Δ0 ura3Δ0 cdc13-1::HIS rnh1::KAN rnh201::HYG pBL189 (2μ GPD-URA3)	Pires et al., 2023
yVP2606	MATa his3Δ1 leu2Δ0 ura3Δ0 + pBL189 (EV)	Pires et al., 2023
yVP2609	MATa his3Δ1 leu2Δ0 ura3Δ0 + pBB39 (2μ GPD-RNH1-URA3)	Pires et al., 2023
yVP2612	MATalpha his3Δ1 leu2Δ0 ura3Δ0 cdc13-1::HIS + pBL189 (EV)	Pires et al., 2023
yVP2615	MATalpha his3Δ1 leu2Δ0 ura3Δ0 cdc13-1::HIS + pBB39 (2μ GPD-RNH1-URA3)	Pires et al., 2023
yVP2618	MATa his3Δ1 leu2Δ0 ura3Δ0 dls1::KAN + pBL189 (EV)	Pires et al., 2023
yVP2621	MATa his3Δ1 leu2Δ0 ura3Δ0 dls1::KAN + pBB39 (2μ GPD-RNH1-URA3)	Pires et al., 2023
yVP2624	MATalpha his3Δ1 leu2Δ0 ura3Δ0 cdc13-1::HIS dls1::KAN + pBL189 (EV)	Pires et al., 2023
yVP2627	MATalpha his3Δ1 leu2Δ0 ura3Δ0 cdc13-1::HIS dls1::KAN + pBB39 (2μ GPD-RNH1-URA3)	Pires et al., 2023
yVP2634	MATalpha his3Δ1 leu2Δ0 ura3Δ0 cdc13-1::HIS + pBL189 (EV)	Pires et al., 2023
yVP2637	MATalpha his3Δ1 leu2Δ0 ura3Δ0 cdc13-1::HIS + pBB39 (2μ GPD-RNH1-URA3)	Pires et al., 2023
yVP2640	MATalpha his3Δ1 leu2Δ0 ura3Δ0 ira2::KAN + pBL189 (EV)	Pires et al., 2023
yVP2643	MATalpha his3Δ1 leu2Δ0 ura3Δ0 ira2::KAN + pBB39 (2μ GPD-RNH1-URA3)	Pires et al., 2023
yVP2646	MATa his3Δ1 leu2Δ0 ura3Δ0 cdc13-1::HIS ira2::KAN + pBL189 (EV)	Pires et al., 2023
yVP2649	MATa his3Δ1 leu2Δ0 ura3Δ0 cdc13-1::HIS ira2::KAN + pBB39 (2μ GPD-RNH1-URA3)	Pires et al., 2023
yVP2658	MATa his3Δ1 leu2Δ0 ura3Δ0 cdc13-1::HIS + pBL189 (EV)	Pires et al., 2023

yVP2661	MATa his3Δ1 leu2Δ0 ura3Δ0 cdc13-1::HIS + pBB39 (2μ GPD-RNH1-URA3)	Pires et al., 2023
yVP2664	MATalpha his3Δ1 leu2Δ0 ura3Δ0 dpb3::KAN + pBL189 (EV)	Pires et al., 2023
yVP2667	MATalpha his3Δ1 leu2Δ0 ura3Δ0 dpb3::KAN + pBB39 (2μ GPD-RNH1-URA3)	Pires et al., 2023
yVP2670	MATa his3Δ1 leu2Δ0 ura3Δ0 cdc13-1::HIS dpb3::KAN + pBL189 (EV)	Pires et al., 2023
yVP2673	MATa his3Δ1 leu2Δ0 ura3Δ0 cdc13-1::HIS dpb3::KAN + pBB39 (2μ GPD-RNH1-URA3)	Pires et al., 2023
yVP2685	MATa/MATalpha his3Δ1/his3Δ1 leu2Δ0/leu2Δ0 ura3Δ0/ura3Δ0 EST2/est2::KAN RNH1/NAT-G1-3myc-RNH1-TAP-HIS RNH201/rnh201::HYG	this study
KP54	W303 MATa leu2-3,112 trp1-1 can1-100 ura3-1 ade2-1 his3-11,15	K. Paeschke Lab
KP91	W303 MATa leu2-3,112 trp1-1 can1-100 ura3-1 ade2-1 his3-11,15, pif1-m2	K. Paeschke Lab

#### 4.1.2 Plasmids

Identifier	Description	Source
pBB39	pRS426 <i>pGPD-RNH1-HA</i> , 2μ, <i>URA3</i>	Balk et al., 2013
pBL189	pRS426 <i>pGPD</i> , 2μ, <i>URA3</i>	Balk et al., 2013
pBL190	pRS423 <i>pGPD</i> , 2μ, <i>HIS3</i>	M. Peter Lab
pBL192	pRS423 <i>pGPD-RNH1-HA</i> , 2μ, <i>HIS3</i>	Balk et al., 2013
pBL332	pYM19, 9MYC, <i>HIS3</i>	Janke et al., 2004 <sup>556</sup>
pBL710	pRS423 <i>pGPD-RNH1-D193N-HA</i> , 2μ, <i>HIS3</i>	this study
pBL975	p5476 <i>FMP45</i> , <i>KanMX</i> , 2μ, <i>LEU2</i>	Ho et al., 2009 <sup>557</sup>
pBL982	p5476 <i>ZDS2</i> , <i>KanMX</i> , 2μ, <i>LEU2</i>	Ho et al., 2009
pBL983	p5476 <i>PAN2</i> , <i>KanMX</i> , 2μ, <i>LEU2</i>	Ho et al., 2009
pBL1000	p5476 <i>YGR045C</i> , <i>KanMX</i> , 2μ, <i>LEU2</i> (EV)	Ho et al., 2009
KP447	pSANG10-3F-BG4	Biffi et al., 2013 <sup>523</sup>

#### 4.1.3 Oligonucleotides

Identifier	Use	Sequence (5' → 3')
oAL29	<i>RNH201-9MYC</i> Rv	TATGTAGTATTACATGAAGATATATAGTATGT GCAAACCTGGAGGTGATCAATCGATGAATTCCG AGCTCG
oAL30	<i>RNH201-9MYC</i> Fw	CTAAGCCTGTTAGAAGGAAGAGGCTGAGAA CCCTAGATAATTGGTACCGGCGTACGCTGC AGGTCCGAC
oAL31	check <i>RNH201-9MYC</i> Fw	ATGGACAGCAGGAAGAACG
oAL77	check <i>RNH202-9MYC</i> Fw	CAAGGTAGTTATGGCTACAA
oAM47	qPCR (18S rDNA Fw)	TCCAATTGTTCCCTCGTTAAG
oAM48	qPCR (18S rDNA Rv)	ATTCAGGGAGGTAGTGACAA
oBL29	KO/tag confirmation Rv	CTGCAGCGAGGAGCCGTAAT



oBL207	DOT BLOT	CACCACACCCACACACCACACCCACA
oBL256	<i>RNH1</i> Fw	GGAATTCATGGCAAGGCAAGGGAAGCTTC
oBL292	qPCR (Actin Fw)	CCCAGGTATTGCCGAAAGAATGC
oBL293	qPCR (Actin Rv)	TTTGTTGGAAGGTAGTCAAAGAAGCC
oBL295	qPCR (1L Fw)	CGGTGGGTGAGTGGTAGTAAGTAGA
oBL296	qPCR (1L Rv)	ACCCTGTCCCATTCAACCATAC
oBL358	Telo-PCR (1L Fw)	GCGGTACCAGGGTTAGATTAGGGCTG
oBL359	Telo-PCR (G oligo Rv)	CGGGATCCGGGGGGGGGGGGGGGGGGGG
oBL361	Telo-PCR (Y' Fw)	TTAGGGCTATGTAGAAGTGCTG
oFB171	qPCR (SUF2 Fw)	TATGATTCTCGCTTAGGGTGCGGGAGG
oFB172	qPCR (SUF2 Rv)	CATTAACATTGGTCTTCTCCAGCTTACTC
oLK49	qPCR (6Y' Fw)	GGCTTGGAGGAGACGTACATG
oLK50	qPCR (6Y' Rv)	CTCGCTGTCACTCCTTACCCG
oLK57	qPCR (15L Fw)	GGGTAACGAGTGGGGAGGTAA
oLK58	qPCR (15L Rv)	CAACACTACCCTAATCTAACCCCTGT
oRM1	<i>RNH1-D193N</i> mutagenesis Fw	GTCTATGAACGTTTACTGTAATGGTTCAAGT TTTGAAACGGCAC
oRM2	<i>RNH1-D193N</i> mutagenesis Rv	TTGTTGTACATGGTATTGCTAGAAAGCTTATA CTTAGATTCAAAAC
oTW18	M13 Rv	CAGGAAACAGCTATGAC
oVP3	<i>RNH202-9MYC</i> Rv	CACCACCGAGTTATAGCATTCAAATTGCTGT TTAATTATGATACTAGCTAATCGATGAATTG AGCTCG
oVP4	<i>RNH202-9MYC</i> Fw	CAAAAGTAGCCATAGGAAAAGGGGCCATTG ATGGATTTTTTAAACGTAAGCGTACGCTGCA GGTCGAC
KP390	qPCR (6R Fw)	ATCATTGAGGATCTATAATC
KP391	qPCR (6R Rv)	CTTCACTCCATTGCG
KW195	qPCR (G4 Chr13 Fw)	GCTTCAGCCTGGGGTAAC
KW196	qPCR (G4 Chr13 Rv)	GGCACCATTAGATTCACCAC

#### 4.1.4 Media

##### 4.1.4.1 Liquid media

Medium	Composition
Yeast peptone dextrose (YPD) medium	2 % (w/v) Peptone 1 % (w/v) Bacto yeast extract 2 % (w/v) Glucose
Synthetic complete (SC) medium w/o amino acid	0.192 % (w/v) Yeast synthetic dropout medium w/o amino acids 0.67 % (w/v) Yeast nitrogen base w/o amino acids 2 % (w/v) Glucose/ Raffinose/ Galactose
Lysogeny broth (LB) medium	1 % (w/v) NaCl 1 % (w/v) Bacto tryptone 0.5 % (w/v) Bacto yeast extract
Sporulation (SPO) medium	0.005 % (w/v) Zinc acetate

	1 % (w/v) Potassium acetate
--	-----------------------------

#### 4.1.4.2 Agar plates

Plate	Composition
YPD agar	10 % (w/v) Peptone 5 % (w/v) Bacto yeast extract 10 % (w/v) Agar 2 % (w/v) Glucose
SC complete	0.192 % (w/v) Yeast synthetic dropout medium w/o amino acids 0.67 % (w/v) Yeast nitrogen base w/o amino acids 2.4 % (w/v) Agar 2 % (w/v) Glucose 1 % (w/v) 100x amino acid
SC without amino acid	0.192 % (w/v) Yeast synthetic dropout medium w/o amino acids 0.67 % (w/v) Yeast nitrogen base w/o amino acids 2.4 % (w/v) Agar 2 % (w/v) Glucose/ Raffinose/ Galactose
SC	0.67 % (w/v) Yeast nitrogen base w/o amino acids 2.4 % (w/v) Agar 2 % (w/v) Glucose
SC without amino acid + 5-FOA	0.192 % (w/v) Yeast synthetic dropout medium w/o amino acids (and w/o uracil) 0.67 % (w/v) Yeast nitrogen base w/o amino acids 0.005% (w/v) uracil 2.4 % (w/v) Agar 2 % (w/v) Glucose 0.1% (w/v) 5-FOA in ddH <sub>2</sub> O at 65°C 0.2% (v/v) missing amino acids
LB	0.5 % (w/v) Bacto yeast extract 1 % (w/v) Bacto tryptone 1 % (w/v) NaCl 1.5 % (w/v) Agar
Pre-sporulation (PRE-SPO)	3 % (w/v) Standard nutrient broth 1 % (w/v) Bacto yeast extract 2 % (w/v) Agar 5 % (w/v) Glucose

<b>Antibiotics (single or multiple, added after autoclaving) were used in the following concentrations:</b>	
Carbenicillin disodium salt	100 µg/mL
G418 disulfate solution (Kanamycin)	300 µg/mL
Hygromycin B	300 µg/mL

Nourseothricin-dihydrogen sulfate (ClonNAT)	100 µg/mL
---	-----------

#### 4.1.5 Buffers and Solutions

Buffer/Solution	Composition
LiAc-Mix	100 mM Lithium acetate in 1x TE
PEG-Mix	40 % (v/v) Polyethylene glycol 400 in LiAc-Mix Sterile filter
10x PBS	1.37 M NaCl 30 mM KCl 80 mM Na <sub>2</sub> HPO <sub>4</sub> x2 H <sub>2</sub> O 20 mM KH <sub>2</sub> PO <sub>4</sub> pH adjusted to 7.4 Autoclaved
EDTA	500 mM disodium EDTA x2 H <sub>2</sub> O pH adjusted to 7.5 or 8.0
FA lysis buffer	50 mM HEPES pH 7.5 140 mM NaCl 1 mM EDTA pH 8.0 1 % (v/v) Triton X-100
FA lysis buffer + SOD	50 mM HEPES pH 7.5 140 mM NaCl 1 mM EDTA pH 8.0 1 % (v/v) Triton X-100 0.1 (w/v) sodium deoxycholate (SOD)
FA lysis buffer 500	50 mM HEPES pH 7.5 0.5 M NaCl 1 mM EDTA pH 8.0 1 % (v/v) Triton X-100 0.1 % (w/v) Sodium deoxycholate (SOD)
Buffer III	10 mM Tris-HCl pH 8.0 1 mM EDTA pH 8.0 250 mM LiCl 1 % (v/v) NP-40 1 % (w/v) Sodium deoxycholate (SOD)
10x TE	100 mM TRIS pH 7.5 10 mM EDTA pH 8.0
Elution Buffer B	50 mM Tris-HCl pH 7.5 1 % (v/v) SDS 10 mM EDTA pH 8.0
10x TBE	0.89 M Tris base 0.89 M Boric acid 20 mM Na <sub>2</sub> EDTA pH 8.0 Sterile filter
Solution 1 (protein extraction)	1.85 M NaOH 1.09 M β-mercaptoethanol

Solution 2 (protein extraction)	50 % (v/v) Trichloroacetic acid in ddH <sub>2</sub> O
Solution 3 (protein extraction)	100 % (v/v) Acetone
Potassium phosphate buffer pH 7.4 (100 mM)	80.2 mM K <sub>2</sub> HPO <sub>4</sub> 19.8 mM KH <sub>2</sub> PO <sub>4</sub>
Sorbitol	2 M Sorbitol in ddH <sub>2</sub> O
Spheroblasting buffer (Chromatin binding assay)	1 M Sorbitol 50 mM Potassium phosphate buffer pH 7.4 1 mM DTT
Extraction buffer (Chromatin binding assay)	500 mM Tris-HCl pH 6.8 100 mM KCl 2.5 mM MgCl <sub>2</sub>
Sucrose solution	30 % (w/v) sucrose in ddH <sub>2</sub> O
Triton X-100	10 % (v/v) Triton X-100 in ddH <sub>2</sub> O
Urea Buffer	120 mM Tris-HCL pH 6.8 5 % (v/v) Glycerol 8 M Urea 143 mM β-mercaptoethanol 8 % (v/v) SDS Bromophenol blue to color
10x SDS running buffer	0.1 % (v/v) SDS 250 mM Tris base 1.92 M Glycine sterile filter
Transfer buffer	1x BioRad transfer buffer in ddH <sub>2</sub> O 2 % (v/v) Absolute ethanol
1x PBST	1x PBS in ddH <sub>2</sub> O, 0.1 % Tween-20
Blocking buffer (western blot)	5 % (w/v) Skim milk powder in 1x PBST
Stripping buffer (western blot)	62.5 mM Tris pH 6.8 2 % (v/v) SDS 100.4 mM β-mercaptoethanol
IP buffer	50 mM Tris pH 7.5 150 mM NaCl 5 mM MgCl <sub>2</sub> 4 tablets Protease Inhibitor Cocktail 1 mM PMSF
IP buffer + NP-40	50 mM Tris pH 7.5 150 mM NaCl 5 mM MgCl <sub>2</sub> 0.2 % (v/v) NP-40 4 tablets Protease Inhibitor Cocktail 1 mM PMSF
Hybridization solution (ssDNA dot blot)	50% (v/v) Formamide 5x SSC 5x Denhardt's 5 mM EDTA 10 mM PIPES pH 6.4 0.04 % (w/v) yeast RNA

	1 % (v/v) SDS Sterile filter
20x SSC	3 M NaCl 0.3 M Sodium citrate tribasic dihydrate pH adjusted to 7.0
Washing solution I (ssDNA dot blot)	2x SSC 0.1 % (v/v) SDS
Washing solution II (ssDNA dot blot)	0.5x SSC 0.1 % (v/v) SDS
10x Blocking solution (ssDNA dot blot)	10% (w/v) Blocking reagent Maleic acid buffer pH 7.5
5x DIG wash buffer pH 7.5 (ssDNA dot blot)	0.5 M Maleic acid pH adjusted to 7.5 0.75 M NaCl 1.5 % (v/v) Tween-20 Sterile filter
Malic acid buffer pH 7.5	100 mM Maleic acid 150 mM NaCl pH adjusted to 7.5 sterile filter
DIG-detection buffer pH 9.5	130 mM Tris-HCl 75 mM NaCl pH adjusted to 9.5 sterile filter

If indicated, buffers and solutions were autoclaved for 20 min at 121°C.

## 4.1.6 Antibodies, Kits and Reagents

### 4.1.6.1 Antibodies

Reagent	Supplier	Identifier	Dilution
Immun-Star goat anti-mouse (GAM)-HRP conjugate	BioRad	Cat#170-5047; RRID: AB_11125753	1:3000
Immun-Star goat anti-rabbit (GAM)-HRP conjugate	BioRad	Cat#170-5046; RRID: AB_11125757	1:3000
Mouse monoclonal anti-DNA-RNA Hybrid (S9.6)	Kerafast	Cat#ENH001; RRID: AB_2687463	4µg/DRIP sample
Mouse monoclonal anti-HA.11 (clone 16B12)	Abcam	Cat#ab81656; RRID: AB_1658369	1:2000
Mouse monoclonal anti-MYC-tag (clone 9B11)	Cell Signaling Technology	Cat#2276S; RRID: AB_331783	1:1000
Mouse monoclonal anti-phosphoglycerate kinase (22C5D8)	Invitrogen	Cat#459250; RRID: AB_2532235	1:200 000
Mouse monoclonal anti-Rad53 (EI7.E1)	Abcam	Cat#ab166859; RRID: AB_2801547	1:1000

Rabbit peroxidase anti-peroxidase soluble complex (PAP)	Sigma-Aldrich	Cat#P1291; RRID: AB_1079562	1:1000
Rabbit polyclonal anti-histone H3	Abcam	Cat#ab1791; RRID: AB_302613	1:1000
Rabbit polyclonal anti-RFA (Baker's yeast replication factor A)	Agrisera Antibodies	Cat#AS07 214; RRID: AB_1031803	1µL/ChIP sample
Rabbit polyclonal anti-RNR3 (Ribonucleoside-diphosphate reductase large chain 2)	Agrisera Antibodies	Cat# AS09 574; RRID: AB_1966947	1:1000
Sheep polyclonal anti-Digoxigenin-AP, Fab fragments	Roche	Cat#11093274910; RRID: AB_2734716	1:5000

#### 4.1.6.2 Kits

Kit	Supplier	Identifier
DIG Oligonucleotide 3'-End Labeling Kit, 2nd generation	Roche	Cat#3353575910
DyNAmo Flash SYBR Green qRT-PCR kit	Thermo Scientific	Cat#10334009
Gentra Puregene Yeast/Bact. Kit B	Qiagen	Cat#158567
MinElute PCR Purification Kit	QIAGEN	Cat#28004
QIAprep Spin Miniprep Kit	Qiagen	Cat#27106
QIAquick Gel Extraction Kit	Qiagen	Cat#28706
QIAquick PCR purification Kit	Qiagen	Cat#28106
Qubit® dsDNA HS Assay Kit	Fisher Scientific	Cat#10606433
Trans-blot® Turbo™ RTA Midi Nitrocellulose Transfer Kit	BioRad	Cat#1704271

#### 4.1.6.3 Reagents

Reagent	Supplier	Identifier
<b><u>Enzymes</u></b>		
Benzonase® Nuclease	Sigma-Aldrich	Cat#E1014
DNase I (RNase free)	Qiagen	Cat#79254
Exonuclease I ( <i>E.coli</i> )	New England Biolabs	Cat#M0293L
KLD Enzyme Mix	New England Biolabs	Cat#M0554S
Lyticase	Sigma-Aldrich	Cat#L4025
Q5® High-Fidelity 2x Master Mix	New England Biolabs	Cat#M0492L
Q5® HotStart High-Fidelity DNA Polymerase	New England Biolabs	Cat#M0493L
Proteinase K (20 mg/mL)	Qiagen	Cat#19133
RNase A (10 mg/mL)	Thermo Scientific	Cat#EN0531
Taq Master Mix (2x)	New England Biolabs	Cat#M0270L
Terminal Transferase	New England Biolabs	Cat#M0315L
Zymolyase T100	Zymo Research	Cat#E1005

Zymolyase® 20T ( <i>Arthrobacter luteus</i> )	Amsbio	Cat#120491-1
<b>Chemicals</b>		
2-mercaptoethanol	Sigma-Aldrich	Cat#M6250
3-Indoleacetic acid (IAA)	Sigma-Aldrich	Cat#I2886-5G
5-Fluoroorotic Acid (5-FOA)	Zymo Research	Cat#F9001-1
Acetone	Sigma-Aldrich	Cat#100014
Agar	Sigma-Aldrich	Cat#05040
Agarose	Sigma-Aldrich	Cat#A9539
Alpha-factor mating pheromone	Zymo Research	Cat#Y1001
Bacto yeast extract	BD Biosciences	Cat#BD-212750
Bacto tryptone	BD Biosciences	Cat#BD-211705
Bardford solution	Applichem	Cat#A6932
Boric acid	Sigma-Aldrich	Cat#31146
Bromocresol green	Sigma-Aldrich	Cat#114359
Bromophenol blue	Sigma-Aldrich	Cat#B0126
Carbenicillin disodium salt	Sigma-Aldrich	Cat#C1389
CDP-Star®	Roche	Cat#1204167700 1
cOmplete Mini EDTA-free Protease Inhibitor Cocktail tablets	Roche	Cat#4693159001
CutSmart® buffer	New England Biolabs	Cat#B7204S
dATP [ $\alpha$ - <sup>32</sup> P]	Hartmann Analytic	Cat#SRP-203
Dimethyl sulfoxide (DMSO)	Sigma-Aldrich	Cat#D8418
Dithiothreitol (DTT)	Sigma-Aldrich	Cat#43816
DNA ladder, 1 kb	New England Biolabs	Cat#N3232L
DNA ladder, 100 bp	New England Biolabs	Cat#N3231S
Dynabeads™ Protein G	Invitrogen	Cat#10607605
Ethanol absolute	VWR	Cat#85033
Ethylenediaminetetraacetic acid (EDTA)	Sigma-Aldrich	Cat#03620
Ethylenediaminetetraacetic acid disodium salt dihydrate (Na <sub>2</sub> EDTA)	Applichem	Cat#A3553
Exonuclease I Reaction Buffer (10x)	New England Biolabs	Cat# B0293S
Ficoll 400	Applichem	Cat#A2252
Formaldehyde solution 30 %, low-methanol	Roth	Cat#4235.1
Formaldehyde solution 37%	Applichem	Cat#A0877
G418 disulfate solution	Applichem	Cat#A6798
Galactose (D+)	Applichem	Cat#1421731211
Glucose (D+)	Applichem	Cat#A1422
Glycerol	Fisher Scientific	Cat#11433297
Glycine	Applichem	Cat#A1067
HEPES buffer pH 7.5	Applichem	Cat#A6916
Hydroxyurea	Sigma-Aldrich	Cat#H8627
Hygromycin B gold solution	InvivoGen	Cat#ANT-HG-5
IgG Sepharose™ 6-Fast-Flow-Medium	GE Healthcare	Cat#11574955
Isopropanol	Sigma-Aldrich	Cat#I9516

KLD 2x Reaction Buffer	New England Biolabs	Cat#B0554S
Lithium acetate	Sigma-Aldrich	Cat#517992
Lithium chloride	Applichem	Cat#A6286
Magnesium chloride (MgCl <sub>2</sub> )	Sigma-Aldrich	Cat#208337
Methyl methanesulfonate	Sigma-Aldrich	Cat#129925
NEBuffer™ 4	New England Biolabs	Cat#B7004S
Nonidet P40	Applichem	Cat#A1694
Nourseothricin-dihydrogen sulfate (ClonNAT)	WERNER BioAgents	Cat#5002000
NuPAGE™ 10% Bis-Tris gel	Thermo Scientific	Cat#NP0301
NuPAGE™ 20x MES buffer	Thermo Scientific	Cat#NP0002
NuPAGE™ 4x LDS sample buffer	Thermo Scientific	Cat#NP0008
NuPAGE™ LDS Sample Buffer 4x	Life Technologies	Cat#NP0008
Orange G	Applichem	Cat#A1404
Peptone	Sigma-Aldrich	Cat#70169
PhosSTOP tablets	Roche	Cat#0490684500 1
PMSF BioChemica	Applichem	Cat#A0999
Poly(ethylene glycol) - PEG 400	Sigma-Aldrich	Cat#81240
Ponceau S solution	Sigma-Aldrich	Cat#P7170
Potassium acetate	Sigma-Aldrich	Cat#P1190
Potassium chloride (KCl)	Sigma-Aldrich	Cat#12636
Potassium hydroxide (KOH)	Applichem	Cat#A1575
Potassium phosphate monobasic (KH <sub>2</sub> PO <sub>4</sub> )	Sigma-Aldrich	Cat#P9791
Potassium phosphate dibasic (K <sub>2</sub> HPO <sub>4</sub> )	Sigma-Aldrich	Cat#P8281
Prestained protein marker, Broad Range (11-190 kDa)	New England Biolabs	Cat#P7706L
Protease Inhibitor Cocktail	Sigma-Aldrich	Cat# P8215-5ML
Raffinose x5 H <sub>2</sub> O (D+)	Applichem	Cat#A6882
Skim milk powder	Sigma-Aldrich	Cat#70166
Sodium acetate (NaAc)	Sigma-Aldrich	Cat#S2889
Sodium azide	Sigma-Aldrich	Cat#S2002
Sodium citrate tribase dihydrate	Sigma-Aldrich	Cat#W302600
Sodium chloride (NaCl)	Sigma-Aldrich	Cat#31434
Sodium deoxycholate (SOD)	Sigma-Aldrich	Cat#D6750
Sodium dodecyl sulfate (SDS) solution 20%	Applichem	Cat#A0675
Sodium hydroxide (NaOH)	Sigma-Aldrich	Cat#30620
Sodium phosphate dibasic (Na <sub>2</sub> HPO <sub>4</sub> x 2 H <sub>2</sub> O)	Sigma-Aldrich	Cat#S7907
Sodium thiosulfate (Na <sub>2</sub> S <sub>2</sub> O <sub>3</sub> )	Applichem	Cat#A1670
Sorbitol (D+)	Sigma-Aldrich	Cat#51876
Standard Nutrient Broth No.1	Sigma-Aldrich	Cat#70122
Sucrose	Sigma-Aldrich	Cat#S0389
SuperSignal West Pico PLUS Chemiluminescent Substrate	Thermo Scientific	Cat#34578
SuperSignal West Femto Chemiluminescent Substrate	Thermo Scientific	Cat#34094
SYBR Gold	Invitrogen	Cat#S11494



SYBR Safe DNA gel stain	Fisher Scientific	Cat#10328162
SYTOX Green nucleic acid stain	Thermo Scientific	Cat#S7020
Trichloroacetic acid (TCA)	Sigma-Aldrich	Cat#27242
Tris (Trizma base)	Sigma-Aldrich	Cat#T1503
Triton X-100	Sigma-Aldrich	Cat#X100
Trypsin	Sigma-Aldrich	Cat#T6567
Tween-20	Sigma-Aldrich	Cat#P1379
Urea	Sigma-Aldrich	Cat#U5378
Xylene cyanol	Sigma-Aldrich	Cat#X4126
Yeast nitrogen base w/o amino acids	Sigma-Aldrich	Cat#Y0626
Yeast synthetic dropout medium supplement w/o amino acid (SC or SD)	MP Biomedicals	
Yeastmaker™ carrier DNA	Clontech	Cat#630440
Zinc acetate	Sigma-Aldrich	Cat#383317

#### 4.1.7 Additional Materials

Name	Source	Identifier
15 mL BioRuptor® Pico tubes and sonication beads	Diagenode	Cat#C01020031
Falcon® 96-well Clear Flat Bottom TC-treated Culture Microplate	Corning	Cat#353072
Amersham Hybond-NX Nylon Membrane	GE Healthcare	Cat#10712237
Amersham Protran Premium Nitrocellulose Membrane	GE Healthcare	Cat#15219804
Hard-Shell 384-well PCR plates	BioRad	Cat#HSP3805
Lysing Matrix C tubes	MP Biomedicals	Cat#11492410
Microscopic Cover Glasses 22 x 22 mm	Novoglas	Cat#01-2222/x
Microscope slides	NeoLab	Cat#1-6274
Microseal 'B' PCD Adhesive seal	BioRad	Cat#MSB1001
Mini-Protean® TGX Stain-Free™ Protein Gels (7.5/ 10/ 4-15 %, 10/ 15 well)	BioRad	
Replica plater for 96-well plate	Sigma-Aldrich	
TubeSpin® Bioreactor 50	TPP	Cat#TPP87050

#### 4.1.8 Electronic Devices and Software

Electronic Device	Supplier
BD FACSVerser	Becton Dickinson
BD LSRFortessa SORP	Becton Dickinson
BioRuptor Pico	Diagenode
BioRuptor Water Cooler Minichiller	Diagenode
Chemidoc Touch Imaging System	BioRad
Dissection Microscope MSM 400	Singer Instruments

Hybridisation Oven OV3	Biometra
FastPrep-25	MP Biomedicals
Leica DM1000 LED	Leica
PowerPac Basic	BioRad
NanoDrop 2000	Thermo Scientific
Qubit 2.0 Fluorometer	Thermo Scientific
Real Time PCD Detection System CFX384 Touch	BioRad
Sonifier 450	Branson
Spectrophotometer Ultrospec 2100 pro	Biochrom
Thermal Cycler C1000 Touch	BioRad
Trans-Blot Turbo Transfer System	BioRad
Typhoon FLA 9500	GE Healthcare
UV Stratalinker 2400	Stratagene
<b>Software</b>	<b>Supplier</b>
BD FACSDiva Software v9.0.1	Becton Dickinson RRID:SCR_001456
Bio-Rad CFX Manager 3.1	BioRad RRID:SCR_018057
FACSuite V1.0.5	Becton Dickinson
Fiji 1.51d	ImageJ RRID:SCR_002285
FileMaker Pro 10	FileMaker Inc
FlowJo v10.6.1	Becton Dickinson RRID:SCR_008520
GraphPad Prism 9	GraphPad RRID:SCR_002798
Illustrator CC2020	Adobe
ImageLab V5.2	BioRad
MaxQuant	Max-Planck-Institute of Biochemistry RRID:SCR_014485
Mendeley Desktop	Elsevier
Microsoft Office for Windows 2016	Microsoft
R	The R Foundation RRID:SCR_001905
SnapGene 4.0.8	GSL Biotech

## 4.2 METHODS

### 4.2.1 Yeast Strains and Culture

All yeast strains used in this study are derived from the *Saccharomyces cerevisiae* parental laboratory strain S288C<sup>558</sup>, more specifically derivatives of the BY4741 background (MATa *his3Δ1 leu2Δ0 met15Δ0 ura3Δ0*)<sup>555</sup>. Strains were grown under standard conditions in YPD (1% [w/v] yeast extract, 2% [w/v] peptone supplemented with 2% glucose) or SC (0.2% [w/v] Synthetic Complete without amino acids, 1% [w/v] yeast nitrogen base supplemented with 2% glucose) media at the appropriate temperature. For strain generation, standard yeast genetics protocols were used<sup>559</sup>, detailed procedures as follows.

#### 4.2.1.1 Yeast Mating and Sporulation

Haploid yeast strains of opposite mating types (MATa and MATα) were mated by patching on YPD plates and grown overnight at the appropriate temperature to obtain diploid strains. Diploids were selected by streaking for single colonies on double-selection plates, incubated at the appropriate temperature for 3 days. Single colonies of diploids were patched on PRE-SPO plates and grown overnight at the appropriate temperature, subsequently cells were transferred into 3 mL SPO media cultures and incubated at 23°C, until efficient sporulation was observed ( $\geq 4$  days). A 1:1 mixture of sporulation culture and lyticase (2.5 mg/mL, Sigma) incubated at room temperature (RT) for 20 min, was then seeded onto YPD or selective plates for tetrad dissection by micromanipulation. Plates were incubated at the appropriate temperature for 3 days, and the genotypes were determined by replica plating onto the appropriate selection plates.

#### 4.2.1.2 Yeast Transformation

To generate competent yeast cells, 25 mL of exponentially growing liquid yeast cultures (0.4-0.8 OD<sub>600</sub> units) were centrifuged 3 min, 1500 rcf at RT and washed with 5 mL LiAc-mix. Cells were centrifuged again 3 min, 1500 rcf at RT and resuspended in 250  $\mu$ L LiAc-mix. The competent yeast cells were either used directly for transformation or stored at -80°C with 7 % DMSO for later use. The transformation reaction contains 100  $\mu$ L of competent cells, 10  $\mu$ L of Yeastmaker<sup>TM</sup> Carrier DNA, 0.5  $\mu$ g of plasmid or 10 $\mu$ L of PCR product and 700  $\mu$ L of PEG-mix, and was incubated for 30 min rotating at RT. After a 15 min heat shock at 42°C (or 37°C for temperature sensitive (*ts*) strains), cells were centrifuged 3 min, 1500 rcf at RT and resuspended in 300  $\mu$ L of YPD medium. For plasmid transformation, cells were incubated for 30 min at 30°C (or lower temperatures for *ts* strains)

and plated on appropriate selective plates. For integration, cells were plated on YPD and allowed to grow overnight at the appropriate temperature, before replica plating onto appropriate selective plates. Selection plates were incubated at the appropriate temperature for 2-3 days.

#### 4.2.1.3 Strain Construction

The *RNH201-6MYC* and *RNH202-9MYC* alleles were created by amplifying the *9MYC-HIS* cassette by PCR from the plasmid pBL332 using the oligonucleotide pairs oAL29 + oAL30, and oVP3 + oVP4, respectively and which were designed according to Janke et al., 2004. The PCR reaction composition included 100 ng pBL332, 25 µL Q5 2x Mastermix, 0.64 µL of each 5 µM oligonucleotide and water to a final volume of 50 µL. The PCR was performed as follows: 98°C 30 sec, 98°C 10 sec, 72°C 30 sec, 72°C 1 min (to step 2 x 34 times), 72°C 10 min. The correct size of the PCR product was verified by agarose gel, and subsequently 10 µL of the PCR reaction were transformed into yBL7 and plated on SC – HIS plates, incubated at 30°C for 3 days. Colonies were restreaked on SC – HIS to exclude false positives, those which could re-grow were confirmed by PCR to verify correct integration on genomic DNA, which was extracted with the Puregene Yeast/Bact. Kit B. Correct integration was verified by PCR and sequencing with the oligonucleotide pairs oAL31 + oBL29 and oAL77 + oBL29, respectively, and the reaction was composed of 200 ng genomic DNA, 5 µL of each 2.5 µM oligonucleotide, 12.5 µL Q5 2x Mastermix and water to a final volume of 25 µL. The PCR was performed as follows: 98°C 30 sec, 98°C 10 sec, 65°C 30 sec, 72°C 1 min (to step 2 x 34 times), 72°C 5 min. The correct size of the PCR product was verified by agarose gel and sequenced with the QIAquick PCR Purification Kit. Expression of the tagged proteins was confirmed by western blot.

#### 4.2.1.4 Site Directed Mutagenesis for Plasmid Construction

For construction of the pBL710 plasmid (*pRS423 pGPD-RNH1-D193N-HA*), a catalytic dead version of *RNH1*, site directed mutagenesis with the Q5® High-Fidelity 2x Master Mix was performed using the plasmid pBL192 (*pRS423 pGPD-RNH1-HA*) as a template and the primers oRM1 + oRM2, as mutation drivers. The PCR was performed as follows: 98°C 30 sec, 98°C 10 sec, 60°C 15 sec, 72°C 4 min 15 sec (to step 2 x 34 times), 72°C 2 min. The amplified PCR product was later treated with a KLD mix, for 1 h RT, and transformed into DH5α *E.coli*. The QIAprep Spin Miniprep Kit was used, according to manufacturer's instruction, to prepare plasmids. Mutagenesis on the plasmids was verified by sequencing with the oligonucleotides oTW18 + oBL256. Validation of *RNH1-D193N* functionality was performed after plasmid transformation into wild type (yBL7) and *rnh1*

*rnh201* (yVP1025) cells, and spotting onto selection plates with methyl methanesulfonate (MMS).

## 4.2.2 Bacterial Transformation

50  $\mu$ L of competent DH5 $\alpha$  *E.coli* cells were mixed with 0.5  $\mu$ g of plasmid and incubated for 30 min on ice. After a 1 min heat shock at 42°C, the transformation reaction was incubated 1 min on ice and subsequently 300  $\mu$ L of LB medium were added. The reaction was further incubated for 30 min at 37°C, before plating 100  $\mu$ L on LB plates containing carbenicillin and grown overnight at 37°C.

## 4.2.3 Spotting Assay

Yeast cells, from overnight cultures incubated at the appropriate temperature in YPD or SC medium, were diluted to 0.5 OD<sub>600</sub> units and spotted in ten-fold dilutions onto the appropriate agar plates. The plates were incubated at the appropriate temperature for the indicated times, and subsequently imaged with the Bio-Rad ChemiDoc™ Touch Imaging System.

## 4.2.4 Growth Curve Assay

Yeast cells, from 5 mL overnight cultures incubated at the appropriate temperature in YPD or SC medium, were diluted to 0.05 OD<sub>600</sub> units in 100  $\mu$ L appropriate medium and transferred to a 96-well plate in triplicates. OD<sub>600</sub> measurements were taken every hour at the appropriate temperature for 15 h using a TECAN Spark® microplate reader. The measured OD<sub>600</sub> was plotted against time and the doubling times (PD) were derived from measurements taken throughout the exponential growth phase and calculated using the following formula from Roth 2006<sup>560</sup>:

$$\text{Doubling Time} = \frac{\text{duration} * \log(2)}{\log(\text{FinalConcentration}) - \log(\text{InicialConcentration})}$$

In this calculation, duration is the time between two measurements in hours and the initial and final concentration values correspond to the measured OD<sub>600</sub> of the cell cultures at the

determined time points. PD values were calculated separately for each biological replicate per genotype, and the average and standard deviation (SD) were plotted. For statistical analysis one-way ANOVA test with Bonferroni correction for multiple comparisons was applied.

#### 4.2.5 Senescence Curve

Telomerase negative spores of dissected diploids, grown for 3 days at the appropriate temperature after dissection, were inoculated to 0.01 OD<sub>600</sub> units (or 0.02 OD<sub>600</sub> units for *rad52* curves) in 5 mL of appropriate media (YPD medium unless indicated otherwise) and incubated for 24 h at the appropriate temperature. The cultures' OD<sub>600</sub> was measured daily and each culture was re-diluted to 0.01 OD<sub>600</sub> units in 5 mL of new media, until all cultures re-gained the initial viability. Viability was measured by setting the starting culture OD<sub>600</sub> to 100% and comparing each daily measurement to the initial one, for each sample. 5-6 biological replicates were performed for each genotype. Population doublings (PD) were calculated daily as the  $\log_2(\text{OD}_{600}/0.01)$  or  $\log_2(\text{OD}_{600}/0.02)$ , where the OD<sub>600</sub> is the average cell density measured after 24 h for each genotype. PD values calculated do not account for the colony growth on the dissection plate (~25 generations). Graphs were plotted using Prism8 (GraphPad).

For senescence curves with overexpression plasmids, the diploid strain was firstly transformed with a wild type copy of the *EST2* gene on a URA plasmid (pBL354) and dissected to obtain the genotypes of interest. The haploids of interest were transformed with pBL190, pBL192 or pBL710 and plated on SD-URA-HIS plates to select for both plasmids, for 3 days at 30°C. Transformed colonies were then streaked out for single colonies on SD-HIS + 5-FOA plates to counter-select for the pBL354 plasmid. Plates were incubated for 3 days at 30°C and similar size single clones, which lost the pBL354 plasmid, were inoculated for the senescence curve. Loss of pBL354 plasmid was confirmed by streaking the colonies used for the curve into SC-URA and checking for lack of growth.

#### 4.2.6 Senescence Spotting Assay

Telomerase negative spores of dissected diploids, grown for 3 days at the appropriate temperature after dissection, were diluted to 0.5 OD<sub>600</sub> units and spotted in ten-fold dilutions onto YPD agar plates. The plates were incubated at the appropriate

temperature for 3 days, and images were taken after 48 and 72 hours with the Bio-Rad ChemiDoc™ Touch Imaging System. Re-spotting occurred every 48 h allowing for subsequent passages and telomere shortening, stopping when senescence was observed for all telomerase negative genotypes.

#### 4.2.7 Cell Cycle Synchronization and Release

Exponentially growing MATa cultures (~0.4 OD<sub>600</sub> units) in YPD medium at the appropriate temperature were treated with 4 µg/mL of α-factor and incubated at the appropriate temperature for 2 h 15 min. Confirmation of G1 arrest was determined qualitatively by looking at cell morphology (shmoo formation in >90% of cells) at the light microscope. For the synchronous release from a G1 arrest, cells were pelleted at 1500 rcf for 3 min and washed three times with pre-warmed sterile ddH<sub>2</sub>O (25°C) and further grown at 25°C in a water bath. Samples were collected every 15 min.

#### 4.2.8 Protein Extraction and Western Blot

2 OD<sub>600</sub> units of exponentially growing cells were centrifuged 2 min at 16 500 rcf, resuspended in 150 µL of ice-cold Solution 1 (1.85 M NaOH, 1.09 M 2-mercaptoethanol) and incubated for 10 min on ice. 150 µL of ice-cold Solution 2 (50% TCA) were then added and, after vortexing, samples were incubated for 10 min on ice. Samples were then centrifuged 2 min at 16 500 rcf at 4°C and the pellets were washed with 1 mL ice-cold Solution 3 (acetone). Samples were centrifuged again 2 min at 16 500 rcf at 4°C and pellets were resuspended in 100 µL of urea buffer (120 mM Tris-HCl pH 6.8, 5% glycerol, 8M urea, 143 mM 2-mercaptoethanol, 8% SDS, bromophenol blue indicator), incubated for 5 min at 75°C, or 50°C if post-translational modifications were analysed, and spin down 30 sec at 16 500 rcf. 5 – 10 µL of protein samples were loaded onto Mini Protean TGX Precast gels (7.5 %, 10 % or 4-15 % gradient), and run at 100 - 150 V with 1x SDS running buffer. Gels were blotted onto pre-wet nitrocellulose membranes, with 1x Transfer buffer, using the TurboBlot system and the “High Molecular Weight” program. The membranes were stained with Ponceau solution to monitor transfer efficiency and loading, and afterwards blocked with Blocking buffer shaking for 1 h at RT. The primary antibody diluted in Blocking buffer was incubated overnight 4°C with gentle shaking (antibody dilutions described in the antibody section of Materials and Methods). After washing three times with 1x PBST, the

membranes were incubated for 1 h with the appropriate secondary antibody diluted in Blocking buffer at RT (antibody dilutions described in [antibody section of Materials and Methods](#)). Membranes were afterwards washed three times with 1x PBST and once with 1x PBS and signals were detected by chemiluminescence, and imaged with the Bio-Rad ChemiDoc™ Touch Imaging System.

#### 4.2.9 DNA Content Analysis by Flow Cytometry

0.18 OD<sub>600</sub> units of cells were centrifuged 2 min at 16 500 rcf and washed with 1 mL ddH<sub>2</sub>O. Pellets were resuspended in 70% ethanol and fixed overnight at 4°C, and afterwards centrifuged 5 min at 16 500 rcf and washed with 1 mL ddH<sub>2</sub>O. Pellets were then resuspended in 500 µL of 50 mM Tris-HCl pH 7.5, supplemented with 10 µL of RNase A (10 mg/mL) and incubated for 3 h at 37°C. Afterwards, 25 µL of Proteinase K (20 mg/mL) were added and incubated for 1 h at 50°C. Cells were centrifuged 5 min at 16 500 rcf, resuspended in 500 µL of 50 mM Tris-HCl pH 7.5 and either stored at 4°C or directly prepared for measuring. For measuring, samples were sonicated manually using the Branson Sonifier 450 for 10 sec (constant mode) or subjected to sonication using the BioRuptor Pico for 2x 10 sec with 10 sec intervals between runs. Samples were transferred to FACS tubes and 500 µL of 4 µM Sytox Green in 50 mM Tris-HCl pH 7.5 was added. Tubes were kept in the dark and each sample was vortexed immediately before analysis with the BD FACSVerser or BD LSRFortessa™ cell analysers. Data analysis was performed with the BD FACS Suite software and the FlowJo software (v10.6.1).

#### 4.2.10 Telomere PCR (TELO-PCR)

Yeast cells (50mL), from the senescence curve, were grown in YPD or SC medium at 30°C for exponential growth. Genomic DNA was extracted using the Gentra Puregene Yeast/Bact. Kit (Qiagen), according to the manufacturer's instructions. 1µL 100ng/µL genomic DNA was mixed with 3.1µL water and 0.9µL NEBuffer 4. The solution was boiled for 10min at 96°C before it was cooled down to 4°C. Afterward, 0.2µL terminal transferase (New England Biolabs), 0.1µL NEBuffer 4, 0.1µL 10mM dCTP and 4.6µL water were added. The C-tailing reaction was allowed to take place for 30min at 37°C, before the reaction was heated up to 65°C for 10min and afterward to 96°C for 5min. Thereafter, the PCR mix was added (21µL water, 4µL 10x PCR buffer (670mM Tris-HCl pH 8.8, 160mM (NH<sub>4</sub>)SO<sub>4</sub>, 50%



glycerol, 0.1% Tween-20, in water), 4  $\mu$ L 2mM dNTPs, 0.3  $\mu$ L 100  $\mu$ M oBL358 (1L) or oBL361 (Y'), 0.3  $\mu$ L 100  $\mu$ M oBL359, 0.4  $\mu$ L Q5 HotStart (New England Biolabs)). The PCR program was as follows: 98°C for 3min, 98°C for 30s, 63°C for 15s, 72°C for 20s (last three steps repeated 44 times), 72°C for 5min. The PCR products were analysed via gel electrophoresis on a 1.8% agarose gel. Gels were imaged on ChemiDoc™ Touch Imaging System (BioRad), telomere length for each lane was determined with the ImageLab (BioRad) software. Calculation of the telomere shortening rates was performed by linear regression of the average daily telomere length for 3-4 consecutive days, where the rate = (slope)/population doubling. Graphs were plotted using Prism7.

#### 4.2.11 Chromatin Binding Assay (CBA)

50 mL of exponentially growing cells (0.6-0.8 OD<sub>600</sub> units) in YPD at 30°C, were collected for genomic DNA extraction using the Gentra Puregene Yeast/Bact. kit (Qiagen). Cell pellets were washed with cold Spheroblasting Buffer, spun down at 3000 rcf, 4°C for 3 min and 12 OD<sub>600</sub> units were resuspended in a final volume of 1 mL in Spheroblasting Buffer. 1  $\mu$ L zymolyase and 1  $\mu$ L DTT were added to each sample, followed by incubation 30°C for 40 min. Spheroblasts were collected by centrifugation at 400 rcf, 4°C for 2 min and were resuspended in 300  $\mu$ L Extraction Buffer containing a protease inhibitor cocktail and phosSTOP. Each sample was then split in whole-cell extract (50  $\mu$ L, corresponding to 2 OD<sub>600</sub> units), soluble (50  $\mu$ L, corresponding to 2 OD<sub>600</sub> units) and chromatin (200  $\mu$ L, corresponding to 8 OD<sub>600</sub> units) fractions. To each sample 0.25% final concentration of Triton X-100 was added, followed by incubation for 5 min on ice. Preparation of whole cell extract fraction: 1  $\mu$ L Benzonase was added to each sample followed by incubation for 15 min on ice. Preparation of soluble fraction: samples were centrifuged and the supernatant was transferred to a fresh tube. Preparation of chromatin fraction: 1 mL of cold 30% sucrose solution was added to each sample, followed by centrifugation at 20 000 rcf, 4°C for 10 min. The pellet was then resuspended in 200  $\mu$ L Extraction Buffer and 5  $\mu$ L 10% Triton X-100. The sucrose step was repeated again and the pellet was finally resuspended in 50  $\mu$ L Extraction Buffer and 0.25% final concentration of Triton X-100. 1  $\mu$ L Benzonase was then added to the samples, followed by incubation for 15 min on ice. To all fractions 20  $\mu$ L Urea buffer were added and samples were boiled for 5 min at 95°C. Samples were then loaded onto 4%–15% precast gel.

#### 4.2.12 Chromatin Immunoprecipitation (ChIP), DNA-RNA Immunoprecipitation (DRIP) and qPCR

Yeast cells in exponential growth phase (0.6-1 OD<sub>600</sub> units) were inhibited with 0.01% sodium azide and subsequently diluted to the same OD<sub>600</sub> values for crosslinking. Samples were crosslinked for 10min (RPA ChIP and DRIP) with 1.2% formaldehyde and quenched with 360mM glycine for 5min. After an incubation on ice of at least 15min, the cells were pelleted and washed twice with 1x PBS. Cells were resuspended in FA lysis buffer (50mM HEPES-KOH pH 7.5, 140mM NaCl, 1mM EDTA pH 8, 1% Triton X-100, protease inhibitor cocktail) and lysed with Matrix C tubes via Fastprep (MP Biomedicals; 6.5M/s, 2x 30sec with 1min on ice in between runs). Cell extracts were recovered adding FA lysis buffer containing 0.1% sodium deoxycholate (SOD), centrifuged and the soluble portion of the lysate was discarded. Pellets were resuspended in FA lysis buffer with SOD + 0.263% SDS. The chromatin was sonicated 2x 30sec ON/OFF for 10 cycles at 4°C, with a 10min break on ice in between with Bioruptor Pico (Diagenode). After centrifugation, the supernatant (ChIP extract) was diluted to 1mg/mL protein concentration in FA lysis buffer + SOD and used for immunoprecipitation (IP). An input sample representing 5% of the ChIP extract used for IP served for qPCR normalization. To verify sonication efficiency, a ChIP extract sample was incubated O/N with 0.75mg/mL proteinase K (QIAGEN) at 65°C. The sample was purified by EtOH precipitation, treated with 10µg RNase A (Thermo Scientific) for 30min at 37°C and analysed on an 1.5% agarose gel. Bead preparation consisted on 1x PBS wash, followed by blocking with 5% BSA for 1h at 4°C and subsequent FA lysis buffer wash. 1mg/mL extracts were precleared with Dynabeads™ Protein G (Invitrogen) for 1h at 4°C. IPs were performed O/N at 4°C with Protein G beads in the presence or absence of 4µg of antibody for DRIP: S9.6 antibody (Kerafast), and 1µL RPA ChIP: α-RFA (Agrisera Antibodies). Beads were washed with: FA lysis buffer + SOD, FA lysis buffer 500 (500nM NaCl added to FA lysis buffer), buffer III (10mM Tris-HCl pH 8, 0.1mM EDTA pH8, 250mM LiCl, 1% Nonidet P-40 and 1% SOD) and TE (pH 8). All washing steps were performed at 4°C for 5min. Bead-bound DNA was eluted twice in 100µL elution buffer B (50mM Tris-HCl pH 7.5, 1% SDS and 10mM EDTA pH 8) for 8min at 65°C. To reverse the crosslinking, IPs and input samples were treated O/N with 0.75mg/mL proteinase K (QIAGEN) at 65°C. DNA was purified with QIAquick PCR Purification Kit (QIAGEN). qPCR analysis was performed using CFX384 Touch Real-Time PCR Detection System (BioRad) and SYBR-Green (Thermo Scientific) detection with 60°C annealing temperature. Oligonucleotides used are listed in the [oligonucleotide section of Materials and Methods](#). Measured Cq values were corrected to input and graphs were created with Prism9 (GraphPad).

BG4 ChIP was performed, by Mona Hajikazemi in Katrin Paeschke's lab, as described previously<sup>524</sup> with minor changes for *S. cerevisiae*. The full protocol can be found in Pires et al. 2023<sup>515</sup>. The enrichment of G4s and percentage of input recovery was quantified using qPCR with specific primers, listed in the [oligonucleotide section of Materials and Methods](#).

#### 4.2.13 ssDNA Dot Blot

Yeast cells (50 mL) were grown in YPD or SC medium at 23°C for exponential growth. The cultures were shifted to 30°C for 2h, in a water bath. Genomic DNA was extracted using the Gentra Purgene Yeast/Bact. Kit (Qiagen), with slight modifications: 10 units Zymolyase 20T (Amsbio) and 23 mM 2-mercaptoethanol were used instead of the Lytic Enzyme Solution and the 65°C step was omitted to prevent denaturation of DNA (non-denaturing conditions). Calculations for the DNA amount took into account the DNA concentration measured by Qubit-Fluorometer (Invitrogen) and also the relative intensity of 1 µL DNA loaded onto a 0.8% agarose gel and imaged with the Bio-Rad ChemiDoc™ Touch Imaging System. 75 ng of DNA were spotted onto a nylon membrane (Amersham), with 1:2 serial dilutions in 1x SSC using a Bio-Dot Apparatus (BioRad). DNA was cross-linked to the membrane with UV light (auto crosslink, Stratalinker). As a loading control, 30 µg of DNA were denatured with 0.2 M NaOH for 15 min at 65°C. ssDNA was digested for 2 h at 37°C by 40 units of Exonuclease I (NEB) in a total volume of 50 µL. The membrane was pre-hybridized for 1h at 47.5°C. The telomeric C-probe (oBL207) was DIG-labelled (Roche) and hybridized overnight at 47.5°C. The membrane was washed twice with 2x SSC 0.1% SDS and twice with 0.5x SSC 0.1% SDS at 47.5°C. The membrane was blocked with 1x Blocking Reagent (Roche) in malic acid buffer pH 7.5 for 30min at RT, and subsequently hybridized with an α-DIG-AP antibody (Roche) for 30min at RT. The signal was detected using CDP-star (Roche) on ChemiDoc™ Touch Imaging System (BioRad), and quantified by the ImageJ software.

#### 4.2.14 Mass Spectrometry

Yeast cells were incubated overnight at 30°C in SC-HIS medium. The cultures were diluted to 0.1 OD<sub>600</sub> units in SC-HIS medium and incubated at 30°C. Exponential cells (0.6 – 0.7 OD<sub>600</sub> units) were collected. 0.5 OD<sub>600</sub> units of exponentially growing cells were collected by centrifugation for 3 min at 1500 rcf, and stored at 80°C. The samples were

resuspended in 1x LDS buffer containing 0.1M Dithiothreitol and denatured for 10 min at 70°C. The proteins were separated on a 10% NuPAGE NOVEX Bis-Tris gel (Thermo Fisher) for 8 min in 1x MES buffer (Thermo Fisher) at 180 V. The gel was fixated and stained with Coomassie Brilliant Blue G250 (Sigma), followed by destaining overnight in water. The in-gel digestion was performed according to the previous protocol<sup>561</sup>. After trypsin digestion the peptides were bound and desalted on C18-StageTips<sup>562</sup> and stored at 4°C until mass spectrometric (MS) measurement. For the MS analysis, the peptides were separated on a 50 cm capillary (New Objective) with 75 µm inner diameter packed in-house with ReproSil-Pur 120 C18-AQ (Dr Maisch GmbH) mounted to an EASY-nLC 1200 (Thermo Fisher). The HPLC system was coupled to an Exploris 480 mass spectrometer (Thermo Fisher). Peptide elution was performed during a 103-min gradient from 3% to 40% acetonitrile with 0.1% formic acid at a constant flow rate of 250 nL min<sup>-1</sup>. The mass spectrometer was operated with a top 20 MS/MS data-dependent acquisition method per MS full scan. The raw data was processed using MaxQuant (version 1.6.10.43)<sup>563</sup> and searched against the Saccharomyces Genome Database (version R64-3-1, 6,716 entries). Data base searches were performed with standard settings using the label free quantification (LFQ) algorithm<sup>564</sup>. Carbamidomethylation was set as fixed modification while methionine oxidation and protein N-acetylation were considered as variable modifications. The option “match between runs” was activated. In a filtering step, contaminants, reverse database hits, protein groups only identified by site and protein groups with less than 2 peptides of which at least one was a unique peptide, were removed. Missing LFQ values were imputed at the lower end of LFQ values within each sample. Data analysis and graphical representation was performed in R (version 3.6.2) using existing libraries (knitr, reshape2, dplyr, ggplot2, ggrepel) and in-house scripts.

## 5 REFERENCES

---

1. Giraud-Panis, M. J. *et al.* One identity or more for telomeres? *Front. Oncol.* **3**, 1–16 (2013).
2. Linger, B. R. & Price, C. M. Conservation of telomere protein complexes: Shuffling through evolution. *Crit. Rev. Biochem. Mol. Biol.* **44**, 434–446 (2009).
3. Palm, W. & de Lange, T. How Shelterin Protects Mammalian Telomeres. *Annu. Rev. Genet.* **42**, 301–334 (2008).
4. Larrivée, M., LeBel, C. & Wellinger, R. J. The generation of proper constitutive G-tails on yeast telomeres is dependent on the MRX complex. *Genes Dev.* **18**, 1391–1396 (2004).
5. Wellinger, R. J., Wolf, A. J. & Zakian, V. A. Saccharomyces Telomeres Acquire Single-Strand TG1-3 Tails Late in S Phase. *Cell* **72**, (1993).
6. Wellinger, R. J. & Zakian, V. A. Everything you ever wanted to know about *Saccharomyces cerevisiae* telomeres: Beginning to end. *Genetics* **191**, 1073–1105 (2012).
7. Lange, T. De. Shelterin-Mediated Telomere Protection. (2018).
8. Dionne, I. & Wellinger, R. J. Cell cycle-regulated generation of single-stranded G-rich DNA in the absence of telomerase. *Proc. Natl. Acad. Sci.* **93**, 13902–13907 (1996).
9. Dionne, I. & Wellinger, R. J. Processing of telomeric DNA ends requires the passage of a replication fork. *Nucleic Acids Res.* **26**, 5365–5371 (1998).
10. Wellinger, R. J., Wolf, A. J. & Zakian, V. A. Origin Activation and Formation of Single-Strand TG1.3 Tails Occur Sequentially in Late S Phase on a Yeast Linear Plasmid. *Mol. Cell. Biol.* **13**, 4057–4065 (1993).
11. Frank, C. J., Hyde, M. & Greider, C. W. Regulation of Telomere Elongation by the Cyclin-Dependent Kinase CDK1. *Mol. Cell* **24**, 423–432 (2006).
12. Zakian, V. A., Blanton, H. M. & Wetzels, L. Distribution of telomere-associated sequences in yeast. *Basic Life Sci.* **40**, 493–498 (1986).
13. Horowitz, H., Thorburn, P. & Haber, J. E. Rearrangements of Highly Polymorphic Regions Near Telomeres of *Saccharomyces cerevisiae*. *Mol. Cell. Biol.* **4**, 2509–2517 (1984).
14. Chan, C. S. M. & Tye, B. K. Organization of DNA sequences and replication origins at yeast telomeres. *Cell* **33**, 563–573 (1983).
15. Brigati, C., Kurtz, S., Balderes, D., Vidali, G. & Shore, D. An Essential Yeast Gene Encoding a TTAGGG Repeat-Binding Protein. *Mol. Cell. Biol.* **13**, 1306–1314 (1993).
16. Louis, E. J. The chromosome ends of *Saccharomyces cerevisiae*. *Yeast* **11**, 1553–1573 (1995).
17. Chan, C. S. M., Tye, B. K. & Herskowitz, I. A family of *Saccharomyces cerevisiae* repetitive autonomously replicating sequences that have very similar genomic environments. *J. Mol. Biol.* **168**, 505–523 (1983).
18. Louis, E. J. & Haber, J. E. The Structure and Evolution of Subtelomeric Y' Repeats in *Saccharomyces cerevisiae*. *Genetics* **131**, 559–574 (1992).
19. Walmsley, R. W., Chant, C. S. M., Tye, B. & Petes, T. D. Unusual DNA sequences associated with the ends of yeast chromosomes. *Nature* **310**, 157–160 (1984).
20. Louis, E. J. & Haber, J. E. The subtelomeric Y' repeat family in *Saccharomyces cerevisiae*: an experimental system for repeated sequence evolution. *Genetics* **124**, 533–545 (1990).
21. Kupiec, M. Biology of telomeres : lessons from budding yeast. *FEMS Microbiol. Rev.* **38**, 144–171 (2014).
22. Gilson, E., Roberge, M., Giraldo, R., Rhodes, D. & Gasser, S. M. Distortion of the DNA double helix by RAP1 at silencers and multiple telomeric binding sites. *J. Mol. Biol.* **231**, 293–310 (1993).
23. Gao, H., Cervantes, R. B., Mandell, E. K., Otero, J. H. & Lundblad, V. RPA-like proteins mediate yeast telomere function. *Nat. Struct. Mol. Biol.* **14**, 208–214 (2007).
24. König, P., Giraldo, R., Chapman, L. & Rhodes, D. The crystal structure of the DNA-binding domain of yeast RAP1 in complex with telomeric DNA. *Cell* **85**, 125–136 (1996).
25. Shore, D. & Nasmyth, K. Purification and cloning of a DNA binding protein from yeast that binds to both silencer and activator elements. *Cell* **51**, 721–732 (1987).
26. Wotton, D. & Shore, D. A novel Rap1p-interacting factor, Rif2p, cooperates with Rif1p to regulate telomere length in *Saccharomyces cerevisiae*. *Genes Dev.* **11**, 748–760 (1997).
27. Hardy, C. F., Sussel, L. & Shore, D. A RAP1-interacting protein involved in transcriptional silencing and telomere length regulation. *Genes Dev.* **6**, 801–814 (1992).
28. Bonetti, D. *et al.* Shelterin-like proteins and Yku inhibit nucleolytic processing of *Saccharomyces cerevisiae* telomeres. *PLoS Genet.* **6**, e1000966 (2010).
29. Anbalagan, S., Bonetti, D., Lucchini, G. & Longhese, M. P. Rif1 supports the function of the CST complex in yeast telomere capping. *PLoS Genet.* **7**,

- e1002024 (2011).
30. McGee, J. S. *et al.* Reduced Rif2 and lack of Mec1 target short telomeres for elongation rather than double-strand break repair. *Nat. Struct. Mol. Biol.* **17**, 1438–1445 (2010).
  31. Moretti, P., Freeman, K., Coodly, L. & Shore, D. Evidence that a complex of SIR proteins interacts with the silencer and telomere-binding protein RAP1. *Genes Dev.* **8**, 2257–2269 (1994).
  32. Rusche, L. N., Kirchmaier, A. L. & Rine, J. The establishment, inheritance, and function of silenced chromatin in *Saccharomyces cerevisiae*. *Annu. Rev. Biochem.* **72**, 481–516 (2003).
  33. Gottschling, D. E., Aparicio, O. M., Billington, B. L. & Zakian, V. A. Position effect at *S. cerevisiae* telomeres: reversible repression of Pol II transcription. *Cell* **63**, 751–762 (1990).
  34. Hecht, A., Strahl-Bolsinger, S. & Grunstein, M. Spreading of transcriptional repressor SIR3 from telomeric heterochromatin. *Nature* **383**, 92–96 (1996).
  35. Strahl-Bolsinger, S., Hecht, A., Luo, K. & Grunstein, M. SIR2 and SIR4 interactions differ in core and extended telomeric heterochromatin in yeast. *Genes Dev.* **11**, 83–93 (1997).
  36. Aparicio, O. M., Billington, B. L. & Gottschling, D. E. Modifiers of position effect are shared between telomeric and silent mating-type loci in *S. cerevisiae*. *Cell* **66**, 1279–1287 (1991).
  37. Boulton, S. J. & Jackson, S. P. Components of the Ku-dependent non-homologous end-joining pathway are involved in telomeric length maintenance and telomeric silencing. *EMBO J.* **17**, 1819–1828 (1998).
  38. Grandin, N., Reed, S. I. & Charbonneau, M. Stn1, a new *Saccharomyces cerevisiae* protein, is implicated in telomere size regulation in association with Cdc13. *Genes Dev.* **11**, 512–527 (1997).
  39. Grandin, N., Damon, C. & Charbonneau, M. Ten1 functions in telomere end protection and length regulation in association with Stn1 and Cdc13. *EMBO J.* **20**, 1173–1183 (2001).
  40. Grandin, N., Damon, C. & Charbonneau, M. Cdc13 cooperates with the yeast Ku proteins and Stn1 to regulate telomerase recruitment. *Mol. Cell. Biol.* **20**, 8397–8408 (2000).
  41. Anderson, E. M., Halsey, W. A. & Wuttke, D. S. Delineation of the high-affinity single-stranded telomeric DNA-binding domain of *Saccharomyces cerevisiae* Cdc13. *Nucleic Acids Res.* **30**, 4305–4313 (2002).
  42. Schramke, V. *et al.* RPA regulates telomerase action by providing Est1p access to chromosome ends. *Nat. Genet.* **36**, 46–54 (2004).
  43. Hughes, T. R., Weilbaecher, R. G., Walterscheid, M. & Lundblad, V. Identification of the single-strand telomeric DNA binding domain of the *Saccharomyces cerevisiae* Cdc13 protein. *Proc. Natl. Acad. Sci. U. S. A.* **97**, 6457–6462 (2000).
  44. Qian, W. *et al.* Ten1p promotes the telomeric DNA-binding activity of Cdc13p: Implication for its function in telomere length regulation. *Cell Res.* **19**, 849–863 (2009).
  45. Qian, W., Fu, X. H. & Zhou, J. Q. Purification and characterization of Stn1p, a single-stranded telomeric DNA binding protein. *Protein Expr. Purif.* **73**, 107–112 (2010).
  46. Petreaca, R. C. *et al.* Chromosome end protection plasticity revealed by Stn1p and Ten1p bypass of Cdc13p. *Nat. Cell Biol.* **8**, 748–755 (2006).
  47. Sun, J. *et al.* Stn1-Ten1 is an Rpa2-Rpa3-like complex at telomeres. *Genes Dev.* **23**, 2900–2914 (2009).
  48. Petreaca, R. C., Chiu, H.-C. & Nugent, C. I. The role of Stn1p in *Saccharomyces cerevisiae* telomere capping can be separated from its interaction with Cdc13p. *Genetics* **177**, 1459–1474 (2007).
  49. Puglisi, A., Bianchi, A., Lemmens, L., Damay, P. & Shore, D. Distinct roles for yeast Stn1 in telomere capping and telomerase inhibition. *EMBO J.* **27**, 2328–2339 (2008).
  50. Grossi, S., Puglisi, A., Dmitriev, P. V., Lopes, M. & Shore, D. Pol12, the B subunit of DNA polymerase alpha, functions in both telomere capping and length regulation. *Genes Dev.* **18**, 992–1006 (2004).
  51. Garvik, B., Carson, M. & Hartwell, L. Single-stranded DNA arising at telomeres in *cdc13* mutants may constitute a specific signal for the RAD9 checkpoint. *Mol. Cell. Biol.* **15**, 6128–6138 (1995).
  52. Polotnianska, R. M., Li, J. & Lustig, A. J. The yeast Ku heterodimer is essential for protection of the telomere against nucleolytic and recombinational activities. *Curr. Biol.* **8**, 831–835 (1998).
  53. Bianchi, A., Negrini, S. & Shore, D. Delivery of yeast telomerase to a DNA break depends on the recruitment functions of Cdc13 and Est1. *Mol. Cell* **16**, 139–146 (2004).
  54. Giraud-Panis, M.-J., Teixeira, M. T., Géli, V. & Gilson, E. CST meets shelterin to keep telomeres in check. *Mol. Cell* **39**, 665–676 (2010).
  55. Nugent, C. I., Hughes, T. R., Lue, N. F. & Lundblad, V. Cdc13p: A Single-Strand Telomeric DNA-Binding Protein with a Dual Role in Yeast Telomere Maintenance. *Science (80- )*. **274**, 249–252 (1996).
  56. Diede, S. J. & Gottschling, D. E.

- Telomerase-mediated telomere addition in vivo requires DNA primase and DNA polymerases alpha and delta. *Cell* **99**, 723–733 (1999).
57. Qi, H. & Zakian, V. A. The *Saccharomyces* telomere-binding protein Cdc13p interacts with both the catalytic subunit of DNA polymerase alpha and the telomerase-associated est1 protein. *Genes Dev.* **14**, 1777–1788 (2000).
  58. Gravel, S., Larrivée, M., Labrecque, P. & Wellinger, R. J. Yeast Ku as a regulator of chromosomal DNA end structure. *Science* **280**, 741–744 (1998).
  59. Larcher, M. V., Pasquier, E., MacDonald, R. S. & Wellinger, R. J. Ku Binding on Telomeres Occurs at Sites Distal from the Physical Chromosome Ends. *PLoS Genet.* **12**, e1006479 (2016).
  60. Martin, S. G., Laroche, T., Suka, N., Grunstein, M. & Gasser, S. M. Relocalization of telomeric Ku and SIR proteins in response to DNA strand breaks in yeast. *Cell* **97**, 621–633 (1999).
  61. Roy, R., Meier, B., McAinsh, A. D., Feldmann, H. M. & Jackson, S. P. Separation-of-function mutants of yeast Ku80 reveal a Yku80p-Sir4p interaction involved in telomeric silencing. *J. Biol. Chem.* **279**, 86–94 (2004).
  62. De Lange, T. How Telomeres Solve the End-Protection Problem. *Science* **326**, 948–952 (2009).
  63. Lydall, D. Taming the tiger by the tail : modulation of DNA damage responses by telomeres. *EMBO J.* **28**, 2174–2187 (2009).
  64. Dewar, J. M. & Lydall, D. Similarities and differences between ‘uncapped’ telomeres and DNA double-strand breaks. *Chromosoma* **121**, 117–130 (2012).
  65. Casari, E. *et al.* To Fix or Not to Fix : Maintenance of Chromosome Ends Versus Repair of DNA Double-Strand Breaks. (2022).
  66. Tomaska, L., Makhov, A. M., Griffith, J. D. & Nosek, J. t-Loops in yeast mitochondria. *Mitochondrion* **1**, 455–459 (2002).
  67. Tomaska, L., Willcox, S., Slezakova, J., Nosek, J. & Griffith, J. D. Taz1 binding to a fission yeast model telomere: formation of telomeric loops and higher order structures. *J. Biol. Chem.* **279**, 50764–50772 (2004).
  68. Muñoz-Jordán, J. L., Cross, G. A., de Lange, T. & Griffith, J. D. t-loops at trypanosome telomeres. *EMBO J.* **20**, 579–588 (2001).
  69. Cesare, A. J., Quinney, N., Willcox, S., Subramanian, D. & Griffith, J. D. Telomere looping in *P. sativum* (common garden pea). *Plant J.* **36**, 271–279 (2003).
  70. Cesare, A. J., Groff-Vindman, C., Compton, S. A., McEachern, M. J. & Griffith, J. D. Telomere loops and homologous recombination-dependent telomeric circles in a *Kluyveromyces* lactis telomere mutant strain. *Mol. Cell. Biol.* **28**, 20–29 (2008).
  71. Griffith, J. D. *et al.* Mammalian telomeres end in a large duplex loop. *Cell* **97**, 503–514 (1999).
  72. de Bruin, D., Kantrow, S. M., Liberatore, R. A. & Zakian, V. A. Telomere folding is required for the stable maintenance of telomere position effects in yeast. *Mol. Cell. Biol.* **20**, 7991–8000 (2000).
  73. Poschke, H. *et al.* Rif2 Promotes a Telomere Fold-Back Structure through Rpd3L Recruitment in Budding Yeast. *PLoS Genet.* **8**, (2012).
  74. Wagner, T. *et al.* Chromatin modifiers and recombination factors promote a telomere fold-back structure, that is lost during replicative senescence. *PLoS Genet.* **16**, e1008603 (2020).
  75. Smith, J. S. *et al.* Rudimentary G-quadruplex-based telomere capping in *Saccharomyces cerevisiae*. *Nat. Struct. Mol. Biol.* **18**, 478–486 (2011).
  76. Ohle, C. *et al.* Transient RNA-DNA Hybrids Are Required for Efficient Double-Strand Break Repair. *Cell* **167**, 1001–1013.e7 (2016).
  77. McClintock, B. The Production of Homozygous Deficient Tissues with Mutant Characteristics by Means of the Aberrant Mitotic Behavior of Ring-Shaped Chromosomes. *Genetics* (1938).
  78. Sandell, L. L. & Zakian, V. A. Loss of a Yeast Telomere : Arrest , Recovery , and Chromosome Loss. *Cell* **75**, 729–739 (1993).
  79. Olovnikov, A. M. Principle of marginotomy in template synthesis of polynucleotides. *Dokl. Akad. Nauk SSSR* **201**, 1496–1499 (1971).
  80. Watson, J. D. Origin of concatemeric T7 DNA. *Nat. New Biol.* **239**, 197–201 (1972).
  81. Gladych, M., Wojtyla, A. & Rubis, B. Human telomerase expression regulation. *Biochem. Cell Biol.* **89**, 359–376 (2011).
  82. Takai, H., Smogorzewska, A., Lange, T. De & de Lange, T. DNA Damage Foci at Dysfunctional Telomeres. *Curr. Biol.* **13**, 1549–1556 (2003).
  83. d’Adda di Fagagna, F. *et al.* A DNA damage checkpoint response in telomere-initiated senescence. *Nature* **426**, 194–198 (2003).
  84. Jafri, M. A., Ansari, S. A., Alqahtani, M. H. & Shay, J. W. Roles of telomeres and telomerase in cancer , and advances in telomerase- targeted therapies. *Genome Med.* (2016) doi:10.1186/s13073-016-0324-x.
  85. Martínez, P. & Blasco, M. A. Telomere-driven diseases and telomere-targeting therapies. *Journal Cell Biol.* **216**, 875–887 (2017).
  86. Cleal, K., Norris, K. & Baird, D. Telomere Length Dynamics and the Evolution of Cancer Genome Architecture. 1–17 (2018) doi:10.3390/ijms19020482.

87. Rossiello, F., Jurk, D., Passos, J. F. & d'Adda di Fagagna, F. Telomere dysfunction in ageing and age-related diseases. *Nat. Cell Biol.* **24**, 135–147 (2022).
88. Waterman, D. P., Haber, J. E. & Smolka, M. B. Checkpoint Responses to DNA Double-Strand Breaks. *Annu. Rev. Biochem.* **89**, 103–133 (2020).
89. Usui, T., Ogawa, H. & Petrini, J. H. J. A DNA Damage Response Pathway Controlled by Tel1 and the Mre11 Complex. *Mol. Cell* **7**, 1255–1266 (2001).
90. Frank-Vaillant, M. & Marcand, S. Transient Stability of DNA Ends Allows Nonhomologous End Joining to Precede Homologous Recombination. *Mol. Cell* **10**, 1189–1199 (2002).
91. Daley, J. M., Palmbo, P. L., Wu, D. & Wilson, T. E. Nonhomologous End Joining in Yeast. *Annu. Rev. Genet.* **39**, 431–451 (2005).
92. Mathiasen, D. P. & Lisby, M. Cell cycle regulation of homologous recombination in *Saccharomyces cerevisiae*. *FEMS Microbiol. Rev.* **38**, 172–184 (2014).
93. Zou, L. & Elledge, S. J. Sensing DNA Damage Through ATRIP Recognition of RPA-ssDNA Complexes. *Science (80-. )*. **300**, 1542–1548 (2003).
94. Cejka, P. & Symington, L. S. DNA End Resection : Mechanism and Control. *Annu. Rev. Genet.* **55**, 285–307 (2021).
95. Chang, H. H. Y., Pannunzio, N. R., Adachi, N. & Lieber, M. R. Non-homologous DNA end joining and alternative pathways to double - strand break repair. *Mol. Cell Biol.* **18**, 495–506 (2017).
96. Mimitou, E. P. & Symington, L. S. Ku prevents Exo1 and Sgs1-dependent resection of DNA ends in the absence of a functional MRX complex or Sae2. *EMBO J.* **29**, 3358–3369 (2010).
97. Shim, E. Y. *et al.* *Saccharomyces cerevisiae* Mre11/Rad50/Xrs2 and Ku proteins regulate association of Exo1 and Dna2 with DNA breaks. *EMBO J.* **29**, 3370–3380 (2010).
98. Ivanov, E. L., Sugawara, N., White, C. I., Fabre, F. & Haber, J. E. Mutations in XRS2 and RAD50 Delay but Do Not Prevent Mating-Type Switching in *Saccharomyces cerevisiae*. *Mol. Cell. Biol.* **14**, 3414–3425 (1994).
99. Lee, S. E. *et al.* *Saccharomyces* Ku70, Mre11/Rad50, and RPA Proteins Regulate Adaptation to G2 / M Arrest after DNA Damage. *Cell* **94**, 399–409 (1998).
100. Mimitou, E. P. & Symington, L. S. Sae2 , Exo1 and Sgs1 collaborate in DNA double-strand break processing. *Nature* **455**, 770–775 (2008).
101. Paques, F. & Haber, J. E. Multiple Pathways of Recombination Induced by Double-Strand Breaks in *Saccharomyces cerevisiae*. *Microbiol. Mol. Biol. Rev.* **63**, 349–404 (1999).
102. Garcia, V., Phelps, S. E. L., Gray, S. & Neale, M. J. Bidirectional resection of DNA double-strand breaks by Mre11 and Exo1. *Nature* **479**, 241–244 (2011).
103. Chanut, P., Britton, S., Coates, J., Jackson, S. P. & Calsou, P. Coordinated nuclease activities counteract Ku at single-ended DNA double-strand breaks. *Nat. Commun.* **7**, (2016).
104. Tsubouchi, H. & Ogawa, H. Exo1 Roles for Repair of DNA Double-Strand Breaks and Meiotic Crossing Over in *Saccharomyces cerevisiae*. *Mol. Biol. Cell* **11**, 2221–2233 (2000).
105. Zhu, Z., Chung, W., Shim, E. Y., Lee, S. E. & Ira, G. Sgs1 Helicase and Two Nucleases Dna2 and Exo1 Resect DNA Double-Strand Break Ends. *Cell* **134**, 981–994 (2008).
106. Jimeno, S., Mejías-Navarro, F., Prados-Carvajal, R. & Huertas, P. Controlling the balance between chromosome break repair pathways. *Adv. Protein Chem. Struct. Biol.* **115**, 95–134 (2019).
107. Bonetti, D., Martina, M., Clerici, M., Lucchini, G. & Longhese, M. P. Article Multiple Pathways Regulate 3' Overhang Generation at *S. cerevisiae* Telomeres. *Mol. Cell* **35**, 70–81 (2009).
108. Gravel, S., Chapman, J. R., Magill, C. & Jackson, S. P. DNA helicases Sgs1 and BLM promote DNA double-strand break resection. *Genes Dev.* **22**, 2767–2772 (2008).
109. Wold, M. S. REPLICATION PROTEIN A : A Heterotrimeric , Single-Stranded DNA-Binding Protein Required for Eukaryotic DNA Metabolism. *Annu. Rev. Biochem.* **66**, 61–92 (1997).
110. Yates, L. A. *et al.* A structural and dynamic model for the assembly of Replication Protein A on single-stranded DNA. *Nat. Commun.* **9**, (2018).
111. New, J. H., Sugiyama, T., Zaitseva, E. & Kowalczykowski, S. C. Rad52 protein stimulates DNA strand exchange by Rad51 and replication protein A. *Nature* **391**, 407–410 (1998).
112. Sung, P. Function of Yeast Rad52 Protein as a Mediator between Replication Protein A and the Rad51 Recombinase. *J. Biol. Chem.* **272**, 28194–28197 (1997).
113. Shinohara, A. & Ogawa, T. Stimulation by Rad52 of yeast Rad51- mediated recombination. *Nature* **391**, 404–407 (1998).
114. Mehta, A. & Haber, J. E. Sources of DNA Double-Strand Breaks and Models of Recombinational DNA Repair. *Cold Spring Harb. Perspect. Biol.* **6**, (2014).
115. Nakada, D., Matsumoto, K. & Sugimoto, K. ATM-related Tel1 associates with double-strand breaks through an Xrs2-dependent mechanism. *Genes Dev.* **17**, 1957–1962 (2003).
116. Uziel, T. *et al.* Requirement of the MRN



- complex for ATM activation by DNA damage. *EMBO J.* **22**, 5612–5621 (2003).
117. Lee, J.-H. & Paull, T. T. Direct activation of the ATM protein kinase by the Mre11/Rad50/Nbs1 complex. *Science* **304**, 93–96 (2004).
118. Lee, J.-H. & Paull, T. T. ATM activation by DNA double-strand breaks through the Mre11-Rad50-Nbs1 complex. *Science* **308**, 551–554 (2005).
119. You, Z., Chahwan, C., Bailis, J., Hunter, T. & Russell, P. ATM activation and its recruitment to damaged DNA require binding to the C terminus of Nbs1. *Mol. Cell. Biol.* **25**, 5363–5379 (2005).
120. Cassani, C. *et al.* Tel1 and Rif2 Regulate MRX Functions in End-Tethering and Repair of DNA Double-Strand Breaks. *PLoS Biol.* **14**, e1002387 (2016).
121. Lisby, M., Barlow, J. H., Burgess, R. C. & Rothstein, R. Choreography of the DNA damage response: spatiotemporal relationships among checkpoint and repair proteins. *Cell* **118**, 699–713 (2004).
122. Sanchez, Y. *et al.* Control of the DNA damage checkpoint by chk1 and rad53 protein kinases through distinct mechanisms. *Science* **286**, 1166–1171 (1999).
123. Sun, Z., Hsiao, J., Fay, D. S. & Stern, D. F. Rad53 FHA domain associated with phosphorylated Rad9 in the DNA damage checkpoint. *Science* **281**, 272–274 (1998).
124. Usui, T., Foster, S. S. & Petrini, J. H. J. Maintenance of the DNA-damage checkpoint requires DNA-damage-induced mediator protein oligomerization. *Mol. Cell* **33**, 147–159 (2009).
125. Blankley, R. T. & Lydall, D. A domain of Rad9 specifically required for activation of Chk1 in budding yeast. *J. Cell Sci.* **117**, 601–608 (2004).
126. Lazzaro, F. *et al.* Histone methyltransferase Dot1 and Rad9 inhibit single-stranded DNA accumulation at DSBs and uncapped telomeres. *EMBO J.* **27**, 1502–1512 (2008).
127. Segurado, M. & Diffley, J. F. X. Separate roles for the DNA damage checkpoint protein kinases in stabilizing DNA replication forks. *Genes Dev.* **22**, 1816–1827 (2008).
128. Lydall, D. & Weinert, T. Yeast checkpoint genes in DNA damage processing: implications for repair and arrest. *Science* **270**, 1488–1491 (1995).
129. Gilbert, C. S., Green, C. M. & Lowndes, N. F. Budding yeast Rad9 is an ATP-dependent Rad53 activating machine. *Mol. Cell* **8**, 129–136 (2001).
130. Sweeney, F. D. *et al.* *Saccharomyces cerevisiae* Rad9 acts as a Mec1 adaptor to allow Rad53 activation. *Curr. Biol.* **15**, 1364–1375 (2005).
131. Alcasabas, A. A. *et al.* Mrc1 transduces signals of DNA replication stress to activate Rad53. *Nat. Cell Biol.* **3**, 958–965 (2001).
132. Tanaka, K. & Russell, P. Mrc1 channels the DNA replication arrest signal to checkpoint kinase Cds1. *Nat. Cell Biol.* **3**, 966–972 (2001).
133. Katou, Y. *et al.* S-phase checkpoint proteins Tof1 and Mrc1 form a stable replication-pausing complex. *Nature* **424**, 1078–1083 (2003).
134. Osborn, A. J. & Elledge, S. J. Mrc1 is a replication fork component whose phosphorylation in response to DNA replication stress activates Rad53. *Genes Dev.* **17**, 1755–1767 (2003).
135. Michelson, R. J., Rosenstein, S. & Weinert, T. A telomeric repeat sequence adjacent to a DNA double-stranded break produces an antieckpoint. *Genes Dev.* **19**, 2546–2559 (2005).
136. Ribeyre, C. & Shore, D. Antieckpoint pathways at telomeres in yeast. *Nat. Struct. Mol. Biol.* **19**, 307–313 (2012).
137. Miyake, Y. *et al.* RPA-like mammalian Ctc1-Stn1-Ten1 complex binds to single-stranded DNA and protects telomeres independently of the Pot1 pathway. *Mol. Cell* **36**, 193–206 (2009).
138. Surovtseva, Y. V. *et al.* Conserved telomere maintenance component 1 interacts with STN1 and maintains chromosome ends in higher eukaryotes. *Mol. Cell* **36**, 207–218 (2009).
139. Price, C. M. *et al.* Evolution of CST function in telomere maintenance. *Cell Cycle* **9**, 3157–3165 (2010).
140. Hirano, Y. & Sugimoto, K. Cdc13 telomere capping decreases Mec1 association but does not affect Tel1 association with DNA ends. *Mol. Biol. Cell* **18**, 2026–2036 (2007).
141. Vodenicharov, M. D., Laterreur, N. & Wellinger, R. J. Telomere capping in non-dividing yeast cells requires Yku and Rap1. *EMBO J.* **29**, 3007–3019 (2010).
142. Vodenicharov, M. D. & Wellinger, R. J. DNA degradation at unprotected telomeres in yeast is regulated by the CDK1 (Cdc28/Cln) cell-cycle kinase. *Mol. Cell* **24**, 127–137 (2006).
143. Weinert, T. A. & Hartwell, L. H. Cell cycle arrest of cdc mutants and specificity of the RAD9 checkpoint. *Genetics* **134**, 63–80 (1993).
144. Mersaoui, S. Y., Bonnell, E. & Wellinger, R. J. Nuclear import of Cdc13 limits chromosomal capping. *Nucleic Acids Res.* **46**, 2975–2989 (2018).
145. Jia, X., Weinert, T. & Lydall, D. Mec1 and Rad53 inhibit formation of single-stranded DNA at telomeres of *Saccharomyces cerevisiae* cdc13-1 mutants. *Genetics* **166**, 753–764 (2004).
146. Xu, L., Petreaca, R. C., Gasparyan, H. J., Vu, S. & Nugent, C. I. TEN1 is essential for CDC13-mediated telomere capping. *Genetics* **183**, 793–810 (2009).
147. Langston, R. E., Palazzola, D., Bonnell,

- E., Wellinger, R. J. & Weinert, T. Loss of Cdc13 causes genome instability by a deficiency in replication-dependent telomere capping. *PLoS Genet.* **16**, e1008733 (2020).
148. Douglas, M. E. & Diffley, J. F. X. Budding yeast Rap1, but not telomeric DNA, is inhibitory for multiple stages of DNA replication in vitro. *Nucleic Acids Res.* **49**, 5671–5683 (2021).
149. Makovets, S., Herskowitz, I. & Blackburn, E. H. Anatomy and dynamics of DNA replication fork movement in yeast telomeric regions. *Mol. Cell. Biol.* **24**, 4019–4031 (2004).
150. Foster, S. S., Zubko, M. K., Guillard, S. & Lydall, D. MRX protects telomeric DNA at uncapped telomeres of budding yeast *cdc13-1* mutants. *DNA Repair (Amst)*. **5**, 840–851 (2006).
151. Mimitou, E. P. & Symington, L. S. DNA end resection: many nucleases make light work. *DNA Repair (Amst)*. **8**, 983–995 (2009).
152. Maringele, L. & Lydall, D. EXO1-dependent single-stranded DNA at telomeres activates subsets of DNA damage and spindle checkpoint pathways in budding yeast *yku70Delta* mutants. *Genes Dev.* **16**, 1919–1933 (2002).
153. Zubko, M. K., Guillard, S. & Lydall, D. Exo1 and Rad24 differentially regulate generation of ssDNA at telomeres of *Saccharomyces cerevisiae cdc13-1* mutants. *Genetics* **168**, 103–115 (2004).
154. Zheng, L. *et al.* Human DNA2 is a mitochondrial nuclease/helicase for efficient processing of DNA replication and repair intermediates. *Mol. Cell* **32**, 325–336 (2008).
155. Ngo, H.-P. & Lydall, D. Survival and growth of yeast without telomere capping by Cdc13 in the absence of Sgs1, Exo1, and Rad9. *PLoS Genet.* **6**, e1001072 (2010).
156. Dewar, J. M. & Lydall, D. Pif1- and Exo1-dependent nucleases coordinate checkpoint activation following telomere uncapping. *EMBO J.* **29**, 4020–4034 (2010).
157. Zhou, J. Q., Monson, E. K., Teng, S. C., Schulz, V. P. & Zakian, V. A. Pif1p helicase, a catalytic inhibitor of telomerase in yeast. *Science (80- )*. **289**, 771–774 (2000).
158. Chang, M. *et al.* Telomerase is essential to alleviate pif1-induced replication stress at telomeres. *Genetics* **183**, 779–791 (2009).
159. Pike, J. E., Burgers, P. M. J., Campbell, J. L. & Bambara, R. A. Pif1 helicase lengthens some Okazaki fragment flaps necessitating Dna2 nuclease/helicase action in the two-nuclease processing pathway. *J. Biol. Chem.* **284**, 25170–25180 (2009).
160. Lopes, J. *et al.* G-quadruplex-induced instability during leading-strand replication. *EMBO J.* **30**, 4033–4046 (2011).
161. Paeschke, K., Capra, J. A. & Zakian, V. A. DNA Replication through G-Quadruplex Motifs Is Promoted by the *Saccharomyces cerevisiae* Pif1 DNA Helicase. *Cell* **145**, 678–691 (2011).
162. Bonetti, D., Clerici, M., Manfrini, N., Lucchini, G. & Longhese, M. P. The MRX complex plays multiple functions in resection of Yku- and Rif2-protected DNA ends. *PLoS One* **5**, e14142 (2010).
163. Porter, S. E., Greenwell, P. W., Ritchie, K. B. & Petes, T. D. The DNA-binding protein Hdf1p (a putative Ku homologue) is required for maintaining normal telomere length in *Saccharomyces cerevisiae*. *Nucleic Acids Res.* **24**, 582–585 (1996).
164. Foster, S. S., Balestrini, A. & Petrini, J. H. J. Functional interplay of the Mre11 nuclease and Ku in the response to replication-associated DNA damage. *Mol. Cell. Biol.* **31**, 4379–4389 (2011).
165. Feldmann, H. & Winnacker, E. L. A putative homologue of the human autoantigen Ku from *Saccharomyces cerevisiae*. *J. Biol. Chem.* **268**, 12895–12900 (1993).
166. Teo, S. H. & Jackson, S. P. Telomerase subunit overexpression suppresses telomere-specific checkpoint activation in the yeast *yku80* mutant. *EMBO Rep.* **2**, 197–202 (2001).
167. Lustig, A. J., Kurtz, S. & Shore, D. Involvement of the silencer and UAS binding protein RAP1 in regulation of telomere length. *Science* **250**, 549–553 (1990).
168. Marcand, S., Pardo, B., Gratias, A., Cahun, S. & Callebaut, I. Multiple pathways inhibit NHEJ at telomeres. *Genes Dev.* **22**, 1153–1158 (2008).
169. Pardo, B. & Marcand, S. Rap1 prevents telomere fusions by nonhomologous end joining. *EMBO J.* **24**, 3117–3127 (2005).
170. Ritchie, K. B. & Petes, T. D. The Mre11p/Rad50p/Xrs2p complex and the Tel1p function in a single pathway for telomere maintenance in yeast. *Genetics* **155**, 475–479 (2000).
171. Hirano, Y., Fukunaga, K. & Sugimoto, K. Rif1 and rif2 inhibit localization of tel1 to DNA ends. *Mol. Cell* **33**, 312–322 (2009).
172. Addinall, S. G. *et al.* Quantitative fitness analysis shows that NMD proteins and many other protein complexes suppress or enhance distinct telomere cap defects. *PLoS Genet.* **7**, e1001362 (2011).
173. Rosas Bringas, F. R., Stinus, S., de Zoeten, P., Cohn, M. & Chang, M. Rif2 protects Rap1-depleted telomeres from MRX-mediated degradation in *Saccharomyces cerevisiae*. *Elife* **11**, (2022).
174. Olovnikov, A. M. A theory of marginotomy. The incomplete copying of template

- margin in enzymic synthesis of polynucleotides and biological significance of the phenomenon. *J. Theor. Biol.* **41**, 181–190 (1973).
175. Hug, N. & Lingner, J. Telomere length homeostasis. *Chromosoma* **115**, 413–425 (2006).
176. Lingner, J., Cooper, J. P. & Cech, T. R. Telomerase and DNA End Replication: No Longer a Lagging Strand Problem? *Science* **269**, 1533–1534 (1995).
177. Greider, C. W. & Blackburn, E. H. The telomere terminal transferase of *Tetrahymena* is a ribonucleoprotein enzyme with two kinds of primer specificity. *Cell* **51**, 887–898 (1987).
178. Greider, C. W. & Blackburn, E. H. Identification of a specific telomere terminal transferase activity in *Tetrahymena* extracts. *Cell* **43**, 405–413 (1985).
179. Greider, C. W. & Blackburn, E. H. A telomeric sequence in the RNA of *Tetrahymena* telomerase required for telomere repeat synthesis. *Nature* **337**, 331–337 (1989).
180. Louis, E. J. & Vershinin, A. V. Chromosome ends: different sequences may provide conserved functions. *Bioessays* **27**, 685–697 (2005).
181. Maestroni, L., Matmati, S. & Coulon, S. Solving the Telomere Replication Problem. *Genes (Basel)*. **8**, (2017).
182. Soudet, J., Jolivet, P. & Teixeira, M. T. Elucidation of the DNA end-replication problem in *Saccharomyces cerevisiae*. *Mol. Cell* **53**, 954–964 (2014).
183. Marcand, S., Brevet, V. & Gilson, E. Progressive cis-inhibition of telomerase upon telomere elongation. *EMBO J.* **18**, 3509–3519 (1999).
184. Singer, M. S. & Gottschling, D. E. TLC1: template RNA component of *Saccharomyces cerevisiae* telomerase. *Science* **266**, 404–409 (1994).
185. Lundblad, V. & Szostak, J. W. A mutant with a defect in telomere elongation leads to senescence in yeast. *Cell* **57**, 633–643 (1989).
186. Mieczkowski, P. A., Mieczkowska, J. O., Dominska, M. & Petes, T. D. Genetic regulation of telomere-telomere fusions in the yeast *Saccharomyces cerevisiae*. *Proc. Natl. Acad. Sci. U. S. A.* **100**, 10854–10859 (2003).
187. Miller, K. M., Rog, O. & Cooper, J. P. Semi-conservative DNA replication through telomeres requires Taz1. *Nature* **440**, 824–828 (2006).
188. Ivessa, A. S., Zhou, J.-Q., Schulz, V. P., Monson, E. K. & Zakian, V. A. *Saccharomyces Rrm3p*, a 5' to 3' DNA helicase that promotes replication fork progression through telomeric and subtelomeric DNA. *Genes Dev.* **16**, 1383–1396 (2002).
189. Sfeir, A. *et al.* Mammalian telomeres resemble fragile sites and require TRF1 for efficient replication. *Cell* **138**, 90–103 (2009).
190. Ye, J. *et al.* TRF2 and apollo cooperate with topoisomerase 2alpha to protect human telomeres from replicative damage. *Cell* **142**, 230–242 (2010).
191. Martínez, P. *et al.* Increased telomere fragility and fusions resulting from TRF1 deficiency lead to degenerative pathologies and increased cancer in mice. *Genes Dev.* **23**, 2060–2075 (2009).
192. Leman, A. R. *et al.* Timeless preserves telomere length by promoting efficient DNA replication through human telomeres. *Cell Cycle* **11**, 2337–2347 (2012).
193. Zeman, M. K. & Cimprich, K. A. Causes and consequences of replication stress. *Nat. Cell Biol.* **16**, 2–9 (2014).
194. Carr, A. M., Paek, A. L. & Weinert, T. DNA replication: failures and inverted fusions. *Semin. Cell Dev. Biol.* **22**, 866–874 (2011).
195. Arudchandran, A. *et al.* The absence of ribonuclease H1 or H2 alters the sensitivity of *Saccharomyces cerevisiae* to hydroxyurea, caffeine and ethyl methanesulphonate: Implications for roles of RNases H in DNA replication and repair. *Genes to Cells* **5**, 789–802 (2000).
196. Jeong, H.-S. S., Backlund, P. S., Chen, H.-C. C., Karavanov, A. A. & Crouch, R. J. RNase H2 of *Saccharomyces cerevisiae* is a complex of three proteins. *Nucleic Acids Res.* **32**, 407–414 (2004).
197. Mischo, H. E. *et al.* Yeast Sen1 helicase protects the genome from transcription-associated instability. *Mol. Cell* **41**, 21–32 (2011).
198. Costantino, L. & Koshland, D. Genome-wide Map of R-Loop-Induced Damage Reveals How a Subset of R-Loops Contributes to Genomic Instability. *Mol. Cell* **71**, 487–497.e3 (2018).
199. Byrd, A. K. & Raney, K. D. Structure and function of Pif1 helicase. *Biochem. Soc. Trans.* **45**, 1159–1171 (2017).
200. Mendoza, O., Bourdoncle, A., Boulé, J.-B., Brosh, R. M. J. & Mergny, J.-L. G-quadruplexes and helicases. *Nucleic Acids Res.* **44**, 1989–2006 (2016).
201. Chung, W.-H. To peep into Pif1 helicase: multifaceted all the way from genome stability to repair-associated DNA synthesis. *J. Microbiol.* **52**, 89–98 (2014).
202. Hou, X.-M. *et al.* Molecular mechanism of G-quadruplex unwinding helicase: sequential and repetitive unfolding of G-quadruplex by Pif1 helicase. *Biochem. J.* **466**, 189–199 (2015).
203. Paeschke, K. *et al.* Pif1 family helicases suppress genome instability at G-quadruplex motifs. *Nature* **497**, 458–462 (2013).
204. Sauer, M. & Paeschke, K. G-quadruplex unwinding helicases and their function in

- vivo. *Biochem. Soc. Trans.* **45**, 1173–1182 (2017).
205. Ribeyre, C. *et al.* The yeast Pif1 helicase prevents genomic instability caused by G-quadruplex-forming CEB1 sequences in vivo. *PLoS Genet.* **5**, e1000475 (2009).
206. Piazza, A. *et al.* Genetic instability triggered by G-quadruplex interacting Phen-DC compounds in *Saccharomyces cerevisiae*. *Nucleic Acids Res.* **38**, 4337–4348 (2010).
207. Zhou, R., Zhang, J., Bochman, M. L., Zakian, V. A. & Ha, T. Periodic DNA patrolling underlies diverse functions of Pif1 on R-loops and G-rich DNA. *Elife* **3**, e02190 (2014).
208. Masuda-Sasa, T., Polaczek, P., Peng, X. P., Chen, L. & Campbell, J. L. Processing of G4 DNA by Dna2 helicase/nuclease and replication protein A (RPA) provides insights into the mechanism of Dna2/RPA substrate recognition. *J. Biol. Chem.* **283**, 24359–24373 (2008).
209. Brosh, R. M. J. *et al.* Functional and physical interaction between WRN helicase and human replication protein A. *J. Biol. Chem.* **274**, 18341–18350 (1999).
210. Wang, Q. *et al.* G-quadruplex formation at the 3' end of telomere DNA inhibits its extension by telomerase, polymerase and unwinding by helicase. *Nucleic Acids Res.* **39**, 6229–6237 (2011).
211. Arnoult, N. *et al.* Replication timing of human telomeres is chromosome arm-specific, influenced by subtelomeric structures and connected to nuclear localization. *PLoS Genet.* **6**, e1000920 (2010).
212. Heun, P., Laroche, T., Raghuraman, M. K. & Gasser, S. M. The positioning and dynamics of origins of replication in the budding yeast nucleus. *J. Cell Biol.* **152**, 385–400 (2001).
213. Ferguson, B. M. & Fangman, W. L. A position effect on the time of replication origin activation in yeast. *Cell* **68**, 333–339 (1992).
214. Newlon, C. S. *et al.* Analysis of replication origin function on chromosome III of *Saccharomyces cerevisiae*. *Cold Spring Harb. Symp. Quant. Biol.* **58**, 415–423 (1993).
215. Friedman, K. L., Brewer, B. J. & Fangman, W. L. Replication profile of *Saccharomyces cerevisiae* chromosome VI. *Genes Cells* **2**, 667–678 (1997).
216. Yamashita, M. *et al.* The efficiency and timing of initiation of replication of multiple replicons of *Saccharomyces cerevisiae* chromosome VI. *Genes Cells* **2**, 655–665 (1997).
217. Poloumienko, A., Dershowitz, A., De, J. & Newlon, C. S. Completion of replication map of *Saccharomyces cerevisiae* chromosome III. *Mol. Biol. Cell* **12**, 3317–3327 (2001).
218. Raghuraman, M. K. *et al.* Replication dynamics of the yeast genome. *Science* **294**, 115–121 (2001).
219. Yabuki, N., Terashima, H. & Kitada, K. Mapping of early firing origins on a replication profile of budding yeast. *Genes Cells* **7**, 781–789 (2002).
220. Méchali, M. Eukaryotic DNA replication origins: many choices for appropriate answers. *Nat. Rev. Mol. Cell Biol.* **11**, 728–738 (2010).
221. Boos, D. & Ferreira, P. Origin Firing Regulations to Control Genome Replication Timing. *Genes (Basel)*. **10**, (2019).
222. McCarroll, R. M. & Fangman, W. L. Time of replication of yeast centromeres and telomeres. *Cell* **54**, 505–513 (1988).
223. Stevenson, J. B. & Gottschling, D. E. Telomeric chromatin modulates replication timing near chromosome ends. *Genes Dev.* **13**, 146–151 (1999).
224. Cosgrove, A. J., Nieduszynski, C. A. & Donaldson, A. D. Ku complex controls the replication time of DNA in telomere regions. *Genes Dev.* **16**, 2485–2490 (2002).
225. Lian, H.-Y. *et al.* The effect of Ku on telomere replication time is mediated by telomere length but is independent of histone tail acetylation. *Mol. Biol. Cell* **22**, 1753–1765 (2011).
226. Peace, J. M., Ter-Zakarian, A. & Aparicio, O. M. Rif1 regulates initiation timing of late replication origins throughout the *S. cerevisiae* genome. *PLoS One* **9**, e98501 (2014).
227. Mattarocci, S., Hafner, L., Lezaja, A., Shyian, M. & Shore, D. Rif1: A Conserved Regulator of DNA Replication and Repair Hijacked by Telomeres in Yeasts. *Front. Genet.* **7**, 45 (2016).
228. Cooley, C., Davé, A., Garg, M. & Bianchi, A. Tel1ATM dictates the replication timing of short yeast telomeres. *EMBO Rep.* **15**, 1093–1101 (2014).
229. Hiraga, S.-I. *et al.* Rif1 controls DNA replication by directing Protein Phosphatase 1 to reverse Cdc7-mediated phosphorylation of the MCM complex. *Genes Dev.* **28**, 372–383 (2014).
230. Hiraga, S.-I. *et al.* Human RIF1 and protein phosphatase 1 stimulate DNA replication origin licensing but suppress origin activation. *EMBO Rep.* **18**, 403–419 (2017).
231. Mattarocci, S. *et al.* Rif1 controls DNA replication timing in yeast through the PP1 phosphatase Glc7. *Cell Rep.* **7**, 62–69 (2014).
232. Bianchi, A. & Shore, D. Early replication of short telomeres in budding yeast. *Cell* **128**, 1051–1062 (2007).
233. Sabourin, M., Tuzon, C. T. & Zakian, V. A. Telomerase and Tel1p preferentially associate with short telomeres in *S. cerevisiae*. *Mol. Cell* **27**, 550–561 (2007).
234. Sridhar, A., Kedziora, S. & Donaldson, A.

- D. At short telomeres Tel1 directs early replication and phosphorylates Rif1. *PLoS Genet.* **10**, e1004691 (2014).
235. Maicher, A., Kastner, L., Dees, M. & Luke, B. Deregulated telomere transcription causes replication-dependent telomere shortening and promotes cellular senescence. *Nucleic Acids Res.* **40**, 6649–6659 (2012).
236. Graf, M. *et al.* Telomere Length Determines TERRA and R-Loop Regulation through the Cell Cycle. *Cell* **170**, 72–85.e14 (2017).
237. Cusanelli, E., Romero, C. A. P. & Chartrand, P. Telomeric Noncoding RNA TERRA Is Induced by Telomere Shortening to Nucleate Telomerase Molecules at Short Telomeres. *Mol. Cell* **51**, 780–791 (2013).
238. Counter, C. M., Meyerson, M., Eaton, E. N. & Weinberg, R. A. The catalytic subunit of yeast telomerase. *Proc. Natl. Acad. Sci. U. S. A.* **94**, 9202–9207 (1997).
239. Lendvay, T. S., Morris, D. K., Sah, J., Balasubramanian, B. & Lundblad, V. Senescence mutants of *Saccharomyces cerevisiae* with a defect in telomere replication identify three additional EST genes. *Genetics* **144**, 1399–1412 (1996).
240. Lingner, J., Cech, T. R., Hughes, T. R. & Lundblad, V. Three Ever Shorter Telomere (EST) genes are dispensable for in vitro yeast telomerase activity. *Proc. Natl. Acad. Sci. U. S. A.* **94**, 11190–11195 (1997).
241. Chan, A., Boulé, J.-B. & Zakian, V. A. Two pathways recruit telomerase to *Saccharomyces cerevisiae* telomeres. *PLoS Genet.* **4**, e1000236 (2008).
242. Mozdy, A. D. & Cech, T. R. Low abundance of telomerase in yeast: implications for telomerase haploinsufficiency. *RNA* **12**, 1721–1737 (2006).
243. Marcand, S., Brevet, V., Mann, C. & Gilson, E. Cell cycle restriction of telomere elongation. *Curr. Biol.* **10**, 487–490 (2000).
244. Gallardo, F. *et al.* Live cell imaging of telomerase RNA dynamics reveals cell cycle-dependent clustering of telomerase at elongating telomeres. *Mol. Cell* **44**, 819–827 (2011).
245. Taggart, A. K. P., Teng, S.-C. & Zakian, V. A. Est1p as a cell cycle-regulated activator of telomere-bound telomerase. *Science (80-. )*. **297**, 1023–1026 (2002).
246. Liu, C.-C., Gopalakrishnan, V., Poon, L.-F., Yan, T. & Li, S. Cdk1 regulates the temporal recruitment of telomerase and Cdc13-Stn1-Ten1 complex for telomere replication. *Mol. Cell. Biol.* **34**, 57–70 (2014).
247. Evans, S. K. & Lundblad, V. Est1 and Cdc13 as comediators of telomerase access. *Science* **286**, 117–120 (1999).
248. Wu, Y. & Zakian, V. A. The telomeric Cdc13 protein interacts directly with the telomerase subunit Est1 to bring it to telomeric DNA ends in vitro. *Proc. Natl. Acad. Sci. U. S. A.* **108**, 20362–20369 (2011).
249. Takata, H., Tanaka, Y. & Matsuura, A. Late S phase-specific recruitment of Mre11 complex triggers hierarchical assembly of telomere replication proteins in *Saccharomyces cerevisiae*. *Mol. Cell* **17**, 573–583 (2005).
250. Teixeira, M. T., Arneric, M., Sperisen, P. & Lingner, J. Telomere length homeostasis is achieved via a switch between telomerase-extendible and nonextendible states. *Cell* **117**, 323–335 (2004).
251. Britt-Compton, B., Capper, R., Rowson, J. & Baird, D. M. Short telomeres are preferentially elongated by telomerase in human cells. *FEBS Lett.* **583**, 3076–3080 (2009).
252. Hemann, M. T., Strong, M. A., Hao, L. Y. & Greider, C. W. The shortest telomere, not average telomere length, is critical for cell viability and chromosome stability. *Cell* **107**, 67–77 (2001).
253. Jacobs, J. J. L. Senescence: back to telomeres. *Nat. Rev. Mol. Cell Biol.* **14**, 196 (2013).
254. Faure, V., Coulon, S., Hardy, J. & Géli, V. Cdc13 and telomerase bind through different mechanisms at the lagging- and leading-strand telomeres. *Mol. Cell* **38**, 842–852 (2010).
255. Nakada, D., Shimomura, T., Matsumoto, K. & Sugimoto, K. The ATM-related Tel1 protein of *Saccharomyces cerevisiae* controls a checkpoint response following phleomycin treatment. *Nucleic Acids Res.* **31**, 1715–1724 (2003).
256. Mallory, J. C. & Petes, T. D. Protein kinase activity of Tel1p and Mec1p, two *Saccharomyces cerevisiae* proteins related to the human ATM protein kinase. *Proc. Natl. Acad. Sci. U. S. A.* **97**, 13749–13754 (2000).
257. Martina, M., Bonetti, D., Villa, M., Lucchini, G. & Longhese, M. P. *Saccharomyces cerevisiae* Rif1 cooperates with MRX-Sae2 in promoting DNA-end resection. *EMBO Rep.* **15**, 695–704 (2014).
258. Bonetti, D., Martina, M., Falcetoni, M. & Longhese, M. P. Telomere-end processing: Mechanisms and regulation. *Chromosoma* **123**, 57–66 (2014).
259. Tseng, S.-F., Lin, J.-J. & Teng, S.-C. The telomerase-recruitment domain of the telomere binding protein Cdc13 is regulated by Mec1p/Tel1p-dependent phosphorylation. *Nucleic Acids Res.* **34**, 6327–6336 (2006).
260. Hector, R. E. *et al.* Tel1p preferentially associates with short telomeres to stimulate their elongation. *Mol. Cell* **27**, 851–858 (2007).
261. Teng, S. C., Chang, J., McCowan, B. & Zakian, V. a. Telomerase-independent

- lengthening of yeast telomeres occurs by an abrupt Rad50p-dependent, Rif-inhibited recombinational process. *Mol. Cell* **6**, 947–52 (2000).
262. Chang, M., Arneric, M. & Lingner, J. Telomerase repeat addition processivity is increased at critically short telomeres in a Tel1-dependent manner in *Saccharomyces cerevisiae*. *Genes Dev.* **21**, 2485–2494 (2007).
263. Goudsouzian, L. K., Tuzon, C. T. & Zakian, V. A. *S. cerevisiae* Tel1p and Mre11p are required for normal levels of Est1p and Est2p telomere association. *Mol. Cell* **24**, 603–610 (2006).
264. Marcand, S., Gilson, E. & Shore, D. A protein-counting mechanism for telomere length regulation in yeast. *Science* **275**, 986–990 (1997).
265. Schulz, V. P. & Zakian, V. A. The *Saccharomyces* PIF1 DNA helicase inhibits telomere elongation and de novo telomere formation. *Cell* **76**, 145–155 (1994).
266. Phillips, J. A., Chan, A., Paeschke, K. & Zakian, V. A. The pif1 helicase, a negative regulator of telomerase, acts preferentially at long telomeres. *PLoS Genet.* **11**, e1005186 (2015).
267. Boulé, J.-B., Vega, L. R. & Zakian, V. A. The yeast Pif1p helicase removes telomerase from telomeric DNA. *Nature* **438**, 57–61 (2005).
268. Teixeira, M. T. *Saccharomyces cerevisiae* as a Model to Study Replicative Senescence Triggered by Telomere Shortening. *Front. Oncol.* **3**, 101 (2013).
269. Maciejowski, J. & de Lange, T. Telomeres in cancer: tumour suppression and genome instability. *Nat. Rev. Mol. Cell Biol.* **18**, 175–186 (2017).
270. Campisi, J. & d'Adda di Fagagna, F. Cellular senescence: when bad things happen to good cells. *Nat. Rev. Mol. Cell Biol.* **8**, 729–740 (2007).
271. Schmidt, J. C. & Cech, T. R. Human telomerase: biogenesis, trafficking, recruitment, and activation. *Genes Dev.* **29**, 1095–1105 (2015).
272. Harley, C. B., Futcher, A. B. & Greider, C. W. Telomeres shorten during ageing of human fibroblasts. *Nature* **345**, 458–460 (1990).
273. Hanahan, D. & Weinberg, R. A. Hallmarks of cancer: the next generation. *Cell* **144**, 646–674 (2011).
274. Barthel, F. P. *et al.* Systematic analysis of telomere length and somatic alterations in 31 cancer types. *Nat. Genet.* **49**, 349–357 (2017).
275. Bryan, T. M., Englezou, A., Dalla-Pozza, L., Dunham, M. A. & Reddel, R. R. Evidence for an alternative mechanism for maintaining telomere length in human tumors and tumor-derived cell lines. *Nat. Med.* **3**, 1271–1274 (1997).
276. Lansdorp, P. M. Telomeres, stem cells, and hematology. *Blood* **111**, 1759–1766 (2008).
277. Baker, D. J. *et al.* Clearance of p16Ink4a-positive senescent cells delays ageing-associated disorders. *Nature* **479**, 232–236 (2011).
278. Baker, D. J. *et al.* Naturally occurring p16(Ink4a)-positive cells shorten healthy lifespan. *Nature* **530**, 184–189 (2016).
279. Hernandez-Segura, A., Nehme, J. & Demaria, M. Hallmarks of Cellular Senescence. *Trends Cell Biol.* **28**, 436–453 (2018).
280. Ijpm, A. S. & Greider, C. W. Short telomeres induce a DNA damage response in *Saccharomyces cerevisiae*. *Mol. Biol. Cell* **14**, 987–1001 (2003).
281. Enomoto, S., Glowczewski, L. & Berman, J. MEC3, MEC1, and DDC2 are essential components of a telomere checkpoint pathway required for cell cycle arrest during senescence in *Saccharomyces cerevisiae*. *Mol. Biol. Cell* **13**, 2626–2638 (2002).
282. Khadaroo, B. *et al.* The DNA damage response at eroded telomeres and tethering to the nuclear pore complex. *Nat. Cell Biol.* **11**, 980–987 (2009).
283. Abdallah, P. *et al.* A two-step model for senescence triggered by a single critically short telomere. *Nat. Cell Biol.* **11**, 988–993 (2009).
284. Grandin, N., Bailly, A. & Charbonneau, M. Activation of Mrc1, a mediator of the replication checkpoint, by telomere erosion. *Biol. Cell* **97**, 799–814 (2005).
285. Fallet, E. *et al.* Length-dependent processing of telomeres in the absence of telomerase. *Nucleic Acids Res.* **42**, 3648–3665 (2014).
286. Xu, Z. *et al.* Two routes to senescence revealed by real-time analysis of telomerase-negative single lineages. *Nat. Commun.* **6**, 1–10 (2015).
287. Churikov, D., Charifi, F., Simon, M.-N. & Géli, V. Rad59-facilitated acquisition of Y' elements by short telomeres delays the onset of senescence. *PLoS Genet.* **10**, e1004736 (2014).
288. Lundblad, V. & Blackburn, E. H. An alternative pathway for yeast telomere maintenance rescues est1- senescence. *Cell* **73**, 347–360 (1993).
289. Le, S., Moore, J. K., Haber, J. E. & Greider, C. W. RAD50 and RAD51 define two pathways that collaborate to maintain telomeres in the absence of telomerase. *Genetics* **152**, 143–152 (1999).
290. Teng, S. C. & Zakian, V. A. Telomere-telomere recombination is an efficient bypass pathway for telomere maintenance in *Saccharomyces cerevisiae*. *Mol. Cell Biol.* **19**, 8083–93 (1999).
291. Lydeard, J. R., Jain, S., Yamaguchi, M. & Haber, J. E. Break-induced replication and telomerase-independent telomere maintenance require Pol32. *Nature* **448**,

- 820–823 (2007).
292. Claussin, C. & Chang, M. The many facets of homologous recombination at telomeres. *Microb. Cell* **2**, 308–321 (2015).
293. Chen, Q., Ijima, A. & Greider, C. W. Two survivor pathways that allow growth in the absence of telomerase are generated by distinct telomere recombination events. *Mol. Cell. Biol.* **21**, 1819–1827 (2001).
294. Larrivée, M. & Wellinger, R. J. Telomerase- and capping-independent yeast survivors with alternate telomere states. *Nat. Cell Biol.* **8**, 741–747 (2006).
295. Cohen, H. & Sinclair, D. A. Recombination-mediated lengthening of terminal telomeric repeats requires the Sgs1 DNA helicase. *Proc. Natl. Acad. Sci. U. S. A.* **98**, 3174–3179 (2001).
296. Huang, P. *et al.* SGS1 is required for telomere elongation in the absence of telomerase. *Curr. Biol.* **11**, 125–129 (2001).
297. Johnson, F. B. *et al.* The *Saccharomyces cerevisiae* WRN homolog Sgs1p participates in telomere maintenance in cells lacking telomerase. *EMBO J.* **20**, 905–913 (2001).
298. Misino, S., Bonetti, D., Luke-Glaser, S. & Luke, B. Increased TERRA levels and RNase H sensitivity are conserved hallmarks of post-senescent survivors in budding yeast. *Differentiation* **100**, 37–45 (2018).
299. Misino, S., Busch, A., Wagner, C. B., Bento, F. & Luke, B. TERRA increases at short telomeres in yeast survivors and regulates survivor associated senescence (SAS). *Nucleic Acids Res.* **50**, 12829–12843 (2022).
300. Episkopou, H. *et al.* Alternative Lengthening of Telomeres is characterized by reduced compaction of telomeric chromatin. *Nucleic Acids Res.* **42**, 4391–4405 (2014).
301. Ng, L. J., Cropley, J. E., Pickett, H. A., Reddel, R. R. & Suter, C. M. Telomerase activity is associated with an increase in DNA methylation at the proximal subtelomere and a reduction in telomeric transcription. *Nucleic Acids Res.* **37**, 1152–1159 (2009).
302. Simon, M.-N., Churikov, D. & Géli, V. Replication stress as a source of telomere recombination during replicative senescence in *Saccharomyces cerevisiae*. *FEMS Yeast Res.* **16**, (2016).
303. Jacobs, J. J. L. & de Lange, T. Significant role for p16INK4a in p53-independent telomere-directed senescence. *Curr. Biol.* **14**, 2302–2308 (2004).
304. Hayflick, L. The Limited IN VITRO Lifetime Of Human Diploid Cell Strains. *Exp. Cell Res.* **37**, 614–636 (1965).
305. Childs, B. G., Durik, M., Baker, D. J. & van Deursen, J. M. Cellular senescence in aging and age-related disease: from mechanisms to therapy. *Nat. Med.* **21**, 1424–1435 (2015).
306. Mortimer, R. K. & Johnston, J. R. Life span of individual yeast cells. *Nature* **183**, 1751–1752 (1959).
307. Hayflick, L. & Moorhead, P. S. The serial cultivation of human diploid cell strains. *Exp. Cell Res.* **25**, 585–621 (1961).
308. Neurohr, G. E. *et al.* Excessive Cell Growth Causes Cytoplasm Dilution And Contributes to Senescence. *Cell* **176**, 1083-1097.e18 (2019).
309. Kim, N. W. *et al.* Specific association of human telomerase activity with immortal cells and cancer. *Science* **266**, 2011–2015 (1994).
310. Bodnar, A. G. *et al.* Extension of life-span by introduction of telomerase into normal human cells. *Science* **279**, 349–352 (1998).
311. Herbig, U., Jobling, W. A., Chen, B. P. C., Chen, D. J. & Sedivy, J. M. Telomere shortening triggers senescence of human cells through a pathway involving ATM, p53, and p21(CIP1), but not p16(INK4a). *Mol. Cell* **14**, 501–513 (2004).
312. Kaul, Z., Cesare, A. J., Huschtscha, L. I., Neumann, A. A. & Reddel, R. R. Five dysfunctional telomeres predict onset of senescence in human cells. *EMBO Rep.* **13**, 52–59 (2011).
313. Dimri, G. P. *et al.* A biomarker that identifies senescent human cells in culture and in aging skin in vivo. *Proc. Natl. Acad. Sci. U. S. A.* **92**, 9363–9367 (1995).
314. Liu, Y. *et al.* Expression of p16(INK4a) in peripheral blood T-cells is a biomarker of human aging. *Aging Cell* **8**, 439–448 (2009).
315. Muñoz-Espín, D. *et al.* Programmed cell senescence during mammalian embryonic development. *Cell* **155**, 1104–1118 (2013).
316. Siegel, R. L., Miller, K. D., Fuchs, H. E. & Jemal, A. Cancer Statistics, 2021. *CA. Cancer J. Clin.* **71**, 7–33 (2021).
317. Vieri, M., Brümmendorf, T. H. & Beier, F. Treatment of telomeropathies. *Best Pract. Res. Clin. Haematol.* **34**, 101282 (2021).
318. Holohan, B., Wright, W. E. & Shay, J. W. Cell biology of disease: Telomeropathies: an emerging spectrum disorder. *J. Cell Biol.* **205**, 289–299 (2014).
319. Mitchell, J. R., Wood, E. & Collins, K. A telomerase component is defective in the human disease dyskeratosis congenita. *Nature* **402**, 551–555 (1999).
320. Parry, E. M. *et al.* Decreased dyskerin levels as a mechanism of telomere shortening in X-linked dyskeratosis congenita. *J. Med. Genet.* **48**, 327–333 (2011).
321. Parry, E. M., Alder, J. K., Qi, X., Chen, J. J.-L. & Armanios, M. Syndrome complex of bone marrow failure and pulmonary fibrosis predicts germline defects in telomerase. *Blood* **117**, 5607–5611

- (2011).
322. Stella, G. M., Balestro, E., Lacedonia, D. & Baraldo, S. Telomeropathies: an emerging spectrum of disorders with important implications for patients with interstitial lung disease. *Minerva Med.* **107**, 9–14 (2016).
323. Armanios, M. Y. *et al.* Telomerase mutations in families with idiopathic pulmonary fibrosis. *N. Engl. J. Med.* **356**, 1317–1326 (2007).
324. Tsakiri, K. D. *et al.* Adult-onset pulmonary fibrosis caused by mutations in telomerase. *Proc. Natl. Acad. Sci. U. S. A.* **104**, 7552–7557 (2007).
325. Armanios, M. & Blackburn, E. H. The telomere syndromes. *Nat. Rev. Genet.* **13**, 693–704 (2012).
326. Alter, B. P., Giri, N., Savage, S. A. & Rosenberg, P. S. Cancer in dyskeratosis congenita. *Blood* **113**, 6549–6557 (2009).
327. Lopez de Silanes, I., Stagno d'Alcontres, M. & Blasco, M. A. TERRA transcripts are bound by a complex array of RNA-binding proteins. *Nat Commun* **1**, 33 (2010).
328. de Silanes, I. L. *et al.* Identification of TERRA locus unveils a telomere protection role through association to nearly all chromosomes. *Nat. Commun.* **5**, 4723 (2014).
329. Deng, Z., Nourse, J., Wiedmer, A., Riethman, H. & Lieberman, P. M. TERRA RNA Binding to TRF2 Facilitates Heterochromatin Formation and ORC Recruitment at Telomeres. *Mol. Cell* **35**, 403–413 (2009).
330. Deng, Z. *et al.* A role for CTCF and cohesin in subtelomere chromatin organization, TERRA transcription, and telomere end protection. *EMBO J.* **31**, 4165–4178 (2012).
331. Montero, J. J., López de Silanes, I., Graña, O. & Blasco, M. A. Telomeric RNAs are essential to maintain telomeres. *Nat. Commun.* **7**, 12534 (2016).
332. Arnoult, N., Van Beneden, A. & Decottignies, A. Telomere length regulates TERRA levels through increased trimethylation of telomeric H3K9 and HP1 $\alpha$ . *Nat. Struct. Mol. Biol.* **19**, 948–956 (2012).
333. Montero, J. J. *et al.* TERRA recruitment of polycomb to telomeres is essential for histone trimethylation marks at telomeric heterochromatin. *Nat. Commun.* **9**, 1548 (2018).
334. Rippe, K. & Luke, B. TERRA and the state of the telomere. *Nat. Struct. Mol. Biol.* **22**, 853–858 (2015).
335. Azzalin, C. M. & Lingner, J. Telomere functions grounding on TERRA firma. *Trends Cell Biol.* **25**, 29–36 (2015).
336. Bettin, N., Oss Pegorar, C. & Cusanelli, E. The Emerging Roles of TERRA in Telomere Maintenance and Genome Stability. *Cells* **8**, (2019).
337. Moravec, M. *et al.* TERRA promotes telomerase-mediated telomere elongation in *Schizosaccharomyces pombe*. *EMBO Rep.* **17**, 999–1012 (2016).
338. Azzalin, C. M., Reichenbach, P., Khoraiuli, L., Giulotto, E. & Lingner, J. Telomeric repeat-containing RNA and RNA surveillance factors at mammalian chromosome ends. *Science* **318**, 798–801 (2007).
339. Luke, B. *et al.* The Rat1p 5' to 3' exonuclease degrades telomeric repeat-containing RNA and promotes telomere elongation in *Saccharomyces cerevisiae*. *Mol. Cell* **32**, 465–477 (2008).
340. Schoeftner, S. & Blasco, M. A. Developmentally regulated transcription of mammalian telomeres by DNA-dependent RNA polymerase II. *Nat. Cell Biol.* **10**, (2008).
341. Nergadze, S. G. *et al.* CpG-island promoters drive transcription of human telomeres. *RNA* **15**, 2186–94 (2009).
342. Pfeiffer, V. & Lingner, J. TERRA promotes telomere shortening through exonuclease 1-mediated resection of chromosome ends. *PLoS Genet.* **8**, (2012).
343. Porro, A., Feuerhahn, S., Reichenbach, P. & Lingner, J. Molecular dissection of telomeric repeat-containing RNA biogenesis unveils the presence of distinct and multiple regulatory pathways. *Mol. Cell. Biol.* **30**, 4808–4817 (2010).
344. Iglesias, N. *et al.* Subtelomeric repetitive elements determine TERRA regulation by Rap1/Rif and Rap1/Sir complexes in yeast. *EMBO Rep.* **12**, 587–593 (2011).
345. Balk, B. *et al.* Telomeric RNA-DNA hybrids affect telomere-length dynamics and senescence. *Nat Struct Mol Biol* **20**, 1199–1205 (2013).
346. Scheibe, M. *et al.* Quantitative interaction screen of telomeric repeat-containing RNA reveals novel TERRA regulators. *Genome Res.* **23**, 2149–2157 (2013).
347. Perez-Romero, C. A., Lalonde, M., Chartrand, P. & Cusanelli, E. Induction and relocalization of telomeric repeat-containing RNAs during diauxic shift in budding yeast. *Curr. Genet.* **64**, 1117–1127 (2018).
348. Arora, R. *et al.* RNaseH1 regulates TERRA-telomeric DNA hybrids and telomere maintenance in ALT tumour cells. *Nat. Commun.* **5**, 5220 (2014).
349. Nanavaty, V., Sandhu, R., Jehi, S. E., Pandya, U. M. & Li, B. Trypanosoma brucei RAP1 maintains telomere and subtelomere integrity by suppressing TERRA and telomeric RNA:DNA hybrids. *Nucleic Acids Res.* **45**, 5785–5796 (2017).
350. Arora, R. & Azzalin, C. M. Telomere elongation chooses TERRA ALTernatives. *RNA Biol.* **12**, 938–941 (2015).
351. Feretzaki, M. *et al.* RAD51-dependent recruitment of TERRA lncRNA to telomeres through R-loops. *Nature* **587**, 303–308 (2020).



352. Feretzaki, M., Renck Nunes, P. & Lingner, J. Expression and differential regulation of human TERRA at several chromosome ends. *RNA* **25**, 1470–1480 (2019).
353. Aguilera, A. & García-Muse, T. R Loops: From Transcription Byproducts to Threats to Genome Stability. *Mol. Cell* **46**, 115–124 (2012).
354. Gan, W. *et al.* R-loop-mediated genomic instability is caused by impairment of replication fork progression. *Genes Dev.* **25**, 2041–2056 (2011).
355. Joyce, C. M. Choosing the right sugar: how polymerases select a nucleotide substrate. *Proc. Natl. Acad. Sci. U. S. A.* **94**, 1619–1622 (1997).
356. McElhinny, S. A. N. *et al.* Genome instability due to ribonucleotide incorporation into DNA. *Nat. Chem. Biol.* **6**, 774–781 (2010).
357. Nick McElhinny, S. A. *et al.* Abundant ribonucleotide incorporation into DNA by yeast replicative polymerases. *Proc. Natl. Acad. Sci. U. S. A.* **107**, 4949–4954 (2010).
358. Lujan, S. A., Williams, J. S., Clausen, A. R., Clark, A. B. & Kunkel, T. A. Ribonucleotides are signals for mismatch repair of leading-strand replication errors. *Mol. Cell* **50**, 437–443 (2013).
359. Clausen, A. R., Zhang, S., Burgers, P. M., Lee, M. Y. & Kunkel, T. A. Ribonucleotide incorporation, proofreading and bypass by human DNA polymerase  $\delta$ . *DNA Repair (Amst)*. **12**, 121–127 (2013).
360. Caldecott, K. W. Ribose - an internal threat to DNA. *Science (80-. )*. **343**, 260–261 (2014).
361. Kellner, V. & Luke, B. Molecular and physiological consequences of faulty eukaryotic ribonucleotide excision repair. *EMBO J.* **39**, 1–16 (2020).
362. Pellegrini, L. The Pol  $\alpha$ -primase complex. *Subcell. Biochem.* **62**, 157–169 (2012).
363. Skourti-Stathaki, K. & Proudfoot, N. J. A double-edged sword: R loops as threats to genome integrity and powerful regulators of gene expression. *Genes Dev.* **28**, 1384–1396 (2014).
364. Costantino, L. & Koshland, D. The Yin and Yang of R-loop biology. *Curr. Opin. Cell Biol.* **34**, 39–45 (2015).
365. Santos-Pereira, J. M. & Aguilera, A. R loops: new modulators of genome dynamics and function. *Nat. Rev. Genet.* **16**, 583–597 (2015).
366. Brickner, J. R., Garzon, J. L. & Cimprich, K. A. Review Walking a tightrope : The complex balancing act of R-loops in genome stability. *Mol. Cell* **82**, 2267–2297 (2022).
367. Niehrs, C. & Luke, B. Regulatory R-loops as facilitators of gene expression and genome stability. *Nat. Rev. Mol. Cell Biol.* **21**, 167–178 (2020).
368. Petermann, E., Lan, L. & Zou, L. Sources, resolution and physiological relevance of R-loops and RNA-DNA hybrids. *Nat. Rev. Mol. Cell Biol.* **23**, 521–540 (2022).
369. Kasahara, M., Clikeman, J. A., Bates, D. B. & Kogoma, T. RecA protein-dependent R-loop formation in vitro. *Genes Dev.* **14**, 360–365 (2000).
370. Zaitsev, E. N. & Kowalczykowski, S. C. A novel pairing process promoted by Escherichia coli RecA protein: inverse DNA and RNA strand exchange. *Genes Dev.* **14**, 740–749 (2000).
371. Wahba, L., Amon, J. D., Koshland, D. & Vuica-Ross, M. RNase H and multiple RNA biogenesis factors cooperate to prevent RNA:DNA hybrids from generating genome instability. *Mol. Cell* **44**, 978–988 (2011).
372. Wahba, L., Gore, S. K. & Koshland, D. The homologous recombination machinery modulates the formation of RNA-DNA hybrids and associated chromosome instability. *Elife* **2**, e00505 (2013).
373. Zatreanu, D. *et al.* Elongation Factor TFIIIS Prevents Transcription Stress and R-Loop Accumulation to Maintain Genome Stability. *Mol. Cell* **76**, 57-69.e9 (2019).
374. Roberts, R. W. & Crothers, D. M. Stability and properties of double and triple helices: dramatic effects of RNA or DNA backbone composition. *Science* **258**, 1463–1466 (1992).
375. Roy, D., Yu, K. & Lieber, M. R. Mechanism of R-loop formation at immunoglobulin class switch sequences. *Mol. Cell. Biol.* **28**, 50–60 (2008).
376. Liu, L. F. & Wang, J. C. Supercoiling of the DNA template during transcription. *Proc. Natl. Acad. Sci. U. S. A.* **84**, 7024–7027 (1987).
377. Roy, D. & Lieber, M. R. G clustering is important for the initiation of transcription-induced R-loops in vitro, whereas high G density without clustering is sufficient thereafter. *Mol. Cell. Biol.* **29**, 3124–3133 (2009).
378. Roy, D., Zhang, Z., Lu, Z., Hsieh, C.-L. & Lieber, M. R. Competition between the RNA transcript and the nontemplate DNA strand during R-loop formation in vitro: a nick can serve as a strong R-loop initiation site. *Mol. Cell. Biol.* **30**, 146–159 (2010).
379. Duquette, M. L., Handa, P., Vincent, J. A., Taylor, A. F. & Maizels, N. Intracellular transcription of G-rich DNAs induces formation of G-loops, novel structures containing G4 DNA. *Genes Dev.* **18**, 1618–1629 (2004).
380. Chan, Y. A. *et al.* Genome-wide profiling of yeast DNA:RNA hybrid prone sites with DRIP-chip. *PLoS Genet.* **10**, e1004288 (2014).
381. El Hage, A., Webb, S., Kerr, A. & Tollervey, D. Genome-wide distribution of RNA-DNA hybrids identifies RNase H targets in tRNA genes, retrotransposons and mitochondria. *PLoS Genet.* **10**,

- e1004716 (2014).
382. Kreuzer, K. N. & Brister, J. R. Initiation of bacteriophage T4 DNA replication and replication fork dynamics: a review in the Virology Journal series on bacteriophage T4 and its relatives. *Virology* **7**, 358 (2010).
383. Itoh, T. & Tomizawa, J. Formation of an RNA primer for initiation of replication of ColE1 DNA by ribonuclease H. *Proc. Natl. Acad. Sci. U. S. A.* **77**, 2450–2454 (1980).
384. Baldacci, G., Chérif-Zahar, B. & Bernardi, G. The initiation of DNA replication in the mitochondrial genome of yeast. *EMBO J.* **3**, 2115–2120 (1984).
385. Xu, B. & Clayton, D. A. RNA-DNA hybrid formation at the human mitochondrial heavy-strand origin ceases at replication start sites: an implication for RNA-DNA hybrids serving as primers. *EMBO J.* **15**, 3135–3143 (1996).
386. Skourti-Stathaki, K., Proudfoot, N. J. & Gromak, N. Human senataxin resolves RNA/DNA hybrids formed at transcriptional pause sites to promote Xrn2-dependent termination. *Mol. Cell* **42**, 794–805 (2011).
387. Castellano-Pozo, M. *et al.* R loops are linked to histone H3 S10 phosphorylation and chromatin condensation. *Mol. Cell* **52**, 583–590 (2013).
388. Skourti-Stathaki, K. & Proudfoot, N. J. Histone 3 s10 phosphorylation: 'caught in the R loop!'. *Mol. Cell* **52**, 470–472 (2013).
389. Ginno, P. A., Lott, P. L., Christensen, H. C., Korf, I. & Chédin, F. R-loop formation is a distinctive characteristic of unmethylated human CpG island promoters. *Mol. Cell* **45**, 814–825 (2012).
390. Arab, K. *et al.* GADD45A binds R-loops and recruits TET1 to CpG island promoters. *Nat. Genet.* **51**, 217–223 (2019).
391. Ginno, P. A., Lim, Y. W., Lott, P. L., Korf, I. & Chédin, F. GC skew at the 5' and 3' ends of human genes links R-loop formation to epigenetic regulation and transcription termination. *TL - 23. Genome Res.* **23**, 1590–1600 (2013).
392. Sun, Q., Csorba, T., Skourti-Stathaki, K., Proudfoot, N. J. & Dean, C. R-loop stabilization represses antisense transcription at the Arabidopsis FLC locus. *Science* **340**, 619–621 (2013).
393. Chen, P. B., Chen, H. V., Acharya, D., Rando, O. J. & Fazzio, T. G. R loops regulate promoter-proximal chromatin architecture and cellular differentiation. *Nat. Struct. Mol. Biol.* **22**, 999–1007 (2015).
394. Michelini, F. *et al.* Damage-induced lncRNAs control the DNA damage response through interaction with DDRNAs at individual double-strand breaks. *Nat. Cell Biol.* **19**, 1400–1411 (2017).
395. D'Alessandro, G. *et al.* BRCA2 controls DNA:RNA hybrid level at DSBs by mediating RNase H2 recruitment. *Nat. Commun.* **9**, (2018).
396. Teng, Y. *et al.* ROS-induced R loops trigger a transcription-coupled but BRCA1/2-independent homologous recombination pathway through CSB. *Nat. Commun.* **9**, 4115 (2018).
397. Marnef, A. & Legube, G. R-loops as Janus-faced modulators of DNA repair. *Nat. Cell Biol.* **23**, 305–313 (2021).
398. Puget, N., Miller, K. M. & Legube, G. Non-canonical DNA/RNA structures during Transcription-Coupled Double-Strand Break Repair: Roadblocks or Bona fide repair intermediates? *DNA Repair (Amst)*. **81**, 102661 (2019).
399. Lu, W.-T. *et al.* Drosha drives the formation of DNA:RNA hybrids around DNA break sites to facilitate DNA repair. *Nat. Commun.* **9**, 532 (2018).
400. Cohen, S. *et al.* Senataxin resolves RNA:DNA hybrids forming at DNA double-strand breaks to prevent translocations. *Nat. Commun.* **9**, (2018).
401. Rawal, C. C. *et al.* Senataxin Ortholog Sen1 Limits DNA:RNA Hybrid Accumulation at DNA Double-Strand Breaks to Control End Resection and Repair Fidelity. *Cell Rep.* **31**, 107603 (2020).
402. Ouyang, J. *et al.* RNA transcripts stimulate homologous recombination by forming DR-loops. *Nature* **594**, 283–288 (2021).
403. Liu, S. *et al.* RNA polymerase III is required for the repair of DNA double-strand breaks by homologous recombination. *Cell* **184**, 1314–1329.e10 (2021).
404. Tan, J. *et al.* An R-loop-initiated CSB-RAD52-POLD3 pathway suppresses ROS-induced telomeric DNA breaks. *Nucleic Acids Res.* **48**, 1285–1300 (2020).
405. Yasuhara, T. *et al.* Human Rad52 Promotes XPG-Mediated R-loop Processing to Initiate Transcription-Associated Homologous Recombination Repair. *Cell* **175**, 558–570.e11 (2018).
406. Li, L. *et al.* DEAD Box 1 Facilitates Removal of RNA and Homologous Recombination at DNA Double-Strand Breaks. *Mol. Cell Biol.* **36**, 2794–2810 (2016).
407. Ortega, P., Mérida-Cerro, J. A., Rondón, A. G., Gómez-González, B. & Aguilera, A. DNA-RNA hybrids at DSBs interfere with repair by homologous recombination. *Elife* **10**, 1–22 (2021).
408. Lindahl, T. Instability and decay of the primary structure of DNA. *Nature* **362**, 709–715 (1993).
409. Hamperl, S. & Cimprich, K. A. The contribution of co-transcriptional RNA:DNA hybrid structures to DNA damage and genome instability. *DNA Repair (Amst)*. **19**, 84–94 (2014).
410. Sollier, J. *et al.* Transcription-coupled

- nucleotide excision repair factors promote R-loop-induced genome instability. *Mol. Cell* **56**, 777–785 (2014).
411. Takahashi, D. T., Burguiere-Slezak, G., Van der Kemp, P. A. & Boiteux, S. Topoisomerase 1 provokes the formation of short deletions in repeated sequences upon high transcription in *Saccharomyces cerevisiae*. *Proc. Natl. Acad. Sci. U. S. A.* **108**, 692–697 (2011).
412. Crossley, M. P., Bocek, M. & Cimprich, K. A. R-Loops as Cellular Regulators and Genomic Threats. *Mol. Cell* **73**, 398–411 (2019).
413. Gómez-González, B. *et al.* Genome-wide function of THO/TREX in active genes prevents R-loop-dependent replication obstacles. *EMBO J.* **30**, 3106–19 (2011).
414. Tuduri, S. *et al.* Topoisomerase I suppresses genomic instability by preventing interference between replication and transcription. *Nat. Cell Biol.* **11**, 1315–1324 (2009).
415. Hamperl, S., Bocek, M. J., Saldivar, J. C., Swigut, T. & Cimprich, K. A. Transcription-Replication Conflict Orientation Modulates R-Loop Levels and Activates Distinct DNA Damage Responses. *Cell* **170**, 774–786.e19 (2017).
416. García-Rubio, M. *et al.* Yra1-bound RNA–DNA hybrids cause orientation-independent transcription– replication collisions and telomere instability. *Genes Dev.* **32**, 965–977 (2018).
417. García-Pichardo, D. *et al.* Histone Mutants Separate R Loop Formation from Genome Instability Induction. *Mol. Cell* **66**, 597–609.e5 (2017).
418. Bayona-Feliu, A., Barroso, S., Muñoz, S. & Aguilera, A. The SWI/SNF chromatin remodeling complex helps resolve R-loop-mediated transcription-replication conflicts. *Nat. Genet.* **53**, 1050–1063 (2021).
419. Bayona-Feliu, A., Casas-Lamesa, A., Reina, O., Bernués, J. & Azorín, F. Linker histone H1 prevents R-loop accumulation and genome instability in heterochromatin. *Nat. Commun.* **8**, 283 (2017).
420. Salas-Armenteros, I. *et al.* Human THO–Sin3A interaction reveals new mechanisms to prevent R-loops that cause genome instability. *EMBO J.* **36**, 3532–3547 (2017).
421. Pan, X. *et al.* FANCM suppresses DNA replication stress at ALT telomeres by disrupting TERRA R-loops. *Sci. Rep.* **9**, 19110 (2019).
422. Silva, B. *et al.* FANCM limits ALT activity by restricting telomeric replication stress induced by deregulated BLM and R-loops. *Nat. Commun.* **10**, 1–16 (2019).
423. Kotsantis, P. *et al.* RTEL1 Regulates G4/R-Loops to Avert Replication-Transcription Collisions. *Cell Rep.* **33**, 108546 (2020).
424. Björkman, A. *et al.* Human RTEL1 associates with Poldip3 to facilitate responses to replication stress and R-loop resolution. *Genes Dev.* **34**, 1065–1074 (2020).
425. Vohhodina, J. *et al.* BRCA1 binds TERRA RNA and suppresses R-Loop-based telomeric DNA damage. *Nat. Commun.* **12**, 3542 (2021).
426. Bayona-Feliu, A. & Aguilera, A. The role of chromatin at transcription-replication conflicts as a genome safeguard. *Biochem. Soc. Trans.* **49**, 2727–2736 (2021).
427. García-Muse, T. & Aguilera, A. R Loops: From Physiological to Pathological Roles. *Cell* **179**, 604–618 (2019).
428. Paull, T. T. RNA-DNA hybrids and the convergence with DNA repair. *Crit. Rev. Biochem. Mol. Biol.* **54**, 371–384 (2019).
429. Uruci, S., Lo, C. S. Y., Wheeler, D. & Taneja, N. R-Loops and Its Chro-Mates: The Strange Case of Dr. Jekyll and Mr. Hyde. *Int. J. Mol. Sci.* **22**, (2021).
430. El Hage, A., French, S. L., Beyer, A. L. & Tollervey, D. Loss of Topoisomerase I leads to R-loop-mediated transcriptional blocks during ribosomal RNA synthesis. *Genes Dev.* **24**, 1546–1558 (2010).
431. Stolz, R. *et al.* Interplay between DNA sequence and negative superhelicity drives R-loop structures. *Proc. Natl. Acad. Sci. U. S. A.* **116**, 6260–6269 (2019).
432. Promonet, A. *et al.* Topoisomerase 1 prevents replication stress at R-loop-enriched transcription termination sites. *Nat. Commun.* **11**, 3940 (2020).
433. Yang, Y. *et al.* Arginine methylation facilitates the recruitment of TOP3B to chromatin to prevent R loop accumulation. *Mol. Cell* **53**, 484–497 (2014).
434. Huertas, P. & Aguilera, A. Cotranscriptionally formed DNA:RNA hybrids mediate transcription elongation impairment and transcription-associated recombination. *Mol. Cell* **12**, 711–721 (2003).
435. Santos-Pereira, J. M. *et al.* The Npl3 hnRNP prevents R-loop-mediated transcription-replication conflicts and genome instability. *Genes Dev.* **27**, 2445–2458 (2013).
436. Gavalda, S., Santos-Pereira, J. M., García-Rubio, M. L., Luna, R. & Aguilera, A. Excess of Yra1 RNA-Binding Factor Causes Transcription-Dependent Genome Instability, Replication Impairment and Telomere Shortening. *PLoS Genet.* **12**, e1005966 (2016).
437. García-Benítez, F., Gaillard, H. & Aguilera, A. Physical proximity of chromatin to nuclear pores prevents harmful R loop accumulation contributing to maintain genome stability. *Proc. Natl. Acad. Sci. U. S. A.* **114**, 10942–10947

- (2017).
438. Li, X. & Manley, J. L. Inactivation of the SR protein splicing factor ASF/SF2 results in genomic instability. *Cell* **122**, 365–378 (2005).
439. Aguilera, A. & Klein, H. L. HPR1, a novel yeast gene that prevents intrachromosomal excision recombination, shows carboxy-terminal homology to the *Saccharomyces cerevisiae* TOP1 gene. *Mol. Cell. Biol.* **10**, 1439–1451 (1990).
440. Gallardo, M., Luna, R., Erdjument-Bromage, H., Tempst, P. & Aguilera, A. Nab2p and the Thp1p-Sac3p complex functionally interact at the interface between transcription and mRNA metabolism. *J. Biol. Chem.* **278**, 24225–24232 (2003).
441. González-Aguilera, C. *et al.* The THP1-SAC3-SUS1-CDC31 complex works in transcription elongation-mRNA export preventing RNA-mediated genome instability. *Mol. Biol. Cell* **19**, 4310–4318 (2008).
442. Tsai, S. *et al.* ARID1A regulates R-loop associated DNA replication stress. *PLoS Genet.* **17**, e1009238 (2021).
443. Abakir, A. *et al.* N6-methyladenosine regulates the stability of RNA:DNA hybrids in human cells. *Nat. Genet.* **52**, 48–55 (2020).
444. Chen, H. *et al.* m(5)C modification of mRNA serves a DNA damage code to promote homologous recombination. *Nat. Commun.* **11**, 2834 (2020).
445. Zhang, C. *et al.* METTL3 and N6-Methyladenosine Promote Homologous Recombination-Mediated Repair of DSBs by Modulating DNA-RNA Hybrid Accumulation. *Mol. Cell* **79**, 425–442.e7 (2020).
446. Stein, H. & Hausen, P. Enzyme from calf thymus degrading the RNA moiety of DNA-RNA Hybrids: effect on DNA-dependent RNA polymerase. *Science* **166**, 393–395 (1969).
447. Cerritelli, S. M. & Crouch, R. J. Ribonuclease H: The enzymes in eukaryotes. *FEBS J.* **276**, 1494–1505 (2009).
448. Nowotny, M. *et al.* Structure of Human RNase H1 Complexed with an RNA/DNA Hybrid: Insight into HIV Reverse Transcription. *Mol. Cell* **28**, 264–276 (2007).
449. Hyjek, M., Figiel, M. & Nowotny, M. RNases H: Structure and mechanism. *DNA Repair (Amst.)* **84**, 102672 (2019).
450. Nowotny, M. *et al.* Specific recognition of RNA/DNA hybrid and enhancement of human RNase H1 activity by HBD. *EMBO J.* **27**, 1172–1181 (2008).
451. Cerritelli, S. M. *et al.* Failure to produce mitochondrial DNA results in embryonic lethality in Rnaseh1 null mice. *Mol. Cell* **11**, 807–815 (2003).
452. Nguyen, H. D. *et al.* Functions of Replication Protein A as a Sensor of R Loops and a Regulator of RNaseH1. *Mol. Cell* **65**, 832–847.e4 (2017).
453. Rice, G. *et al.* Clinical and molecular phenotype of Aicardi-Goutières syndrome. *Am. J. Hum. Genet.* **81**, 713–725 (2007).
454. Chon, H. *et al.* Contributions of the two accessory subunits, RNASEH2B and RNASEH2C, to the activity and properties of the human RNase H2 complex. *Nucleic Acids Res.* **37**, 96–110 (2009).
455. Rychlik, M. P. *et al.* Crystal structures of RNase H2 in complex with nucleic acid reveal the mechanism of RNA-DNA junction recognition and cleavage. *Mol. Cell* **40**, 658–670 (2010).
456. Eder, P. S., Walder, R. Y. & Walder, J. A. Substrate specificity of human RNase H1 and its role in excision repair of ribose residues misincorporated in DNA. *Biochimie* **75**, 123–126 (1993).
457. Murante, R. S., Henricksen, L. A. & Bambara, R. A. Junction ribonuclease: an activity in Okazaki fragment processing. *Proc. Natl. Acad. Sci. U. S. A.* **95**, 2244–2249 (1998).
458. Cerritelli, S. M. & Crouch, R. J. RNases H: Multiple roles in maintaining genome integrity. *DNA repair* vol. 84 102742 (2019).
459. Rydberg, B. & Game, J. Excision of misincorporated ribonucleotides in DNA by RNase H (type 2) and FEN-1 in cell-free extracts. *Proc. Natl. Acad. Sci. U. S. A.* **99**, 16654–16659 (2002).
460. Sparks, J. L. *et al.* RNase H2-Initiated Ribonucleotide Excision Repair. *Mol. Cell* **47**, 980–986 (2012).
461. Nguyen, T. A. *et al.* Analysis of subunit assembly and function of the *Saccharomyces cerevisiae* RNase H2 complex. *FEBS J.* **278**, 4927–4942 (2011).
462. Zimmer, A. D. & Koshland, D. Differential roles of the RNases H in preventing chromosome instability. *Proc. Natl. Acad. Sci.* **113**, 12220–12225 (2016).
463. Bubeck, D. *et al.* PCNA directs type 2 RNase H activity on DNA replication and repair substrates. *Nucleic Acids Res.* **39**, 3652–3666 (2011).
464. Lockhart, A. *et al.* RNase H1 and H2 Are Differentially Regulated to Process RNA-DNA Hybrids. *Cell Rep.* **29**, 2890–2900.e5 (2019).
465. Castillo-Guzman, D. & Chédin, F. Defining R-loop classes and their contributions to genome instability. *DNA Repair (Amst.)* **106**, 103182 (2021).
466. Lim, Y. W., Sanz, L. A., Xu, X., Hartono, S. R. & Chédin, F. Genome-wide DNA hypomethylation and RNA:DNA hybrid accumulation in Aicardi-Goutières syndrome. *Elife* **4**, (2015).
467. Cristini, A. *et al.* RNase H2, mutated in Aicardi-Goutières syndrome, resolves co-transcriptional R-loops to prevent DNA

- breaks and inflammation. *Nat. Commun.* **13**, 2961 (2022).
468. Figiel, M. & Nowotny, M. Crystal structure of RNase H3-substrate complex reveals parallel evolution of RNA/DNA hybrid recognition. *Nucleic Acids Res.* **42**, 9285–9294 (2014).
469. Stone, J. E. E. *et al.* RNase H and postreplication repair protect cells from ribonucleotides incorporated in DNA. *Mol. Cell* **45**, 99–110 (2012).
470. O'Connell, K., Jinks-Robertson, S. & Petes, T. D. Elevated Genome-Wide Instability in Yeast Mutants Lacking RNase H Activity. *Genetics* **201**, 963–975 (2015).
471. Chon, H. *et al.* RNase H2 roles in genome integrity revealed by unlinking its activities. *Nucleic Acids Res.* **41**, 3130–3143 (2013).
472. Aiello, U. *et al.* Sen1 is a key regulator of transcription-driven conflicts. *Mol. Cell* **82**, 2952–2966.e6 (2022).
473. Moreira, M.-C. *et al.* Senataxin, the ortholog of a yeast RNA helicase, is mutant in ataxia-ocular apraxia 2. *Nat. Genet.* **36**, 225–227 (2004).
474. Alzu, A. *et al.* Senataxin associates with replication forks to protect fork integrity across RNA-polymerase-II-transcribed genes. *Cell* **151**, 835–846 (2012).
475. Appanah, R., Lones, E. C., Aiello, U., Libri, D. & De Piccoli, G. Sen1 Is Recruited to Replication Forks via Ctf4 and Mrc1 and Promotes Genome Stability. *Cell Rep.* **30**, 2094–2105.e9 (2020).
476. San Martín-Alonso, M., Soler-Oliva, M. E., García-Rubio, M., García-Muse, T. & Aguilera, A. Harmful R-loops are prevented via different cell cycle-specific mechanisms. *Nat. Commun.* **12**, 1–14 (2021).
477. Boulé, J.-B. & Zakian, V. A. The yeast Pif1p DNA helicase preferentially unwinds RNA DNA substrates. *Nucleic Acids Res.* **35**, 5809–5818 (2007).
478. Pohl, T. J. & Zakian, V. A. Pif1 family DNA helicases: A helpmate to RNase H? *DNA Repair (Amst)*. **84**, 102633 (2019).
479. Kim, S. *et al.* ATAD5 restricts R-loop formation through PCNA unloading and RNA helicase maintenance at the replication fork. *Nucleic Acids Res.* **48**, 7218–7238 (2020).
480. Sessa, G. *et al.* BRCA2 promotes DNA-RNA hybrid resolution by DDX5 helicase at DNA breaks to facilitate their repair. *EMBO J.* **40**, e106018 (2021).
481. Mersaoui, S. Y. *et al.* Arginine methylation of the DDX5 helicase RGG/RG motif by PRMT5 regulates resolution of RNA:DNA hybrids. *EMBO J.* **38**, e100986 (2019).
482. Hodroj, D., Serhal, K. & Maiorano, D. Ddx19 links mRNA nuclear export with progression of transcription and replication and suppresses genomic instability upon DNA damage in proliferating cells. *Nucleus* **8**, 489–495 (2017).
483. Song, C., Hotz-Wagenblatt, A., Voit, R. & Grummt, I. SIRT7 and the DEAD-box helicase DDX21 cooperate to resolve genomic R loops and safeguard genome stability. *Genes Dev.* **31**, 1370–1381 (2017).
484. Sridhara, S. C. *et al.* Transcription Dynamics Prevent RNA-Mediated Genomic Instability through SRPK2-Dependent DDX23 Phosphorylation. *Cell Rep.* **18**, 334–343 (2017).
485. Pérez-Calero, C. *et al.* UAP56/DDX39B is a major cotranscriptional RNA-DNA helicase that unwinds harmful R loops genome-wide. *Genes Dev.* **34**, 898–912 (2020).
486. Mosler, T. *et al.* R-loop proximity proteomics identifies a role of DDX41 in transcription-associated genomic instability. *Nat. Commun.* **12**, 7314 (2021).
487. Yoo, H. H. & Chung, I. K. Requirement of DDX39 DEAD box RNA helicase for genome integrity and telomere protection. *Aging Cell* **10**, 557–571 (2011).
488. Maestroni, L. *et al.* Eroded telomeres are rearranged in quiescent fission yeast cells through duplications of subtelomeric sequences. *Nat. Commun.* **8**, 1684 (2017).
489. Phillips, D. D. *et al.* The sub-nanomolar binding of DNA-RNA hybrids by the single-chain Fv fragment of antibody S9.6. *J. Mol. Recognit.* **26**, 376–381 (2013).
490. Pfeiffer, V., Crittin, J., Grolimund, L. & Lingner, J. The THO complex component Thp2 counteracts telomeric R-loops and telomere shortening. *EMBO J.* **32**, 2861–2871 (2013).
491. Wahba, L., Costantino, L., Tan, F. J., Zimmer, A. & Koshland, D. S1-DRIP-seq identifies high expression and polyA tracts as major contributors to R-loop formation. *Genes Dev.* **30**, 1327–1338 (2016).
492. Yu, T.-Y., Kao, Y. & Lin, J.-J. Telomeric transcripts stimulate telomere recombination to suppress senescence in cells lacking telomerase. *Proc. Natl. Acad. Sci. U. S. A.* **111**, 3377–3382 (2014).
493. Fernandes, R. V., Feretzaki, M. & Lingner, J. The makings of TERRA R-loops at chromosome ends. *Cell Cycle* **20**, 1745–1759 (2021).
494. Lee-Soety, J. Y. *et al.* Yeast hnRNP-related proteins contribute to the maintenance of telomeres. *Biochem. Biophys. Res. Commun.* **426**, 12–17 (2012).
495. Pérez-Martínez, L., Öztürk, M., Butter, F. & Luke, B. Npl3 stabilizes R-loops at telomeres to prevent accelerated replicative senescence. *EMBO Rep.* **21**, e49087 (2020).
496. Aguilera, A. & Gómez-González, B. Genome instability: a mechanistic view of its causes and consequences. *Nat. Rev. Genet.* **9**, 204–217 (2008).

497. Hu, Y. *et al.* RNA-DNA Hybrids Support Recombination-Based Telomere Maintenance in Fission Yeast. *Genetics* **213**, 431–447 (2019).
498. Lee, J. Y., Kozak, M., Martin, J. D., Pennock, E. & Johnson, F. B. Evidence that a RecQ helicase slows senescence by resolving recombining telomeres. *PLoS Biol.* **5**, e160 (2007).
499. Luke-Glaser, S. & Luke, B. The Mph1 helicase can promote telomere uncapping and premature senescence in budding yeast. *PLoS One* **7**, e42028 (2012).
500. Lafuente-Barquero, J. *et al.* The Smc5/6 complex regulates the yeast Mph1 helicase at RNA-DNA hybrid-mediated DNA damage. *PLoS Genet.* **13**, 1–25 (2017).
501. Li, J.-R. *et al.* Pif1 regulates telomere length by preferentially removing telomerase from long telomere ends. *Nucleic Acids Res.* **42**, 8527–8536 (2014).
502. Apte, M. S. & Cooper, J. P. Life and cancer without telomerase: ALT and other strategies for making sure ends (don't) meet. *Crit. Rev. Biochem. Mol. Biol.* **52**, 57–73 (2017).
503. Sobinoff, A. P. & Pickett, H. A. Alternative Lengthening of Telomeres: DNA Repair Pathways Converge. *Trends Genet.* **33**, 921–932 (2017).
504. Pan, X. *et al.* FANCM, BRCA1, and BLM cooperatively resolve the replication stress at the ALT telomeres. *Proc. Natl. Acad. Sci. U. S. A.* **114**, E5940–E5949 (2017).
505. Dilley, R. L. *et al.* Break-induced telomere synthesis underlies alternative telomere maintenance. *Nature* **539**, 54–58 (2016).
506. Roumelioti, F.-M. *et al.* Alternative lengthening of human telomeres is a conservative DNA replication process with features of break-induced replication. *EMBO Rep.* **17**, 1731–1737 (2016).
507. Min, J., Wright, W. E. & Shay, J. W. Alternative Lengthening of Telomeres Mediated by Mitotic DNA Synthesis Engages Break-Induced Replication Processes. *Mol. Cell. Biol.* **37**, (2017).
508. Nguyen, D. T. *et al.* The chromatin remodelling factor ATRX suppresses R-loops in transcribed telomeric repeats. *EMBO Rep.* **18**, 914–928 (2017).
509. Flynn, R. L. *et al.* TERRA and hnRNPA1 orchestrate an RPA-to-POT1 switch on telomeric single-stranded DNA. *Nature* **471**, 532–536 (2011).
510. Lee, Y. W., Arora, R., Wischniewski, H. & Azzalin, C. M. TRF1 participates in chromosome end protection by averting TRF2-dependent telomeric R loops. *Nat. Struct. Mol. Biol.* **25**, 147–153 (2018).
511. Amon, J. D. & Koshland, D. RNase H enables efficient repair of R-loop induced DNA damage. *Elife* **5**, 1–20 (2016).
512. Conomos, D., Pickett, H. A. & Reddel, R. R. Alternative lengthening of telomeres: remodeling the telomere architecture. *Front. Oncol.* **3**, 27 (2013).
513. Chawla, R. & Azzalin, C. M. The telomeric transcriptome and SMG proteins at the crossroads. *Cytogenet. Genome Res.* **122**, 194–201 (2008).
514. Cusanelli, E. & Chartrand, P. Telomeric repeat-containing RNA TERRA: A noncoding RNA connecting telomere biology to genome integrity. *Front. Genet.* **6**, 1–9 (2015).
515. Pires, V. B. *et al.* RNA-DNA hybrids prevent resection at dysfunctional telomeres. *Cell Rep.* **42**, 112077 (2023).
516. Chedin, F., Hartono, S. R., Sanz, L. A. & Vanoosthuysse, V. Best practices for the visualization, mapping, and manipulation of R-loops. *EMBO J.* **40**, 1–13 (2021).
517. Wu, Z. J. *et al.* CDC13 is predominant over STN1 and TEN1 in preventing chromosome end fusions. *Elife* **9**, 1–25 (2020).
518. Addinall, S. G. *et al.* A Genomewide Suppressor and Enhancer Analysis of cdc13-1 Reveals Varied Cellular Processes Influencing Telomere Capping in *Saccharomyces cerevisiae*. *Genetics* **180**, 2251–2266 (2008).
519. Weinert, T. A., Kiser, G. L. & Hartwell, L. H. Mitotic checkpoint genes in budding yeast and the dependence of mitosis on DNA replication and repair. *Genes Dev.* **8**, 652–665 (1994).
520. Grandin, N., Damon, C. & Charbonneau, M. Cdc13 prevents telomere uncapping and Rad50-dependent homologous recombination. *EMBO J.* **20**, 6127–6139 (2001).
521. Bochman, M. L., Paeschke, K. & Zakian, V. A. DNA secondary structures: stability and function of G-quadruplex structures. **13**, 770–780 (2012).
522. Jurikova, K. *et al.* Role of folding kinetics of secondary structures in telomeric G-overhangs in the regulation of telomere maintenance in *Saccharomyces cerevisiae*. *J. Biol. Chem.* **295**, 8958–8971 (2020).
523. Biffi, G., Tannahill, D., McCafferty, J. & Balasubramanian, S. Quantitative Visualization of DNA G-quadruplex Structures in Human Cells. **5**, 182–186 (2013).
524. Hänsel-hertsch, R., Spiegel, J., Marsico, G., Tannahill, D. & Balasubramanian, S. Genome-wide mapping of endogenous G-quadruplex DNA structures by chromatin immunoprecipitation and high-throughput sequencing. *Nat. Publ. Gr.* **13**, 551–564 (2018).
525. Booth, C., Griffith, E., Brady, G. & Lydall, D. Quantitative amplification of single-stranded DNA (QAOS) demonstrates that cdc13-1 mutants generate ssDNA in a telomere to centromere direction. *Nucleic Acids Res.* **29**, 4414–4422 (2001).
526. Johnson, C., Gali, V. K., Takahashi, T. S. & Kubota, T. PCNA Retention on DNA into

- G2/M Phase Causes Genome Instability in Cells Lacking Elg1. *Cell Rep.* **16**, 684–695 (2016).
527. Hombauer, H., Srivatsan, A., Putnam, C. D. & Kolodner, R. D. Mismatch Repair, But Not Heteroduplex Rejection, Is Temporally Coupled to DNA Replication. *Science (80-. )*. **334**, 1713–1716 (2011).
528. Matmati, S., Lambert, S., Géli, V. & Coulon, S. Telomerase Repairs Collapsed Replication Forks at Telomeres. *Cell Rep.* **30**, 3312–3322.e3 (2020).
529. Wagner, C. B. & Luke, B. DNA–RNA Hybrids at Telomeres in Budding Yeast. in *Methods Mol Biol* (eds. Aguilera, A. & Ruzov, A.) 145–157 (Springer US, 2022). doi:10.1007/978-1-0716-2477-7\_10.
530. Pérez-Martínez, L., Wagner, T. & Luke, B. Telomere Interacting Proteins and TERRA Regulation. *Front. Genet.* **13**, 1–8 (2022).
531. Bertuch, A. A. & Lundblad, V. EXO1 Contributes to Telomere Maintenance in Both Telomerase-Proficient and Telomerase-Deficient *Saccharomyces cerevisiae*. *Genetics* **166**, 1651–1659 (2004).
532. Maringele, L. & Lydall, D. EXO1 Plays a Role in Generating Type I and Type II Survivors in Budding Yeast. *Genetics* **166**, 1641–1649 (2004).
533. Wanat, J. J. *et al.* TERRA and the histone methyltransferase Dot1 cooperate to regulate senescence in budding yeast. *PLoS One* **13**, 1–23 (2018).
534. Daley, J. M. *et al.* Specificity of end resection pathways for double-strand break regions containing ribonucleotides and base lesions. *Nat. Commun.* **11**, 1–12 (2020).
535. Jimeno, S. *et al.* ADAR-mediated RNA editing of DNA:RNA hybrids is required for DNA double strand break repair. *Nat. Commun.* **12**, (2021).
536. Evans, S. K. & Lundblad, V. Positive and negative regulation of telomerase access to the telomere. *J. Cell Sci.* **113 Pt 19**, 3357–3364 (2000).
537. Pennock, E., Buckley, K. & Lundblad, V. Cdc13 delivers separate complexes to the telomere for end protection and replication. *Cell* **104**, 387–396 (2001).
538. Chandra, A., Hughes, T. R., Nugent, C. I. & Lundblad, V. Cdc13 both positively and negatively regulates telomere replication. *Genes Dev.* **15**, 404–414 (2001).
539. Churikov, D., Corda, Y., Luciano, P. & Géli, V. Cdc13 at a crossroads of telomerase action. *Front. Oncol.* **3**, 39 (2013).
540. Li, S. *et al.* Cdk1-dependent phosphorylation of Cdc13 coordinates telomere elongation during cell-cycle progression. *Cell* **136**, 50–61 (2009).
541. Hang, L. E., Liu, X., Cheung, I., Yang, Y. & Zhao, X. SUMOylation regulates telomere length homeostasis by targeting Cdc13. *Nat. Struct. Mol. Biol.* **18**, 920–926 (2011).
542. Wu, Y., DiMaggio, P. A. J., Perlman, D. H., Zakian, V. A. & Garcia, B. A. Novel phosphorylation sites in the *S. cerevisiae* Cdc13 protein reveal new targets for telomere length regulation. *J. Proteome Res.* **12**, 316–327 (2013).
543. Miglietta, G., Russo, M. & Capranico, G. G-quadruplex-R-loop interactions and the mechanism of anticancer G-quadruplex binders. *Nucleic Acids Res.* **48**, 11942–11957 (2020).
544. García-Muse, T. & Aguilera, A. Transcription-replication conflicts: How they occur and how they are resolved. *Nat. Rev. Mol. Cell Biol.* **17**, 553–563 (2016).
545. Gómez-González, B. & Aguilera, A. Transcription-mediated replication hindrance: a major driver of genome instability. *Genes Dev.* **33**, 1008–1026 (2019).
546. Britton, S. *et al.* DNA damage triggers SAF-A and RNA biogenesis factors exclusion from chromatin coupled to R-loops removal. *Nucleic Acids Res.* **42**, 9047–9062 (2014).
547. Lee, H. *et al.* RNase H is an exo- and endoribonuclease with asymmetric directionality, depending on the binding mode to the structural variants of RNA:DNA hybrids. *Nucleic Acids Res.* **50**, 1801–1814 (2022).
548. Petzold, C., Marceau, A. H., Miller, K. H., Marqusee, S. & Keck, J. L. Interaction with Single-stranded DNA-binding Protein Stimulates *Escherichia coli* Ribonuclease HI Enzymatic Activity. *J. Biol. Chem.* **290**, 14626–14636 (2015).
549. Indiviglio, S. M. & Bertuch, A. A. Ku's essential role in keeping telomeres intact. *Proc. Natl. Acad. Sci. U. S. A.* **106**, 12217–12218 (2009).
550. Teixeira-Silva, A. *et al.* The end-joining factor Ku acts in the end-resection of double strand break-free arrested replication forks. *Nat. Commun.* **8**, 1982 (2017).
551. Krasner, D. S., Daley, J. M., Sung, P. & Niu, H. Interplay between Ku and Replication Protein A in the Restriction of Exo1-mediated DNA Break End Resection\*. *J. Biol. Chem.* **290**, 18806–18816 (2015).
552. Cristini, A., Groh, M., Kristiansen, M. S. & Gromak, N. RNA/DNA Hybrid Interactome Identifies DXH9 as a Molecular Player in Transcriptional Termination and R-Loop-Associated DNA Damage. *Cell Rep.* **23**, 1891–1905 (2018).
553. Bader, A. S., Hawley, B. R., Wilczynska, A. & Bushell, M. The roles of RNA in DNA double-strand break repair. *Br. J. Cancer* **122**, 613–623 (2020).
554. Wang, I. X. *et al.* Human proteins that interact with RNA/DNA hybrids. *Genome Res.* **28**, 1405–1414 (2018).

555. Winston, F., Dollard, C. & Ricupero-Hovasse, S. L. Construction of a set of convenient *Saccharomyces cerevisiae* strains that are isogenic to S288C. *Yeast* **11**, 53–55 (1995).
556. Janke, C. *et al.* A versatile toolbox for PCR-based tagging of yeast genes: New fluorescent proteins, more markers and promoter substitution cassettes. *Yeast* **21**, 947–962 (2004).
557. Ho, C. H. *et al.* A molecular barcoded yeast ORF library enables mode-of-action analysis of bioactive compounds. *Nat. Biotechnol.* **27**, 369–377 (2009).
558. Mortimer, R. K. & Johnston, J. R. Genealogy of principal strains of the yeast genetic stock center. *Genetics* **113**, 35–43 (1986).
559. Guthrie, C. & Fink, G. *Guide to Yeast Genetics and Molecular Biology. Methods Enzymol.* (Academic Press, 1991).
560. Roth, V. Doubling Time Computing. <http://www.doubling-time.com/compute.php> (2006).
561. Shevchenko, A., Tomas, H., Havlis, J., Olsen, J. V & Mann, M. In-gel digestion for mass spectrometric characterization of proteins and proteomes. *Nat. Protoc.* **1**, 2856–2860 (2006).
562. Rappsilber, J., Mann, M. & Ishihama, Y. Protocol for micro-purification, enrichment, pre-fractionation and storage of peptides for proteomics using StageTips. *Nat. Protoc.* **2**, 1896–1906 (2007).
563. Cox, J. & Mann, M. MaxQuant enables high peptide identification rates, individualized p.p.b.-range mass accuracies and proteome-wide protein quantification. *Nat. Biotechnol.* **26**, 1367–1372 (2008).
564. Cox, J. *et al.* Accurate Proteome-wide Label-free Quantification by Delayed Normalization and Maximal Peptide Ratio Extraction, Termed MaxLFQ. *Mol. Cell. Proteomics* **13**, 2513–2526 (2014).



# CURRICULUM VITAE

---

## PERSONAL DETAILS

Name: Vanessa Borges Pires

Date of birth: 19 September 1991

Nationality: Portuguese

## EDUCATION

August 2017- Present

- Faculty of Biology of Johannes Gutenberg University Mainz (Germany)
- PhD Student (Cotutelle) in the International PhD Program (IPP) of the Institute of Molecular Biology – Co-supervision

January 2017-Present

- Instituto de Ciências Biomédicas Abel Salazar, University of Porto (Portugal)
- PhD Student (Cotutelle) in the Graduate Program in Areas of Basic and Applied Biology (GABBA) of the University of Porto – Co-supervision

July-August 2018

- Yeast Genetics and Genomics Course at Cold Spring Harbor Laboratory (USA)  
Helmsley Scholarship from CSHL and Funding for Female Researcher from the JGU Mainz awarded to cover course and travel expenses

September 2013-December 2015

- Faculty of Sciences, University of Lisbon (Portugal)  
Master in Molecular Biology and Genetics  
Dissertation title: Testing short LNA-modified oligonucleotides for Duchenne Muscular Dystrophy gene therapy  
Final average grade: 17 (out of 20) with Dissertation grade of 19 (out of 20)

September 2009- July 2013

- Faculty of Sciences, University of Lisbon (Portugal)  
Graduation in Biology, Branch of Molecular Biology and Genetics with a Minor in Biochemistry  
Final average grade: 14

## WORK EXPERIENCE

August 2017 – December 2022

- PhD Student in Prof. Dr. Brian Luke's Lab at the Institute of Molecular Biology (IMB), Mainz (Germany)  
Project: The regulation of Telomeric R-loops through the RNase H enzymes  
Techniques performed: Yeast genetics, Western Blot, Southern Blots, ChIP.

December 2015 – December 2016

- Internship, in Prof. Dr. Maria Carmo-Fonseca's Lab at the Instituto de Biologia Molecular, Lisbon (Portugal)  
Techniques performed: Cell culture, Purification of RNA, qRT-PCR and RT-PCR, Immunofluorescence coupled with RNA-FISH Microscopy.

September 2014 – December 2015

- Internship for Dissertation, in Prof. Dr. M. Carmo-Fonseca's Lab at the Instituto de Biologia Molecular, Lisbon (Portugal)  
Project: Testing short LNA-modified oligonucleotides for Duchenne Muscular Dystrophy gene therapy  
Techniques performed: Cell culture, Western Blot, Purification of RNA, qRT-PCR and RT-PCR, Immunofluorescence/Fluorescence Microscopy.

July-August 2013

- Summer Internship at the Microbiology Laboratory at the Quality Control Department of the SCC – Sociedade Central de Cervejas e Bebidas, SA. – Heineken Group, Vialonga (Portugal)  
Techniques performed: Sample collection and laboratorial analysis.

## PERSONAL SKILLS

### Language Skills

- Native Language: Portuguese
- Other Languages: English – Advanced; French – Basic; German – Basic

**Communication Skills** – Good spirit of teamwork, good interpersonal relationships and good project leadership skills acquired in an academic and lab context by performing assignments and projects.

**Organization Skills** – punctuality, attendance, good power of synthesis and good time management skills.

**Computer Skills** – Microsoft Office™, GraphPad Prism, Illustrator, Image J and Image Lab.  
Good understanding of Internet tools and websites.

## **ADDITIONAL INFORMATION**

### **Publications**

- Pires VB, Simões R, Mamchaoui K, Carvalho C, Carmo-Fonseca M (2017) Short (16-mer) locked nucleic acid splice-switching oligonucleotides restore dystrophin production in Duchenne Muscular Dystrophy myotubes. PLOS ONE 12(7): e0181065.
- Bousard A, Raposo AC, Żylicz JJ, Picard C, Pires VB, Qi Y, Gil C, Syx L, Chang HY, Heard E, da Rocha ST (2019) The role of Xist-mediated Polycomb recruitment in the initiation of X-chromosome inactivation. EMBO Rep. 20(10):e48019.
- Lockhart A, Pires VB, Bento F, Kellner V, Luke-Glaser S, Yakoub G, Ulrich HD, Luke B (2019) RNase H1 and H2 Are Differentially Regulated to Process RNA-DNA Hybrids. Cell Rep. 29(9):2890-2900.e5.
- Pires VB, Lohner N, Wagner T, Wagner CB, Wilkens M, Hajikazemi M, Paeschke K, Butter F, Luke B. RNA-DNA hybrids prevent resection at dysfunctional telomeres. Cell Rep. 2023 Feb 1;42(2):112077.

### **Conference Attendance**

- Oral presentation at the “1st Yeast Munich Meeting”, Germany, on 9 September 2019.
- Poster presentation at the “Telomeres and Telomerase” virtual meeting, CSHL, 14-17 December 2021.
- Poster presentation at the “DGDR-Krupp 2022 Symposium on DNA Repair and Human Disease” in Jena, Germany, on 6-9 April 2022, awarded Best Poster Prize.
- Poster presentation at the “IMB/SFB 1361 Conference - Restore, Reorganise, Repurpose: The many faces of DNA repair” in Mainz, Germany, on 20-23 September 2022.